Myco-transformation of Polystyrene Sulfonate by *Curvularia dactyloctenicola* VJP08: A Mechanistic Perspective

Thesis

Submitted in partial fulfillment

of the requirement for the degree of

DOCTOR OF PHILOSOPHY

By

Vishalakshi Bhanot

Under the supervision of

Prof. Jitendra Panwar

BIRLA INSTITUTE OF TECHNOLOGY AND SCIENCE, PILANI

2023

BIRLA INSTITUTE OF TECHNOLOGY AND SCIENCE, PILANI

CERTIFICATE

This is to certify that the thesis titled **"Myco-transformation of Polystyrene Sulfonate by *Curvularia dactyloctenicola* VJP08: A Mechanistic Perspective"** submitted by **Vishalakshi Bhanot,** ID No. **2017PHXF0032P** for award of Ph.D. of the Institute embodies original work done by him/her under my supervision.

Signature of the Supervisor:

Name in capital letters: JITENDRA PANWAR

Designation: **PROFESSOR**

Date:

Acknowledgements

First of all, I am obliged to the Lord almighty, merciful, gracious and passionate, for providing me the support to proceed patiently and the capability to complete my thesis.

I express my sincere gratitude to my supervisor, Prof. Jitendra Panwar for the guidance, encouragement, advice, constructive criticisms and hand-written notes he has provided throughout my research work. My learnings and improvements in scientific writing, data representation and designing schematic diagrams are solely an output of his guidance that improved me as a researcher. He has truly been an amazing mentor throughout my Ph.D. venture, and I strongly believe that it's his mentorship that crafts students to be independent future researchers.

I am thankful to the DNA Sequencing Facility, South Campus, University of Delhi for carrying out the sequencing of the fungal isolates. I am thankful to the staff of Sophisticated Instrumentation Facility, BITS Pilani, Pilani Campus, Mr. Sandeep, Mr. Om Prakash, Mr. Abhishek and Mr. Suman for helping me in performing Raman spectroscopy, SEM, GC-MS/MS and Confocal microscopy for my samples. I am especially grateful to Prof. Suresh Gupta, Dept. of Chemical Engineering, BITS Pilani, Pilani Campus, for helping me out in DSC analysis.

I am thankful to my family and my husband for their continuous support and patience. None of this would have been possible without the everlasting support and innumerable blessings of my grandmother, bade papa-mumma, my brothers, my sister-in laws and my beautiful little nephews. Special thanks to my husband Mr. Rachit Shukla for his continuous support, tremendous patience, and cooperation with my questionable spending whenever I felt over-worked. Everyone's endearment has been a constant source of my strength and happiness.

I am thankful to the Vice Chancellor, Director, and Deans of Birla Institute of Technology & Science (BITS), Pilani, Pilani Campus for providing necessary facilities and financial support. I am thankful to all the faculty members of Department of Biological Sciences and my Doctoral advisory committee (DAC) members Prof. Prabhat N. Jha and Dr. Pankaj K. Sharma who were always there to support me and spared their valuable time to proof-read this thesis. Their honest criticisms and valuable suggestions have immensely helped in enrichment of this thesis. I would like to thank non-teaching staff of the Department of Biological Sciences, Mr. Ajay, Mr. Naresh, Mr. Kamlesh, Mr. Subhash, Ms. Kaushalya, Dr.

Iti; and staff of AGSR Division Mr. Mahipal, Mr. Murali and Mr. Nitesh for their help and support.

I acknowledge my gratitude to my friend Dr. Tripti Misra for her companionship during this journey. I am especially thankful to my group members: Shobham and Mamta, who have truly been a strong support system throughout my journey. I am thankful to my seniors Dr. Arpit Bhargava, Dr. Monika Jangir, Dr. Sandeep Kumar, Dr. Shahid Khan, Dr. Shraddha Mishra, Dr. Poonam, Dr. Vikram Pareek, Dr. Vidushi and colleagues Shreya, Snigdha, Kamesh and Anil for their support and help during this period. I would also like to thank my furry friends for making my hostel stay very warm and happy.

I dedicate this thesis to my parents, Mr. Ajay Bhanot and Mrs. Seema Bhanot. It is all because of their love, motivation and encouragement that strengthened me to embark and complete this journey. When me and my brother were kids, my parents always allowed us to focus on ourselves, made our dreams theirs' and flooded us with a lot of interesting books, which turned the both of us into avid readers, that especially allowed me to go through so many articles for my research. Thanks for encouraging us to be independent thinkers and having confidence in our abilities to go after new things that inspired us.

Lastly, I wish to apologize if I forgot to acknowledge anyone who had helped me in any way.

Vishalakshi Bhanot

Abstract

Plastics are a ubiquitous class of synthetic polymers with applicability in virtually all commercial and industrial sectors. The majority of global plastics consists of polymers with carbon-carbon backbones, whose environmental persistence and low cost have resulted in a massive reservoir of plastic waste that resides in landfills and the environment. PS is an aromatic polymer formed as a result of polymerization of aromatic styrene monomers attached via vinyl side-chains. PS is used in manufacturing of various products including single use plastics *e.g.*, foam containers & trays for food take away, protective packaging, heat insulation as well as copolymers like acrylonitrile butadiene styrene (ABS), latex, and rubber. Therefore, the majority of the PS-derived products are single-use or throw-away products. Since majority of the plastic waste is comprised of single-use plastics, the development of PS degradation strategy is crucial at this point.

Biodegradation of plastics has been a topic of interest for researchers from more than a decade now, and yet the understanding of the degradation enzymes and their pathways is largely lacking. To the present date, polyethylene terephthalate (PET) is the only plastic for which the degradation enzymes namely cutinases/esterases/PETases have been identified. However, the degradation of plastics such as polyethylene, polystyrene and polypropylene that are composed of C-C bonds and lack functional bonds is fairly difficult to achieve. The aromatic and long-chain C-C bonds require higher bind dissociation energies; thus the above-mentioned plastics are recalcitrant to biodegradation and remain persistent in the environment. Additionally, the basis of selection of microorganisms to understand the plastic biodegradation process is very random, therefore limiting the probability of finding highly functional set of enzymes.

In the present study, the phylloplane of the xerophytic plants is selected as a substrate for isolation of fungi to be explored for their plastic degradation abilities. The phylloplane of plants is composed of a wide array of functional polymers such as cellulose, lignin, suberin, rubber latex components and cuticle, of impressive physiochemical properties. These polymers, particularly cuticle, display properties such as water insolubility, durability, and resistance to physical, chemical, or biological degradation, which are similar to synthetic plastics. Since the biodiversity and occurrence of microbes is strongly dependent on their ecological habitat, it is plausible that the phylloplanic microflora may be explored towards their ability to degrade synthetic polymers. Xerophytic plants possess thicker cuticle layer in order to avoid water-loss via transpiration, therefore the phytopathogenic fungi capable of

breaching the cuticle barrier might display similar functionality for plastic degradation. Hence, the phylloplanes of two xerophytic plants, namely *Calotropis procera* and *Salvadora persica* were collected across seasonal survey and a total of 20 fungi were isolated via leaf imprinting method. Pure cultures of 20 fungal isolates (VJP01-20) were used for the molecular identification of each fungal isolate, followed by their sequence submission on NCBI.

Simultaneously, the collected leaf samples were studied for the effect of temporal variation on the surface micromorphology and chemical composition of cuticular waxes by using SEM, CLSM and GC-MS/MS. The surface analysis revealed that the cuticular arrangement onto the leaves of both the plant species displayed assorted wax morphologies along with the appearance of trichomes. The wax crystals appeared ovate crystalloids and platelets in *C. procera* and *S. persica*, respectively. While the wax content of both the plants was observed to be maximum during the summer season. Additionally, the chemical composition of both the plants revealed the presence of similar class of components belonging to alkanes, fatty acids, aldehydes, alcohols, ketones, alkenes and terpenoids.

Further, the 20 fungal isolates from VJP01-VJP20 were screened towards their PSS utilization ability. Based on the change in the fresh fungal biomass, fungal isolates namely, *Cladosporium* sp. VJP04, *C. dactyloctenicola* VJP08, *Aspergilus ochraceus* VJP10, *Aspergillus nidulans* VJP11, *Aspergillus foveolatus* VJP13, *Alternaria alstroemeriae* VJP18 and *Aspergillus welwitschiae* VJP20 were observed to be potential PSS transformers. These short-listed fungal isolates were further evaluated for their transformation ability by Raman spectroscopy and *C. dactyloctenicola* VJP08 was selected for further studies. The independent variables, such as exposure duration, temperature, and pH were evaluated to determine the best-suited conditions for PSS transformation by change in fresh fungal biomass, Raman spectroscopy and GC-MS/MS analysis. The results indicated that the temperature of 28 °C, pH of 7.2, and the exposure duration between 15 to 20 days were the optimum conditions for PSS transformation by *C. dactyloctenicola* VJP08. The isolate VJP08 displayed significant decrease in the key Raman peaks of PSS corresponding to aromatic C-H bands stretch 3248.26 and 3387.59 cm^{-1}, in addition to the presence of cellular metabolites in the exometabolomic profile indicating the utilization of PSS for its growth and metabolism.

To understand the possible mechanism behind the PSS transformation ability of *C. dactyloctenicola* VJP08, the protein extracts precipitated from the fungal secretome across different exposure durations (day 5 to 20) were analysed for the presence of putative enzymes

involved in PSS myco-transformation by quantitative proteomic analysis. The obtained results showed enhanced expression of oxidoreductases, CAZymes and transport proteins at day 15 of exposure duration. The oxidoreductases and biosurfactant proteins combinedly function for PSS utilization. Oxidoreductases such as laccase were predicted to be involved in depolymerization of PSS into its oligomers and monomers and their subsequent conversion into cellular metabolites. Simultaneously, other enzymes such as tyrosinase, dehydrogenases, and peroxidases function to cleave the aromatic ring of styrene sulfonate (SS) into 2,2-vinyl muconic acid which is subsequently fed into the Krebs cycle. The PSS utilization may also occur via side-hain cleavage, however, the enzymes involved in aromatic ring cleavage were predominantly present in the secretome. Moreover, *in silico* analysis of biosurfactant cerato-platanin and laccase revealed their possible association with each other and individually with SS.

Further, the ability of *C. dactyloctenicola* VJP08 was also evaluated towards degradation of commercially available PS using SEM, EDS, changes in weight and thickness, DSC and GC-MS/MS analysis. The results indicated that *C. dactyloctenicola* VJP08 was able to colonize the PS with its mycelium breaching the surface of PS leading to the appearance of cracks and holes, indicating that PS-derived carbon has been extracted for fungal growth. Further, decrease in weight and thickness were observed in the fungal treated PS samples. The decrease in T_g also confirmed the fungal-induced alteration in the mechanical properties of PS. At last, the GC-MS/MS analysis confirmed significant decrease in the concentration of benzene and related aromatic derivatives as a result of fungal action.

Another fungal isolate, *L. ramosa* AJP11 isolated from the rhizosphere of plants growing in heavy metal rich sites was also evaluated towards its PSS myco-transformation ability. The data revealed that over a period of 30 days, the fungal isolate was able to transform PSS into cellular metabolites such as alkanes and fatty acids which are subsequently fed into the Krebs cycle. Further, SDS-PAGE revealed the overexpression of three proteins at 14.4 kDa, 46.8 kDa and 107.9 kDa in the secretome of *L. ramosa* AJP11 exposed to PSS as sole carbon source, indicating their possible involvement in PSS transformation. Using peptide mass fingerprinting, the proteins were identified to be hydrophobic surface binding protein, universal stress protein (and PRP-1 splicing factor, respectively. Based on these results, the putative molecular mechanism was proposed as follows: nutrient stress induces *Usp* gene in nucleus resulting in maximizing cellular transcript level (by PRP-1 splicing protein) in order to utilize PSS. Among various synthesized transcripts, an extracellular Hsb was also synthesized which

adheres to the hydrophobic PSS assiting its myco-trasnformation into organic compounds. These results were also supported by *in silico* analysis revealing higher probabilty of binding between Hsb and SS.

Overall, this study fills important knowledge gaps in plastic biodegradation by identifying the proteins involved in the PSS myco-transformation and their predicted mode of action. To the best of our knowledge, this is the first study where the phytopathogenic fungus *C. dactyloctenicola* VJP08 has been studied to successfully transform PSS and commercially available PS products. The present study suggests that owing to the similarities between the plant cuticle and plastics, the phytopathogenic fungi possess powerful protein arsenal capable of degrading recalcitrant plastics and other associated xenobiotic pollutants.

Table of Contents

List of Tables

List of Figures

	Fatty acids; SER: Smooth Endoplasmic Reticulum; RER: Rough Endoplasmic Reticulum; Hsb: Hydrophobic Surface Binding Proteins. Dotted lines represent the hypothetical series of events where the participating biomacromolecule is unknown	

List of Abbreviations

Symbol	Abbreviation
%	Percentage
µg	Microgram
µl	Microlitre
ΔG	Gibbs free energy
2,3-DCMSB	(2,3-diphenylcyclopropyl)methylsulfanylbenzene
2,4-DTBP	2,4-Di-tert-butylphenol
2D	Two-dimensional
3D	Three-dimensional
A	Adenine
ABC Transporter	ATP-binding cassette Transporters
ADT	AutoDock Tools
Ala	Alanine
A. oryzae	*Aspergillus oryzae*
Arg	Arginine
ASTM	American Society for Testing and Materials
ATP	Adenosine triphosphate
au	Arbitory unit
BDE	Bond dissociation energy
BITS	Birla Institute of Technology and Science
BLAST	Basic local alignment search tool
bp	Base pair
C	Cytosine
℃	Celsius
CAZymes	Carbohydrate-active enzymes
CBB	Coomassie Brilliant Blue
C-C	Carbon-Carbon
CFF	Cell-free filtrate
C-H	Carbon-Hydrogen
C-O	Carbon-Oxygen
C=O	Ester bond
CLSM	Confocal laser scanning microscopy
Cu-bd	Copper-binding

cm	Centimeter
D	Day
dH_2O	Distilled water
DLS	Dynamic light scattering
DNA	Deoxyribonucleic acid
DSC	Differential scanning calorimetry
EDS	Energy dispersive spectroscopy
FA	Fatty acids
FAD	Flavin adenine dinucleotide
FC	Fold change
FDR	False discovery rate
FE-SEM	Field-emission Scanning electron micrpscopy
FRAP	Fluorescence recovery after photobleaching
FW	Fresh weight
g	Gram
G	Guanine
GA	Gum arabic
GC	Gas chromatography
GC-MS/MS	Gas chromatograph-Mass spectroscopy
GHG	Greenhouse gases
Gln	Glutamine
Glu	Glutamate
Gly	Glycine
GMC	Glucose-methanol-choline
GRAVY	Grand average of hydropathicity
H_2O_2	Hydrogen peroxide
h	Hour
HCCA	A-Cyano-4-hydroxycinnamic acid
HDPE	High density polyethylene
HR	High resolution
Hsb	Hydrophobic surface binding protein
Ile	Isoleucine
ITS	Internal transcribed spacer
IMTech	Institute of Microbial Technology

kDa	Kilo dalton
keV	Kilo electron volt
kJ	Kilo joules
kPa	Kilopascal
kV	Kilo volt
L	Leucine
LC-MS/MS	Liquid chromatograph-Mass spectroscopy
LDPE	Low-density polyethylene
L. ramose AJP11	*Lichtheimia ramose* AJP11
Lys	Lysine
M	Molar
mA	Milli Ampier
MEGA	Molecular Evolutionary Genetics Analysis
mg	Milli gram
min	Minutes
mL	Milli litre
mM	Milli Molar
mm	Micrometer
MO	Monooxygenase
MP	Microplastics
MSA	Minimal salt agar
MSM	Minimal salt media
mV	Mili Volt
MVA	Mevalonate
M_w	Molecular weight
m/z	Mass/charge number
NADH	Nicotinamide adenine dinucleotide+Hydrogen
NAD	Nicotinamide adenine dinucleotide
NADPH	Reduced nicotinamide adenine dinucleotide phosphate
NCBI	National centre for biotechnology information
NCIM	National collection of industrial microorganisms
nm	Nanometer
NIST	National Institute of Standards & Technology

NP	Nanoplastics
PA	Polyamide
PAALDH	Phenylacetaldehyde dehydrogenase
PACoA Ligase	Phenylacetyl coenzyme A ligase
PAH	Polycyclic aromatic hydrocarbons
PBAT	Poly(butylene adipate-co-terephthalate)
PBS	Poly(butylene succinate)
PBSA	Poly(butylene succinate-co-adipate)
PC	Polycarbonate
PCA	Principal component analysis
PCL	Polycaprolatone
PCR	Polymerase chain reaction
PDA	Potato dextrose agar
PDB	Potato dextrose broth
PDB file	Protein data bank file
PDBQT	Protein data bank, Partial charge (Q), & Atom type (T)
PE	Polyethylene
PES	Polyethersulfone
PET	Polyethylene terephthalate
ɣ PGA	Polyglycolic acid
PHB	Polyhydroxybutyrate
PHBV	Polyhydroxybutyrate and hydroxyvalerate
Phe	Phenylalanine
PHHA	Poly(hydroxyhexadecanoate)
PLA	Polylactic acid
PLA-DA	Partial least squares discriminant analysis
pmol	Picomole
PP	Polypropylene
PS	Polystyrene
PSS	Poly(sodium 4-styrenesulfonate)
PTFE	Polytetrafluoroethylene
PU	Polyurethane
PVC	Polyvinyl chloride

PVOH	Polyvinyl alcohol
QCM	Quartz crystal microbalance
R	Arginine
RER	Rough endoplasmic reticulum
RNA	Ribonucleic acid
RNAseq	RNA Sequencing analysis
ROS	Reactive Oxygen species
rpm	Rotation per minute
RT	Room temperature
S. No.	Serial number
SAVES6	Structural Analysis and Verification Server 6
SD	Standard deviation
SDF	Simulation description format
SDS-PAGE	Sulfate-polyacrylamide gel electrophoresis
SEM	Scanning electron microscopy
SER	Smooth endoplasmic reticulum
SMO	Styrene monooxygenase
SO	Styrene oxide
SO_2	Sulfur dioxide
SOI	Styrene oxide isomerase
SS	Styrene sulfonate
SSP	Small-secreted proteins
sp	species
T	Thymine
TCA	Trichloroacetic acid
TCEP	Tris (2-carboxyethyl) phosphine hydrochloride
TEF 1- α	Translation elongation factor 1-α
TEP	Triethyl phosphate
Tf	Final thickness
Tg	Glass transition temperature
TGA	Thermogravimetric analysis
Thr	Threonine
Ti	Initial thickness
TS	Transverse section

Tyr	Tyrosine
Usp	Universal stress protein
UV	Ultra-violet
v/v	Volme by volume
Val	Valine
VIP	Variable importance in the projection
VLCFA	Very Long Chain Fatty Acids
Wi	Initial weight
Wf	Final weight
Y	Tyrosine

Chapter 1

General Introduction

Part of the work presented in this chapter has been published as per the following details:

- Bhanot et al. (2020) Myco-degradation of plastics. In: *New and Future Developments in Microbial Biotechnology and Bioengineering*, Singh, J. and Gehlot, P. (Eds.), Elsevier, Amesterdam, Netherlands, pp. 25-34.

1.1 Plastics: Evolutionary History and Current Scenario

For decades, human activities culminating in rapid growth of industrialisation and globalisation have led to the contamination of soil and water with several damaging xenobiotic compounds [Ceci et al. 2019]. The presence of these pollutants in the environment exerts a long-term disbalance in the biogeochemical equilibrium and hence, interfere with the functionality of the natural processes and resources. Since early ages (~1600 BC), there have been records of humans exploiting natural resources such as rubber, waxes and resins for their polymeric applications, which significantly upscaled with the invention of synthetic polymers such as vulcanised rubber in the mid-1800s [Andrady and Neal, 2009]. Later, in 1856, the first synthetic thermoplastic plastic, 'Parkesine' was created by combining cellulose and nitric acid, to be used as an 'eco-friendly' substitute for ivory. Shortly, another type of modified synthetic plastic, celluloid, was discovered to be used as photographic films in cinematographic industries [Rhodes, 2018]. The twentieth century experienced incremental production of various new classes of synthetic polymers. The first commercially successful synthetic polymer 'Bakelite' was introduced in 1907 by Leo Baekeland which was synthesized by combining phenol and formaldehyde under heat and pressure [Worm et al. 2017]. Ironically, the Bakelite manufacturers adopted the symbol 'infinity', somewhat insightful pertaining to the current situation of plastics. The invention of Bakelite was a time turning event in introducing plastics into the commercial market. It was the World War II that sky-rocketed the plastic production to be used in clothing, parachutes etc., marking the beginning of an unending era of 'Plastics' [Worm et al. 2017].

The word plastic comes from the Greek word *Plastikos*, which means 'able to be molded into different shapes' [Joel, 1995]. Plastics are synthetic polymers composed of monomers forming long chains of carbon and hydrogen atoms as the backbone to which oxygen, sulfur or nitrogen atoms may be attached. These monomeric units are linked via highly stable and strong covalent bonds [Chamas et al. 2020]. Their versatility, flexibility, durability, strength, and economic feasibility makes them an attractive replacement for the metals and wood. Now, that plastics have marked their componential dominance in various sectors such as furniture, cutlery, entertainment, automobiles, aeronautics, etc., the waste generated is getting difficult to be taken hold of. The production of plastics has remarkably accelerated since 1950s, and is estimated to reach up to 1900 million tonnes in 2050 [Rhodes, 2018]. Plastics have become a global concern as their accumulation in the environment has become evident and inevitable, acting as a high-risk carrier for the human health [Wright et al. 2017]. About

58% of the total plastic produced is discarded as waste on land and oceans, which can be witnessed by the infamous 'The Great Garbage Patch' in the Pacific Ocean filled with >80 trillion plastic pieces, increasing every day at an unprecedented scale [Geyer et al. 2017; Lebreton and Andrady, 2019]. These plastic fragments may serve as niches for a wide spectrum of microbes, including pathogens, which may be transported to long distances [Barnes et al. 2009]. Around 89% of the plastic waste occupying the depths of water bodies consists of 'single use plastics' [Chiba et al. 2018]. The vastness and seriousness of the issue can be estimated by the genesis of 'plastic-specific' new terminologies, such as *Plastisphere* and *Plastiglomerate*. Plastisphere defining the plastic debris acting as a superficial niche for the microbial communities and other microscopic life, specifically in the oceans, facilitating the dispersal of microbial communities across distances, affecting the aquatic ecology [Amaral-Zettler et al. 2020]. Plastiglomerate is a conglomerate of rock fragments, sand grains, organic materials (shells, wood, coral debris) combined with plastic debris resulting in the formation of the one of its kind anthropogenic stone [Corcoran and Jazvac, 2020]. As human-induced activities continue to add up the plastic dump into the environment, it is important to access the impact of our actions. Given, the environment harbours a multitude of habitats and diverse groups of microbes, little has been explored to utilise them for efficient biotransformation of plastics. Although the phenomenon of biodegradation is known to occur, however, the functional significance of the specific biomacromolecules that might play a major role in plastic degradation are yet to be explored.

1.2 Types of Plastics

Plastics are classified on the basis of their origin (synthetic/bio-based), structural arrangements (theromosets/thermoplastics), and biodegradability (biodegradable/non-biodegradable). These factors influence various properties such as crystallinity, molecular weight, strength, melting temperature, inertness, recyclability, etc [Sánchez, 2020]. Additionally, the presence of identical/different monomeric units also classify them as homo- or heteropolymer, respectively [Eyerer, 2010]. The above-mentioned categories have been briefly described below:

1.2.1 Synthetic and Bio-based Plastics

Synthetic plastics are highly stable plastics derived from hydrocarbons and petrochemicals, and do not readily enter the degradation cycle, such as polyethylene (PE), polypropylene (PP), polystyrene (PS), polyethylene terephthalate (PET), polyamide (PA),

polycarbonate (PC), polyvinyl chloride (PVC) and polyurethane (PU). On the other hand, according to American Society for Testing and Materials (ASTM), bio-based plastics are organic material in which carbon is derived from a renewable resource via biological processes, such as polylactic acid (PLA), polyhydroxybutyrate (PHB), polycaprolatone (PCL), poly(butylene adipate-co-terephthalate) (PBAT), poly(butylene succinate) (PBS), poly(butylene succinate-co-adipate) (PBSA), polyethersulfone (PES), polyvinyl alcohol (PVOH), polyglycolic acid (ɣ PGA), etc [Johnston et al. 2018]. Since bio-based plastics are known to be derived from biological sources, it is a misconception to assume all bio-based plastics as biodegradable.

1.2.2 Thermosets and Thermoplastics

Thermosets are highly dense plastics forming crosslinked networks on polymerization, namely, Bakelite, PU, PA, etc. They have low melting viscosity, low processing cost and cannot be reshaped or recycled, once they have been molded into a particular shape. Whereas thermoplastics have no crosslinks, have high melting viscosity, and can be repeatedly reshaped by heating without losing their chemical/mechanical properties. Examples of thermoplastics include, PE, PS, PP, PET and PVC [Obande et al. 2019].

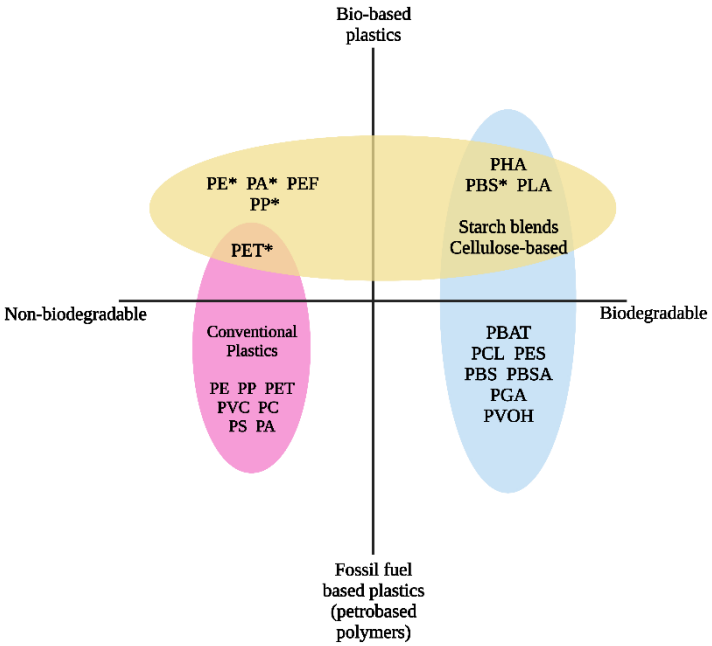

Figure 1.1 Schematic representation of conventional and bio-based plastics categorised as biodegradable and non-biodegradable. The * indicates polymers that have bio-based origins plus fossil fuel synthesis routes [Johnston et al. 2018].

1.2.3 Biodegradable and Non-Biodegradable Plastics

On the basis of biodegradability, plastics may be divided into three sub-classes: (1) Non-biodegradable bio-based plastics derived from renewable raw material, usually combined with conventional plastics (PE*, PA*, PP*, PEF); (2) Biodegradable bio-based plastics (PHA, PBS, PLA, starch blends and cellulose based) and lastly, (3) Fossil-based biodegradable plastics (PCL, PES, PBAT, PVOH, PBS, etc) [Johnston et al. 2018]. The diversity and classification of plastics types has been furnished in the given schematic [Figure 1.1].

All the above-mentioned plastic types have their own challenges in biodegradation. Various studies have highlighted the degradation of mostly bio-based plastics, PE, PVC and PET, ignoring the more persistent plastic types. Considering the large applicability of PS in disposable items, accounting for significant proportion in waste generated throughout, and lack of substantial reports on mechanistic insight of biodegradation of PS, it is equitable to look deeper into the details of properties, problems and current biodegradation scenario of PS, so as to get a directive approach for its sustainable removal from waste.

1.3 Why Degrading Polystyrene is Important?

Polystyrene $(C_8H_8)_n$ is a high molecular weight, synthetic and non-biodegradable polymer composed of aromatic styrene monomers with substantial applicability in throw away products [Ho et al. 2018]. Due to its good mechanical properties and structural stability, PS has been extensively used in commercial market since 1930s for manufacturing products such as disposable cutlery, packaging, laboratory consumables, medical items, etc. and is also the first synthetic polymer to be detected as a contaminant in euphotic zone of the ocean in 1970s [Carpenter et al. 1972; Pilevar et al. 2019]. Although PS is recyclable, the cost of recycling is more than the manufacturing cost, restricting the process, leading to a large waste accumulation of this ‘one time use’ plastic [Ali and Ghaffar, 2017]. According to the Plastics Europe Report, by 2020, the global plastic production has reached almost 370 million tonnes, with packaging industry emerging as a major sector contributing about 40% of the total plastic demand [Plastics Europe, 2020]. The widespread production and consumption of polystyrene in the packaging industry, combined with lack of recycling and incompetent waste management approaches, have led to severe effects and drawbacks sinking the overall environmental health. The overall properties, applications and challenges associated with the disposal of PS have been furnished in Figure 1.2.

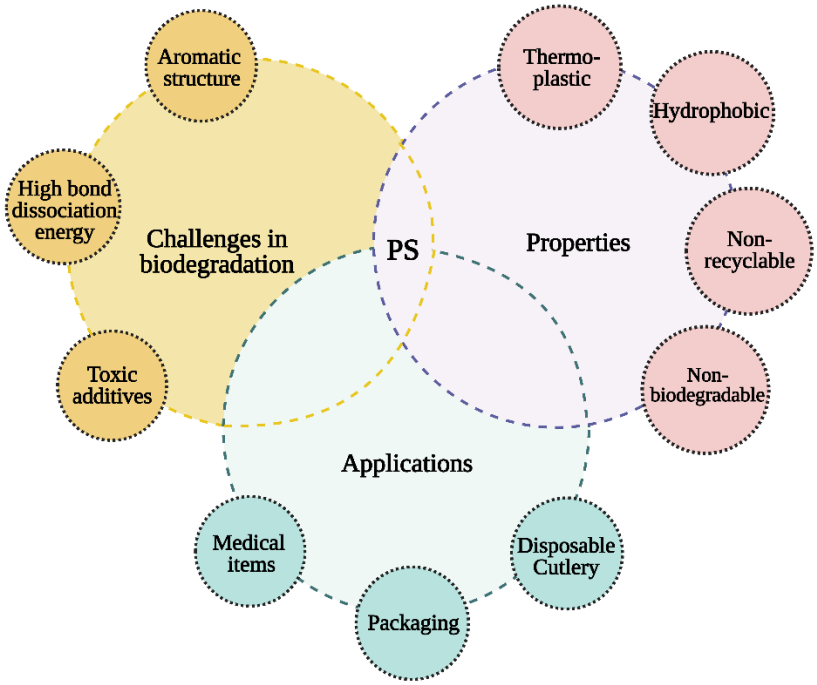

Figure 1.2 General properties, applications, and challenges in biodegradation of PS.

The aromatic structure of the PS (Figure 1.3) imparts structural stability and hydrophobic character that makes it highly resistant to biodegradation. Moreover, the high molecular weight and extensive carbon-carbon bonds present in the aromatic structure and the backbone make PS highly resistant to enzymatic cleavage by the oxidation-reduction processes [Ho et al. 2018]. High thermal stability of PS is also one of the factors for its resistant attribute. PS shows no sign of degradation even at temperature as high as 200℃. Partial degradation of the backbone could be observed at ~350℃, leaving its monomeric unit 'styrene' as the main end product [Kik et al. 2020]. Also, the inexorable character of the PS chemical structure makes it difficult to be blended with different biocompatible substrates. The antioxidants, processing lubricants, flame retardants, dyes and stabilizers added during the manufacturing process increase its shelf life by adding resistance to oxidation and biodegradation. The additives such as phthalates, bisphenol, benzophenones, hindered amines and antimicrobial agents (in case of food packaging) of high toxic capacity are slowly released into the environment during prolonged disposal of PS [Warner and Flaws, 2019]. Along with these chemical additives, the exerted environmental forces lead to the disintegration of PS to its micro- and nano-forms. Since the monomeric unit, styrene, itself has been classified as a potent carcinogen, its sub-particle forms have also been studied to show ecotoxicological effects. Due to the high surface area, PS microplastics (MPs) and PS nanoparticles (NPs) are likely to be accumulate in the

marine and terrestrial animals. PS-MPs are mostly ingested via food and water, whereas PS-NPs may penetrate organisms through various routes, i.e. skin, respiratory and digestive tracts by the interaction between the protein corona and cellular membranes. Moreover, the discarded MPs/NPs adsorb metal ions and chemical pollutants, leading to the many-folds increase in their toxicity potential. Among other plastic pollutants, PS-MPs/NPs are the most predominant type accounting up to 4500 μg L^{-1} in densely polluted zones, which is 4500 times more than the threshold leading to chronic exposure [Reisser et al. 2015; Kik et al. 2020]. Studies have been conducted to partially fill the gaps in assessing the toxicokinetic and toxicodynamic of the PS-MPs, highlighting the effects of PS-MPs/NPs at molecular and organismal level leading to cellular oxidative stress, mitochondrial depolarization, disruption of scaffold and junction proteins, lung and pulmonary dysfunction [Yang et al. 2019; Dong et al. 2020]. Due to their broad size range (<0.1-5000 μm), it is impossible to filter out all the MPs and NPs from the ground water/or treated effluents, hence, a convenient degradation method is required for treating PS waste.

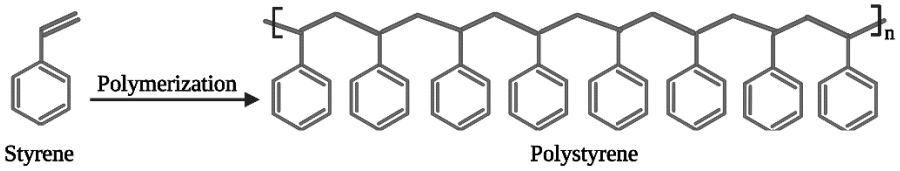

Figure 1.3 Chemical structure of monomeric unit-styrene (vinylbenzene) and polystyrene [Ho et al. 2018].

Although, the microbial degradation of polystyrene by various microbes has been demonstrated in recent years, unfortunately, no detailed study covering the enzymes involved in the degradation pathway has been published [Danso et al. 2019; Amobonye et al. 2021]. Briefly, bacteria such as Archaeons, *Rhodococcus* sp. and *Actinobacterium* have been tested to show PS degradation at a very slow rate, peaking up to 0.04-0.57% degradation in several months. The extremely insignificant low productivity, lack of well-manufactured degradation systems and required high capital input are the major reasons due to which opportunities have not been further explored and practiced [Amobonye et al. 2021]. Recently, studies focusing on the gut microbiome of plastic eating larvae have surfaced, showing the role of *Acinetobacter* sp. isolated from the gut of *Tribolium castaneum*, in PS degradation over a period of 60 days [Wang et al. 2020]. Similarly, the gut microbiome of the superworm *Zophobas atratus* has also been studied to aide in the digestion of Styrofoam as sole carbon source [Yang, et al. 2020].

Additionally, the conduciveness of the gut microbiome of *Tenebrio molitor* towards PS biodegradation was monitored, showing the cohesive involvement of the emulsifying factors (30-100 kDa) secreted by the mealworm, with the respiratory factors (<30 kDa) released from the gut microbiota, collectively increasing the bioavailability of PS for biodegradation [Brandon et al. 2021]. The effect of PS-MPs on the gut of mice has revealed the toxic consequences causing decreased intestinal mucus secretion, drastically altering the microbial communities, disturbing metabolic pathways leading to metabolic disorders and dysbiosis [Jin et al. 2019]. These studies could be theorized leading to binary inference, firstly the toxic capacities of the sub-forms of PS have been highlighted and secondly, the polystyrene degradation and mineralization potential of microbes has been displayed, although major gaps lie in the detailed information about the metabolic by-products and the biomacromolecules involved in the process of degradation. Moreover, since various ethically approved niches could be explored for isolating microbes with PS degradation capabilities, there seems no compulsion to sacrifice larvae for the same.

1.4 Biodegradation of Plastics and Associated Challenges

Polymer degradation is defined as the conversion of polymer into smaller subunits by breaking bonds through physical, chemical, or biological processes leading to alterations in the physico-chemical properties of polymer. Abiotic processes including thermal, photo-oxidation, ozone-based degradation, catalytic and mechanochemical methods are also known to play a role in polymer degradation [Singh and Sharma, 2008; Amaral-Zettler et al. 2020]. The above-mentioned methods only partially degrade the plastic waste, with incineration (thermal degradation) as an exception. However, incinerating plastics is accompanied by the release of toxic greenhouse gases (GHGs) and MPs of unique physiochemical micro- and nanoscale properties which adversely affect human health [Peiponen et al. 2019; Yang et al. 2021]. With the current incremental stats of plastic production, it is estimated that the global carbon footprint would elevate by15% in the next two decades [Zheng and Suh, 2019].

Due to the aforementioned problems and lack of natural analogues, plastics do not easily undergo extensive degradation under marine/terrestrial ecosystems. As a source of abundant carbon, plastics could be used as carbon reservoirs by microbes through biodegradation, transforming the physico-chemical properties of polymer to release respective oligomers and monomers. It is a relatively slow process in which cleavage of polymer backbone by bond scission leads to generation of carbonyl groups (oxidation) to be utilized by

the microbes [Sivan, 2011]. Studies showing the potential of microbes towards degrading different types of plastics (including PS) are published consistently, although, limited data is available on their biodegradation capacity. However, the monomeric unit, styrene, has been studied and has shown degradable properties. In bacteria, under aerobic conditions, the oxidation of styrene takes place under two different pathways: either via attacking the vinyl side chain; or by attacking the aromatic ring, releasing 3-vinylcatechol, 2-phenyl ethanol and phenylacetic acid as primary intermediates. Although, the cleavage of aromatic ring is somewhat a less understood process; the key enzymes, namely, styrene monooxygenase, styrene oxide isomerase and phenylacetaldehyde dehydrogenase, participating in the oxidation of vinyl side chain have been thoroughly studied [Tischler et al. 2009; Morrison et al. 2013; Crabo et al. 2017]. The intermediates namely, phenylacetic acid and 3- vinylcatechol, produced during the vinyl side chain and aromatic cleavage, respectively, are converted to acetyl-CoA, and subsequently fed into the Krebs cycle [Figure 1.4] [Ho et al. 2018; Danso et al. 2019]. Nevertheless, questions such as, how common this phenomenon in nature is; how much of this process contributes to the naturally occurring process of biodegradation; and are the microbial isolates used for the biodegradation studies isolated from the right source, and lastly, do fungi utilise similar or different bio-macromolecular functional units for PS degradation, remain unanswered. The predicted routes of extracellular plastic degradation by involvement of fungal hydrophobins (described in section 1.5) and catalytic enzyme and the bacterial intracellular utilization of styrene monomer via vinyl side chain cleavage have been furnished below [Figure 1.4].

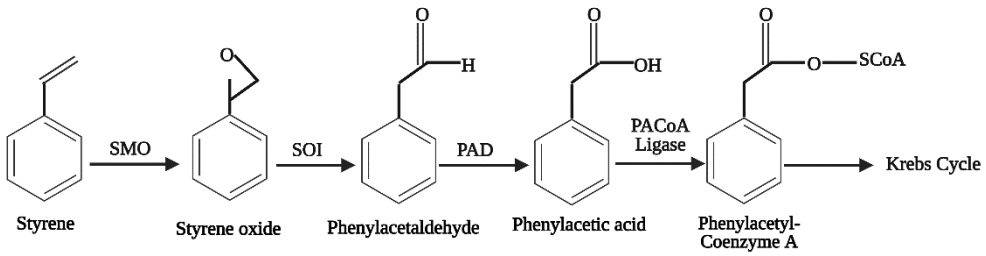

Figure 1.4 Bacterial degradation pathway of styrene via vinyl chain cleavage. Abbreviations: SMO: styrene monooxygenase, SOI: styrene oxide isomerase, PAALDH: phenylacetaldehyde dehydrogenase, PACoA ligase: phenylacetyl coenzyme A ligase [Ho et al. 2018].

1.5 Rationale Behind the Study: Plant Cuticle as a Natural Plasticizer

Plants synthesize a wide array of functional starch and non-starch polymers such as cellulose, lignin, suberin, rubber latex components and cuticle, of impressive physiochemical properties. These polymers are mainly composed of hydrocarbons and have very low or no solubility in water. These polymers are laid as network that frame the cells and aide in maintaining shape, protecting the plant from mechanical/osmotic damage, and act as a barrier at the interfaces of plant system and its outer environment [Bhanot et al. 2021]. Interestingly, synthetic plastics also exhibit similar properties such as water insolubility, durability, and resistance to physical, chemical, or biological degradation. The chemical segments of natural non-starch polymeric substances such as cellulose and cuticle components, resemble the chemical unit of different plastics due to the presence of hydrocarbon chains attached to various functional groups [Table 1.1] and have also been widely used for the synthesis of bioplastics [Marichevlam et al. 2019; Chen et al. 2020]. Furthermore, as plastics are derived from crude oil, the chemical bonds constituting and linking the monomeric units of the plastics are found to be similar to those in natural polymers. Certain wax components, such as *n*-alkanes, *n*-alcohols, and *n*-acids, have similar features to plastics, such as hydrophobicity and resistance to abiotic factors, and have been found to be preserved as fossils [Logan et al. 1995].

Recently, few studies have explored the applicability of superhydrophobic surfaces such as cuticular waxes towards sustainable replacement of synthetic plastics. It has been reported that the phylloplane shows superhydrophobicity, low adhesion and self-cleaning property due to the epicuticular wax load over its surface [Riglet et al. 2021]. Recent studies reported various cuticle-inspired bioplastics with properties similar to existing plastics, for example, poly(hydroxyhexadecanoate) (PHHA), a ω-hydroxy fatty acid derived biopolyester showed comparative water barrier properties as well as toughness that suggest it as a suitable option for packaging material [Singha et al. 2021]. Comparison of cuticle components to various plastics has been discussed at length by Guzmán-Puyol et al. (2021). They reported fabrication of plant cuticle-like composites by the blending of cutin-inspired polymers with waxes and polysaccharides making it an interesting strategy to improve mechanical properties and hydrophobicity. Considering the similarity between physical, mechanical & thermal properties of various monomeric units of plant cuticle to the synthetic plastics, it can be explored as replacements for plastics [Yaradoddi et al. 2020]. Given the compelling evidence of the physical, mechanical, and thermal similarities amongst plastics, it is conceivable to search for phylloplane microorganisms, primarily phytopathogens, that penetrate the external

cuticle barrier for the establishment of infection. The enzymes that break down these natural polymers, such as cuticular waxes, may thus also be able to break down plastic polymers [Chen et al. 2020; Ueda et al. 2021].

Table 1.1 Outlook of the chemical linkage similarities between the plant based non-starch polymers and synthetic polymers [Chen et al. 2020].

Polymer class	**Linkage type**	**Species**	**Main components**	**Backbone linkage**
Non-starch plant biomass	Non-polysaccharide biomass	Cutin	Oxygenated fatty acid	Ester bond
		Natural rubber	C5H8 isoprene	C-C bond
		Lignin	Aromatic subunit	C-C and C-O bonds
	Polysaccharide biomass	Cellulose	Glucose	Glycosidic bond
		Hemicellulose	Xylose, mannose, glucose, galactose, arabinose	Glycosidic bond
		Pectin	Galacturonic acid	Glycosidic bond
Synthetic polymer	C-C bond polymer	Polyethylene	Ethylene	C-C bond
		Polypropylene	Propylene	C-C bond
		Polystyrene	Ethylbenzene	
		Polyvinyl chloride	Vinyl chloride	C-C bond
	Hydrolysable bond polymer	Polyurethane	Polyol and isocyanate	Urethane bond
		Polyethylene terephthalate	Ethylene and terephthalate	Ester bond

The biodiversity and occurrence of microbes is strongly dependent on their ecological habitat. Since the plant-derived polymers show comparable mechano-chemical properties to the synthetic plastics, it is plausible to look for the microbes inhabiting these polymers under natural conditions and evaluate their biodegradation potential towards synthetic polymers. As starch and cellulose are glucose-derived polymers, their microbial degradation is well established. On contrary, plant cuticle which occurs as a continuous shield covering the epidermal cells, is well known to be preserved as fossil, resisting degradation over a prolonged exposure to environmental factors [Guignard, 2019; Bhanot et al. 2021]. Since 1970s, cuticle has been described as the outermost layer of low water permeability, with water droplets rolling down its surface. With its hydrophobicity a thousand times more than that of the cell wall, it qualifies to be comparable with the synthetic polymers [Schreiber and Schönherr, 2009]. Its hydrophobic attribute is a consequence of the cutin monomer layered over with the epicuticular wax deposits. The hydrophobic character of cuticle limits the water loss occurring due to the excessive heat and temperature rise. Xerophytic plants which thrive in arid regions have more cuticle thickness with high wax deposition on their leaves as compared to the mesophytic plants from wetter climates [Sharma et al. 2019]. The stable, resistant and outstanding water repellence of the cuticle are due to the presence of carbon-based monomeric units of cutin and epicuticular wax [Figure 1.5] [Ensikat et al. 2011]. In comparison to the other natural polymers, components of the cuticle show high similarities in chemical structure, mechanical, thermal and hydration profiles to the synthetic polymers [Khanal and Knoche, 2017; Gómez-Patiño et al. 2020].

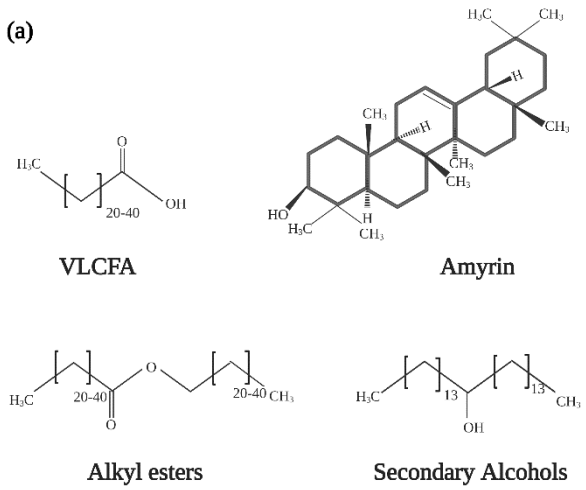

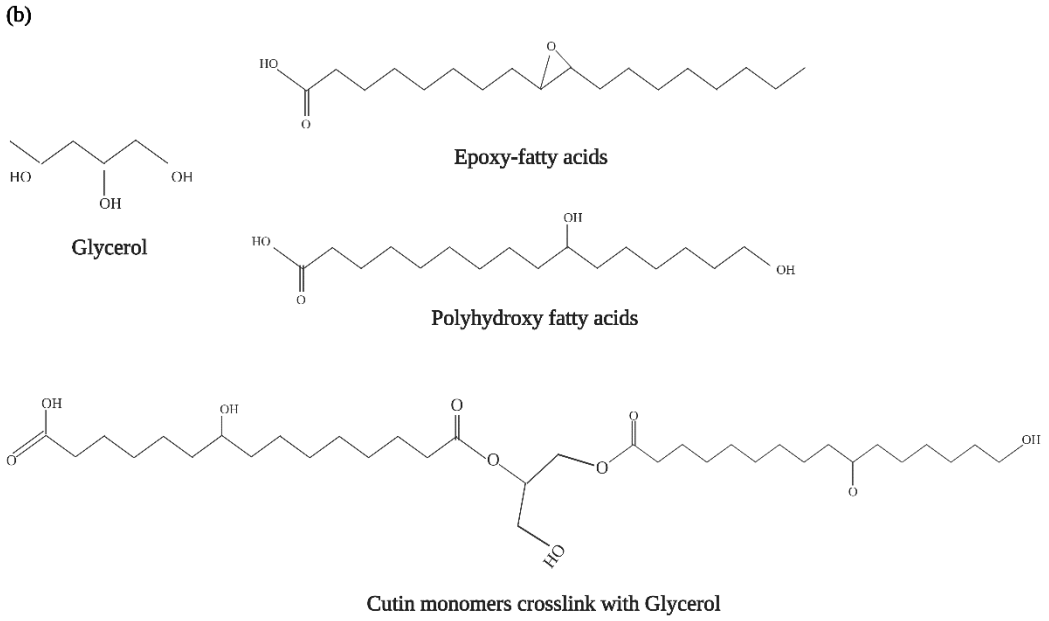

Figure 1.5 Chemical structures of complex hydrocarbon-based monomeric units comprising the plant cuticle: (a) linear and aromatic monomeric units of epicuticular wax, (b) fatty acid units crosslinking with glycerol to form cutin. Abbreviation: VLCFA: Very Long Chain Fatty Acids

The phylloplane of a plant houses numerous microbes that exhibit a close functional relationship with the host plant. The phylloplanic microbes could either have beneficial, mutualistic effects such as increase in resource uptake, providing nutrients, aiding plant growth and development, inferring resistance to abiotic/ biotic stresses, etc., or pathogenic effect to the plant [Berg et al. 2014]. Since cuticle is the outermost covering and the first line of defence, phylloplanic microbes live in close association with it. Certain bacterial and fungal phytopathogens are known to secrete cutinases that are capable of depolymerizing cuticle. The microbial cutinases studied to date belong to the large α/β-hydrolase family of lipases/esterases and are considered to form a structurally distinct class owing to the lack of a lid covering the active site [Chen et a. 2013]. In lipases, the active site remains covered by the lid until the interaction with a substrate causes a conformational change in the enzyme. On the contrary, in cutinases, the active site is exposed, and two hydrophobic loops located above the active site appear to be sufficient to initiate interaction with substrates. Additionally, cutinases have been demonstrated to be better in enantioselective catalysis and accommodating substrates with steric hinderance and bulky substituents [Su et al. 2020]. Owing to more ‘open’ architecture,

cutinases have been demonstrated to exhibit ‘better’ surface erosive degradation by cleaving the ester bond of PBS in comparison to lipases. In contrast, lipases have been demonstrated to slightly over-perform biodegradative action of cutinases in PCL depolymerization [Shi et al. 2019; Shi et al. 2020]. The contradicting results indicate that the enzyme dynamics covering the substrate structure, substrate-specificity and catalytic activity are highly variable and crucial in investigating the process of biodegradation. Since the environmental factors are also impactful in deciding microbial survival and gene expression, the above-stated facts make bacterial/fungal cutinases, inhabiting the phylloplane, a promising enzymatic route for designing a sustainable solution for plastic degradation.

The functional aspects of cutinases/lipases are being continuously explored, with studies focusing on the thermal stability, substrate-mediated conformational changes, site-directed mutagenesis, catalytic domain engineering, and creating bifunctional enzyme systems, targeting plastic degradation [Numoto et al. 2018; Ma et al. 2018; Furukawa et al. 2019]. Studies have featured the engineered variants of PET hydrolase in understanding the enzyme-substrate interaction involving key residues such as arginine (R61), tyrosine (Y58), leucine (L88) and isoleucine (I179) present in the substrate-binding groove. The hydrophobic interaction between the substrate and the enzyme is particularly influenced by isoleucine (I179), which acts as a deciding factor, and absence of which leads to the loss of enzymatic activity. However, its substitution by a rather more hydrophobic residue, phenylalanine, reflected stronger effect on the substrate localization and multi-fold escalation in the catalytic activity [Ma et al. 2018]. The thermodynamics and conformational kinetics of cutinase have also been monitored and improvised for improved catalytic PET hydrolysis by modifying the cutinase via glycosylation impeding the enzyme aggregation and stabilizing the enzyme at higher temperature (70°C) with improved catalytic activity [Shirke et al. 2018]. Recently, the crystal structure of PETase has also been reported by various research groups [Han et al. 2017; Joo et al. 2018; Fecker et al. 2018 and Liu et al. 2018], nevertheless, studies highlighting the employment of cutinase isolated from different microbes towards degradation of polymers (apart from PET) are being conducted for establishing a better understanding of the versatility and functionality of the enzyme in a catalytic active environment [Liu et al. 2019; Shi et al. 2019; Tan et al. 2021]. Since, the defining role of cutinase in biodegradation has been established for a few polymer types, it is convincing that the phylloplanic microbes be explored for identifying novel enzymes capable of conducting biodegradation of recalcitrant plastics. Moreover, the mechanistic aspect of biodegradation for recalcitrant plastics such as PP and PS, constituting the majority of the plastic waste, remains to be understood.

1.6 Unique Amphiphilic Fungal Proteins

As the primary decomposers of the environment, fungi have developed a robust and complex enzyme system that allows absorption of nutrients from highly resistant substrates. Besides the production of lipases/esterases known to be involved in the biodegradation of plastics, fungi secrete another class of surface-active proteins called the 'Hydrophobins'. Uniquely to filamentous fungi, these are low molecular weight proteins with remarkable properties, one of which is the ability to self-assemble at hydrophilic-hydrophobic interfaces. This property changes a surface from hydrophilic to hydrophobic and vice-versa. These are secreted as soluble proteins constituting 70-350 amino acids in length, with a signal peptide directing the proteins to be exported from the cell [Wösten and Scholtmeijer, 2015]. These proteins show low sequence conservation and are characterized by hydrophobicity profiles, idiosyncratic pattern of eight conserved cysteine residues forming four disulphide bridges [Sunde et al. 2008]. Based on their hydropathy patterns and solubility characteristics, class I and class II hydrophobins have been identified. Class I hydrophobins are produced by Ascomycota and Basidiomycota fungi, and form assemblies of amyloid-like rodlets that are SDS insoluble, resistant to heat, and resistant to acidic conditions. Class II hydrophobins, which to date have only been identified among the Ascomycota, are readily identified as their sequences are comparatively conserved. Their assemblies are less stable than class I assemblies and can be disassociated by SDS-alcohol mixtures [Bayry et al. 2012]. Typically, a single fungal species only expresses either class I or class II hydrophobins. However previous studies showed that few species have the ability to express both class I and class II hydrophobins [Linder et al. 2005]. Moreover, fungi may also synthesize intermediate forms of hydrophobins which may not be clearly divided into the above classes [Jensen et al. 2010]. Hydrophobins are expressed under different stages of fungal life cycle participating in numerous important roles including aiding aerial hyphal growth, coating of spores and mediating interactions with host. Besides their noteworthy functions, hydrophobins also play a key role in helping the fungi to survive and adapt under different environmental conditions by affecting the mechanical properties of the mycelium and their ability to interact with surfaces [Linder et al. 2005; Appels et al. 2018].

Since hydrophobins can self-assemble themselves at hydrophilic-hydrophobic interfaces, their functional aspect may be explored to overcome one of the challenges in plastic degradation, the hydrophobicity of plastics. The large and exposed hydrophobic patches on the protein surface display a clustering of surface charged residues that is likely to underpin the

observed high surface activity of these proteins [Lienemann et al. 2013]. Recently, Pham et al. (2018) determined that hydrophobins have a significant level of conformational plasticity, with the nature of the interfacial assemblies being highly dependent on the specific interface the proteins are interacting with. Their versatile properties make them conducive to a broad and growing potential application space including construction of drug delivery systems, biosensors, antimicrobial coatings, biomineralization, etc [Berger and Sallada, 2019]. Due to the high stability of hydrophobin layers, the polystyrene surface in the biosensor was functionalized by coating hydrophobins over it resulting in increased sensitivity of the biosensor [Hennig et al. 2016]. This suggests that hydrophobins might also play an integral role in plastics biodegradation systems. It is noteworthy that a few studies have reported the role of hydrophobins in myco-degradation of biodegradable plastics. Takahashi et al. (2005) reported the role of RolA (a hydrophobin) produced by *Aspergillus oryzae*, in biodegradation of PBSA, by coating the hydrophobic surface of PBSA, followed by conformational change, and subsequently recruiting cutinase for stimulating PBSA hydrolysis. Later, another hydrophobic surface binding protein, namely, HsbA, secreted by *Aspergillus oryzae*, was reported to specifically work in a similar manner to previously reported RolA [Ohtaki et al. 2006]. Recently, Puspitasari et al. (2021) reported that RolA extracted from *A. oryzae* could also elevate the degradation of PET, alongwith PBSA. It is speculated that the wetting effect of RolA acts on PET surface converts PET to become hydrophilic that leads PETase easier to contact and attack the surface. Hence, it could be concluded that the functional aspects of hydrophobins to be tested for synthetic recalcitrant plastics are yet to be understood. Since the phylloplanic fungi harbour a hydrophobic surface under natural conditions, their inherent potential for production and release of hydrophobins and other bioactive proteins can be utilized for the biodegradation of synthetic plastics.

1.7 Gaps in Existing Research

The awareness of plastic pollution is relatively recent and was highlighted to concentrate on plastic debris in the oceans. The widespread use of plastics has led to a staggering amount of plastic pollution in man-made and natural environments, clearly identifying plastic waste as first-order environmental issue. Plastic debris of all size classes is rapidly accumulating without any practicable options for its removal, majorly constituting the waste generated from ‘throw away’ products. Besides, the identified harmful effects of plastic debris on human and wildlife health, the lack of a plausible solution has become a larger problem to be dealt with. Since the mobility of plastic fragments varies under different

environments, the parameters which influence its mobility and fragmentation of plastic debris are yet to be explored. Moreover, no global data is available on the proportion of various types of plastic waste that is generated, disposed, recycled, and landfilled. The basic knowledge about the general production stats and 'after-life' fate of plastic products remains unknown. Thinking of plastic pollution like an iceberg: we only know what is on the surface. To understand the problem, we need to understand the scope of the problem.

Biodegradation of plastics is one possible solution and a key factor to reduce the impact of plastic pollution. However, the scientific knowledge covering the degradation of different plastics by a few identified microbes is scattered across scientific publications. Moreover, the available data regarding the rationale behind isolation of plastic-degrading microbes and involvement of biomacromolecules participating in biodegradation is largely undetermined. Although, biodegradation of a few biodegradable and largely recyclable plastics such as PHAs and PET has been widely explored, the horizons of the research remain unexpanded. Among synthetic plastics, degradation studies have been majorly conducted on low-density polyethylene (LDPE), whereas degradation of recalcitrant and non-recyclable plastics such as PS and PP are lacking. Moreover, since PS is regarded as the most persistent plastic comprising the majority of the waste generated, no conclusive studies have been published regarding the enzymes involved in its biodegradation. In addition, the selection of microbial species used for plastic degradation have been very random and without any scientific rationale behind their selection. Since, epicuticular wax and cutin share chemical similarities to the plastics, the microflora of the phylloplane of the xerophytes can be explored towards their plastic degradation abilities. Given that, the rate of plastic biodegradation may be affected by parameters such as temperature, pH, and exposure duration, the optimization processes for efficient biodegradation are lacking. The mechanism of plastic degradation has also not been explored fully till date due to which large scale degradation of plastic waste is still a dream. As biodegradation is a complex phenomenon, detailed pattern and mechanism is still being predicted. The discovery of novel plastic degrading enzymes occurring in nature and their interaction with the plastics as substrates shall improve our current understanding necessary to construct a suitable biotechnical application of enzymes for plastic biodegradation.

1.8 Objectives

Based on the above-mentioned considerations, the present thesis aims to fulfil the following objectives:

1. Collection, isolation, and identification of phylloplane fungi capable of polystyrene sulfonate transformation
2. Screening, optimization studies and determination of polystyrene sulfonate transformation by fungal isolate(s)
3. Characterization of participating biomolecule(s) and exposition of polystyrene sulfonate transformation mechanism(s)

Chapter 2

Molecular Identification of Phylloplanic Fungi Isolated from Xerophytic Plants

2.1 Introduction

Plastics have emerged as one of the most integral parts of today's era and it shall be for the decades to follow. This is because of their outstanding properties that evolve through time such as low price, stability, and resilience due to their polymeric characteristics which make plastics indispensable part for every aspect of our daily lives [Ali et al. 2021]. However, these properties also resist any notable degradation in the environment. When plastic waste enters the environment, it is acted upon by a combination of various abiotic and biotic factors such as photodegradation, thermo-oxidation, hydrolysis, and biodegradation [Andrady, 2011]. The abiotic factors result in the generation of various hazardous micro- and nano-sized plastic particles, while the biotic action results in the conversion of plastics mainly into CO_2, organic intermediates, and microbial biomass. Hence, microbial-degradation or biodegradation of plastics seems to be the most plausible method for managing plastic waste.

Microorganisms have been evolving for millions of years in advancing their metabolic capacity, enabling them to favour their growth and survival under extreme environmental conditions [Amobonye et al. 2021; Aleklett and Boddy, 2021]. Among various microbial communities, fungi have expanded and strengthened their extra- and intra-cellular enzyme system concluding in their emergence as potent decomposers. Their tolerance to high concentrations of pollutants in the dynamically active environments makes them as potential systems for mediating degradation and remediation of organic pollutants. For instance, the lignocellulosic biomass and plant cuticle are one of the most complex and recalcitrant substrates for enzyme degradation due to extensive C-C bonding throughout their chemical structure [Andlar et al. 2018; Bhanot et al. 2021]. However, various fungal genera have been reported to actively depolymerize these naturally occurring rigid polymers by releasing extra-cellular enzymes [Gupta et al. 2016].

Similar to lignocelluloses and plant cuticle, plastics also display an extensive C-C bonded chemical structure that makes it resistant to biodegradation. Based on their chemical structure, plastics may exist as homo- and hetero- plastics, mainly consisting of only C-C backbone and C-O backbone, respectively [Ali et al. 2021]. For, hetero-plastics such as polyurethane (PU) or polyethylene terephthalate (PET), enzymatic depolymerization by esterases such as PETases has been widely reported since these bonds are comparatively easier to break. However, homo-plastics containing highly recalcitrant C–C bonds in their backbones have no dedicated enzymes reported (as yet) and might undergo degradation at a very slow

pace [Tournier et al. 2020; Tiso et al. 2022]. Moreover, detailed studies concentrating on the biodegradation of various homo-plastics such as polypropylene (PP) and polystyrene (PS) are scarce and lack the scientific rationale behind the selection of microorganisms for conducting degradation experiments.

Despite the powerful prospects of fungi in metabolising complex pollutants, limited studies have been conducted to understand the functional abilities and specific myco-macromolecules involved in the process of fungal-mediated plastic degradation. Moreover, studies focussing on the biodegradation plastics have selected random microbial isolates without any scientific rationale causing lack in the detailed outlook of the process. There are many reports concentrating on the enzyme-mediated degradation of PET, which is already one of the most recycled plastics, ignoring the more rigid and frequently used plastics (namely, PP and PS) due to which large scale degradation of plastic waste is still a dream. Considering the physical and chemical similarities between the hydrophobic cuticle (which covers the phylloplane of the leaves) and plastics, well-adapted microbes isolated from the phylloplane of xerophytic plants growing in harsh environmental conditions of Indian arid zone can be a better source for plastic degradation. Since xerophytes have been known to possess thicker cuticle in comparison to mesophytic plants, we aimed to isolate the well-adapted phylloplanic fungi of the xerophytic plants and to test their ability for plastic degradation.

2.2 Materials and Methods

The microbiological media ingredients, molecular biology kits and PCR reagents were purchased from HiMedia (HiMedia Laboratories, India), Qiagen (Qiagen, Germany) and Promega (Promega, Germany), respectively. Primers used for the amplification of ITS region and Translation elongation factor 1-α (*TEF 1- α*) were obtained from Sigma-Aldrich (Sigma-Aldrich, USA). All other chemicals were procured from Merck Chemicals (Merck KGaA, Germany) unless otherwise stated. Milli-Q Biocel water purification system (Merck KGaA, Germany) was used for obtaining Milli-Q water.

The experimental handling of fungal isolates was carried out following the guidelines given in the “Handbook for Institutional Biosafety Committee, (IBSC), 2020” notified by Department of Biotechnology, Ministry of Science & Technology, Govt. of India.

2.2.1 Sampling Sites and Isolation of Fungi

Phylloplane samples of naturally growing xerophytic plants viz. *Calotropis procera* and *Salvadora persica* were collected from various sites of four districts of western Rajasthan, namely, Jhunjhunu, Sikar, Churu and Nagaur during summer (June, 2019), monsoon (September, 2019), and winter (January, 2020) seasons. Being semi-arid regions of Rajasthan, these districts witness extended dry summer, insufficient rainfall, and extreme winter during the year. Table 2.1 summarizes the district-wise sampling location sites and their respective geographic coordinates.

Table 2.1 The sampling locations in western Rajasthan and plant species used for phylloplane samples.

District	Location	Geographical co-ordinates	Plant species
Jhunjhunu	Site 1	28°30'37"-75°3'12"	*Calotropis procera* *Salvadora persica*
	Site 2	28°2'32"-75°63'12"	
	Site 3	28°16'24"-75°4'85"	
	Site 4	28°15'94"-75°4'23"	
Sikar	Site 5	28°73'24"-75°22'16"	*Calotropis procera* *Salvadora persica*
	Site 6	27°57'75"-75°18'90"	
Churu	Site 7	27°72'34"-74°71'45"	*Calotropis procera*
Nagaur	Site 8	27°64'91"-74°44'80"	*Calotropis procera*
	Site 9	27°64'43"-74°42'64"	

A total of nine sampling sites were studied across four districts [Table 2.1]. At each sampling site, three spatially distant points with a minimum of 5 m distance were selected for the collection of healthy leaves from individual plant of respective species. Leaves were chosen at random in order to avoid local fluctuations in fungal populations. The leaves were picked using sterile forceps and immediately packed in sterile sealed plastic bags which were then placed in an insulated carrier during transport and immediately refrigerated at 4 °C. The samples for fungal isolation were processed the same day, and the samples for cuticle characterization were processed within three days of their collection.

Isolation of fungi was carried out using the leaf imprinting technique [Meyling and Eilenberg, 2006]. Briefly, the leaf sample was picked with sterile forceps and imprinted (pressed firmly) from both adaxial (upper) and abaxial (lower) surfaces on to Rose Bengal Agar media plates (pH 7.2±0.2) supplemented with 30 μg mL^{-1} of chloramphenicol. After incubating the plates for 3-4 days at 28°C under dark conditions, the obtained individual fungal colonies were isolated and further purified by repeated sub-culturing on potato dextrose agar (PDA) medium (pH 5.6±0.2). Preliminary identification of fungal isolates was performed on the basis of morphological characters [Table 2.2]. Glycerol stock of all the morphologically distinct fungi were prepared and stored at -80˚ C for future use.

2.2.2 Molecular Characterization of Fungal Isolates

The individual fungal isolates were inoculated separately in 25 mL of Czapek's dox broth medium (pH 7.3±0.2) in 100 mL Erlenmeyer flasks in order to prepare fresh cultures. The flasks were incubated at 28 ˚C for 72 h under dark conditions. The grown mycelia were separated from the media by centrifugation (8000 rpm, 4 °C, 10 min). The obtained mycelia were washed thrice using autoclaved MilliQ® water followed by its mechanical crushing in liquid nitrogen using pre-chilled mortar and pestle. The genomic DNA was extracted using the spin column kit (HiMedia) following the manufacturer's instructions and the obtained DNA pellet was mixed in 50 μL of molecular grade water.

For all fungal isolates, the internal transcribed spacer (ITS) regions of ribosomal DNA was amplified using primers ITS-1 (5´TCCGTAGGTGAACCTGCGG) and ITS-4 (5´TCCTCCGCTTATTGATATGC) [White et al. 1990]. Wherever required, amplification of other house-keeping gene was also performed for conclusive species level identification. Translation elongation factor (*TEF 1-α*) gene was partially amplified using the complete length primer 2218R (5`ATGACACCRACRGCRACRGTYTG) [Rehner and Buckley, 2005]. Polymerase chain reaction (PCR) was performed in total volume of 50 μL containing Taq Buffer A (10 mM Tris-HCl, 50 mM KCl, and 1.5 mM $MgCl_2$, pH 8.3), 50 μM each of deoxynucleoside triphosphates, 50 pmol of each of ITS-1 and ITS-4 primers (30 pmol in case of *TEF 1-α* primer), 1 unit of TaqDNA polymerase and 100-150 ng of template genomic DNA. The reactions were carried out on Veriti® Thermal Cycler (Applied Biosystems, USA) using the optimized PCR conditions [Table 2.2]. The obtained PCR products were separated on 1 % (w/v) agarose gel along with standard DNA ladder SM0241 (Fermentas Life Sciences, Canada). The purified PCR products were sequenced using an ABI 3500x1 genetic analyser

(Life Technologies, USA). The obtained nucleotide sequences were compared using Basic Local Alignment Search Tool (BLAST) network services of the National Centre for Biotechnology Information (NCBI) database. The most closely related species were determined based on the existing Type strain entries. The sequences were further submitted to GenBank database, and the accession numbers were obtained.

The multiple alignment of obtained ITS1-5.8S-ITS2 gene complex sequences of the fungal isolates was performed using built-in CLUSTAL W function in Molecular Evolutionary Genetic Analysis software (MEGA 11) [Thompson et al. 1994]. The phylogenetic tree was constructed using Neighbor-joining method and with 1000 bootstraps run in MEGA 11 software [Tamura et al. 2021]. The substitution model was based on Jukes and Cantor (1969).

Table 2.2 PCR conditions used for amplification of selected regions/genes for molecular identification of fungal isolates.

Region/ Gene	**Stages of PCR Amplification Conditions**					
	Initial Denaturation	**Denaturation**	**Annealing**	**Elongation**	**Final Elongation**	**Cycles**
ITS	94°C (2 min)	94°C (1 min)	57°C (1.5 min)	72°C (2 min)	72°C (4 min)	30
TEF 1-α	94°C (3 min)	94°C (0.75 min)	55°C (0.75 min)	72°C (1.5 min)	72°C (4 min)	30

2.3 Results and Discussion

2.3.1 Morphological Identification of Fungal Isolates

Preliminary identification of fungal isolates was performed on the basis of morphological parameters like form, size, elevation, margin/border, surface, opacity, colour, back pigmentation and microscopic parameters like hyphal branching pattern and spore shape, size and arrangement etc. recorded for all isolates. A total of 20 morphologically distinct fungal isolates were purified based on the above-mentioned parameters [Table 2.3]. Out of which, 13 fungal isolates were isolated from the phylloplane of *C. procera* and 7 were isolated from *S.*

persica. The difference in the fungal abundance over the different plant species could be an attribute of the phylloplanic area, which was larger in case of *C. procera* in comparison to *S. persica*. Furthermore, the fungal abundance peaked in the summer season (14 isolates) and was lowest in the monsoon (2 isolates). This could be due to the windy sandstorms that occur during summer season, leading to the increased fungal diversity, whereas, the heavy rains wash out the phylloplane of the plants, resulting in lesser number of fungal isolates remaining on the surface.

Table 2.3 Morphology (as observed on PDA medium) of axenic fungal isolates derived from phylloplanes of selected xerophytic plants.

Fungal Isolate	Morphology	Texture
VJP01	Thick olive-green mat	Velvety
VJP02	Very dark green mat with dark reverse	Woolly
VJP03	Aqua green spores	Sporulous
VJP04	Olive-black with black reverse	Velvety
VJP05	Brown-greenish mat with whitish granules	Granular
VJP06	Dull mustard spores	Sporulous
VJP07	Cotton white mat	Cottony
VJP08	Brown woolly mat	Woolly
VJP09	Mauve and white mat	Woolly
VJP10	Mustard spores	Sporulous
VJP11	Dark green mat with whitish centre	Woolly
VJP12	Brownish with white margin	Wrinkled
VJP13	Tree-bark ring mat	Wrinkled
VJP14	Cream-brown	Wrinkled
VJP15	Mehndi green spores	Granular
VJP16	Yellowish snow-flake	Wrinkled
VJP17	Black-grey fluffy mat	Woolly
VJP18	Dark green mat	Woolly

VJP19	Aqua green and yellowish mat	Chalky
VJP20	Black spores	Sporulous

2.3.2 Molecular Identification

Molecular characterization was performed by the comparative sequence analysis of ITS regions of ribosomal DNA for all the fungal isolates. The rRNA operon sequence is the most widely used candidate for the molecular phylogenetic studies. Amplification of the ITS regions resulted in PCR products of 532-668 bp with considerable variation. In case, where the ITS region sequence was not adequate, the comparative sequence analysis of partial *TEF 1-α* gene was also performed for conclusive characterization. The fungal isolate *Curvularia* sp. VJP08 showed less percent similarity for ITS region, and hence, *TEF 1- α* gene was amplified which resulted in PCR product of 849 bp. The sequences generated from these PCR products were submitted to the GenBank database of NCBI, and the accession numbers were obtained [Table 2.4 and 2.5].

2.3.3 Fungal Diversity

Clustering of obtained nucleotide sequences resulted in the distribution of 20 morphologically distinct fungal isolates into 17 different species across 8 different genera [Figure 2.1]. *Aspergillus* and *Penicillium* were found to be the most abundant genera with 8 and 3 species each among the fungal isolates, respectively. The fungal biodiversity of the xerophytic plants including *Calotropis* sp. and *Salvadora* sp. has been reported to be abundant in *Aspergillus* sp., *Fusarium* sp., *Curvularia* sp., *Cladosporium* sp., *Penicillium* sp., and *Alternaria* sp., [Yadav and Meena, 2021].

The phylogenetic tree was constructed to study the evolutionary relationship among the fungal isolates [Figure 2.2]. The analysis revealed the presence of five major clades comprised of *Alternaria, Cladosporium, Curvularia, Epicoccum, Fusarium, Penicillium* and *Purpureocillium* genera, whereas a single aggregated clade representing *Aspergillus* genus was also observed. The appearance of similar aggregated clades of *Aspergillus* species were also observed and found to be closely related to *Penicillium* species [Samson et al. 2014]. It is noteworthy that these phylloplane fungal genera are also reportedly plant pathogens, which have the ability to degrade plant leaf cuticle in order to facilitate its adhesion and promote early stages of infection [Ziv et al. 2018; Jayawardena et al. 2021]. As discussed in Chapter 1, that the plant polymers share similar chemical linkages as plastics, it would be interesting to

investigate and identify the ability of these fungal isolates towards their transformation potential against PSS.

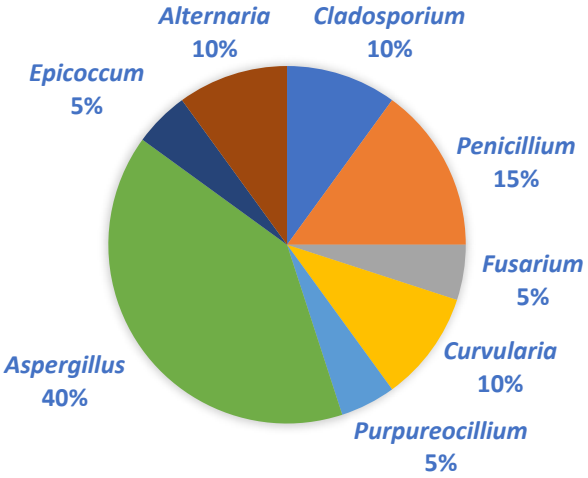

Figure. 2.1 Pie chart depicting various fungal genera.

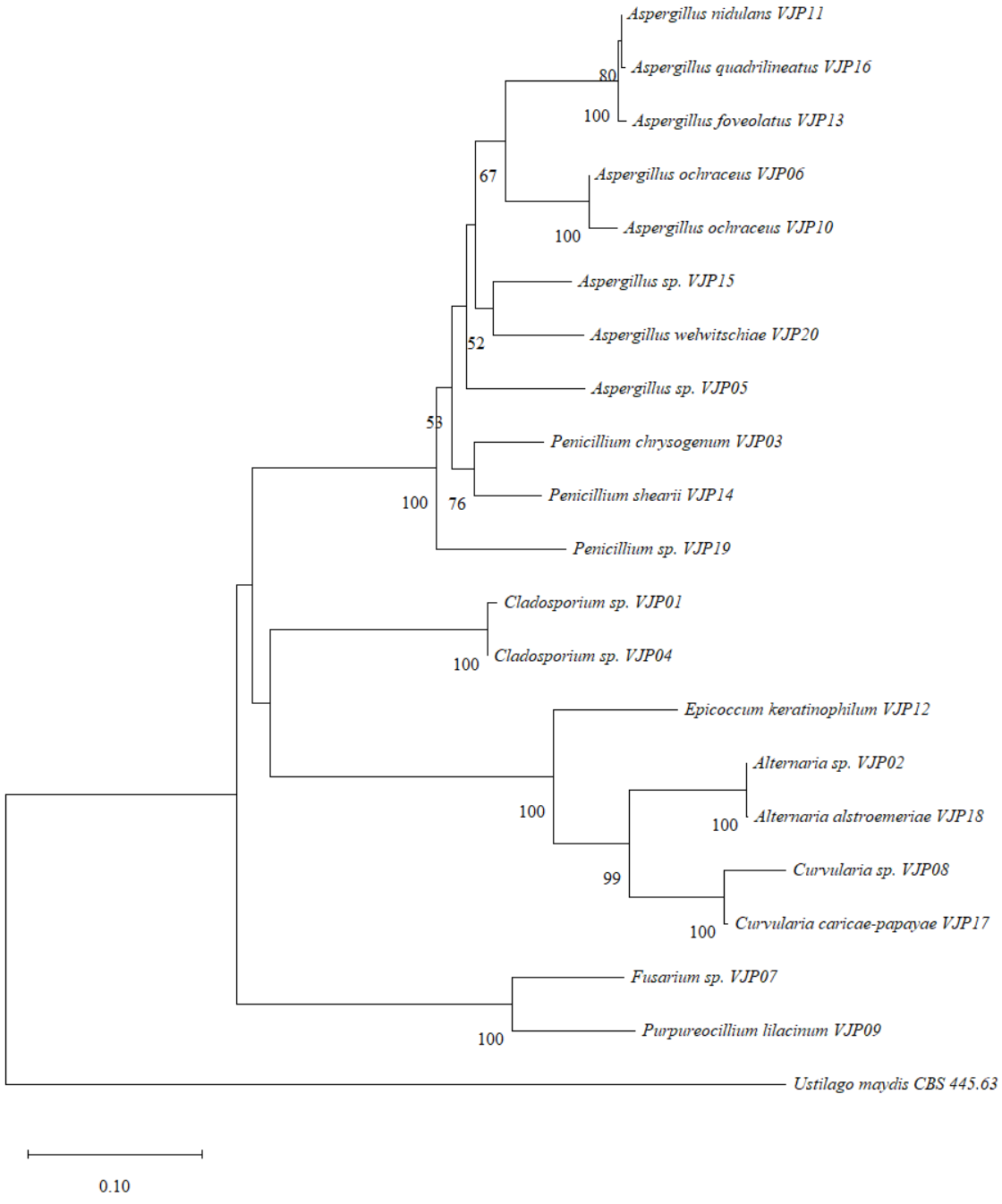

Figure 2.2 Molecular phylogenetic analysis of ITS gene sequences of fungal isolates from phylloplane of xerophytic plants. *Ustilago maydis* CBS 445.63 was used as outgroup. Bootstrap support values ≥50% are presented below the nodes.

Table 2.4 Analysis of ITS region sequences of fungal isolates with their reference sequences from NCBI GenBank database.

Fungus	Isolate	Accession Number	Sequence Length					BLAST Analysis				
			18S	ITS1	5.8S	ITS2	28S	Max. Score	Query Coverage	Max. Identity	Closest Match	Reference
Cladosporium sp.	VJP01	OM920724	<79	70	149	149	49>	990	90%	99.63%	NR_119729.1 [T]	Schubert et al. 2009
Alternaria sp.	VJP02	OM944048	<58	165	207	158	62>	1033	94%	99.65%	NR_163686.1 [T]	Vu et al. 2019
Penicillium chrysogenum	VJP03	OM944049	<33	173	152	168	62>	1072	99%	99.66%	NR_077145.1 [T]	Rakeman et al. 2005
Cladosporium sp.	VJP04	OM944607*	-	169	158	148	62>	966	97%	99.81%	NR_148192.1 [T]	Sandoval-Denis et al. 2015
Aspergillus sp.	VJP05	OM945716	<17	176	158	150	61>	941	99%	96.98%	NR_111412.1 [T]	Schoch et al. 2014
Aspergillus ochraceus	VJP06	OM945723	<33	168	155	180	60>	1044	99%	98.49%	NR_077150.1 [T]	Haugland et al. 2004
Fusarium sp.	VJP07	OM945732*	-	164	158	156	50>	876	98%	96.96%	NR_172283.1 [T]	Vu et al. 2019
Curvularia sp.	VJP08	OM967375	<28	175	158	165	58>	900	100%	94.89%	NR_172405.1 [T]	Tan et al. 2018
Purpureocillium lilacinum	VJP09	OM945734	<17	188	157	161	61>	1037	96%	100%	NR_165946.1 [T]	Luangsa-Ard et al. 2011
Aspergillus ochraceus	VJP10	OM952173	<16	169	158	172	120>	1057	100%	99.83%	NR_077150.1 [T]	Haugland et al. 2004
Aspergillus nidulans	VJP11	OM945811	<33	152	158	165	45>	1000	98%	99.63%	NR_133684.1 [T]	Henry et al. 2000
Epicoccum keratinophilum	VJP12	OM945845	<18	139	158	156	52>	918	98%	98.47%	NR_158278.1 [T]	Valenzuela-Lopez et al. 2017

Aspergillus foveolatus	VJP13	OM946598	<33	152	158	165	61>	1013	99%	98.77%	NR_151791.1 [T]	Chen et al. 2016
Penicillium shearii	VJP14	OM946586*	-	188	158	166	40>	987	93%	99.81%	NR_111495.1 [T]	Houbraken et al. 2010
Aspergillus sp.	VJP15	OM946588	<17	181	158	166	61>	1077	100%	100%	NR_171607.1 [T]	Frisvad et al. 2019
Aspergillus quadrilineatus	VJP16	OM946591*	-	168	158	164	12>	1000	99%	99.64%	NR_131289.1 [T]	Peterson, 2008
Curvularia caricae-papayae	VJP17	OM946592	<14	160	158	153	55>	998	100%	100%	NR_147458.1 [T]	Madrid et al. 2014
Alternaria alstroemeriae	VJP18	OM946594	<16	162	174	141	46>	977	98%	99.63%	NR_137143 [T]	Pryor and Bigelow, 2003
Penicillium sp.	VJP19	OM946595*	-	187	139	179	96>	911	95%	96.56%	NR_121325.1 [T]	Peterson and Horn, 2009
Aspergillus welwitschiae	VJP20	OM952175	<16	185	172	142	57>	1064	100%	99.66%	NR_137513.1 [T]	Meijer et al. 2011

*Incomplete ITS sequence; [T] Type strain

Table 2.5 Analysis of partial *TEF 1-α* gene sequence of selected fungal isolate with the reference sequences from NCBI GenBank database.

Fungus	**Isolate**	**Gene**	**Accession number**	**Coding Sequence Length**	**BLAST Results**				
					Max. score	**Query Coverage**	**Max. identity**	**Closest Match**	**Reference**
Curvularia dactyloctenicola	VJP08	*TEF 1-α* (Partial)	ON108652	<1……>846	1520	99%	99.17%	MF490858.1 [T]	Marin-Felix et al. 2017

[T] Type strain

Table 2.6 Phylogenetic classification of fungal isolates derived from phylloplane of xerophytic plants.

Fungus	**Isolate**	**Classification*** **Kingdom[1], Phyllum[2], Subphyllum[3], Class[4], Subclass[5], Order[6], Family[7], Genus[8]**
Cladosporium sp.	VJP01	Fungi[1], Ascomycota[2], Pezizomycotina[3], Dothideomycetes[4], Dothideomycetidae[5], Capnodiales[6], Davidiellaceae[7], *Cladosporium*[8]
Alternaria sp.	VJP02	Fungi[1], Ascomycota[2], Pezizomycotina[3], Dothideomycetes[4], Pleosporomycetidae[5], Pleosporales[6], Pleosporaceae[7], *Alternaria*[8]
Penicillium sp.	VJP03	Fungi[1], Ascomycota[2], Pezizomycotina[3], Eurotiomycetes[4], Eurotiomycetidae[5], Eurotiales[6], Trichocomaceae[7], *Penicillium*[8]
Cladosporium sp.	VJP04	Fungi[1], Ascomycota[2], Pezizomycotina[3], Dothideomycetes[4], Dothideomycetidae[5], Capnodiales[6], Davidiellaceae[7], *Cladosporium*[8]
Aspergillus sp.	VJP05	Fungi[1], Ascomycota[2], Pezizomycotina[3], Eurotiomycetes[4], Eurotiomycetidae[5], Eurotiales[6], Trichocomaeceae[7], *Aspergillus*[8]
Aspergillus ochraceus	VJP06	Fungi[1], Ascomycota[2], Pezizomycotina[3], Eurotiomycetes[4], Eurotiomycetidae[5], Eurotiales[6], Trichocomaeceae[7], *Aspergillus*[8]
Fusarium sp.	VJP07	Fungi[1], Ascomycota[2], Pezizomycotina[3], Sorariomycetes[4], Hypocreomycetidae[5], Hypocreales[6], Nectriaceae[7], *Fusarium*[8]
Curvularia dactyloctenicola	VJP08	Fungi[1], Ascomycota[2], Pezizomycotina[3], Dothideomycetes[4], Pleosporomycetidae[5], Pleosporales[6], Didymellaceae[7], *Curvularia*[8]

Purpureocillium lilacinum	VJP09	Fungi[1], Ascomycota[2], Pezizomycotina[3], Sorariomycetes[4], Sardariomycelidae[5], Hypocreales[6], Ophiocordycipitaceae[7], *Purpureocillium*[8]
Aspergillus ochraceus	VJP10	Fungi[1], Ascomycota[2], Pezizomycotina[3], Eurotiomycetes[4], Eurotiomycetidae[5], Eurotiales[6], Trichocomaeceae[7], *Aspergillus*[8]
Aspergillus nidulans	VJP11	Fungi[1], Ascomycota[2], Pezizomycotina[3], Eurotiomycetes[4], Eurotiomycetidae[5], Eurotiales[6], Trichocomaeceae[7], *Aspergillus*[8]
Epicoccum keratinophilum	VJP12	Fungi[1], Ascomycota[2], Pezizomycotina[3], Dothideomycetes[4], Pleosporomycetidae[5], Pleosporales[6], Didymellaceae[7], *Epicoccum*[8]
Aspergillus foveolatus	VJP13	Fungi[1], Ascomycota[2], Pezizomycotina[3], Eurotiomycetes[4], Eurotiomycetidae[5], Eurotiales[6], Trichocomaeceae[7], *Aspergillus*[8]
Penicillium shearii	VJP14	Fungi[1], Ascomycota[2], Pezizomycotina[3], Eurotiomycetes[4], Eurotiomycetidae[5], Eurotiales[6], Trichocomaceae[7], *Penicillium*[8]
Aspergillus sp.	VJP15	Fungi[1], Ascomycota[2], Pezizomycotina[3], Eurotiomycetes[4], Eurotiomycetidae[5], Eurotiales[6], Trichocomaeceae[7], *Aspergillus*[8]
Aspergillus quadrilineatus	VJP16	Fungi[1], Ascomycota[2], Pezizomycotina[3], Eurotiomycetes[4], Eurotiomycetidae[5], Eurotiales[6], Trichocomaeceae[7], *Aspergillus*[8]
Curvularia caricae-papayae	VJP17	Fungi[1], Ascomycota[2], Pezizomycotina[3], Dothideomycetes[4], Pleosporomycetidae[5], Pleosporales[6], Didymellaceae[7], *Curvularia*[8]
Alternaria alstroemeriae	VJP18	Fungi[1], Ascomycota[2], Pezizomycotina[3], Dothideomycetes[4], Pleosporomycetidae[5], Pleosporales[6], Pleosporaceae[7], *Alternaria*[8]
Penicillium sp.	VJP19	Fungi[1], Ascomycota[2], Pezizomycotina[3], Eurotiomycetes[4], Eurotiomycetidae[5], Eurotiales[6],

		Trichocomaceae[7], *Penicillium*[8]
Aspergillus welwitschiae	VJP20	Fungi[1], Ascomycota[2], Pezizomycotina[3], Eurotiomycetes[4], Eurotiomycetidae[5], Eurotiales[6], Trichocomaeceae[7], *Aspergillus*[8]

*Source: Mycobank (http://www.mycobank.org)

The phylogenetic classification indicated that all the identified fungal isolates belonged to phylum *Ascomycota* [Table 2.6]. *Ascomycota* constitutes the most variable phylum of fungal kingdom, accounting for >65% of the currently described fungi [Harms et al. 2011]. Fungal species of this phylum represent all the modes of nutrition (parasitic, symbiotic or saprotrophic) and are able to colonize very diverse niches [Olicón-Hernández, 2017]. The degradative capability of *Ascomycota* fungi has been studied for aromatic substances such as polycyclic aromatic hydrocarbons (PAHs) and chlorinated hydrocarbons indicating them as potential degraders [González-Abradelo et al. 2019; Germain et al. 2021]. In addition, *Ascomycota* genus namely, *Aspergillus* sp., *Acremonium* sp., *Cladosporium* sp., *Penicillium* sp., *Paecilomyces* sp., and *Fusarium* sp. have been utilised in many bioremediation studies [Sharma and Malaviya, 2016]. Despite this wide distribution, the utilization of *Ascomycota* fungal species for plastic biodegradation has been least explored.

2.4 Conclusion

During the seasonal survey, a total of 20 morphologically different fungi were isolated, pure-cultured and identified, all of which were belonging to phylum *Ascomycota*. Overall, the fungal abundance peaked in the summer season and was lowest in the monsoon. *Aspergillus* was found to be the most dominating genera constituting about 40% of the total fungal species, followed by *Penicillium* sp. (15%), *Cladosporium* sp. (10%), *Curvularia* sp. (10%), and *Alternaria* sp. (10%), respectively. *Ascomycetous* fungi could be ideal biodegraders due to their ability to grow in wide range of habitats and in extreme conditions due to their outstanding metabolic diversity and versatility. Considering the chemical similarities of phylloplane constituents (epicuticular wax and cutin) to the complex synthetic plastics, the phylloplanic fungi can be explored towards their plastic degradation potential. Hence, these fungal isolates were further explored and screened as potential candidates for plastic degradation.

Chapter 3

Temporal Variations in the Surface Micromorphology and Chemical Composition of Cuticular Wax in Xerophytic Plants

Part of the work presented in this chapter has been published as per the following details:

- Bhanot et al. (2021) *Environmental and Experimental Botany* 183, 104364

3.1 Introduction

The phylloplane is the leaf surface environment which serves as the 'communication platform' between the plant leaf and external abiotic & biotic factors. The anatomy of the phylloplane is multi-layered and formed by chemically distinct regions, one of which is the 'cuticle' that lies above the cell wall of the leaf epidermal cells. The development of cuticle coating has been noted as one of the most important adaptations during the evolutionary events of plants' habitat transition [Bhanot et al. 2021]. The evolution of cuticle has been documented in early studies perceiving cuticle solely as an extracellular lipid deposit over the epidermal cells [Martens, 1933]. Later studies concluded that the cuticle does not lie as an independent entity, but rather occurs in a complex association with the cell wall of epidermal cells [Meyer, 1937; Sargent, 1976]. The transverse section (TS) of the leaf boundary would show the polysaccharide cell wall of epidermal cells physical overlined by the cuticle components occurring as a specialised lipid modification of the cell wall [Yeats and Rose, 2013]. Chemically, the cuticle is divided into two domains: the lower domain 'cuticle layer', composed of an interconnection between cell wall polysaccharides and cutin polymers, whereas the upper domain 'cuticle proper' is enriched in intra-cuticular waxes within the cutin matrix, which are in-turn sealed by the extrinsic deposits of epicuticular wax that displays distinct morphologies [Figure 3.1] [Bhanot et al. 2021].

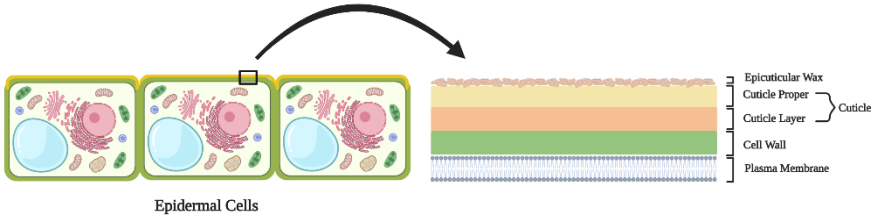

Figure 3.1 A schematic diagram of transverse section of a leaf showing epidermal cell and overlaying domains of cuticle and epicuticular wax deposits [Bhanot et al. 2021].

Waxes are essential structural and fundamental element of the plant surface which have functional and ecological importance [Barthlott et al. 1998]. The cuticular waxes are majorly composed of heterogeneous mixtures of very long chain hydrocarbon backbone with common components including n-alkanes, aldehydes, fatty acids, alkyl esters, primary and secondary alkanols, ketones, alkenes and terpenoids etc. [Aragón et al. 2017]. The cuticular waxes can be extracted using organic solvents such as chloroform, acetone, ethyl acetate, hexane, and methanol, whereas the cross-linked polymeric network of cutin makes it insoluble and difficult

to extract [Nawrath, 2006]. These assorted hydrocarbons establishing the cuticular wax impart hydrophobicity and water impermeability, making the phylloplanic surface superhydrophobic [Zeisler-Diehl et al. 2018]. Waxes often form complex three-dimensional crystalline microstructures such as platelets, rods, and tubules [Koch and Barthlott, 2006a]. The assorted chemical composition and structural arrangement of cuticular waxes display an alteration in response to varying environmental factors such as temperature, drought, etc. Based on the appearance and arrangement of epicuticular wax on the surface, Barthlott et al (1998) proposed classification and terminology for about 23 wax types by analysing at least 13,000 species to systemize the micromorphological diversity. These classifications included the appearance of wax as granules, platelets, threads, rodlets, tubules and wax chimneys with further introduced sub-divisions. Additionally, these ultrastructures are also observed to appear in correlation to the chemical composition of wax.

Functionally, these wax crystals exhibit a protection barrier against microorganisms such as bacteria and fungi [Domínguez et al. 2011]. In addition, there is evidence of the modulation and involvement of the cuticular wax components in establishing a 'reversible' transpiration barrier under different conditions of water availability. Although, the exact mechanism has not yet been fully identified, but the components have shown to modify and adjust in controlling water loss [Zhang et al. 2021]. Moreover, the hydration level of the cutin-rich layer beneath the cuticular waxes also regulates the water permeation [Kamtsikakis et al. 2021].

The present study aims to examine the temporal dynamics in the surface micromorphology and chemical composition of the cuticular wax of *Calotropis procera* and *Salvadora persica* growing in the arid regions of Indian Thar Desert. The micromorphology of cuticular waxes was investigated using SEM imaging and confocal microscopy, while the chemical composition was studied using GC-MS/MS for the leaf samples collected during summer, monsoon, and winter season, respectively.

3.2 Materials and Methods

3.2.1 Materials

All chemicals were of analytical grade and the solvents were of GC grade and procured from Sigma Aldrich (India) or Merck (India) unless otherwise stated. Fully mature leaves of *C. procera* and *S. persica* were obtained from naturally growing plants located in four districts of Rajasthan namely, Jhunjhunu, Sikar, Churu and Nagaur during summer (June, 2019),

monsoon (September, 2019), and winter (January, 2020) seasons. The area has been classified as arid desert (hot) by the Köppen-Geiger climate classification system [Peel et al. 2007]. Macroclimatic data are available with the Indian Meteorological Department, Ministry of Earth Sciences, India. The leaf samples were immediately transferred in self-sealing plastic bags and placed in an insulated box during transport. The samples were processed within 1 day of collection.

3.2.2 Field-Emission Scanning Electron Microscopy (FE-SEM)

The leaves were cut along the mid-rib into 1×1 cm^2 using a clean scalpel blade and air-dried overnight at room temperature to slowly reduce the water content [Pathan et al. 2008]. The dried leaves were fixed on aluminium stubs using an adhesive carbon tape and sputter coated with gold palladium for 60-120 s at 40 mA (Quorum Q150T ES Plus, United Kingdom), followed by investigation of three-dimensional surface micromorphology using FE-SEM (ApreoS FEI/ FESEM, Thermo Fischer, USA). A voltage between 5 and 10 kV was maintained while imaging the samples.

3.2.3 Staining of Tissue Sections

The transverse section (TS) of leaves were cut by free-hand sectioning using sterilized blade and transferred into a drop of distilled water (dH_2O) placed on the microscope slides [Lux et al. 2005]. The excess water was removed using tissue paper and the sections were stained according to the method described by Buda et al. 2009. Briefly, two stains, namely, Auramine O and Calcofluor white M2R (Sigma-Aldrich), were used to visualize the cuticle and cell wall under confocal laser scanning microscope. Calcofluor white M2R stain was prepared in dH_2O by dissolving 0.1 % (w/v) dye powder. Auramine O stain was freshly prepared by dissolving 0.1 % Auramine O (w/v) in 50 mM Tris/HCl at pH 7.2. After staining with Calcofluor white M2R for 2 min and gently rinsing with dH_2O, the T.S. were transferred aseptically to microscope slides and then stained with Auramine O for 15 min. After washing with dH_2O, the sections were suspended in 50 % glycerol (v/v) on a microscope slide, and a coverslip was sealed to the slide with transparent nail-polish.

3.2.4 Confocal Laser Scanning Microscopy (CLSM)

Confocal laser imaging was performed using Zeiss LSM880 Airyscan confocal microscopy (Carl Zeiss, Jena, Germany) with a 63x/1.4 oil immersion objective. The image processing was done using the Zeiss ZEN 2.3 SP1 software. Auramine O was excited using a

458 nm argon laser, and emission was collected between 491 to 563 nm. Calcofluor White M2R was excited with a 405 nm near UV-diode, and emission was collected between 415 to 448 nm [Buda et al. 2009].

3.2.5 Extraction and Quantification of Cuticular Wax

The cuticular wax *C. procera* and *S. persica* leaves were extracted separately using chloroform immediately after the seasonal sample collection. Ten leaves of each plant type were used for the total wax extraction using the method described by Zhu et al. (2018). Briefly, the leaves were dipped in 15 mL of chloroform in separate glass beakers (pre-weighted) and stirred at room temperature for 30 s. The chloroform containing the extracted wax was evaporated to dryness, followed by the measurement of the wax dry weight. The amount of total wax was calculated using the following formula and presented as weight per unit surface area (μg cm^{-2}).

Total amount of wax = final weight-initial weight (of glass beaker)/area of leaf sample.

3.2.6 Gas Chromatography-Mass Spectroscopy Analysis

For GC-MS/MS analysis, samples are derivatized in order to improve the chromatographic separation, peak shape and enhance the detection sensitivity [Rasmussen and Huang, 2012]. Hence, 50 μL N,O-bis(trimethylsilyl)trifluoroacetamide (BSTFA, Aldrich, GC grade) containing 1% trimethylchlorosilane (Aldrich) was added to the dried wax sample, followed by heating in a dry bath at 70 °C for 1 h. The dried samples was dissolved in 600 μL chloroform and filtered through 0.22 μm polytetrafluoroethylene (PTFE) filter [Kim et al. 2007].

For each sample, 1μL filtrate (chloroform containing extracted wax) was analysed by GC-MS/MS (Model TQ 8040, Shimadzu, Japan). The capillary column Rtx-5 (0.10 μm film thickness, 0.25 mm i.d., 30 m length) was used for the gas chromatography using helium as a carrier gas with head pressure of 47.5 kPa, and flow rate of 1.0 mL min^{-1}. The initial oven temperature was held at 80 °C for 1 min, which was then increased @ 15 °C /min till it reached to 260 °C and then held at 260 °C held for 10 min. The temperature was further increased by 5 °C /min up to 290 °C, where the temperature was held for 20 min. The conditions used during MS/MS analysis were as follows: scan mode, start time of 5 min, end time of 49 min, scan

speed 1666 u, event time 0.3 s, start m/z 45, and end m/z 500. The obtained data were compared with the inbuilt standard mass spectra library system (NIST 16).

3.3 Results and Discussion

3.3.1 Surface Micromorphology of Cuticular Wax

SEM micrographs of the phylloplane of *C. procera* and *S. persica* elucidated the surface morphology of the wax crystals. Although, the adaxial as well as abaxial sides of the particular plant species equally covered by trichomes, the FE-SEM micrographs of adaxial sides are represented in Figure 3.2. The micromorphology of the phylloplane of *C. procera* leaves collected during seasonal survey showed consistency in the appearance of flattened, slender, and elongated ribbon trichomes that densely covered the phylloplane [Figure 3.2 a, c & e]. Contrastingly, the phylloplane of *S. persica* exhibited 'simple' trichomes which were sparsely present and appeared to be 'standing' over the leaf epidermal cells [Figure 3.2 b, d & f]. These special structures can protect from herbivory by mammals, insect, and pathogens attacks, increase the light reflectance, regulate temperature, and decrease water loss [Wagner et al. 2004]. In *C. procera*, the presence of dense trichomes did not allow the clear imaging of stomata, although giant wax deposits could be visualised which were either lying or embedded into the pits of the trichome laden surface.

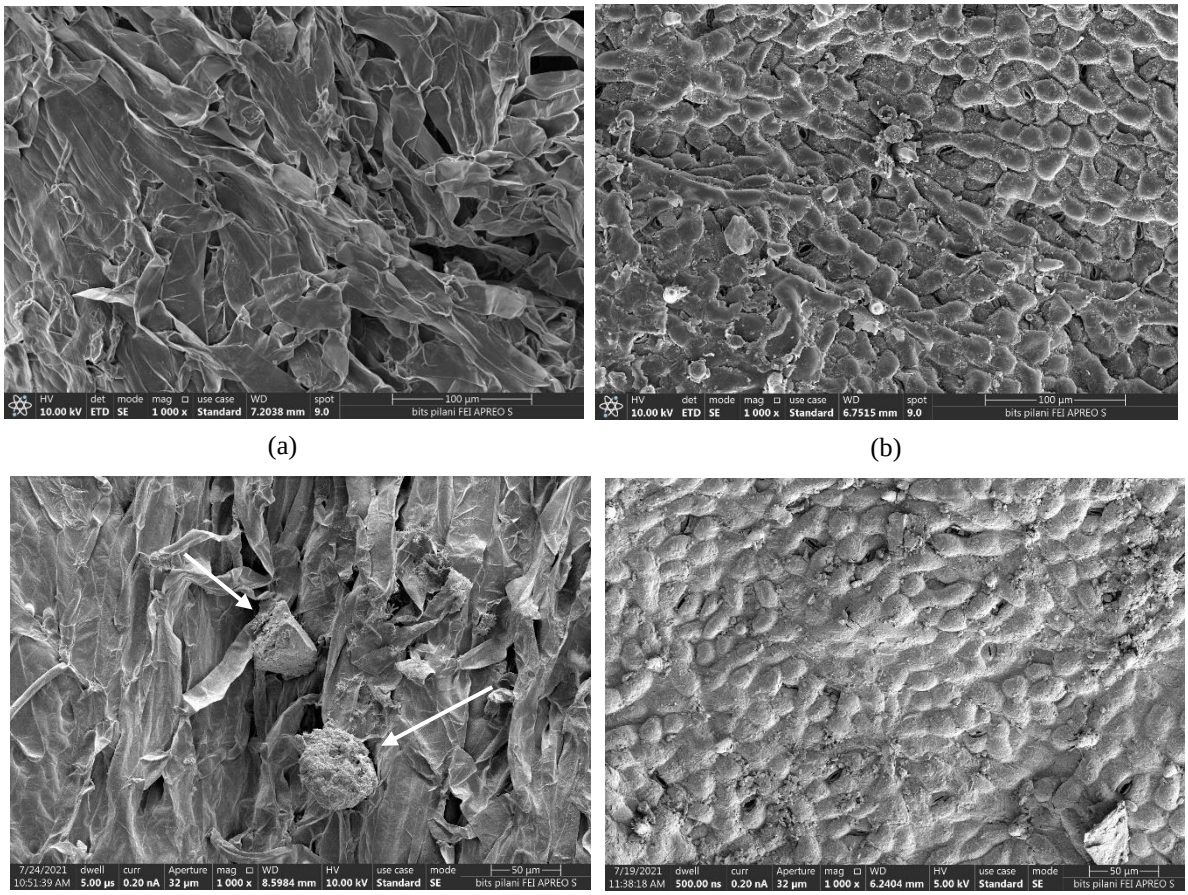

III

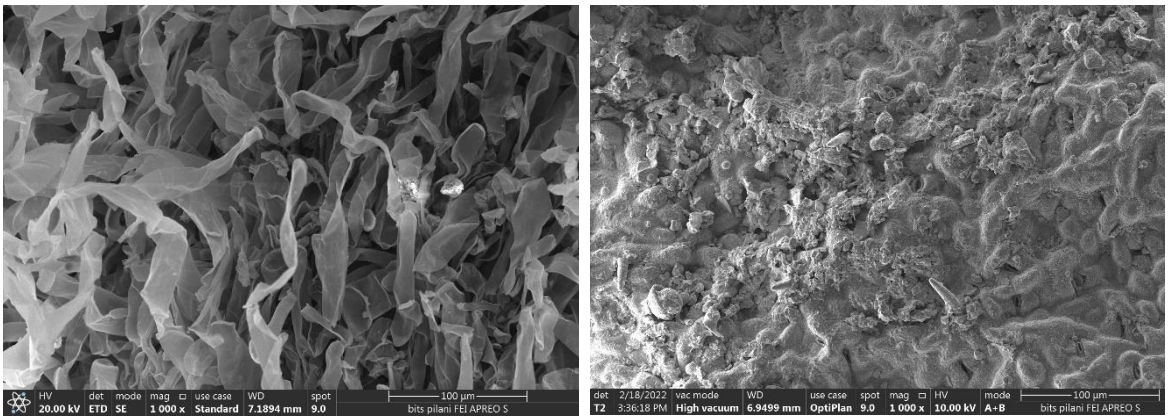

(e) (f)

Figure 3.2 Micromorphology of the cuticular wax on the adaxial surface of *C procera* (a, c, e) and *S. persica* (b, d, f) of the phylloplane samples collected during summer (I), monsoon (II) and winter (III) seasons. The magnification of each image is 1000x.

In addition to the appearance of different types of trichomes, both the plant species showcased the deposits of cuticular wax in distinct manner. The wax microstructures were identified based on the classification of wax morphology proposed by Barthlott et al. (1998), however some of the samples showed previously unidentified wax morphologies as well. In case of *C. procera*, large ovate wax crystalloids were observed lying over the trichomes. During the summer season, the trichomes on *C. procera* were densely packed with wax particles lying over their surface [Figure 3.2 a], whereas in *S. persica*, trichomes were sparsely present, with large wax crystalloids as well as aggregated wax platelets covering the surface. Additionally, continuous patches of wax crust were also observed as shown in the upper and lower left portions of Figure 3.2 b. Furthermore, comparatively larger portions of exceptionally thick wax crusts were also observed exclusively during summers which would have deposited to minimize the transpiration rate [Figure 3.3 a & b]. During the monsoon, *C. procera* exhibited dominant presence of large crystalloids lying over the trichomes, with some unusual 'snowflake' like spikey wax crystals spread all over the leaf surface [Figure 3.2 c]. The surface of *S. persica* mostly displayed thick aggregates of wax platelets spread across the surface, while a large rectangular wax platelet was also observed standing over the surface as shown in the right bottom of Figure 3.2 d. In comparison to summer season, a relatively thin continuous wax coating/crust covering the centre of the leaf surface was observed during monsoon. Interestingly, the phylloplane of *S. persica* also displayed 'disco-ball' like wax entity lying over its adaxial surface [Figure 3.3 c]. The surficial pattern of the phylloplane of *C. procera* varied in the packaging of the trichomes during the winters. The trichomes were comparatively loosely arranged, with smaller wax granules/ crystalloids scattered throughout the surface

[Figure 3.2 e]. In contrast, there were no visual changes observed in the number and appearance of trichomes in *S. persica* leaves during winters. Nonetheless, the large aggregates of morphologically unidentified wax crystals merged with each other were observed [Figure 3.2 f].

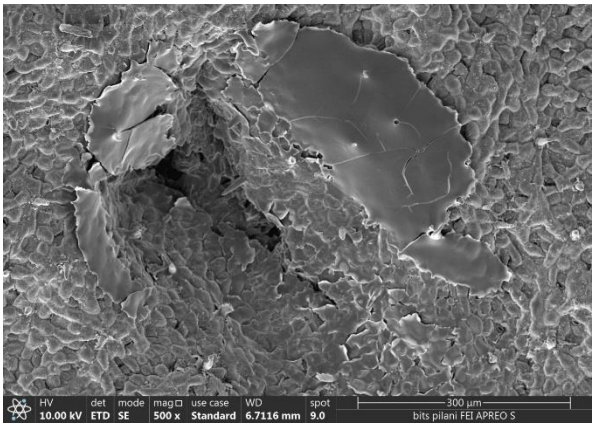

(a)

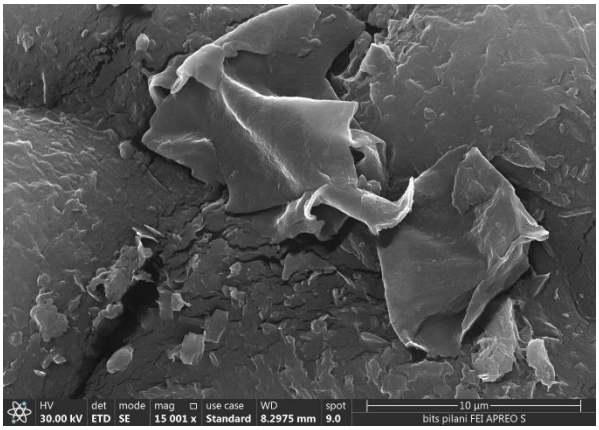

(b)

(c)

Figure 3.3 Unique wax structures on the adaxial surface of *S. persica* appearing as (a) thick wax crust with fractures (summer season); (b) folded crust lying between the depts of the leaf cells (summer season); (c) wax particle in the shape of distinct 'disco-ball' associated with wax aggregates (monsoon season).

Overall, in *C. procera*, the crystalloid wax forms usually occurred as single crystalloids and were irregularly dispersed over the leaf surface. Whereas the phylloplane of *S. persica* displayed 'platelet' forming wax crystals densely covering the overall surface, however, some spots showed aggregation of these platelets into large chunks. As documented by Barthlott et al. (1998), platelets are one of the most prevalent wax crystals forms which are attached to the surface via different angles and may possess regular or irregular margins showing high level of variability in the morphology. The platelet formation by *S. persica* were observed to be irregular platelets with high width to height ratio. Additionally, the phylloplane samples of *S. persica* collected during the summer survey showcased the presence of massive thick wax coverings, called the 'crusts'. The occurrence of crusts is rare and might appear as continuous or broken [Barthlott et al. 1998]. In present study, the crusts were individually present as

separate entities appeared to be fractured at some points, which could be due to the expansion of epidermal cells and wax production proceeding at a different rate. Overall, both the plant species displayed consistent yet unique surface micromorphology across different seasons.

CLSM analysis of T.S. of *C. procera* and *S. persica* leaves was performed for the qualitative and quantitative analysis of structural integrity and thickness of cuticle and cell wall layers in order to check the temporal variation. Dichromatic staining with Auramine O and Calcofluor allowed distinct visual separation of cuticle and cell wall since, Auramine O shows differential affinity toward the various cuticular layers, whereas Calcofluor white M2R provides precise localization of the cell wall of leaf epidermal cells [Buda et al. 2009]. The dichromatic staining differentially resolved the cuticle layer as a bright pink coloured boundary covering the underlying cell wall appeared blue in colour [Figure 3.4].

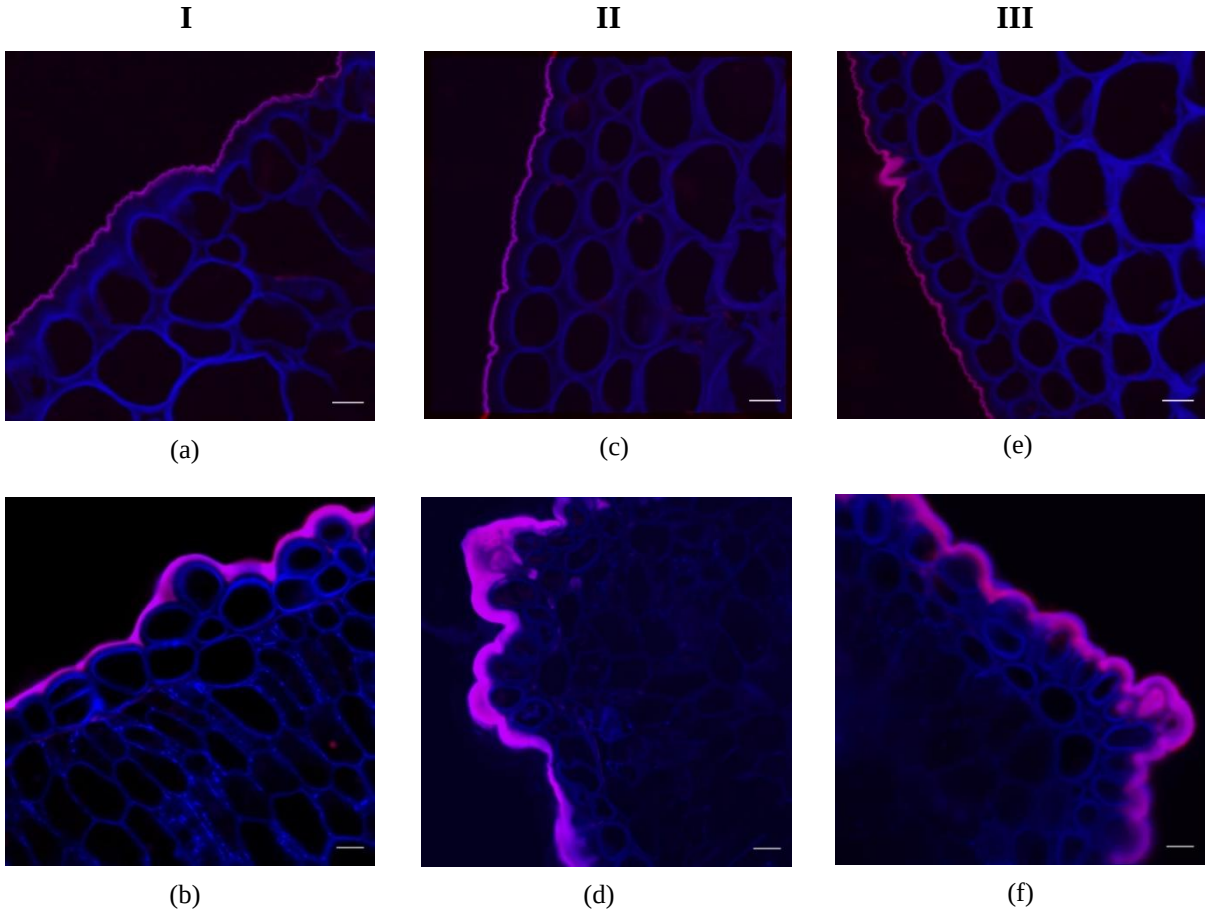

Figure 3.4 CLSM images of TS of *C. procera* (a, c, e) and *S. persica* (b, d, f) leaves collected during summer (I), monsoon (II) and winter (III) seasons. Scale bar in all images is equivalent to 10 μm.

The T.S. of *C. procera* showed consistent appearance of cuticle layer over the epidermal cells. Under FE-SEM, the presence of trichomes hindered the visualisation of wax crystals, therefore, confocal microscopy compensated the distinct appearance of cuticle layer lying over the epidermal cells. There were not many variations observed in the thickness of the cuticle layer of *C. procera* across the three seasons [Figure 3.4 a, c & d].

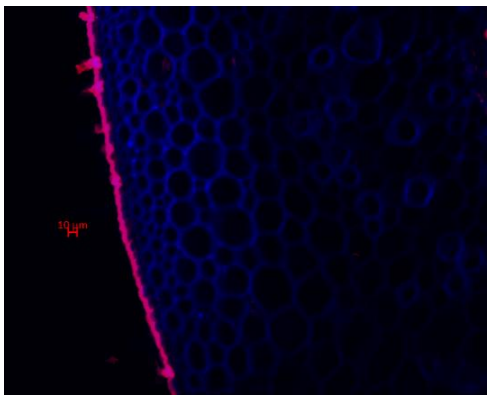

Figure 3.5 Standing trichomes over the phylloplane of *C. procera*. Scale bar equivalent to 10 µm.

The cuticle appeared as a fine covering of about 2 µm of thickness. Moreover, the wider view of the T.S. of *C. procera* distinctly displayed the appearance of trichomes standing over the surface of the phylloplane [Figure 3.5]. Similarly, consistent thickness of 3 µm was observed in *S. persica* across the three seasons [Figure 3.4 b, d, f]. Notably, in the leaf samples collected in summer season, the cuticle thickness was observed to be about 5 µm particularly at the edges [Figure 3.4 b]. While, in the monsoon and winter samples, the cuticle showed relatively more variations in thickness ranging from 2-7 µm [Figure 3.4 d and f]. The CLSM results complemented the FE-SEM analysis [Figure 3.2 d & f], where large aggregates of wax were observed at some portions, depicting the uneven thickness of the cuticle. These results were also in coherence with the observations of Barthlott et al. (1998), describing irregular platelets exhibiting high width-height variations.

3.3.2 Quantification and Chemical Composition of Cuticular Wax

The total wax from the phylloplanes of *C. procera* and *S. persica* was extracted via organic extraction using chloroform [Table 3.1]. The effect of seasonal variation on the total amount of wax obtained from *C. procera* leaves was found to range from 525 ± 0.031 to 775 ± 0.019 µg cm^{-2} across different seasons. The cuticular wax content was found to be highest (775 ± 0.019 µg cm^{-2}) during the summer season, whereas the lowest wax content (525 ± 0.031 µg cm^{-2}) during the monsoon season. The total amount of extracted wax obtained from *S. persica* was ranged from 491 ± 0.009 µg cm^{-2} to 777 ± 0.036 µg cm^{-2} across different seasons.

The cuticular wax concentration was highest (777 ± 0.036 μg cm^{-2}) during the summer season and the lowest (491 ± 0.009 μg cm^{-2}) during the winter season.

Table 3.1 Seasonal variation in the total wax content (μg cm^{-2}) of the phylloplane of selected xerophytic plants.

Plant	Summer	Monsoon	Winter
C. procera	775 ± 0.019	525 ± 0.031	610 ± 0.021
S. persica	777 ± 0.036	526 ± 0.009	491 ± 0.009

The metabolic profile of the cuticular wax extracted from the leaves of *C. procera* and *S. persica* collected during summer, monsoon and winter season are displayed in Figure 3.6 I, II & III, respectively. The wax composition of the *C. procera* leaves during summer, monsoon and winter seasons showed presence of 53, 63 and 45 different wax compounds, respectively. The extracted wax displayed the maximum number of different components in *C. procera* during the monsoon season. Similar pattern was observed in case of *S. persica* leaves which showed maximum number of compounds (110) during the monsoon season, whereas the leaves collected during summer and winter had 48 and 49 compounds, respectively. Overall, terpenoids, followed by alkanes were found to be the major components of the cuticular wax in both the plant species. The main components of cuticular wax observed were various terpenoids, steroids, alkanes (C_{11}-C_{54}), fatty acids (C_3-C_{24}), alcohols (C_6-C_{36}), aldehydes (C_{14}-C_{28}), ketones (C_{15}-C_{25}) and alkenes (C_{14}-C_{35}). These results were found to be consistent with the earlier reports [Wu et al. 2017; Chai et al. 2020; Wang et al. 2021] and detailed below.

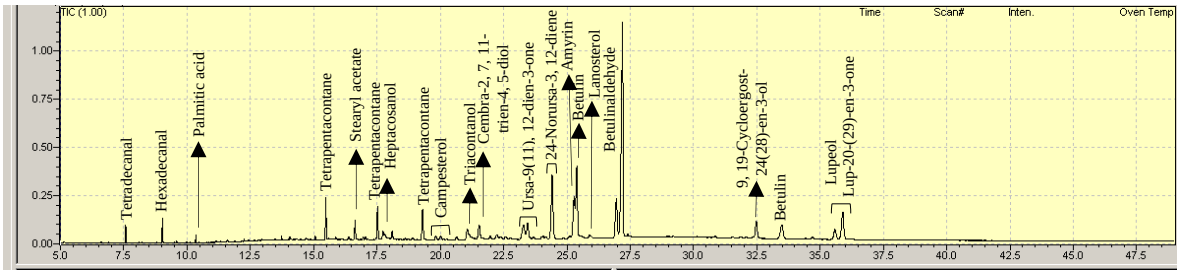

(a)

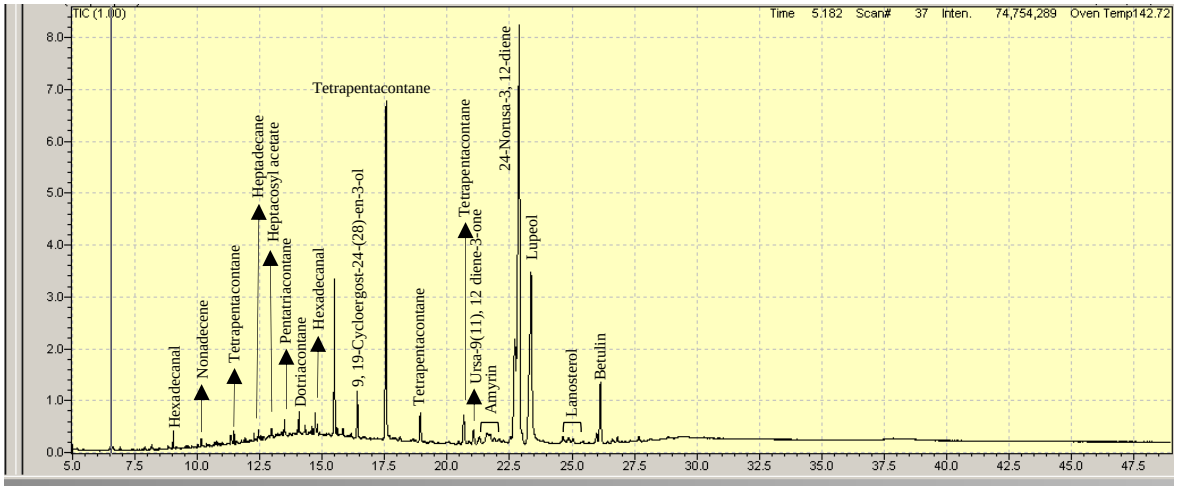

(b)

Figure 3.6 (I) Representative GC-MS/MS chromatogram showing key components of cuticular wax extracted from the leaves of (a) *C. procera* and (b) *S. persica* during summer season.

During summer season, the wax extracted from the leaves of *C. procera* and *S. persica* had the higher number of terpenoids in comparison to other wax metabolites [Figure 3.6 I, a & b]. Terpenoids such as amyrin, betulin, lupeol, 24-norursa-3, 12-diene and ursa-9(11), 12-dien-3-one were common in both the plants, whereas, lup-20-(29)-en-3-one, cembra-2,7,11-trien-4,5-diol and lanosterol were exclusively present in *C. procera* and *S. persica*, respectively. In case of *C. procera*, alcohols (heptacosanol, triacontanol), alkanes (tetrapentacontane, heptacontane and dotriacontane) and aldehydes (tetradecanal and hexadecanal) were present in fairly equal proportions. Whereas, in *S. persica*, alkanes (tetrapentacontane, pentatriacontane, heptacontane and dotriacontane) were found to be the second predominant compounds, followed by aldehydes and alcohols, respectively.

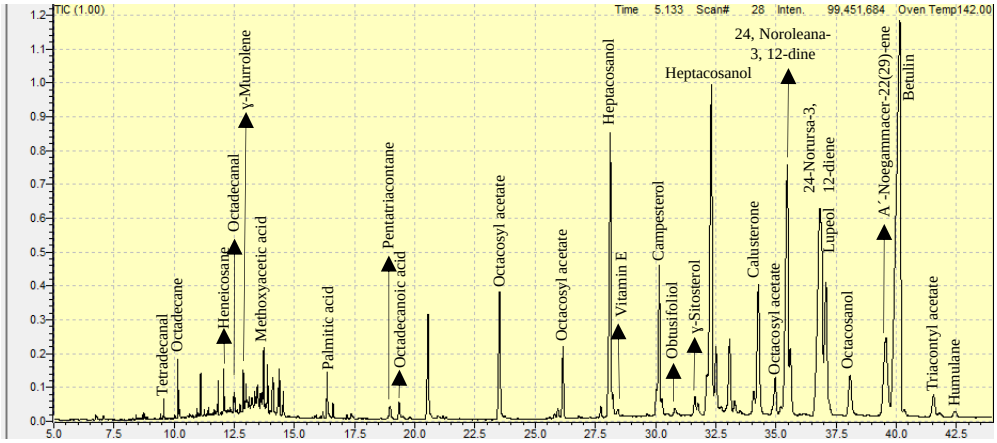

(a)

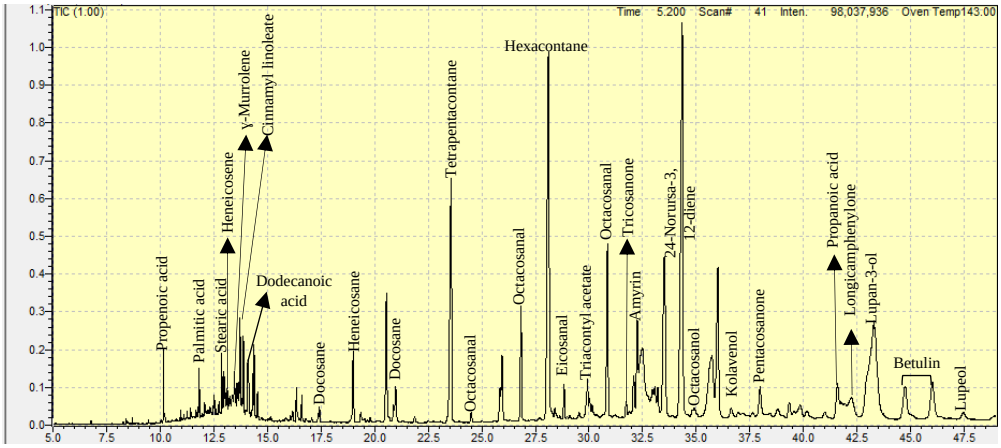

(b)

Figure 3.6 (II) Representative GC-MS/MS chromatogram showing key components of cuticular wax extracted from the leaves of (a) *C. procera* and (b) *S. persica* during monsoon season.

During monsoon season, the wax extract from the leaves of *C. procera* and *S. persica* showcased higher variety of compounds in comparison to the summer season [Figure 3.6 II, a & b]. Both the plant extracts showed similar proportions of terpenoids, alkanes and fatty acids in their composition. Terpenoids such as betulin, lupeol, γ-muurolene and 24-norursa-3, 12-diene were present in the extracts of both the plants. A'-noegammacer-22(29)-ene, 24, noroleana-3, 12-diene and humulane were found to be exclusively present in *C. procera*, whereas, amyrin, kolavenol, lupeol and longicamphenylone were exclusively present in *S. persica.* In *C. procera*, the alkanes (octadecane, heneicosane and pentatriacontane, along with aldehydes (tetradecanal and octadecanal), alcohol (heptacosanol) and fatty acids (palmitic acid and octadecanoic acid) were also present as key components. While in *S. persica*, alkanes (hexacontane, docosane, heneicosane, tetrapentacontane and tetracontane and), along with aldehydes (octadecanal and eicosanal), alcohol (octacosanol) and fatty acids (palmitic acid, propanoic acid, stearic acid and dodecanoic acid) were observed in slightly higher amount in comparison to *C. procera*.

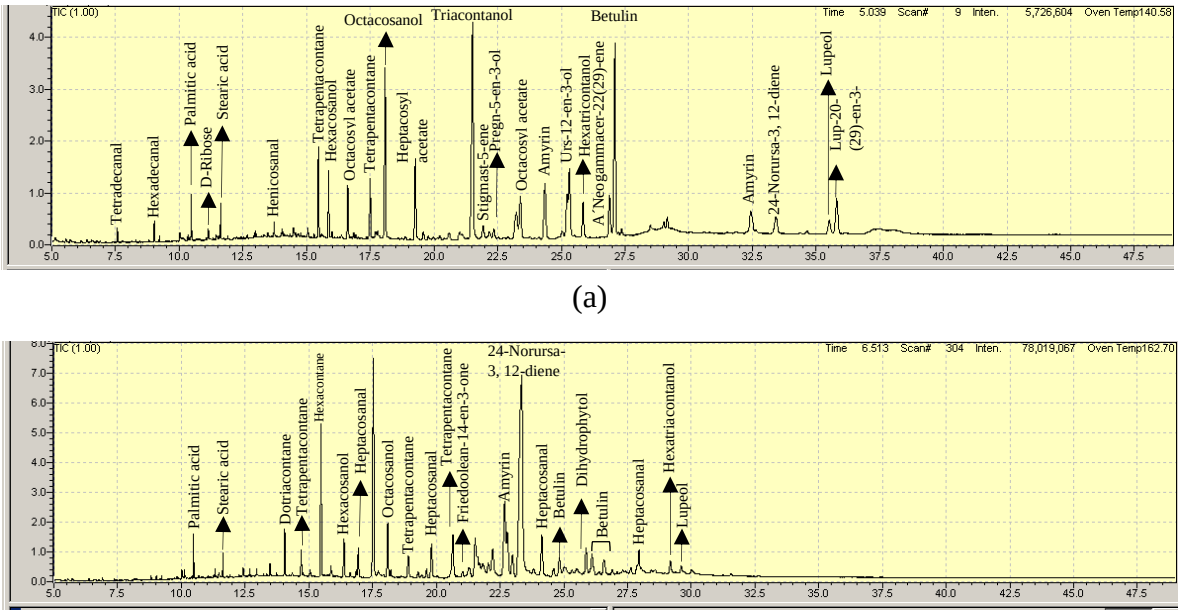

Figure 3.6 (III) Representative GC-MS/MS chromatogram showing key components of cuticular wax extracted from the leaves of (a) *C. procera* and (b) *S. persica* during winter season.

During winter season, the wax extract from the leaves of *C. procera* and *S. persica* showed almost similar proportions of terpenoids, alkanes, alcohols and fatty acids [Figure 3.6 III, a & b]. Various terpenoids such as amyrin, betulin, lupeol and 24-norursa-3, 12-diene were commonly present in both plant extracts. A'-neogammacer-22(29)-ene and ursa-9(11), 12-dien-3-one were found to be exclusively present in *C. procera* and friedoolean-14-en-3-one was exclusively present in *S. persica*. Additionally, alkanes such as tetrapentacontane, alcohols such as hexacosanol and octacosanol and fatty acids such as palmitic acid and stearic acid were also found in both the plant extracts. However, alcohols such as triacontanol, and aldehydes such as tetradecanal, hexadecanal and heneicosanal were exclusively present in *C. procera*, while alkanes such as hexadecane, dotriacontane and aldehydes such as heptacosanal were exclusively present in *S. persica.*

The details of all the wax components and other plant associated bioactive compounds observed during the seasonal survey in both these plant species has been discussed in the following section.

3.3.2.1 Aliphatic Compounds

Wax constituents such as alkanes, primary alcohols, fatty acids, aldehydes, ketones and alkenes combinedly fall into the category of aliphatic wax compounds. It was observed that the proportion of total aliphatic compounds increased from summer season through monsoon, and comparatively declined during the winters in both the plant species. Among the aliphatic wax compounds, alkanes were predominant in *C. procera* constituting ~18% and 30% of the total wax content during the summer and monsoon seasons, respectively [Figure 3.7]. Similarly, for *S. persica*, alkanes majorly constituted ~49% and ~18% of the total wax contents during the summer and monsoon season, respectively [Figure 3.7]. The alkane content was observed to slightly decreased during winters, which could be due to the functional role of alkanes in imparting water-retention property in the waxes [Chai et al. 2020]. Besides alkanes, primary alcohols were consistently present in the cuticular wax of both the plant species throughout seasons. In contrast, fatty acids were significantly present only during the monsoon season representing 19% and ~16% of the total wax components in *C. procera* and *S. persica*, respectively [Figure 3.7]. Diverse homologues of alkanes including hexadecane ($C_{16}H_{34}$), heptadecane ($C_{17}H_{36}$), octadecane ($C_{18}H_{38}$), tetrapentacontane ($C_{54}H_{110}$), and fatty acids such as palmitic acid ($C_{16}H_{32}O_2$) and stearic acid ($C_{18}H_{36}O_2$) were present across all seasons. Additionally, the primary alcohols including 1-hexadecanol ($C_{16}H_{34}O$), 1-hexacosanol ($C_{26}H_{54}O_2$) and 1-octacosanol ($C_{28}H_{58}O$) were consistently present in the wax extracts of both plant species across all seasons. Although in lesser amounts, aldehydes such as eiocosanal ($C_{20}H_{40}O$) and octacosanal ($C_{28}H_{56}O$) were also detected in the wax extract.

The cuticular wax components are very responsive to the environmental stimuli and provides a crucial adaptation for climatological drought, low moisture, salinity and other environmental stresses. In a study, Xu et al. (2016) reported that under dry conditions, the wax extract of *Populus euphratica* leaves exhibited distinctly higher amount of alkanes, alcohols and fatty acids in comparison to the wet conditions. The study demonstrated that the above-mentioned cuticular wax components are closely associated with the plants' adaptation to arid climates. Similarly, the cuticular wax and transcriptomic analysis of two xerophytes namely, *Tetraena mongolica* and *Zygophyllum xanthoxylum* confirmed that presence of higher number of alkanes, alcohols and fatty acids are crucial towards protecting the plants against high temperature and low water availability [Xu et al. 2020]. In addition to conferring adaptability against arid conditions, presence of alkanes, primary alcohols and fatty acids also contribute towards providing resistance against various insects. For instance, presence of shorter (C_8-C_{13})

and mid-length (C_{18}-C_{22}) fatty acids reduced the settling of insect on the leaves of cabbage and raspberry, thus, preventing the crop damage by *Myzus persicae and Amphorophora idaei, respectively* [Sherwood et al. 1981; Shepherd et al. 1999]. However, presence of higher amount of ketones are known to increase the susceptibility of plants towards insect attack [Eigenbrode et al. 1991]. Furthermore, aldehydes were observed to be in slightly lesser variety and quantity in comparison to alkanes. Since, aldehydes are considered as direct precursors of alkanes, their lesser quantity could signify that majority of the aldehydes got transformed to their respective alkanes [Wu et al. 2018]. The aliphatic components constituting the cuticular wax have been listed in Table 3.2.

Table 3.2 Chemical composition of common aliphatic compounds presents in the cuticular wax of *C. procera* and *S. persica*.

S.No.	Compound	Molecular Formula
Alkanes		
1.	Undecane	$C_{11}H_{24}$
2.	Hexadecane	$C_{16}H_{34}$
3.	Heptadecane	$C_{17}H_{36}$
4.	Octadecane	$C_{18}H_{38}$
5.	Nonadecane	$C_{19}H_{40}$
6.	Eicosane	$C_{20}H_{42}$
7.	Heneicosane	$C_{21}H_{44}$
8.	Docosane	$C_{22}H_{46}$
9.	Methyltricosane	$C_{24}H_{50}$
10.	Methylhexacosane	$C_{27}H_{56}$
11.	Triacontane	$C_{30}H_{62}$
12.	Dotriacontane	$C_{32}H_{66}$
13.	Tetratriacontane	$C_{34}H_{70}$
14.	Pentatriacontane	$C_{35}H_{72}$
15.	Tetrapentacontane	$C_{54}H_{110}$

Primary alcohols		
1.	1-Hexanol	$C_6H_{14}O$
2.	1-Dodecanol	$C_{12}H_{26}O$
3.	1-Pentadecanol	$C_{15}H_{32}O$
4.	1-Hexadecanol	$C_{16}H_{34}O$
5.	1-Nonadecanol	$C_{19}H_{40}O$
6.	1-Tetracosanol	$C_{24}H_{50}O$
7.	1-Pentacosanol	$C_{25}H_{52}O$
8.	1-Hexacosanol	$C_{26}H_{54}O$
9.	1-Heptacosanol	$C_{27}H_{56}O$
10.	1-Octacosanol	$C_{28}H_{58}O$
11.	1-Triacontanol	$C_{30}H_{62}O$
12.	1-Hexatriacontanol	$C_{36}H_{74}O$
Fatty acids		
1.	Propanoic acid	$C_3H_6O_2$
2.	Hexanoic acid	$C_6H_{12}O_2$
3.	Nonanoic acid	$C_9H_{18}O_2$
4.	Undecanoic acid	$C_{11}H_{22}O_2$
5.	Myristic acid	$C_{14}H_{28}O_2$
6.	Palmitic acid	$C_{16}H_{32}O_2$
7.	Stearic acid	$C_{18}H_{36}O_2$
8.	Petroselinic acid	$C_{18}H_{34}O_2$
9.	Tetracosanoic acid	$C_{24}H_{48}O_2$
Aldehydes		
1.	Tetradecanal	$C_{14}H_{28}O$
2.	Hexadecanal	$C_{16}H_{32}O$

3.	Octadecanal	$C_{18}H_{36}O$
4.	Eicosanal	$C_{20}H_{40}O$
5.	Heneicosanal	$C_{21}H_{42}O$
6.	Hexacosanal	$C_{26}H_{52}O$
7.	Heptacosanal	$C_{27}H_{54}O$
8.	Octacosanal	$C_{28}H_{56}O$
Ketones		
1.	2-Pentadecanone	$C_{15}H_{30}O$
2.	2-Nonadecanone	$C_{19}H_{38}O$
3.	12-Tricosanone	$C_{23}H_{46}O$
4.	2-Heptacosanone	$C_{27}H_{54}O$
5.	2-Pentacosanone	$C_{25}H_{50}O$
Alkenes		
1.	1,5,9,13-Tetradecatetraene	$C_{14}H_{22}$
2.	1-Heptadecene	$C_{17}H_{34}$
3.	4,6,9-Nonadecatriene	$C_{19}H_{34}$
4.	1-Nonadecene	$C_{19}H_{38}$
5.	3-Eicosene	$C_{20}H_{40}$
6.	Heneicosene	$C_{21}H_{42}$
7.	1-Heptacosene	$C_{27}H_{54}$
8.	17-Pentatriacontene	$C_{35}H_{70}$

3.3.2.2 Cyclic Compounds

The non-polar cyclic compounds constituting the wax components include terpenoids, steroids and flavonoids [Riederer and Müller, 2006]. In the present study, among all the cyclic components, the terpenoids dominated the wax composition throughout seasons in both the plant species. In case of *C. procera*, the proportion of terpenoids was found to be the maximum during summer (38%), showed a significant decrease during the monsoon season (17.46%), and was observed to be increased again in winters (20.40%) [Figure 3.7]. However, in *S persica*, the terpenoid concentration remained almost consistent throughout seasonal variation with maximum concentration during the summer (29.16%), followed by a slight decrease during the monsoon (23.63%) and again reaching up (28.57%) during the winter [Figure 3.7]. On the basis of structural diversity, the terpenoids are classified as di-, tri-, and sesqui-terpenoids. Among various terpenoids amyrins, betulin, lupeol, 24-norusa-3,12-diene were the most common terpenoids found to be predominant in cuticular wax across the seasons [Table 3.3]. However, some of the terpenoids were observed to occur in a season and plant specific manner. For instance, in *C. procera*, cembra-2,7,11, trien-4, humulane-1,6-dien-3-ol and thunbergol were observed during summer season whereas, elemenone and geranylgeraniol were observed during monsoon season. In *S. persica*, kolavenol and longicamohenylone were only found during monsoon, whereas friedoolean-14-en-3-one and methanopicene were observed during the winter season only. Moreover, γ-muurolene was found to be present only during the monsoon season in both the plant species. Terpenoids exhibit wide range of structural diversity and biological activity such as sustaining mechanical strength as well as acting as a functional defensive component against external abiotic and biotic factors [Wu et al. 2018]. In *Arabidopsis thaliana*, the triterpenoids and sesquiterpenoids exhibited their functional role towards strengthening the plant defence against certain phytopathogens [Huang et al. 2012; Cárdenas et al. 2019]. Recently, diterpenoids have also been observed to establish a dual defence against both biotic and abiotic stresses [Lu et al. 2018; Murphy and Zerbe, 2020]. Hence, their increased concentration observed during summer and winter seasons could be due to their above-mentioned functions in *C. procera* and *S. persica*.

Phytosterols are crucial for maintaining the structural integrity and plants' response to various environmental stresses such as UV radiation, cold, drought, temperature, etc. Some of the above-mentioned stress factors, such as UV radiation, has been reported to influence the concentration of sterols in plants [Rogowska and Szakiel, 2020]. However, the direct involvement of sterols in defining the cuticular transpiration barrier remains elusive. In the

present study, GC-MS/MS analysis showed that xerophytic plants synthesise a complex mixture of sterols, such as campesterol, stigmasteirol and sitosterol being some of the most abundant compounds [Table 3.4]. The obtained results are in coherence with the previous studies where the cuticle wax samples were observed to have the above-mentioned sterols constituting a major proportion of phytosterols [Borisjuk et al. 2018; Rogowska and Szakiel, 2020]. The concurrent accumulation of phytosterols such as sitosterol, could enhance the flexibility and mechanical strength of cuticle, facilitating it to withstand changes in the turgor pressure while maintaining the integrity. Furthermore, the presence of campesterol has been observed to be crucial for the plant growth and development whereas stigmasterol has been reported to coordinate the plants' defence towards external stresses via cell signalling [Valitova et al. 2016]. Phytosterols, in correlation with terpenoids have also been identified to significantly participate as 'resistant factors' against infestation [Shepherd et al. 1999].

These preceding cyclic components (terpenoids and phytosterols) of the cuticular wax are synthesised via Mevalonate (MVA) pathway [Trivedi et al. 2019; Bhanot et al. 2021]. Squalene is the key intermediate of this pathway resulting in the formation of phytosterols and key triterpenoids such as lupeol and amyrins [Trivedi et al. 2019]. Noteworthy, GC-MS/MS analysis also showed the presence of squalene, and its resulting terpenoids and phytosterols in the wax extract of *C. procera* and *S. persica* representing the overall wax synthesis pathways.

Table 3.3 Chemical composition of terpenoids in the cuticular wax of *C. procera* and *S. persica*.

S.No.	Compound	Molecular Formula
Diterpenoids		
1.	Cembra-2,7,11-trien-4,5-diol	$C_{20}H_{34}O_2$
2.	Clerodadien	$C_{21}H_{30}O_5$
3.	Geranylgeraniol	$C_{20}H_{34}O$
4.	Kolavenol	$C_{20}H_{34}O$
5.	Thunbergol	$C_{20}H_{34}O$
Triterpenoids		
1.	Amyrins	$C_{30}H_{50}O$

2.	Betulin	$C_{30}H_{50}O_2$
3.	Friedoolean-14-en-3-one	$C_{30}H_{48}O$
4.	Handianol	$C_{30}H_{50}O$
5.	Lanosterol	$C_{30}H_{50}O$
6.	Lupeol	$C_{30}H_{50}O$
7.	Lup-20-(29)-en-3-one	$C_{30}H_{48}O$
8.	6a, 14a-Methanopicene	$C_{23}H_{16}$
9.	24, Noroleana-3, 12-diene	$C_{29}H_{46}$
10.	24-Norursa-3, 12-diene	$C_{29}H_{46}$
11.	A'-Noegammacer-22(29)-ene	$C_{30}H_{50}$
12.	Squalene	$C_{30}H_{50}$
13.	Ursa-9(11), 12-dien-3-one	$C_{30}H_{46}O$
Sesquiterpenoids		
1.	Elemenone	$C_{15}H_{22}O$
2.	Humulane	$C_{15}H_{26}O$
3.	Longicamphenylone	$C_{14}H_{22}O$
4.	γ-Muurolene	$C_{15}H_{24}$

Table 3.4 Chemical composition of phytosterols in the cuticular wax of *C. procera* and *S. persica*

S.No.	Compound	Molecular Formula
1.	Calusterone	$C_{21}H_{32}O_2$
2.	Campesterol	$C_{28}H_{48}O$
3.	9,19-Cycloergost-24(28)-en-3-ol	$C_{32}H_{52}O_2$
4.	Ergosta-5,22-dien-3-ol	$C_{28}H_{46}O$
5.	Obtusifoliol	$C_{30}H_{50}O$

6.	Pregn-5-en-3-ol	$C_{21}H_{34}O$
7.	Stigmast-5-ene	$C_{29}H_{50}$
8.	γ-Sitosterol	$C_{29}H_{50}O$

Further, additional non-wax bioactive compounds including carbohydrates, carboxylic acids, carboxylic esters and various intermediates & precursors of phytochemicals were also observed to constitute the cuticular wax [Table 3.5]. A few specific bioactive compounds such as triacontyl acetate (plant growth stimulator), cinnamyl linolenate (antioxidant), dihydrophytol (intermediate of phytanic acid), vitamin E (antioxidant), 2-palmitoyl glycerol (fatty acid ester) and azulene (precursor of terpenoids such as vetivazulene and guaiazulene) were also present.

Table 3.5 Chemical composition of non-wax metabolites in the cuticular wax of *C. procera* and *S. persica*.

S.No.	**Compound**	**Molecular Formula**
Carbohydrates		
1.	Mannitol	$C_6H_{14}O_6$
2.	D-Ribose	$C_5H_{10}O_5$
3.	L-Ribose	$C_5H_{10}O_5$
Carboxylic acids		
1.	1,2-Benzenedicarboxylic acid	$C_8H_6O_4$
2.	Fumaric acid	$C_4H_4O_4$
3.	Glutaric acid	$C_5H_8O_4$
4.	Methoxyacetic acid	$C_3H_6O_3$
5.	2-Propenoic acid	$C_3H_4O_2$
6.	Trichloroacetic acid	$C_2HCl_3O_2$

Carboxylic esters		
1.	Heptacosyl acetate	$C_{29}H_{58}O_2$
2.	Octacosyl acetate	$C_{30}H_{60}O_2$
Additional bioactive compounds		
1.	Azulene	$C_{10}H_8$
2.	Cinnamyl linolenate	$C_{27}H_{40}O_2$
3.	Dihydrophytol	$C_{20}H_{42}O$
4.	2-Palmitoyl glycerol	$C_{19}H_{38}O_4$
5.	Triacontyl acetate	$C_{32}H_{64}O_2$
6.	Vitamin E	$C_{29}H_{50}O_2$

Comparative percentage of chemical compositions in the total wax content in both the plant species, across seasonal variation, it was observed that alkanes (16.3-42.8 %), primary alcohols (7.1-22.0 %) and terpenoids (19.4-37.5 %) collectively constituted the major proportion of the cuticular wax, whereas aldehydes (4.1-12.4 %), fatty acids (1.7-18.5 %) and ketones (3.4-4.5 %) were present in relatively lower concentrations across seasons [Figure 3.7]. The relative proportion of terpenoids was found to be more during the summer season as compared to the monsoon and winter seasons. Notably, maximum number of alkanes were observed during the summer season in *S. persica*. In general, both the plant species showed presence of similar chemical compounds during respective seasons with slightly varied concentration.

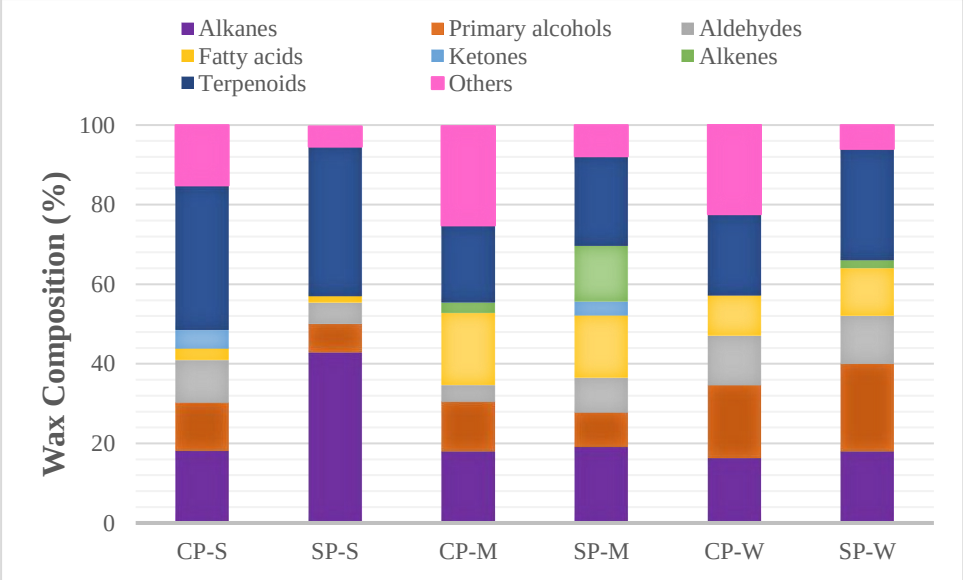

Figure 3.7 Proportion of aliphatic and cyclic compounds constituting the cuticular wax of *C. procera* and *S. persica* in different seasons. Abbreviations: CP- *Calotropis procera*; SP- *Salvadora persica*; S-Summer; M- Monsoon; W-Winter; Others- non-wax metabolites.

3.3.2.3 Correlation between Morphology and Chemical Composition of Wax

In the present study, the cuticular waxes exhibited exceptionally assorted micromorphology in the form of films, layers, crusts, crystalloids, platelets, threads, rodlets, tubules and even as chimneys around the stomata. The self-assembly of waxes into the aforementioned morphologies has been observed to be influenced by their chemical composition [Barthlott et al. 1998; Ding et al. 2018; Roma and Santos, 2021]. However, the chemistry of waxes may have a formative but not exclusive role in determining the morphology [Koch and Ensikat, 2008]. For instance, the alignment of the polar groups of the underlying cutin matrix and external environmental factors may also combinedly influence the wax morphology [Wu et al. 2018]. As mentioned above (section 3.3.1), the FE-SEM analysis of *C. procera* revealed the presence of thread-like trichomes covering the phylloplane surface. The wax deposits were present as independent ovate crystalloids lying over and in-between the trichomes throughout all the seasons [Figure 3.2 a, c & e] The GC-MS/MS results indicate that large wax ovate crystalloids formed due to the presence of large proportions of alkanes and terpenoids in the wax composition. However, the reports directly correlating the occurrence of wax crystalloids with the chemical composition of wax compounds are scarce.

S. persica showed the presence of wax crystals as platelets due to the large proportions of alkanes, alcohols and terpenoids in the wax composition [Figure 3.2 b, d & f]. Previous studies have also indicated that the presence of high proportion of alkanes, aldehydes, alcohols and terpenoids correlate with the formation of platelets by wax crystals [Wu et al. 2018, Boanares, et al. 2021, Wang et al. 2021]. However, it seems that similar wax structures can be formed by different chemical compositions in different plant species. Noteworthy, platelets can also be formed if any of the above-mentioned compounds are solely presence in abundance. For instance, wax platelets in *Sedum rupestre* are characterized by a high amount of triterpenoids, whereas platelets found in the Poaceae (e.g., *Triticum* sp., *Zea* sp.) are generally dominated by the presence of primary alcohols in their wax composition [Koch et al., 2006b; Trivedi et al. 2021]. Since various external factors are also participative in deciding the shape of wax crystals, the wax structures observed on the leaves of *C. procera* and *S. persica* are not only due to their dominant chemical composition but must also be influenced by other factors.

3.4. Conclusion

The present study provides following major conclusions: (i) The wax micromorphology of both the plants showed presence of different types of trichomes. In *C. procera*, the flattened trichomes densely covered the phylloplane surface, while in *S. persica*, 'simple' trichomes were sparsely present in standing position. In *C. procera*, the wax was present as ovate crystalloids, whereas, the phylloplane of *S. persica* showed the presence of numerous wax platelets, with some regions of wax crusts formed during the summers; (ii) The wax content of both the plants was observed to be maximum during the summer season. In *C. procera*, lesser change was observed in the wax content during monsoon and winter seasons, whereas in *S. persica*, the wax content consistently decreased through monsoon to winter; (iii) CSLM analysis showed cuticle and cell wall as two distinct layers. The cuticle of *C. procera* was thinner (~ 2 μm) in comparison to that of *S. persica* (~ 2 to 7 μm) (iv) The main chemical components of the cuticular wax for both the plant species were detected to be aliphatic as well as cyclic compounds. The aliphatic compounds included alkanes (C_{11}-C_{54}), primary alcohols (C_6-C_{36}), fatty acids (C_3-C_{24}), aldehydes (C_{14}-C_{28}), ketones (C_{15}-C_{25}) and alkenes (C_{14}-C_{35}). While the cyclic components included di-, tri- and sesqui- terpenoids. The analysis represented the presence of various long-chain compounds consisting of extensive C-C, C-H, -C=O bonds as well as aromatic components which are also common components of different synthetic plastics including polyethylene, polystyrene, polyethylene terephthalate, etc, indicating similar chemical foundation between the two polymers viz. cuticular wax and plastics. Additionally,

the collective proportions of terpenoids and alkanes were maximum during the summer season, while fatty acids and alkenes were comparatively more during monsoon season. In spite of being comprised of similar chemical families, the specific composition and abundance of compounds under seasonal variations reflects noticeable environmentally related differences. Specifically, the combined dominance of terpenoids and alkanes during the summer season indicates their role in response to high temperature conditions in xerophytes. Also, both the plant species displayed distinct wax microstructure pattern indicating that the physical mechanism to withstand temporal variation could be different. Therefore, understanding of the surface and chemical adaptability of cuticle wax among different xerophytes would be crucial for its practical applicability towards improved tolerance to temporal variation in commercial crops that would broaden the cultivation horizon in arid & semi-arid areas of Indian Thar Desert.

Chapter 4

PSS Transformation Potency of Phylloplane Fungi of Xerophytic Plants

4.1 Introduction

In present era of expedited growth of industries aimed at comforting human lifestyle, plastics and their applicability needs no introduction. Plastics are irreplaceable in their utility and their end-of-fate evidently represents persistence and extreme distribution across various environmental niches. While being constantly exposed to environmental factors, plastics tend to undergo fragmentation forming smaller sized macro-/meso- (> 5 mm), micro- (<5 mm) and nano- (1 nm to 1 mm) particles [Mariano et al. 2021]. Owing to their smaller size and low density, these fragmented particles are easily transported via wind and water across large distances [Syberg et al. 2015]. Additionally, their characteristic physical and chemical properties such as size, porosity, surface area, adsorption, surface affinity, etc, provide a suitable adhesion matrix for other toxic contaminants over their surfaces [Mei et al. 2020]. These plastic particles not only act as transportation vectors but are also mark as multiple contamination threat. Moreover, they also contain various toxic chemicals added during the manufacturing process, while simultaneously transporting the pollutants present in their close affinity via adsorption. For instance, various polycyclic aromatic hydrocarbons, polyfluoroalkyl substances, and persistent organic pollutants such as biphenyls, etc have been reported to adsorb over the plastic surface [Joo et al. 2021]. Hence, plastic waste has a larger significance as an ecological contaminant as compared to other pollutants.

The current scenario of plastic waste management includes three major strategies; (i) alternative eco-friendly polymers to replace plastics, (ii) recycling and (iii) remediation of the plastic waste. However, all the above-mentioned strategies have their own set of limitations. Firstly, the eco-friendly polymers such as starch/cellulose-based polymers possess inherently poor mechanical properties such as low porosity to vapor or oxygen, requiring complex and expensive process treatments for commercialization in order to be at par with conventional plastics [do Val Siqueira et al. 2021]. Moreover, the solution to the challenges associated with these polymers are still at lab-scale and would require a greater effort to reach commercialization. Secondly, although recycling of plastics appears to be one of the best-suited way outs, it has its own challenges that remarkably declines its practice. The recycling of plastics is restrictive for a variety of reasons including plastic properties, inclusion of additives and plastic sorting [Seay et al. 2020]. Nevertheless, recycling does not provide a permanent solution to the plastic waste, but only delays the inevitable fate of plastic ending up in the ecosystem [Hahladakis et al. 2018]. Thirdly, incineration is the most widely used method to remediate plastic waste by heating. However, incineration of plastics leads to the direct release

of toxic gaseous by-products such as dioxins, polychlorinated biphenyls, furans, mercury, etc into the atmosphere [Verma et al. 2016]. Nevertheless, incineration is not the terminator of plastic waste, on the contrary, the generated bottom ash contributes to the release of microplastics into the environment [Yang et al. 2021]. It is clear that neither of the above-mentioned strategies have been clearly indicative of the possible eco-friendly end-of-fate solution to the existing and growing plastic waste. Microbe-assisted remediation has been observed to have certain advantages such as sustainability, high efficiency, broad substrate spectrum, and cost-effectiveness, as compared to traditional remediation strategies.

Among various microbial groups, fungi are a highly diverse clade of eukaryotic, heterotrophic, absorptive organisms found in virtually all environments, and exist in different types including moulds, yeasts, lichens, rusts, and smuts [Naranjo-Ortiz and Gabaldón 2019]. Among the various types of fungi, moulds (filamentous fungi) have evolved a spatially extensive growth form of thread-like hyphae, with the ability of the hyphal networks to spread across over hundreds of acres [Ferguson et al. 2003; Stajich et al. 2009]. The genetics, physiology and ecological adaptations have manifested filamentous fungi to perfectly exploit various nutrient sources, enabling them to fit into extreme environments [Wrzosek et al. 2017]. The filamentous network of fungi can easily undergo continuous remodelling and is therefore highly dynamic, adapting to different underlying nutrient conditions, damage, or assault by meso-fauna [Fricker et al. 2008]. Through these networks, fungi release varied enzymes that help them to survive under unfavourable conditions.

Owing to their remarkable capabilities, fungi have been exploited for their biodegradative abilities towards various toxic and highly resistant xenobiotic compounds. For instance, *Aspergillus fumigatus* has been reported to consume petroleum hydrocarbons from contaminated sludge [Othman et al. 2022]. Similarly, *Alternaria, Trichoderma* and *Purpureocillium* species have also been observed to utilise petroleum hydrocarbons from the contaminated sites [Benguenab and Chibani, 2021; El-Aziz et al. 2021]. Other class of pollutants such as polycyclic aromatic hydrocarbons, benzene, naphthalene, chlorophenol, etc have also been reported to be susceptible against fungal action [Sandhibigraha et al. 2020; Agrawal et al. 2021; Vipotnik et al. 2021; Li et al. 2022]. Generally, fungi involved in hydrocarbons degradation are mesophilic organisms, growing in the range 10-40 °C, reaching the functional optima in the range 20–35 °C [Kirk et al. 2008]. However, an appropriate combination of different factors such as pH, temperature and exposure are required in order to reach effective microbial activity against contaminant degradation [Fester et al. 2014; Liu et

al. 2017]. Moreover, due to the limited number of studies conducted on PS degradation, it is hard to predict the optimal temperature and pH ranges for its enzyme-mediated degradation [Hou and Majumder, 2021].

In the present study, the fungi isolated from the phylloplane of xerophytes (as discussed in Chapter 3) were tested for the potency to transform PSS considering the following reasons: (i) The phylloplane of xerophytes is densely covered by a hydrophobic cuticle, which has physical and chemical similarities to plastics; (ii) The xerophytic phylloplanic fungi are directly exposed to extreme environmental conditions, hence, must be acclimatized to survive under drastic abiotic conditions; (iii) Being eukaryotic and heterotrophic, fungi secrete versatile range of extracellular components with a potential to be explored for remedial purposes. Further, optimization of various process parameters was attempted in order to maximize the output.

4.2 Materials and Methods

4.2.1 Chemicals and Reagents

All chemicals (analytical grade) and solvents (GC grade) used were procured from Sigma Aldrich (India) or Merck (India) unless otherwise stated. All culture media used were purchased from HiMedia (India). Poly(sodium 4-styrenesulfonate) (PSS; M_w ~70,000 Da), Sigma-Aldrich was used as the source of polystyrene. Standard protein molecular weight marker (26610) was obtained from Thermo Fischer, USA. For ultrafiltration of proteins, a 12 kDa cut-off nitrocellulose membrane (Merck) was used.

4.2.2 Screening of Fungal Isolates

All the 20 fungal isolates were screened to check their ability towards PSS myco-transformation. The individual fungal isolates were grown in 100 mL of potato dextrose broth (PDB) in 250 mL Erlenmeyer flasks and incubated under dark conditions at 28℃ for 72 h on a rotary shaker (120 rpm). After incubation, the fungal biomass was separated from the culture medium by centrifugation (5000 rpm; 4 ˚C; 15 min) and washed thrice with autoclaved Milli-Q water to remove all traces of media. Typically, 10 g fresh weight (FW) of fungal biomass was re-suspended in 100 mL of minimal salt media (MSM) containing NH_4NO_3 3 g L^{-1}; KH_2PO_4 & $K_2HPO_4 \cdot 3H_2O$ 0.5 g L^{-1} each; $MgSO_4 \cdot 7H_2O$ 0.008 g L^{-1}; $CuSO_4 \cdot 5H_2O$, $MnSO_4 \cdot H_2O$, $FeSO_4 \cdot 7H_2O$ and $CaCl_2 \cdot 2H_2O$ 0.002 g L^{-1} each; pH 7.0 with 1% PSS as sole carbon source in a 250 mL Erlenmeyer flask and incubated at 28 ˚C for 30 days on a rotatory shaker (150 rpm) under dark conditions. After incubation, the biomass was separated by

centrifugation at the above-mentioned conditions and its FW was measured. The isolate(s) showing maximum increase in fresh weight biomass were selected for further study.

4.2.3 Effect of Various Parameters on PSS Myco-transformation Potency

To monitor the most favourable conditions for the utilization of PSS as sole carbon source, experiments were carried out to test the effect of various reaction parameters viz., exposure duration, temperature, and pH. For optimization of reaction parameters, 20 g FW of short-listed fungal isolate was re-suspended in 200 mL of MSM containing 1% PSS as sole carbon source in a 500 mL Erlenmeyer flask and incubated at 28 ˚C on a rotatory shaker (150 rpm) under dark conditions. After completion of tested incubation period, the fungal biomass was separated by centrifugation (5000 rpm; 4 ˚C; 15 min) & weighed. The supernatant was filtered using Whatman grade 1 filter paper (Whatman Inc., USA) to obtain the cell-free filtrate for further characterization.

The change in the fresh weight of fungal biomass was measured and compared with the initial weight of fungal biomass inoculated at day zero of the respective experiments. The increase in fungal biomass would be indicative of utilization of PSS as sole carbon source for sustaining fungal metabolism. Treatment containing MSM with 3% dextrose was considered as a positive control and treatment containing only MSM (without PSS and no other carbon source) was considered as a negative control w.r.t fungal growth. All the treatments were incubated at 28°C, which is the standard temperature used for cultivation of fungi. The data points represent the mean of independent measurements, and the uncertainties were represented as standard error. Further, Raman spectroscopy and GC-MS/MS analysis of the supernatant were performed to monitor the extend of PSS myco-transformation in comparison to control (MSM+1% PSS) sample. All the experiments were performed in triplicate with respective controls.

4.2.3.1 Effect of Exposure Duration

Effect of PSS exposure duration on the utilization of PSS as sole carbon source was studied by allowing the reactions to run for a period of 30 days during which the reactions were terminated at the duration of day 5, 10, 15, 20 and 30 for all the treatment conditions, namely, MSM+1% PSS and only MSM (negative control). Whereas, MSM+ 3% dextrose (positive control) was terminated at day 5, in order to minimize the appearance of false protein bands. All the experimental flasks were incubated at 28°C, 150 rpm under dark conditions.

4.2.3.2 Effect of Temperature

Effect of temperature was studied by incubating Erlenmeyer flasks of all treatment conditions (stated above) at three different temperatures, viz., 15°C, 28°C and 40°C. The experimental flasks were incubated at 150 rpm at the optimized exposure duration, under dark conditions.

4.2.3.3 Effect of pH

Effect of reaction pH was studied by altering the pH of different treatment conditions (as stated above) before the addition of fungal biomass. For this, 0.1 N HCl or 0.1 N NaOH was added to adjust the final pH of 5.0, 5.5, 6.0, 6.5, 7.0 and 8.0 using a Cyberscan 1100 pH meter (Eutech Instruments, Singapore). The experimental flasks were incubated at 150 rpm at the optimized exposure duration and temperature, under dark conditions.

4.2.4 Characterization of PSS Myco-transformation Ability of Fungal Isolates

4.2.4.1 Raman Spectroscopy Analysis

Raman spectroscopy enables the assessment of the chemical composition of a sample through the acquisition of the inelastic scattering of monochromatic light interacting with the molecule. Using this technique, a spectral fingerprint corresponding to the chemical composition of a molecule can be obtained which is specific to its molecular conformation. Raman spectroscopy was performed for the filtered supernatant (2mL) collected at the termination of the reaction to evaluate the changes in the qualitative features due to myco-transformation using LabRam HR Evolution model (Horiba, France). Optimal conditions for the analysis of polystyrene were as follows: $\lambda = 785$ nm (wavelength) at $P = 20$ mW (power) for an acquisition frame time of five cycles for 30 s using a 50x objective with 0.5 N.A. (numerical aperture). Similarly, control sample containing only MSM+1% PSS was also analysed in order to find out the shifts in the Raman spectra. Each spectral fingerprint was computed according to the peak intensities and Raman shifts (centimetres) using the LabSpec 6- HORIBA Scientific. Noise reduction and base correction of the generated Raman spectra were performed was done using OriginPro 9.0.

4.2.4.2 GC-MS/MS Analysis

To examine the myco-transformation compounds generated during PSS myco-transformation, chromatographic analyses were performed by the following method described by Krueger et al. [2015]. The sample supernatant (2 mL) from fungal treated MSM+1% PSS and control sample containing only MSM+1% PSS were extracted using 500 µL of chloroform. The chloroform phase was extracted, and one microliter of each sample was analysed by gas chromatography mass spectroscopy (Model TQ 8040, Shimadzu, Japan). The capillary column SH-Rxi-5Sil MS (0.25 µm film thickness, 0.25 mm i.d., 30 m length) was used for the gas chromatography with helium as a carrier gas (head pressure 72.5 kPa; flow rate 1.0 mL/min). The initial oven temperature was of 60 °C held for 2 min, which was then increased at 8 °C /min till it reached 280 °C. The temperature was then increased by 2.5 °C /min till it reached 300°C. Injector temperature was set at 280 °C as the transfer line to the mass spectrometer. The mass spectra were acquired at full scan mode in the mass range from 50 u to 500 u. Electron ionization (70 eV) was applied at an ion source temperature of 230°C. The conditions applied to MS analysis were as follows: scan mode, start time of 3 min, end time of 39 min, scan speed 1666, event time 0.3 s, start m/z 45, and end m/z 500. The obtained data were compared with the inbuilt standard mass spectra library system (NIST 16).

The raw data generated during optimization of different process parameters were used to analyse the profile of the myco-transformation compounds using MetaboAnalyst version 5.0 software (McGill University, Montreal, QC, Canada) [Xia and Wishart, 2011; Pang et al. 2021]. To ensure that all samples were normally distributed, the datasets were normalized to their total sample median for the specific parameter. The myco-transformation compounds $\log_{10}$ transformation was performed and data were Pareto-scaled by dividing the mean centred by square root of the standard deviation of each variable in order to identify differentially expressed myco-transformation compounds among the study groups and make individual features more comparable [Dahabiyeh et al. 2020]. The $\log_{10}$ transformation is done to reduce or remove the skewness of the original data, while pareto scaling reduces the relative importance of large values and maintains the originality of the data trend [van den Berg et al. 2006]. For clear and distinct representation of large metabolomics data, principal component analysis (PCA), partial least squares discriminant analysis (PLS-DA), heat map and correlation matrix were performed using Metaboanalyst 5.0 software. For heatmap generation, average clustering method was performed with ‘Euclidean’ distance measuring and ‘Ward’ clustering method.

4.2.5 Protein Precipitation and One-Dimensional Gel Electrophoresis

Based on the results of tested process parameters (exposure duration, temperature and pH) for efficient myco-transformation of PSS, the optimised parameters i.e. 28℃ and pH 7.0 were selected to monitor the extracellular protein profile of *C. dactyloctenicola* VJP08 at all the tested exposure durations (day 5 to day 30). To find out the active role of extracellular fungal proteins in the myco-transformation of PSS, the extracellular proteins present in the fungal cell-free filtrate from the experimental flasks (including controls) were precipitated using modified TCA/acetone precipitation method [Niu et al. 2018]. Briefly, 20% cold TCA/acetone was added to the cell-free filtrate in 1:1 ratio (v/v) at a final concentration of 10%TCA/ 50% acetone. The mixture was gently stirred for 5 min at 4°C, followed by centrifugation (15,000 g, 3 min, 4°C). The resulting protein precipitate was washed twice with 80% acetone. The obtained protein pellet was then re-suspended in minimum volume of 50 mM phosphate buffer (pH 7.2) followed by dialysis using 12 kDa cut-off bag pre-treated as per the manufacturer's instructions. The duly sealed dialysis bag filled with proteins was immersed in dialysis buffer (50 mM phosphate buffer, pH 7.2) and stirred gently at 4°C on a magnetic stirrer for 12 h by changing the buffer at every 3 h. The total protein concentration in the dialysed samples were quantified using QuantiPro BCA assay kit (Merck). The assay was performed according to the manufacturer's protocol and the protein concentration was calculated against the standard protein curve plotted using bovine serum albumin provided in the kit.

Proteins obtained for each treatment were subjected to sodium dodecyl sulfate-polyacrylamide gel electrophoresis (SDS-PAGE) analysis as per standard procedure with adequate modifications [Laemmli, 1970]. All the samples were denatured in 2X sample buffer containing 60 mM Tris (pH 6.8), 25% glycerol, 2% SDS, 14.4 mM 2-mercaptoethanol, 0.1% bromophenol blue by boiling for 5 min followed by centrifugation (8000 rpm, 1 min, 4°C). Electrophoresis was performed on a Mini Protean® Tetra-Cell instrument (BioRad Laboratories, USA) at a constant voltage of 80 kV for 120 min. Standard protein markers were also run with the denatured samples. After electrophoresis, the gel was stained with Coomassie Brilliant Blue (CBB) G-250 dye and observed in a BioRad ChemiDoc^{TM} XRS+ imaging system with Image Lab^{TM} software.

4.3 Results and Discussion

4.3.1 Screening and Short-Listing of Fungal Isolates

All the 20 fungal isolates were screened for their ability to utilize PSS as the sole carbon source. For this, change in the FW of fungal biomass in presence of PSS (1%) as sole carbon source in MSM media after 30 days was measured. Being heterotrophic organism, fungi obtain its nutrient from the surrounding environment by secreting various extracellular enzymes, which breakdown the complex organic compounds. The degraded compounds are then absorbed (ingested) for nutrition. Carbon is a macro-nutrient and an essential source for sustaining all metabolic processes in the fungal cells as well as maintain cellular integrity by the cell wall synthesis. Hence, it must be extracted from the surrounding environment in considerable amount [Bhanot et al. 2023]. Therefore, any increase in the fungal biomass would be indicative of utilization of PSS as carbon source for growth [Bhanot et al. 2023].

Table 4.1 depicts the FW of fungal biomass recorded after 30 days for all the fungal isolates. Considering the initial FW (10g) of fungal biomass, the fungal genera *Aspergillus*, *Alternaria*, *Cladosporium* and *Curvularia* majorly showed an increase in their biomass weight indicating that they could utilize PSS as carbon source. Noteworthy, all the fungal genera which showed growth in MSM with PSS as sole carbon source were major phytopathogens [Marin-Felix et al. 2017; Jayawardena et al. 2021; Singh et al. 2021]. *Curvularia dactylotenicola* VJP08 showed maximum growth and significantly exceeded all other fungal isolates, with an increase of ~52% in the final fungal biomass weight after 30 days of incubation in MSM+1% PSS. In order to short-list the most efficient fungi, all the isolates showing ~ or >15% increase in the biomass weight, namely, *Cladosporium* sp. VJP04, *C. dactyloctenicola* VJP08, *Aspergilus ochraceus* VJP10, *Aspergillus nidulans* VJP11, *Aspergillus foveolatus* VJP13, *Alternaria alstroemeriae* VJP18 and *Aspergillus welwitschiae* VJP20 were further evaluated for their PSS myco-transformation ability using Raman spectroscopy analysis (data not shown). Based on which, the isolate *C. dactylotenicola* VJP08 was short-listed for further studies.

Curvularia is an upcoming fungal genus with many newly discovered species of unexplored potentials [Kiss et al. 2019; Iturrieta-González et al. 2020; Marin-Felix et al. 2020]. Recently, *Curvularia* sp. has received much attention as a potent phytopathogen possessing an extraordinary enzymatic potential, with the ability to infect some of the rarely infected plant species [Sharma et al. 2016; dos Santos et al. 2018; Liang, et al. 2018; Alawlaqi and Alharbi, 2020; Baral et al. 2022]. Moreover, species of *Curvularia* have been reported to synthesize

distinct types of secondary metabolites such as antibiotics, pigments, amino acids, vitamins and organic compounds that perform significant biological activities, and thus, can be explored for several biotechnological applications [Mehta et al. 2022]. Apart from secondary metabolites, genus *Curvularia* has reportably remarkable enzymatic potential capable of surpassing the biodegradation efficiency of other filamentous fungi [Hamad et al. 2021]. For instance, among 20 fungal isolates, *Cochliobolus lunatus* strain CHR4D now classified as *Curvularia lunata*, has been reported as the most promising candidate for the rapid degradation of chrysene, which is a four-ringed high molecular weight polycyclic aromatic hydrocarbon (PAH) [Bhatt et al. 2014].

Table 4.1 The change in the fresh weight (FW) biomass of fungal isolates in MSM+1% PSS after 30 days of incubation. (Initial FW fungal biomass =10 g).

S.No.	Fungus	Isolate	Final Biomass (g)	% Change in FW
1	*Cladosporium* sp.	VJP01	10.8±0.3	8.0
2	*Alternaria* sp.	VJP02	10.5±0.1	5.0
3	*Penicillium chrysogenum*	VJP03	8.7±0.5	-13
4	*Cladosporium* sp.	VJP04	12.5±0.3	25
5	*Aspergillus* sp.	VJP05	10.0±0.2	N/A
6	*Aspergillus ochraceus*	VJP06	9.4±0.4	-6
7	*Fusarium* sp.	VJP07	10.3±0.2	3
8	*Curvularia dactyloctenicla*	VJP08	15.2±0.1	52
9	*Purpureocillium lilacinum*	VJP09	10.1±0.0	1
10	*Aspergillus ochraceus*	VJP10	12.8±0.1	28
11	*Aspergillus nidulans*	VJP11	11.5±0.4	15
12	*Epicoccum keratinophilum*	VJP12	9.7±0.1	-3
13	*Aspergillus foveolatus*	VJP13	11.6±0.3	16
14	*Penicillium shearii*	VJP14	9.0±0.1	-10
15	*Aspergillus sp.*	VJP15	8.5±0.5	-15
16	*Aspergillus quadrilineatus*	VJP16	10.7±0.2	7
17	*Curvularia caricae-papayae*	VJP17	11.0±0.1	10
18	*Alternaria alstroemeriae*	VJP18	13.0±0.0	30
19	*Penicillium* sp.	VJP19	9.1±0.2	-9
20	*Aspergillus welwitschiae*	VJP20	11.7±0.3	17

4.3.2 Effect of Various Parameters on Myco-transformation Potency

The efficiency of any microbe-mediated transformation/degradation of any compound is influenced by the environmental factors which can impact their growth and metabolic activities. To investigate the effect of various physico-chemical conditions on the myco-transformation of PSS by *C. dactylotenicola* VJP08 and to obtain the optimized conditions for identification of participating biomacromolecules, a series of experiments were conducted. Biological processes such as bioremediation or biotransformation heavily rely on the enzymate-mediated reactions that occur at an optimum temperature [Endeshaw et al. 2017]. Additionally, these processes also depend on pH because it affects the enzymatic activities, the cell membrane transport, and the catalytic reaction balance [Bonomo et al. 2001]. Hence, exposure duration, temperature and pH were selected as the key parameters for optimization in order to monitor the process of myco-transformation.

4.3.2 Effect of Exposure Duration

At first, the effect of PSS exposure duration on the growth of *C. dactyloctenicola* VJP08 was studied by monitoring the changes in the FW of fungal biomass. The fungal growth in the MSM+3% dextrose (positive control) showcased an increase of 321.65% over an incubation period of 5 days as dextrose is a readily available carbon source for the growth of fungi (Table 4.2 a). While due to absence of carbon source in only MSM (negative control), the biomass FW of *C. dactyloctenicola* VJP08 was observed to be continuously decrease from 5.35% (at day 5) to 32.83% (at day 30). In case of MSM+ 1% PSS, where PSS was present as sole carbon source, *C. dactyloctenicola* VJP08 exhibited gradual increase in the biomass FW w.r.t initial inoculated biomass. The biomass FW was observed to increase by 57.8% at day 5, which further increased to its maximum potential of 73.8% at day 15. However, in comparison to day 15, the biomass FW was found to eventually decrease by 27.3% by the incubation period of 30 days. These results indicate that *C. dactyloctenicola* VJP08 could utilize PSS which was the sole carbon source to support its growth and metabolism. The maximum growth of *C. dactyloctenicola* VJP08 was observed at day 15. Since, the overall growth profile of *C. dactyloctenicola* VJP08 showed significant increase in biomass FW w.r.t to the initial inoculum FW (20 g) during the tested exposure durations, Raman spectroscopy was employed to further understand the myco-transformation profile of PSS.

Table 4.2 (a) Effect of exposure duration (days) on the growth of *C. dactyloctenicola* VJP08. (Initial fungal biomass FW= 20 g).

Treatment	Fungal biomass FW (g)				
	D5	**D10**	**D15**	**D20**	**D30**
MSM+ 3% Dextrose	84.3±1.4	-	-	-	-
Only MSM	18.9±0.1	18.2±0.2	14.9±0.4	14.0±0.2	13.4±0.8
MSM+ 1% PSS	31.5±1.4	31.8±1.4	34.7±1.1	32.2±0.9	29.3±1.7

D= days; ± represent standard error

4.3.2.1 Raman Spectroscopy

In order to compare and analyse the changes in chemical fingerprint of PSS across different exposure duration (day 5 to day 30), Raman spectra were analysed by employing the stack plot of MSM+1% PSS treatment in comparison to control (untreated MSM+1% PSS) [Figure 4.1]. Raman spectra of PSS showed main vibrations at 789.209, 1125.53, 1208.48, 1407.9, 1648.64, 3248.26 and 3387.59 cm^{-1}. These bands correspond to C-H deformation (789.208 cm^{-1}), C-C stretch (1125.53 cm^{-1}), sulfonic acid (1208.48 cm^{-1}), CH_2 scissoring (1407.9 cm^{-1}), benzene ring stretch (1648 cm^{-1}) and aromatic C-H band stretch (3248.26 and 3387.59 cm^{-1}) [Edwards et al. 2000; Nava et al. 2021]. In comparison to other bands, 3248.26 and 3387.59 cm^{-1} bands showed a broad appearance (higher intensity) due to the presence of hydrogen atom which is lighter than carbon. Moreover, the band ~3200 cm^{-1} represent the carbons in the aliphatic part of carbon chains connecting the styrene units, whereas band at ~3300 cm^{-1} represent the carbons in the aromatic part of carbon ring of styrene.

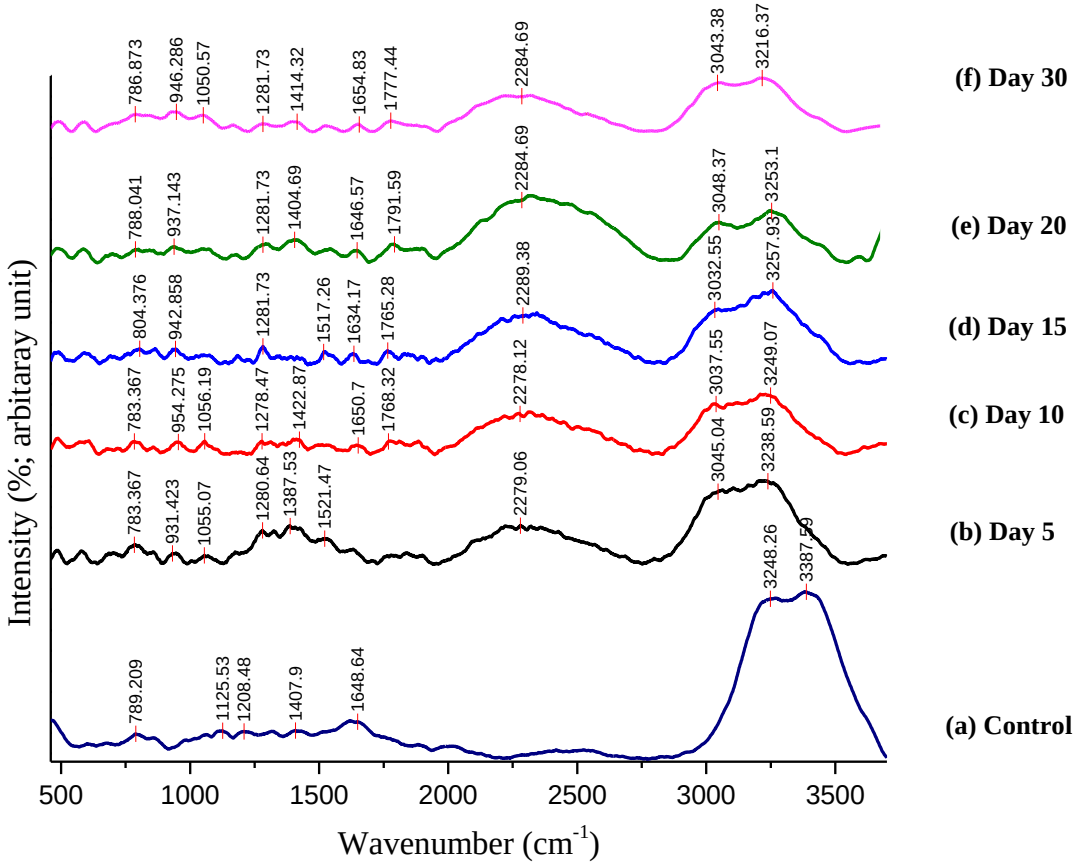

Figure 4.1 Raman spectra of (a) control; (b-f) treatment containing MSM+ 1% PSS samples exposed to *C. dactyloctenicola* VJP08 for the exposure duration from day 5 to day 30.

In comparison to control, samples with *C. dactyloctenicola* VJP08 demonstrated significant variations in the characteristic peaks, in addition to newly generated peaks at ~940, ~1050, ~1770, and ~2280 cm^{-1}. However, the appearance of these newly generated peaks showed slight variation among samples exposed for different exposure durations. A significant gradual decrease in the % intensities for peaks mainly at 3248.26 and 3387.59 cm^{-1} was observed with the increased exposure duration. In control sample, the intensity of these two bands was found to be ~350%. However, at exposure duration of 5 days, the intensity of these bands was observed to be ~160%, which further decreased to 70% by day 30. Along with the decrease in the peak/ band intensity, the Raman peak originally positioned at 3248.26 and 3387.59 cm^{-1} showed an average wavenumber shift to ~3035 and 3240 cm^{-1} respectively. It is due to the change in relative distance and orientation between atoms due to local deformation, causing the change in the strength of corresponding chemical bonds. This subsequently changes in the interaction between electromagnetic wave and chemical bonds of materials leading to shift in Raman peak positions due to changes in the frequencies of Raman-induced phonons

and/or molecular vibrations [Ganesan et al. 1970; Yang et al. 2020]. Furthermore, the newly generated peaks at ~940 cm^{-1} represents aromatic ring bending vibrations and peak at ~2280 cm^{-1} can be assigned to a wide range of bands including C-H and C-C stretching, $=CH_2$ and C-H deformation [Klisińska-Kpoacz et al. 2018]. Moreover, new functional group peaks observed at ~1050 cm^{-1} and ~1770 cm^{-1} represent −C−O− and −C=O stretching, respectively indicating oxidation of the PSS [Song et al. 2020]. The Raman spectroscopy analysis suggest that the *C. dactylocetnicola* VJP08 could utilize both the aliphatic and aromatic carbon components of PSS for its growth and metabolism throughout the incubation period of 30 days, during which the utilization was observed to slow down after 20 days. Noteworthy, the peak intensity of ~2280 cm^{-1} band decreased at 30 days which indicates that fungal-mediated utilization of PSS become restricted. However, the fungus survived by utilizing the products and by-products generated during the earlier days of exposure.

4.3.2.2 Myco-transformation Compounds Analysis

The chemical fingerprint analysis discussed in above section indicated the capability of *C. dactyloctenicola* VJP08 towards PSS utilization. Hence, to further investigate the compounds generated during the myco-transformation of PSS, the treatment extracts were subjected to GC-MS/MS analysis. The extracts from the control (MSM+ 1% PSS) sample showcased the presence of key components of PSS, namely benzene (the monomeric structure of PSS), and two plastic additives: 2,4-Di-tert-butylphenol (2, 4-DTBP) and 1,1'-Biphenyl, 2-3' diol which are commonly added as UV stabilizer and flame retardants. The peaks indicating the compounds leaked from the GC-MS/MS column have not been marked in all the representative chromatograms (Shown in Appendix-III).

Treatment containing MSM+1% PSS exposed to *C. dactyloctenicola* VJP08 displayed presence of various organic compounds, generated as a result of PSS myco-transformation. The profiling resulted in identification of a total 6 compounds in control sample. In comparison, total 29 (day 5), 33 (day 10), 32 (day 15), 28 (day 20) and 24 (day 30) compounds were observed in the treatment containing MSM+1% PSS with fungal biomass [Figure 4.2], respectively. Most of the compounds were found to be common during different exposure durations. Overall, a total of 56 compounds were identified, of which, 22 compounds were uniquely present in different exposure durations. The generated compounds were identified as plastic-derived oxidized molecules, alkanes, alcohols, easters, carboxylic acids, fatty acids and miscellaneous compounds [Figure 4.2]. These results indicate that *C. dactyloctenicola* VJP08 has the ability to myco-transform and utilise PSS as sole carbon source for its metabolism.

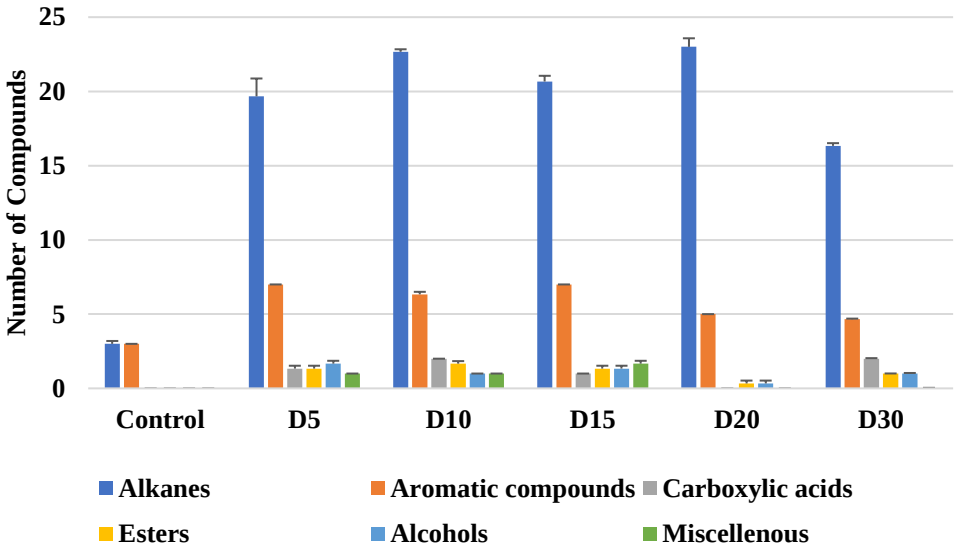

Figure 4.2 Proportion of different compounds generated during myco-transformation of PSS by *C. dactyloctenicola* VJP08 at different exposure durations.

Further, the clustering of control (MSM+ 1% PSS without fungal biomass) sample and treatment (MSM+1% PSS with fungal biomass) samples across different exposure duration were analysed using two-dimensional (2D) principal component analysis (PCA) score plot. The 2D scores PCA plot indicated the natural grouping and clear separation/ differentiation of the control and treated samples at different exposure durations. The treated samples (indicated as green circles) are clustered together due to the similarity in the variation of their component profiles [Figure 4.3 A]. The two principal components used to generate the scores plot accounted for almost 50% of the variance across the data set, with ~ 32% of the variance contributing to the separation between the control and treated samples along the first PC

dimension. Additionally, the compounds with value greater than 1 in variable importance in the projection (VIP) were marked as the most significant myco-transformation compounds [Siddiqui et al. 2022]. The univariate VIP plot clearly indicated the higher expression of PSS-transformation derived aromatic compounds such as benzothiazole, quinoline, octadecanoic acid, and organic compounds such as pentadecane, hexadecane, heptadecane, octadecane, nonadecane, dodecane, docosane & octacosane indicating that PSS has been transformed into organic compounds by *C. dactyloctenicola* VJP08 for its metabolism [Figure 4.3 B]. The generated compounds included alkanes and alcohols of varied carbon chain length ranging from C_7 to C_{54} and C_{10} to C_{22}, respectively. The alkanes are generated as a result of enzyme-mediated plastic depolymerization, subsequently to be utilised through β-oxidation pathway [Ji et al. 2013]. Among the metabolite classes, alkanes were found to be present most dominantly. Pentadecane, heptadecane, octadecane, nonadecane, heneicosane, eicosane, octacosane and tetrapentacontane were the most predominant alkanes synthesized during different exposure durations (days). Generation of various organic compounds such as alkanes, alcohols, carboxylic acids and esters have also been observed during biodegradation of various other types of plastics [Mohanan et al. 2020; Ru et al. 2020; Zadjelovic et al. 2022]. Further multivariate VIP analysis was performed to analyse the component profile during the individual exposure durations [Figure 4.3 C]. The analysis revealed the occurrence of PSS myco-transformation compounds at lower concentrations during the initial exposure duration (day 5), which significantly increased till day 30, with the highest component concentrations at day 15 and day 30. These results can be explained as follows: After exposure to *C. dactyloctenicola* VJP08, PSS myco-transformation occured in a catabolite repression manner, where the transformation exponentially increases till day 15 leading to the generation of organic components, which are preferentially utilized by the growing fungal biomass, leading to their decreased concentration in the sample as observed at day 20. Their depletion stimulates the fungus to further transform the leftover PSS leading to the generation of new organic compounds in higher concentration which were observed at day 30 during GC-MS/MS analysis.

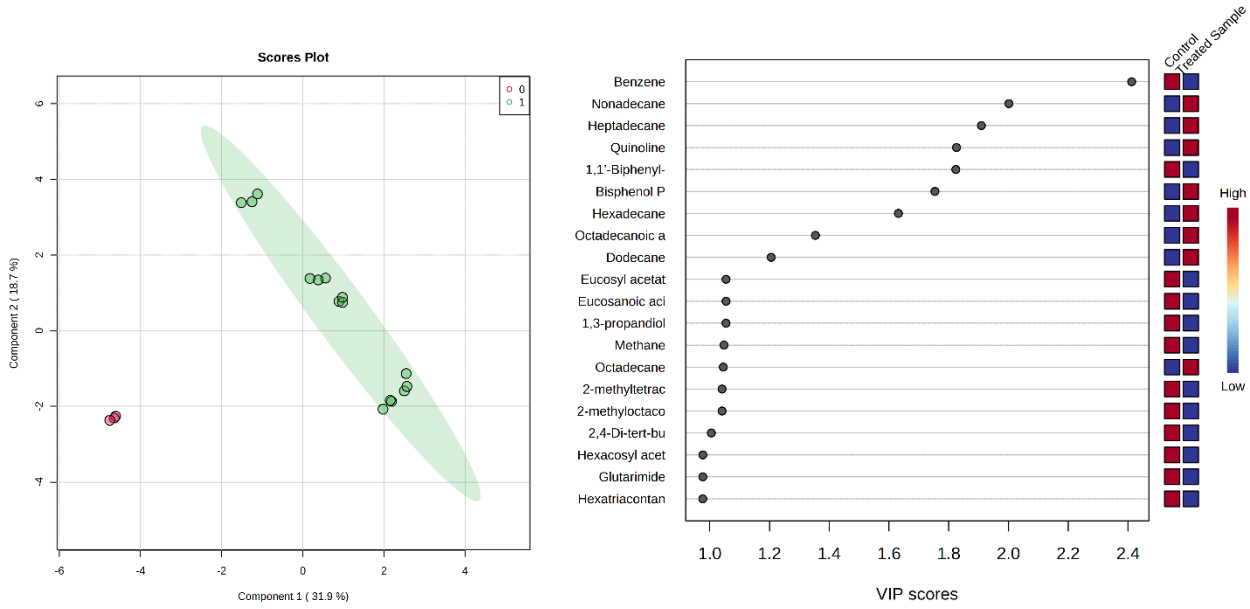

(A) **(B)**

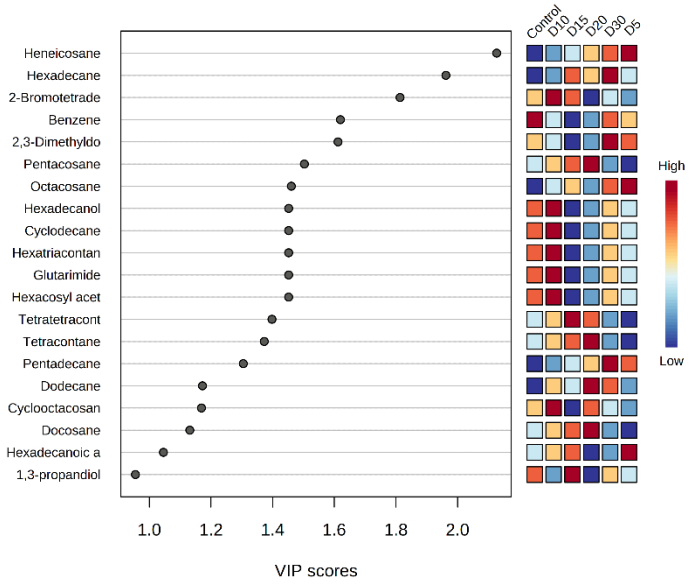

(C)

Figure 4.3 (A) Two-dimensional principal component analysis (2D-PCA) score plot demonstrates statistical clustering of control (shown in red) and treated samples at different exposure durations (shown in green); (B) Univariate variable importance in the projection (VIP) score plot of top 20 identified compounds in control; and treated samples for different exposure durations; (C) Multivariate VIP score plot of top 20 identified compounds in control; and treated samples at different exposure durations.

The clustering of overall component profile of fungal-mediated PSS transformation across different exposure durations could be clearly observed in the heatmap [Figure 4.4]. Since PSS is majorly comprised of rigid aromatic ring structure, its chemical transformation is an essential step for its utilization. The heatmap indicates that key PSS components such as benzene, 2, 4-DTBP and 1,1'-Biphenyl, 2-3' diol were present in highest concentrations in the control sample, which got significantly decreased over the incubation period of 20 days. This chemical transformation was evidently observed by the simultaneous formation of benzenepentanoic acid at day 5 of exposure duration, which is an oxidized form of benzene. It could be hypothesised that this oxidized form of benzene was readily mineralized by the fungus

to synthesize various organic compounds such as alkanes and fatty acids, essential for the fungal growth and metabolism. Further, the generation of sulfurous acid at day 5 indicated that the PSS structure has been catabolically transformed by *C. dactyloctenicola* VJP08.

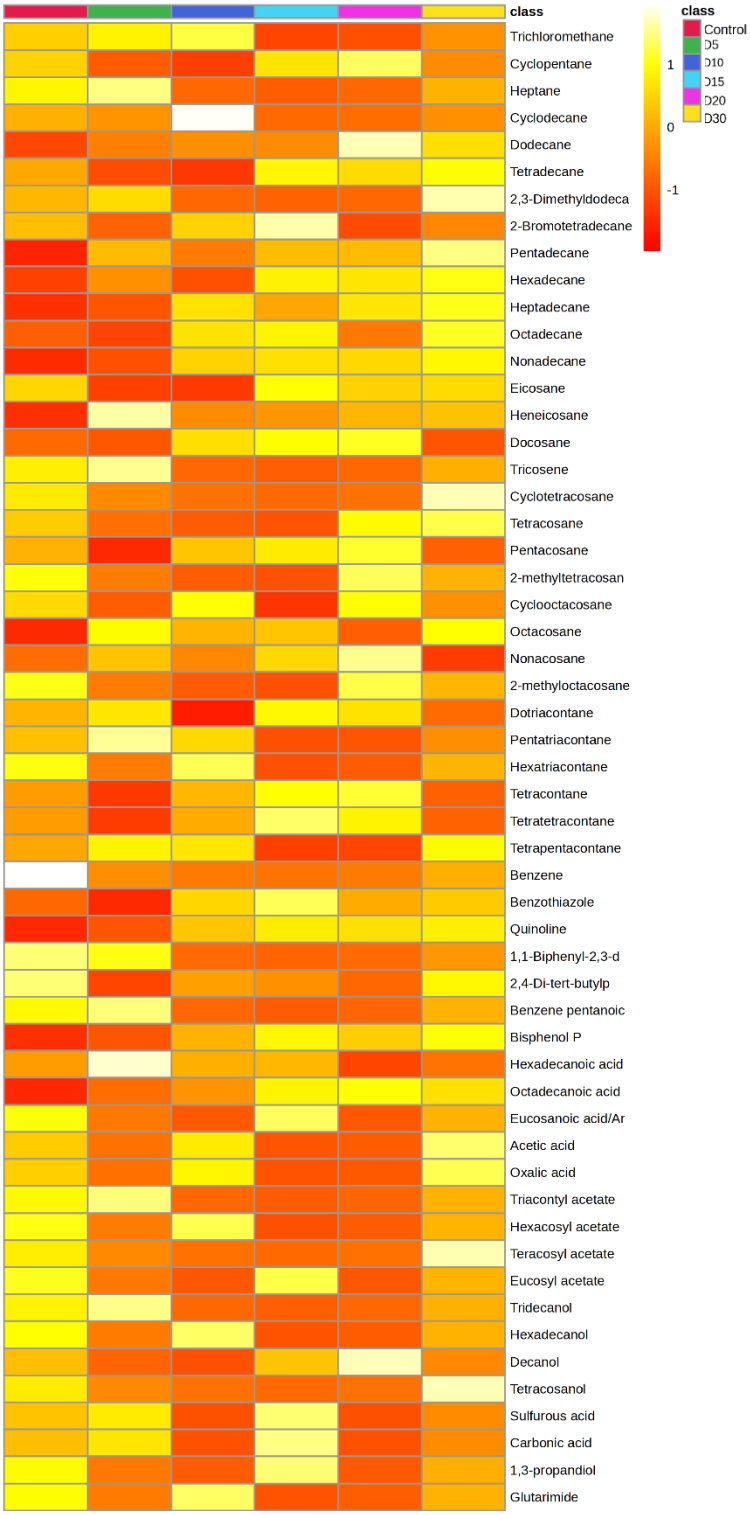

Figure 4.4 Heatmap showing the average clustering of component profiles of PSS myco-transformation products in control and treated samples at different exposure durations.

However, the concentration of other organic compounds were comparatively lesser at day 5 which suggest that at day 5, the catabolic action of fungus towards PSS were at its initial stage. The concentration of organic compoundss were observed to increase with the proceeding exposure duration. The highest concentration of alkanes (hexadecane, heptadecane, octadecane, dodecane, tetracontane, tetratetracntane, dotriacontane, pentacosane, octacosane and nonacosane), carboxylic acids (carbonic acid and sulfurous acid), esters (eucosyl acetate) and fatty acids (eucosanoic acid and octadecanoic acid) were observed at day 15. Similar to our observations, Jindrová et al. (2002) also reported that the microbial degradation of aromatic compounds essentially begins with their oxidation which further facilitates their subsequent conversion into organic compounds. Overall, the reported polystyrene degradation products including cyclopentane, octadecanoic acid, benzenepentanoic acid, etc indicated the catabolism of PSS into metabolically crucial intermediates [Sánchez et al. 2020; Amobonye et al. 2021].

Further, a correlation matrix of myco-transformation compounds was also generated using Pearson's correlation test in order to calculate the correlation coefficients between the myco-transformation compounds [Figure 4.5]. The results exhibited positive correlation of benzene with benzenepentanoic acid and 1’1-biphenyl-2’3-diol, while various organic components such as dodecanol was found to be positively correlated to alkanes including dodecane, hexadecane, tetradecane. Further, teracosyl acetate and hexacosyl acetate were also positively correlated to their respective alcohol derivatives. It is noteworthy that cyclic and acyclic alkanes such as cyclopentane, cyclotetralactosane, cyclotetracosane, cyclodecane, hexadecane, octadecane etc., undergo a series of oxidation reactions leading to the formation of corresponding dicarboxylic acids, which are further metabolized in the cell [Cheng et al. 2002]. These results indicate that complex fungal-mediated biochemical reactions occurred during the myco-transformation of PSS into organic compounds and supported the fungal growth and metabolism.

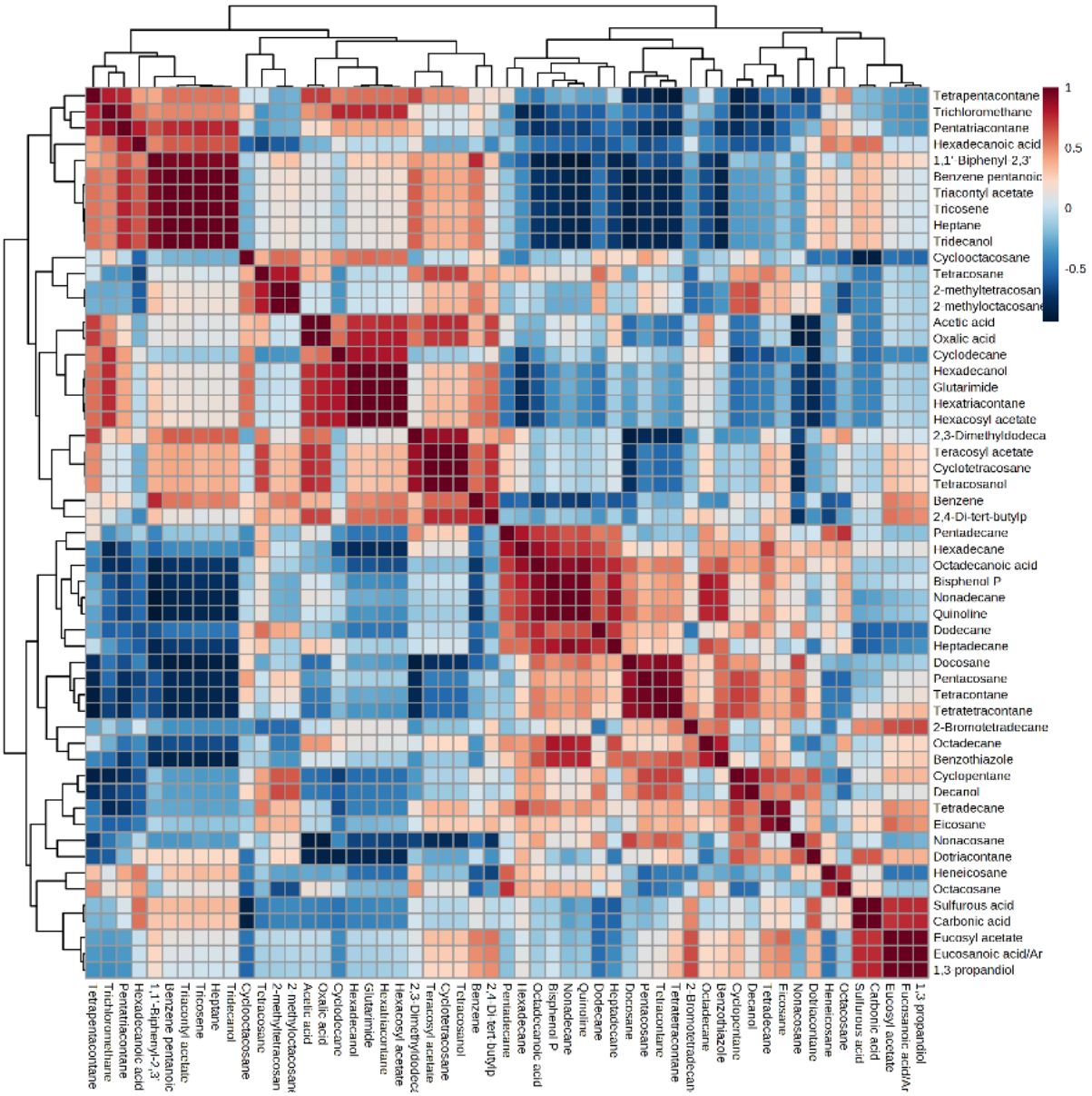

Figure 4.5 Correlation matrix of identified compounds in control and treated samples incubated for different exposure durations.

In summation, the biomass growth, Raman spectroscopy analysis and, myco-transformation compounds profile combinedly indicated that although the fungal mediated PSS myco-transformation continues till day 30, the process was paced down after 15 days. The obtained results suggest that maximum activity of *C. dactyloctenicola* VJP08 towards PSS utilization was at day 15 of incubation. Hence, day 15 was selected as the optimal exposure duration time.

4.3.3 Effect of Temperature

Temperature is one of the most key parameters for any microbial process as it centrally affects the rate of microbial metabolism by affecting the structure and activity of proteins [Tilton Jr et al. 1992]. Diverse and unique metabolic processes allow microbes to adapt to unfavourable environments. However, organisms cannot efficiently shield themselves from temperature in the way they can shield themselves from extreme external pH or salinity by maintaining steep concentration gradients over biological membranes. Hence, the microbes and their biomolecules must adapt to the temperatures of their surrounding environment [Engqvist et al. 2018]. Apart from microbial metabolism, temperature also affects the chemical kinetics of a biodegradation reaction including solubility, diffusion coefficients and volatilization of hydrocarbon constituents [Atlas, 1975]. Thus, temperature is a highly important factor for pollutant biodegradation in test systems and in the environment [Sjøholm et al. 2021]. Generally, most of the environmental microbes operate most effectively in the temperature range of 15-40°C [Yadav et al. 2012; Engqvist et al. 2018]. Hence, we chose three temperatures, i.e. 15°C, 28°C and 40°C to evaluate the efficiency of *C. dactyloctenicola* VJP08 towards myco-transformation of PSS.

The growth and PSS myco-transformation capacity of *C. dactyloctenicola* VJP08 was evaluated under different temperatures by monitoring the change in the fresh weight biomass [Table 4.2 b]. The fungus showed maximum growth when incubated at 28°C, which optimally supports the overall growth and metabolism in fungi. Maximum increase of 321.65% was observed in the biomass FW at 28°C, in comparison to other temperature conditions of 15°C and 40°C, under which the fungus showed biomass increase of 186.65% and 24%, respectively. These obtained results clearly indicated that the fungal metabolism become slow down at 15°C, while largely lags at 40°C. Similar results were observed when *C. dactyloctenicola* VJP08 was incubated in MSM+1% PSS, where the maximum increase of 73.8% was observed in the biomass FW at 28°C, while 36.65% and 13.3% increase was observed under incubation at 15°C and 40°C, respectively. Due to unavailability of any carbon source in only MSM treatment, the biomass FW was observed to decrease under all tested temperature conditions. Drastic decrease of 36.7% in biomass FW at 40°C, followed by 25.2% and 23.5% decrease in biomass FW was observed at 28°C and 15°C, respectively. Under nutrition starved conditions, the higher temperature of 40°C might have stimulated cell lysis, whereas the lower temperature of 15°C slowed down the fungal metabolism leading to the lesser decrease in the fungal biomass in comparison to that at 28°C.

Table 4.2 (b) Effect of temperature on the growth of *C. dactyloctenicola* VJP08. (Initial fungal biomass FW= 20 g; exposure duration= 15 days).

Treatment	Fungal Biomass FW (g)		
	15°C	**28°C**	**40°C**
MSM+3% Dextrose	57.3±2.9	84.3±1.4	24.8±1.3
Only MSM	14.9±0.4	15.3±0.6	12.6±0.6
MSM+1% PSS	27.3±0.8	34.7±1.1	22.6±1.8

± represents standard error

4.3.3.1 Raman Spectroscopy

In order to compare and analyse the changes in chemical fingerprint of PSS under different temperature conditions, Raman spectroscopy was performed, and the obtained graphs were stack plotted for analysis [Figure 4.6]. The key PSS peaks corresponding to aromatic C-H bands stretch (3227.27 and 3387.59 cm^{-1}) were found to show decrease at 15°C followed by 28°C. Highest intensity of $=CH_2$ and C-H deformation peak (2462.81 cm^{-1}) was observed at 15°C, indicating the slow utilization of PSS by *C. dactyloctenicola* VJP08 due to slow fungal growth at this temperature. Additionally, a greater number of new peaks at 957.696, 1042.69, 1209.58, 1307.78, 1537.24, 1798.66, 1873.06 and 2018.47 cm^{-1} were observed at day 15°C as compared to other temperatures. These bands correspond to aromatic bending (957.696 cm^{-1}), C-CH_3 stretch or SO_3 stretch (1042.69cm^{-1}), sulfonic acid or free acid SO_2 (1209.58 cm^{-1}), CH bending (1307.78 cm^{-1}), CCH ring quadrant (1537.24 cm^{-1}), −C=O stretch (1798.66 cm^{-1}), anhydrides such as SO_3 derived from PSS (1873.06 cm^{-1}) and -CH deformation (2018.47 cm^{-1}) [Edwards et al. 2000; Yuniarto et al. 2016]. The appearance of these new peaks indicates that although the PSS transformation took place at 15°C, the generated by-products tend to accumulate and were slowly utilized by *C. dactyloctenicola* VJP08 due to slow fungal growth at 15°C. Previous studies also reported that at low temperatures, mould fungi show slow growth rate as formation of a unit of biomass consume more energy at 15°C [Li et al. 2009].

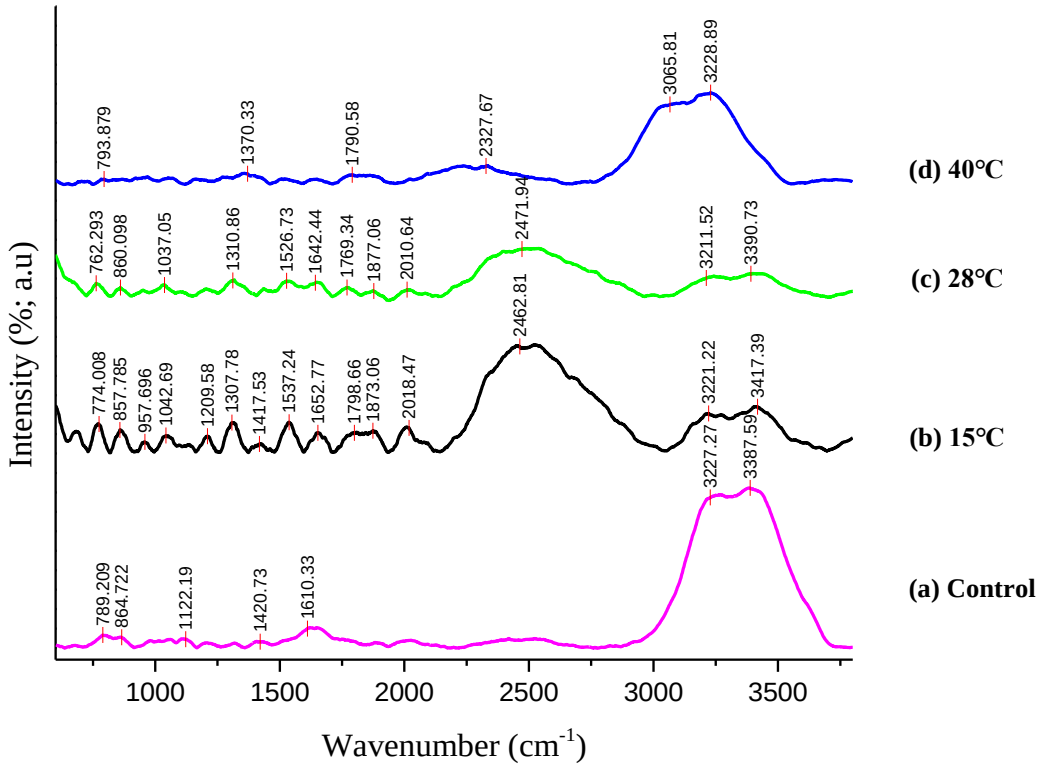

Figure 4.6 Raman spectra of (a) control; (b-d) treatment containing MSM+ 1% PSS samples exposed to *C. dactyloctenicola* VJP08 at 15°C, 28°C and 40°C, respectively.

In comparison to control sample, the intensity of PSS corresponding key peaks at 1610, 3277 and 3387 cm^{-1} were found to decrease significantly the test sample incubated at 28°C. The peaks at 1122.19 and 1420.73 cm^{-1} corresponding to C-C stretch and CH_2 scissoring were observed to be absent in the test sample incubated at 28°C. However, newly generated peaks corresponding to C-CH3 (1037 cm^{-1}), SO_2- asymmetric stretch (1310 cm^{-1}), aromatic ring quadrant (1528 cm^{-1}), −C=O stretch (1798.66 cm^{-1}), anhydrides such as SO_3 derived from PSS (1877.06 cm^{-1}) and -CH deformation (2018.47 cm^{-1}) were observed indicating that *C. dactyloctenicola* VJP08 enabled PSS myco-transformation at 28°C. In contrast, at 40°C, relatively less decrease in the intensity of peaks corresponding to aromatic C-H bands stretch (3065.81 and 3228.89 cm^{-1}) was observed which indicated that due to higher temperature, there was lower -CH deformation in the PSS by fungal action. The obtained results implied that the temperature has a significant influence on the metabolic efficiency and growth rate of fungi under cultural conditions [Venkatachalan et al. 2019]. Further, as compared to other temperatures (15°C and 40°C), based on the maximum decrease in the intensities of PSS corresponding peaks 28°C was selected as the most favourable temperature for fungal-

mediated action over PSS. These results were also aligned with the maximum fungal biomass FW which was observed at 28℃, followed by 15°C and 40°C, respectively (Table 4.2 b).

4.3.3.2 Myco-transformation Compounds Analysis

To further investigate the compounds generated during myco-transformation of PSS at different temperature conditions, the treatment extracts were subjected to GC-MS/MS analysis. The profiling resulted in identification of a total 3 compounds in control sample. In comparison, total 30 (at 15℃), 43 (at 28℃) and 28 (at 40℃) compounds were observed in treatment containing MSM+1% PSS with fungal biomass, respectively. Among all compounds, alkanes were the most dominating class followed by PSS derived aromatic compounds, fatty acids, carboxylic acids, esters and alcohols in all the temperature conditions [Figure 4.7]. Diverse range from C_5 to C_{60} were observed in alkanes, among which tetradecane, heptadecane, octadecane, eicosane, heneicosane, octacosane, nonacosane, tetracontane and tetratetracontane were commonly found in all the tested temperature conditions. A total of 69 compounds were identified, of which, 23 compounds were uniquely present in different temperature conditions.

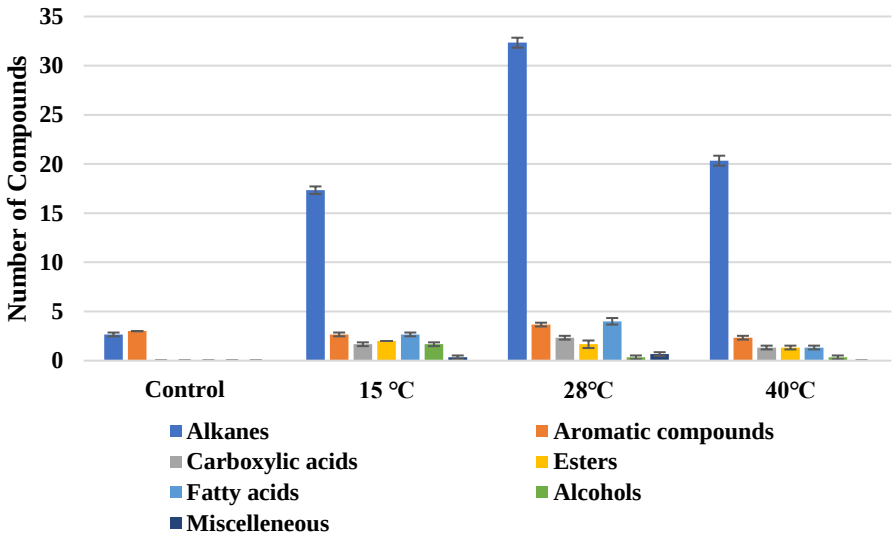

Figure 4.7 Proportion of different compounds generated during myco-transformation of PSS by *C. dactyloctenicola* VJP08 at different temperature conditions.

The 2D PCA scores plot displayed grouping of treated samples incubated at different temperatures, while the control sample displayed clear separation, indicating that although at different magnitudes, PSS was transformed in the treated samples at all the tested temperatures [Figure 4.8 A]. Additionally, the VIP plot clearly indicated that organic compounds such as heptadecane, octadecane, eicosane, heneicosane, etc generated during the myco-transformation

process were found in higher concentrations in the treated samples [Figure 4.8 B]. In order to separately evaluate the process of myco-transformation at different temperatures, multivariate VIP plot was analysed, which revealed variable presence of compounds at tested temperatures [Figure 4.8 C]. Alcohols and esters were found to be dominated at 15℃, while alkanes were more at 28℃ and 40℃, respectively.

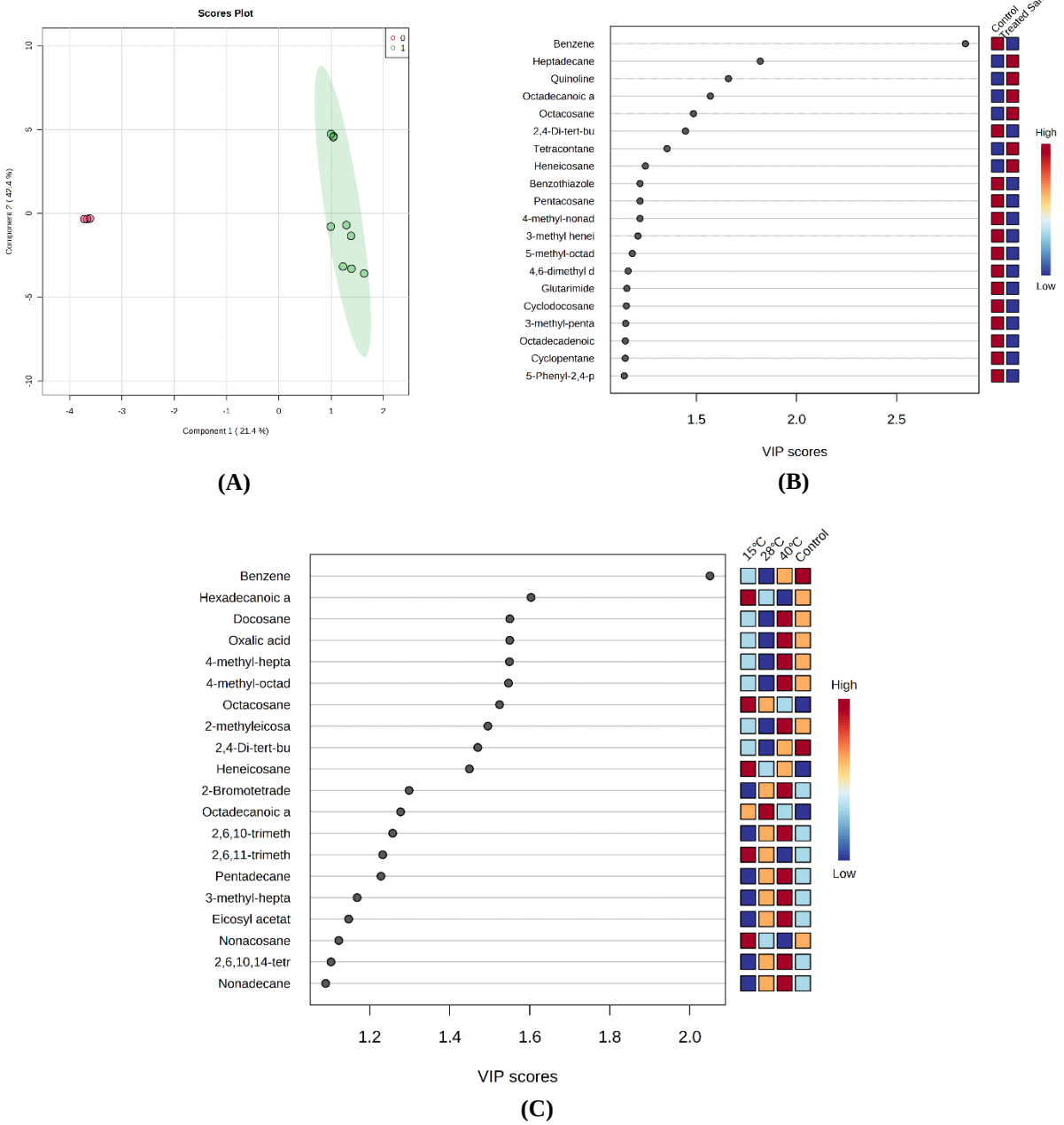

Figure 4.8 (A) 2D-PCA score plot demonstrates statistical clustering of control (shown in red) and treated samples (shown in green); (B) Univariate VIP score plot of top 20 identified compounds under untreated MSM+1% PSS; and treated samples at different temperatures; (c) Multivariate VIP score plot of top 20 identified compounds in control; and treated samples at different temperatures.

Further, the detailed expression of component profile of fungal-mediated PSS transformation across different temperature conditions can be clearly observed in the heatmap [Figure 4.9]. The heatmap clearly indicates higher amount of alkanes such as cyclopentane, pentacosane, cyclodocosane, 4,6-dimethyl dodecane, 3-methyl heneicosane, 3-methyl pentadecane, etc were majorly present in the treatment supernatant incubated at 28℃, while 2,3-dimethyl dodecane, 2,6,10-trimethyldodecane, 6-cyclohexyl tridecane, 2-methyl-tetracosane and pentatriacontane were present in the samples incubated at 15℃, and methylated forms of eicosane such as 2-methyl eicosane, 4-methyl heptadecane and 4-methylated octadecane were uniquely present in the samples incubated at 40℃. The myco-transformation compounds analysis by Raman spectroscopy also revealed higher concentration of sulfurous acid in fungal treated samples incubated at 15℃ and 28℃. Fatty acids such as hexadecenoic acid, octadecanoic acid were also found in the samples incubated at 15℃ and 28℃, while octadecadenoic acid and eicosanoic acid were only found at 28℃. However, treatment incubated at 40℃ displayed presence of only one fatty acid, namely octadecanoic acid. As observed in the heatmap, the least amount of PSS-derived organic compounds were found in the fungal treated samples incubated at 40℃, whereas the highest amount of organic compounds were found in samples incubated at 15℃ and 28℃. It indicates that PSS was transformed at these temperatures by *C. dactyloctenicola* VJP08. The obtained results are in correlation with the change in fungal biomass FW as well as with the results of Raman spectroscopy analysis. The correlation matrix also indicated close association of various organic compounds [Figure 4.10]. Various alkanes such as pentadecane, heptadecane, octadecane and nonadecane and docosane were found to be positively correlated to their methylated forms. For instance, pentadecane was found to be positively correlated with its 2-methyl pentadecane, 6-methyl pentadecane and 2, 6, 11-methylpentadecane, while heptadecane, octadecane, nonadecane and docosane were positively correlated to 2-methyl heptadecane, 3-methyl heptadecane, 3-methyl/4-methyl octadecane, 4-methyl/2,3-dimethyl nonadecane, 2,21-dimethyl/2, 6, 10 trimethyl, 2, 6, 11 trimethyl docosane, respectively.

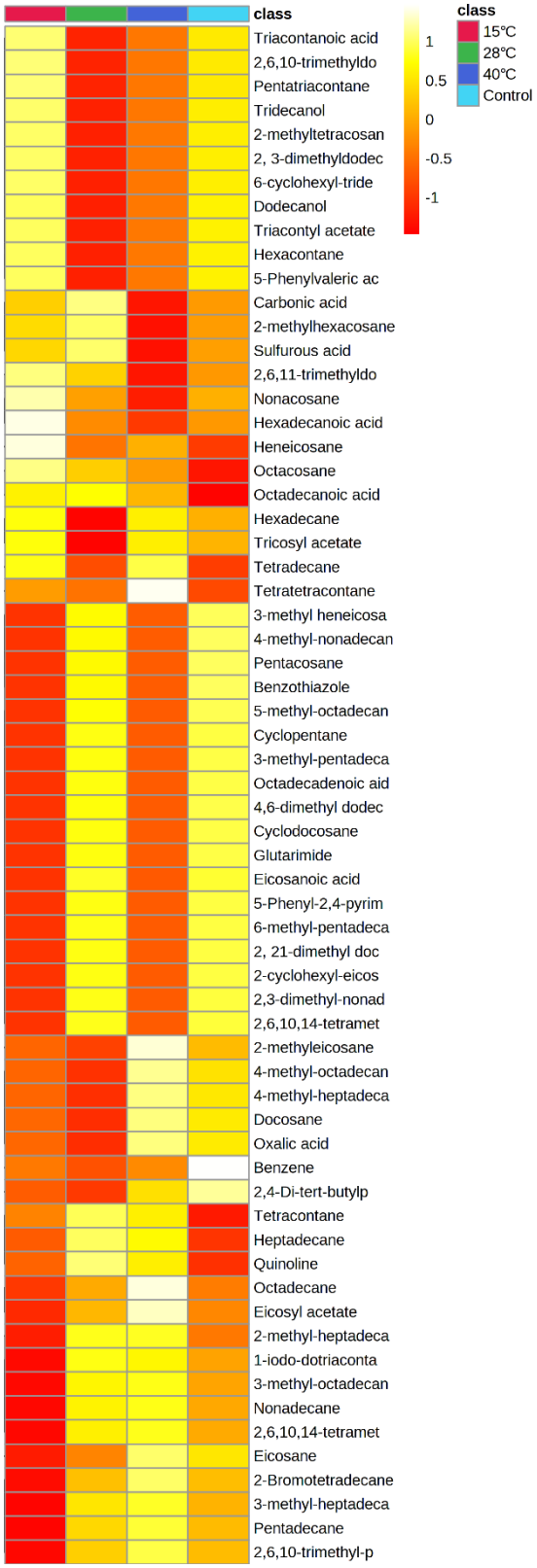

Figure 4.9 Heatmap showing the average clustering of component profiles of PSS myco-transformation products in control and treated samples at different temperature conditions.

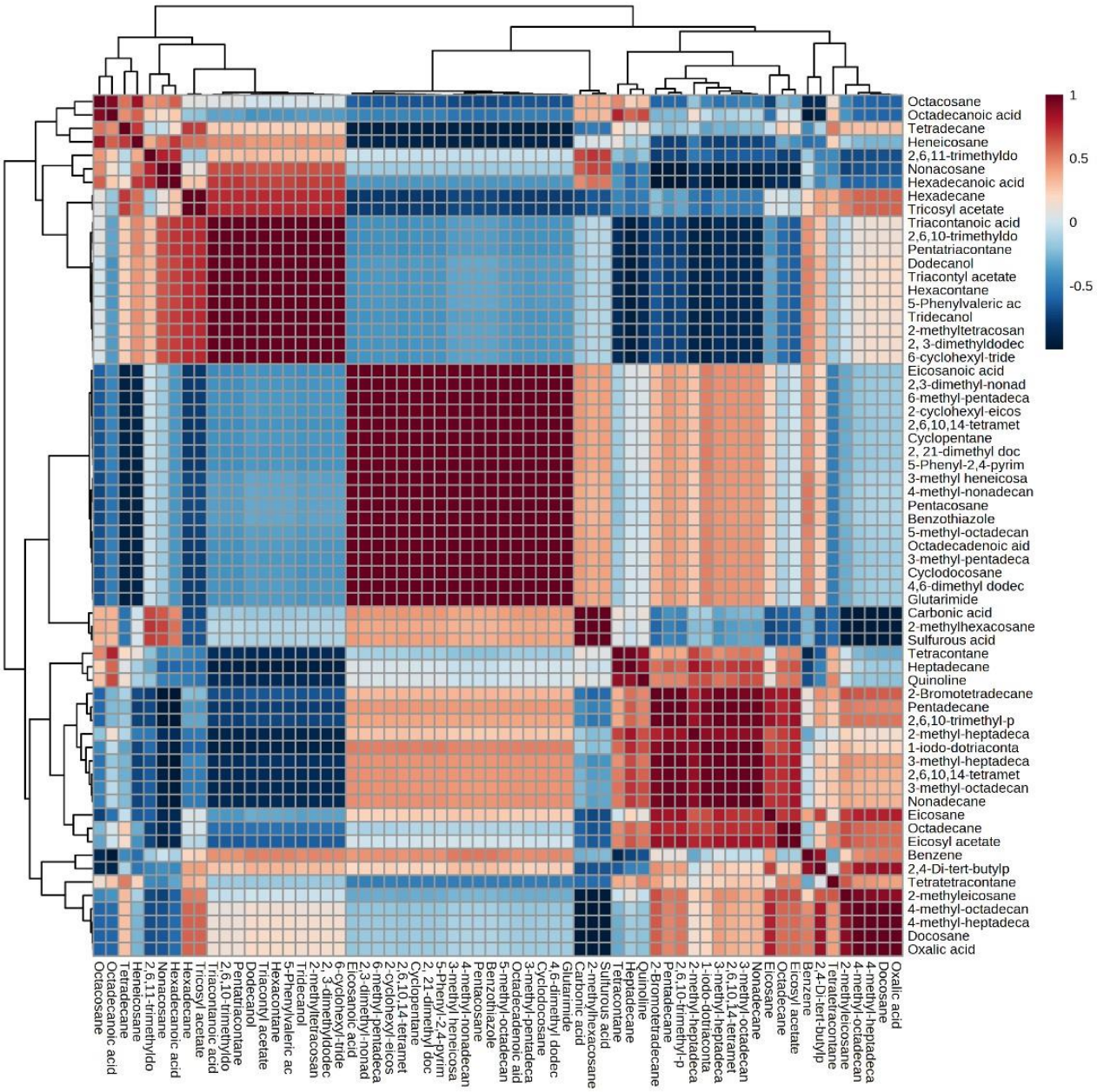

Figure 4.10 Correlation matrix of identified compounds in control and treated samples incubated at different temperature conditions.

Additionally, benzene was positively corelated to one of its derivatives namely, 2,4-DTBP, and other organic compounds such as cyclopentane and cyclodocosane indicating that these cyclic compounds were generated from aromatic benzene ring via fungal-mediated action. These results strongly indicate that various fungal-mediated biochemical reactions resulted in the transformation of PSS into bioactive organic compounds, which actively participated in catabolic and anabolic metabolism that supported fungal growth. Additionally, the results also highlight that fungal metabolism has a different pace at different tested

temperature conditions. In comparison to 28℃, the fungal growth and PSS utilization was found to be slightly slower at 15℃, whereas the least transformation was observed at 40℃, indicating that although *C. dactyloctenicola* VJP08 has the ability to survive and transform PSS (as sole carbon source) at all the tested temperatures, it functions optimally at 28℃. Hence, 28℃ was selected as the optimal temperature to monitor the effect of pH on PSS transformation by *C. dactyloctenicola* VJP08.

4.3.4 Effect of pH

In comparison to other microorganisms, fungi are capable to grow and develop over wide pH ranges. For example, *Aspergillus nidulans and Botrytis cinerea, etc* have been reported to grow in pH ranging from 2.5 to 9.0 [Manteau et al. 2003]. This is because fungi can actively modulate the pH of surrounding environment by secreting acids or alkali [Landraud et al., 2013; Vylkova, 2017]. During the infection process of phytopathogenic fungi, the pH of infected cuticle rises from about 6.3 to 7.7, which is required for the regulation of cuticle-degrading enzymes [Leger et al. 1998].

Considering the importance of pH, the growth and PSS myco-transformation efficiency of *C. dactyloctenicola* VJP08 was studied in pH ranging from 5 to 8 (including the standard pH of MSM media i.e. 7.0±0.2) by monitoring the change in the fungal biomass FW. *C. dactyloctenicola* VJP08 showed maximum growth with an increase of 321.65% at pH7.0±0.2 in MSM+ 3% dextrose treatment, followed by 196.65%, 161.65%, 193.3%, 158.3% and 148.3% at pH 5.0, 5.5, 6.0, 6.5 and 8.0, respectively [Table 4.2 c]. The growth at pH 5.0 and 6.0 as well as pH 5.5 and 6.5 were found to be significantly similar, while the least growth was observed at pH 8.0. Similar trend was observed in case of MSM+1% PSS treatments in which the highest growth of 73.8% was observed at pH 7.0, while ~31% and ~22% increase were observed at pH 5.0/6.0/8.0 and pH 5.5/6.5, respectively. These observations indicated that *C. dactyloctenicola* VJP08 supports versatile growth pattern under nutrient challenging conditions along acidic to alkaline medium. Furthermore, while incubation in only MSM, *C. dactyloctenicola* VJP08 displayed consistent decrease in the biomass FW at the tested pH which may be due to nutrient starvation. However, only on the basis of change in the biomass FW, it was difficult to clearly delimitate the effect of pH on myco-transformation capacity of *C. dactyloctenicola* VJP08. Hence, for further analysis Raman spectroscopy was performed for all the samples exposed to different pH conditions.

Table 4.2 (c) Effect of pH on the growth of *C. dactyloctenicola* VJP08. (Initial fungal biomass FW= 20 g; exposure duration= 15 days; temperature 28°C).

Treatment	Fungal Biomass FW (g)					
	pH 5.0	**pH 5.5**	**pH 6.0**	**pH 6.5**	**pH 7.0**	**pH 8.0**
MSM+3% Dextrose	59.3±4.0	52.3±2.4	58.6±2.3	51.6±2.6	84.3±1.4	49.6±1.7
Only MSM	14.3±0.6	13.0±0.4	14.0±1.08	14.6±0.6	14.9±0.4	13.0±0.7
MSM+1% PSS	26.3±1.0	23.3±1.3	26.3±2.3	24.3±0.6	34.7±1.1	27.6±1.8

± represent standard error

4.3.4.1 Raman Spectroscopy

Figure 4.11 depicts the changes in the signature peaks of PSS at different pH which are represented in the form of stack plot. As observed in the Raman spectra of exposure duration, the PSS peaks corresponding to aromatic C-H bands stretch (3235.36 and 3408.78 cm^{-1}) showed a wavenumber shift (3043.37 and ~3230 cm^{-1}), as a result of altered strength of corresponding chemical bonds indicating the deformation of PSS aromatic rings by *C. dactyloctenicola* VJP08. In addition, the appearance of $=CH_2$ and C-H deformation peaks in the range of 2000-2400 cm^{-1} were also observed across pH 5.0-8.0. Similarly, as observed in previous sections (4.3.2.1 and 4.3.3.1), newly generated peaks at ~805.542, 934.85, 1042.69, 1165.47, 1209.58, 1301.27, 1535.17, 1775.45, 1885.05 and 2283.75 cm^{-1} were also found in all pH treatments, with an exception of peaks at ~1156 and ~1301 cm^{-1} corresponding to C-C stretch and SO_2-asymmetric stretch which were absent in pH 5.0 and 8.0 indicating that either SO_2 was consumed by the fungus; or SO_2 was not released. The newly generated peaks indicate that *C. dactyloctenicola* VJP08 is functionally capable to transform PSS at a wide pH range. However, the peaks at ~3043.38 and ~3223 cm^{-1} corresponding to aromatic C-H band stretch were observed to show the highest decrease in peak intensities at neutral conditions corresponding to pH 7.0.

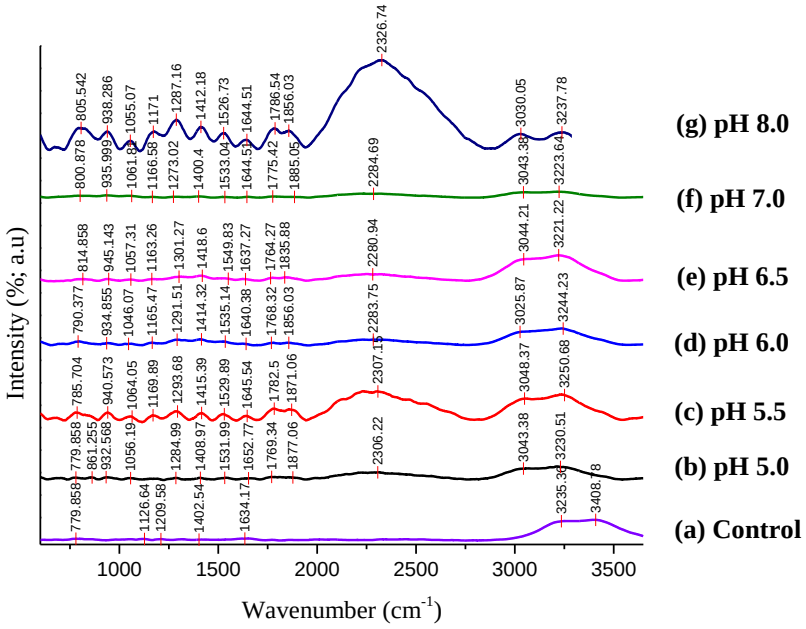

(A)

Figure 4.11 Raman spectra of (a) control; (b-g) treatment containing MSM+ 1% PSS samples exposed to *C. dactyloctenicola* VJP08 at pH 5.0, 5.5, 6.0, 6.5, 7.0 and 8.0, respectively.

4.3.4.2 Myco-transformation Compounds Analysis

The component profile of *C. dactyloctenicola* VJP08 incubated in MSM+1% PSS with pH varying from 5.0 to 8.0 revealed that there were a total of 101 myco-transformation compounds generated in the samples among which 55 were common and 46 were unique at different pH conditions [Figure 4.12]. Similar to other process parameters (exposure duration and temperature), alkane was found to be the most dominating class across the tested pH range. The highest number of alkanes (42) were found to be generated in the sample kept at pH 5.0, followed by pH 7.0 (35), pH 5.5 (34), pH 6.0 (32), pH 8.0 (30) and pH 6.5 (20), respectively. However, the overall component profile was found to be metabolically less diverse at pH 5.0 in comparison to other pH treatments. Furthermore, the 2D PCA scores plot exhibited distinct separation of both control and treatment samples and depicted clustering of all the fungal incubated samples at different pH [Figure 4.13 A]. The results indicated that *C. dactylcotenicola* VJP08 has the ability to successfully transform PSS, present as sole carbon source, into organic components to be utilized for fungal growth and metabolism. The univariate VIP plot clearly indicated the presence of PSS-derived and other fungal-generated organic compounds in treated MSM+1% PSS samples with fungal biomass [Figure 4.13 B]. However, the multivariate VIP analysis indicated mixed proportion of components across different treatment pH range [Figure 4.13 C].

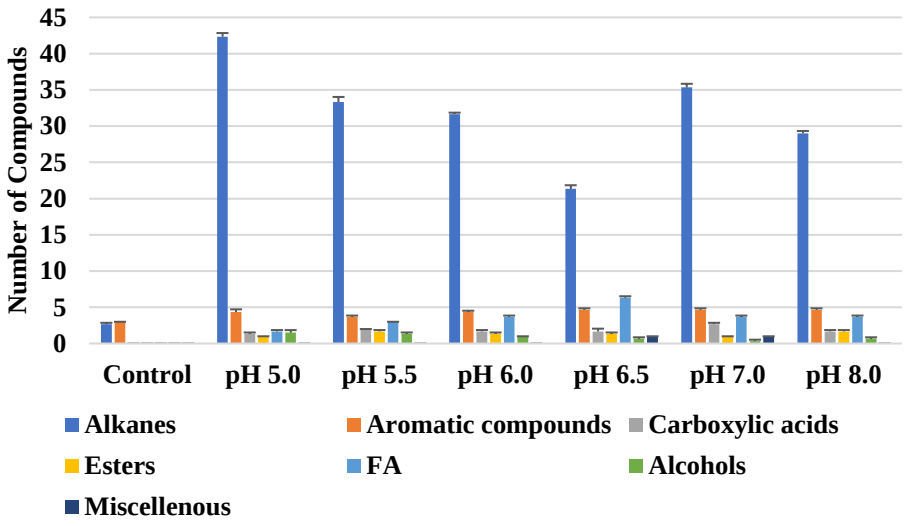

Figure 4.12 Proportion of different compounds generated during myco-transformation of PSS by *C. dactyloctenicola* VJP08 at different pH range.

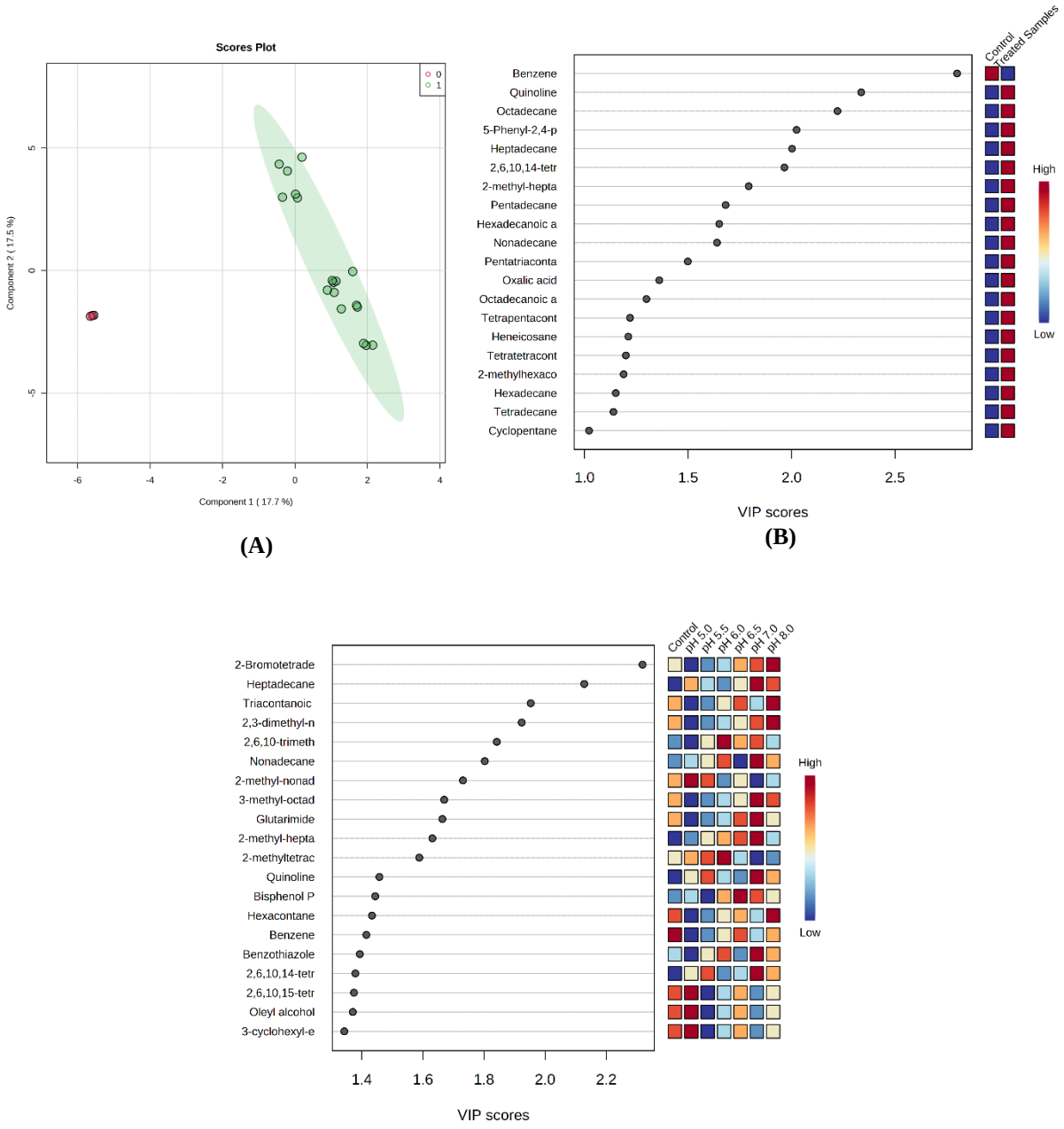

Figure 4.13 (A) 2D-PCA score plot demonstrates statistical clustering of control (shown in red) and treated samples (shown in green); (B) Univariate VIP score plot of top 20 identified compounds under untreated MSM+1% PSS; and treated samples at different pH; (C) Multivariate VIP score plot of top 20 identified compounds in control; and treated samples at different pH.

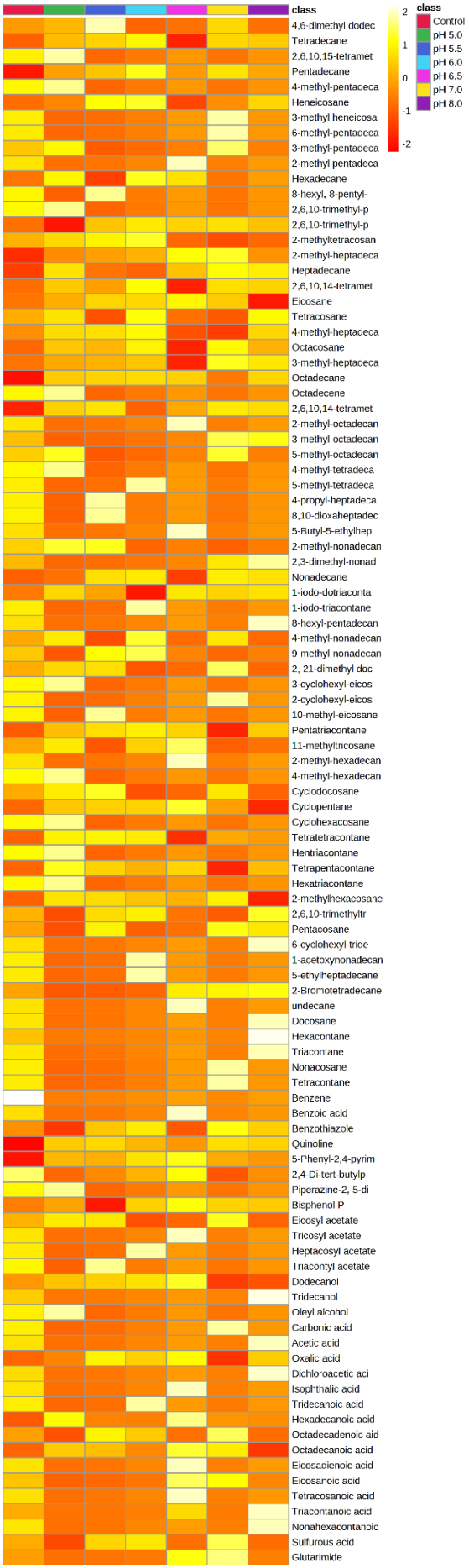

The heatmap further confirmed the variations and clustering of compounds geerated across different pH conditions [Figure 4.14]. Some of the common components include methylated and simple alkanes such as pentadecane, hexadecane, heptadecane, octadecane, nonadecane, heneicosane, eicosane, tetratetracontane, tetrapentacontane, cyclopentane, 2/3-methyl heptadecane, 2-methyl tetracosane; fatty acids such as hexadecenoic acid, octadecanoic acid, octadecadenoic acid, and eicosanoic acid; and benzene derivatives such as benzothiazole, quinoline, 5-Phenyl-2,4-pyrimidinediamine, 2,4-Di-tert-butylphenol etc. in the treated samples at different pH. Whereas some of the methylated alkanes, esters and fatty acids were unique to specific pH conditions.

Figure 4.14 Heatmap showing the average clustering of component profiles of PSS myco-transformation products in control and treated samples at different pH.

Careful analysis suggests that 4-methylpentadecane/hexadecane/ tetradecane, 5-methyl octadecane, cyclohexacosane, hentriacontane, hexatriacontane, oleyl alcohol, piperazine-2,5-dione were uniquely present in fungal treated samples incubated at pH 5.0. Whereas methylated heptadecane/ eicosane/ tridecane/ pentacosane and triacontly acetate were uniquely present in samples at pH 5.5. In addition to methylated, ethylated and acetoxy-alkanes, heptacosyl acetate and tridecanoic acid were found to be uniquely present in samples incubated at pH 6.0 treatments. In addition to methylated alkane, diverse types of fatty acids including eicosadienoic acid, tetracosanoic acid and triacontanoic acid as well as benzene derivative such as benzoic acid and isophthalic acid were found in samples incubated at pH 6.5. At pH 7.0 and pH 8.0, the unique alkanes were majorly found to be methylated. In comparison to other treatment conditions, treatments at pH 7.0 displayed higher collective proportions of alkanes and fatty acids, whereas, treatments at pH 5.0 and pH 6.5 displayed the abundance of only a single compound class (either alkanes or fatty acids).

Although differently modified alkanes and other organic compounds were present in different pH treatments, the correlation matrix analysis displayed varied pattern of interrelations between these components [Figure 4.15]. PSS-derived benzothiazole displayed positive correlation with other transformed compounds including sulfurous acid, octadecanoic acid and alkanes of varied chain length alkanes (C_{15}-C_{24}) such as pentadecane, tetradecane, pentacosane, octacosane, tetracosane, etc. While long-chain tetracontane (C_{40}) was found to be positive correlated with comparatively short-length alkanes including 6-methyl pentadecane, 3-methyl heptadecane, 3-methyl heneicosane, nonacosane and pentacosane, indicating that short-chain length alkanes would have originated from the long chain alkanes via different biochemical reactions by the action of fungal exo-enzymes.

The obtained results suggested that although *C. dactyloctenicola* VJP08 was able to transform PSS under wide pH range, the most significant transformation was observed at pH 7.0.

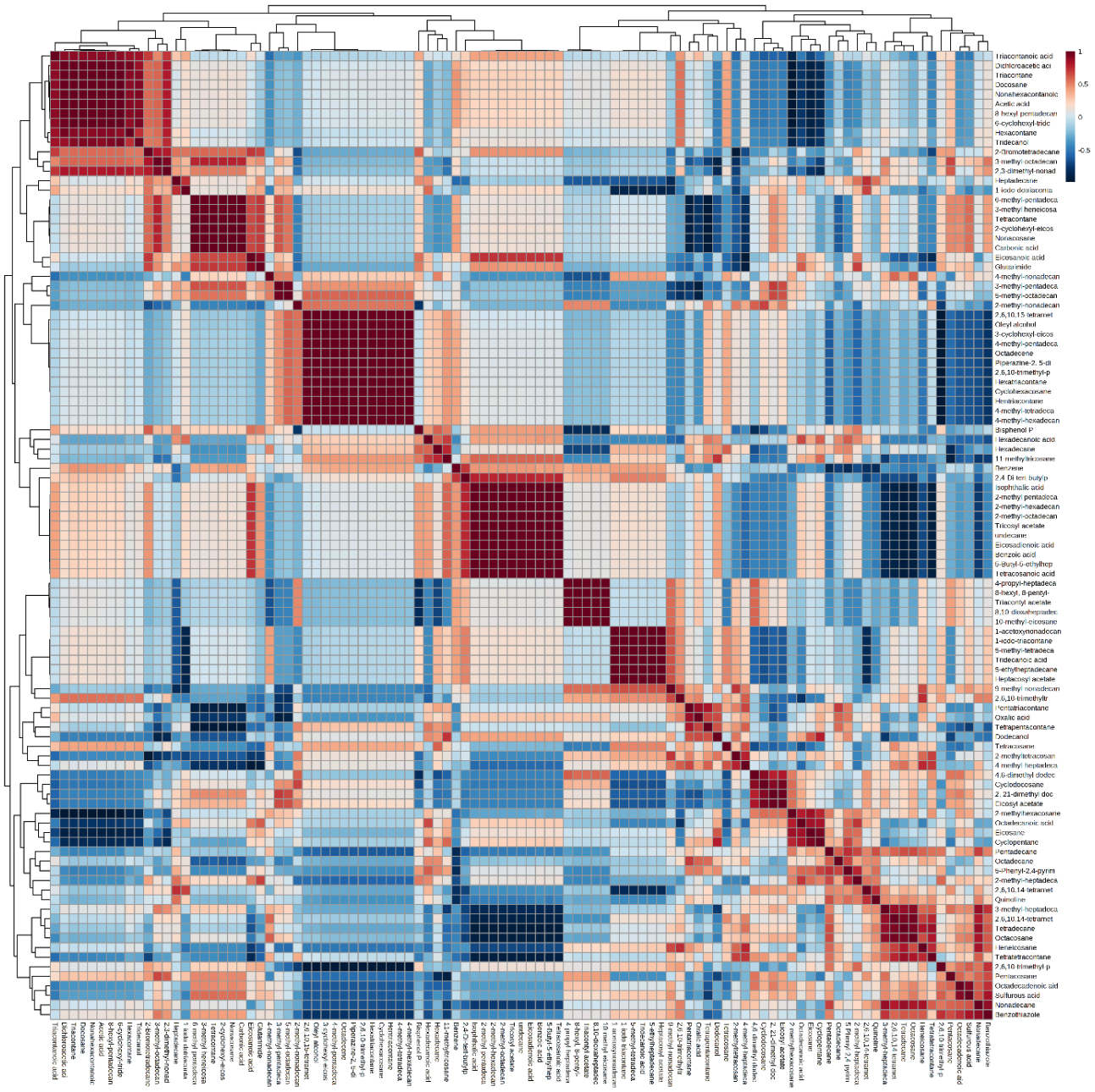

Figure 4.15 Correlation matrix of identified compounds in control and treated samples incubated at different pH.

4.4 Protein Precipitation and One-Dimensional Gel Electrophoresis

Fungi are considered natural decomposers and secrete large amount of extracellular enzymes which have the ability to degrade varied complex macromolecules (nutrient sources) into smaller units and help them to survive in harsh environment under low nutrient conditions [Jeyakumar et al. 2013; Sánchez et al. 2020; El-Gendi et al. 2022]. Since the polymeric molecules need to be broken down into oligomers/monomers (which are comparatively easier to be utilized), extracellular enzymes represent crucial functional components for monitoring such processes [Zhao et al. 2021; Bhanot et al. 2023]. In order to examine the role of extracellular enzymes in PSS transformation, it was important to understand the extracellular protein profile of *C. datyloctenicola* VJP08 under different growth treatments, namely MSM+3% dextrose, only MSM and MSM+1% PSS. The cell-free filtrate displayed significant difference in the concentration of total extracellular proteins under different treatment conditions [Table 4.3].

Table 4.3 Extracellular protein concentration (µg mL^{-1}) of *C. dactyloctenicola* VJP08 in tested treatments at varied exposure duration.

Treatments	**Total extracellular proteins (µg mL^{-1})**				
	D5	**D10**	**D15**	**D20**	**D30**
MSM+3% Dextrose	284.4±19.1	-	-	-	-
Only MSM	177.3±18.1	256.3±26.0	279.3±18.5	228.3±21.1	285.6±12.7
MSM+1% PSS	344.0±12.0	264.4±32.9	278.6±18.7	308.3±40.7	233.3±13.5

D= days; ± represent standard error

The concentration of total extracellular protein was found to be highest in treatment with MSM+1% PSS (344.0 µg mL^{-1}) at day 5. The protein concentration was found to decreased by day 10 and remained broadly constant till day 15, after which a slight increase was observed at day 20, followed by a steep decline at day 30. The observed variation in the protein concentration may be explained such that during the initial exposure duration of 5 days, the fungus released large amount of different proteins to get carbon source from surrounding environment, after which only selected proteins were secreted that were capable in myco-transformation of PSS. However, during the prolonged exposure (20 days), possibility of rupturing a few fungal cells cannot be ignored which could be leading to would have been

ruptured leading to the release of internal cellular proteins causing the increase in total protein concentration. It is also in correlation to the changes observed in fresh weight biomass, which was found to exponentially increase by day 15 followed by decrease till day 30 (Table 4.2 a). At this point, it is important to emphasize that our method does not claim to have extracted all the proteins but only those that were being released and remained stable (not degraded) under the experimental conditions. It could also be possible that the presence of secreted hydrolytic enzymes might have led to degradation of proteins in substantial amounts.

The total extracellular protein profile revealed the presence of varied band patterns across different treatments. For instance, the treatment MSM+3% dextrose showed six distinct protein bands ranging from molecular weight from 14.4 kDa to ~80 kDa [Figure 4.16 A, Lane 2]; while almost similar protein bands were observed in MSM+1% PSS treatment at day 10 and 15, wherein total fourteen discrete bands ranging from ~15.0 kDa to ~90.0 kDa and twelve bands ranging from 60.0 kDa to ~150 kDa, respectively [Figure 4.16 B & C, Lane 2]. Total twenty-three distinct protein bands were observed in MSM+1% PSS treatment at the exposure duration of 20 days ranging from molecular weight of ~11.0 kDa to ~150.0 kDa [Figure 4.16 D, Lane 2]. However, the total number of bands observed at day 30 decreased to12, ranging from ~14 kDa to ~100.0 kDa [Figure 4.16 E, Lane 2]. These results highlight that the PSS transformation ability of *C. dactyloctenicola* VJP08 gets significantly affected by longer exposure duration of 30 days. Hence, the protein sample of day 30 not considered for further proteomics analysis. Noteworthy, the protein bands at ~14.0 kDa, ~37 kDa and ~60-70 kDa (indicated in box) were found to be consistent throughout day 10 to 30 which indicated their possible role in PSS myco-transformation. Among these, the protein band between 14.4 kDa to 18.4 kDa was also present in MSM+3% dextrose treatment. It could be hypothesised that this protein is either a housekeeping or a multi-functional protein. It is important to emphasize that due to extreme jelly-like consistency of extracellular proteins in the cell-free filtrate at day 5, the protein bands could not be resolved through SDS-PAGE and hence, were directly identified using proteomics approach.

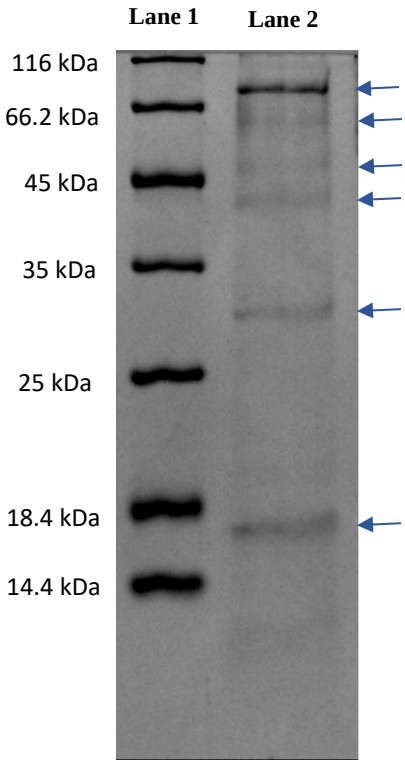
Lane 1
Lane 2
116 kDa
66.2 kDa
45 kDa
35 kDa
25 kDa
18.4 kDa
14.4 kDa

(A)

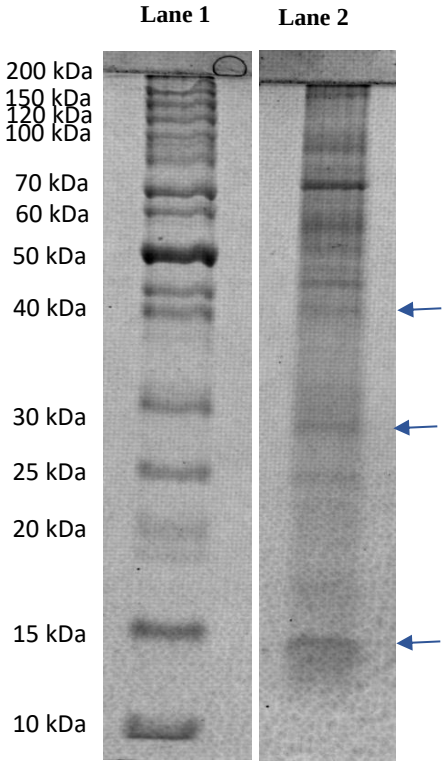
Lane 1
Lane 2
200 kDa
150 kDa
120 kDa
100 kDa
70 kDa
60 kDa
50 kDa
40 kDa
30 kDa
25 kDa
20 kDa
15 kDa
10 kDa

(B)

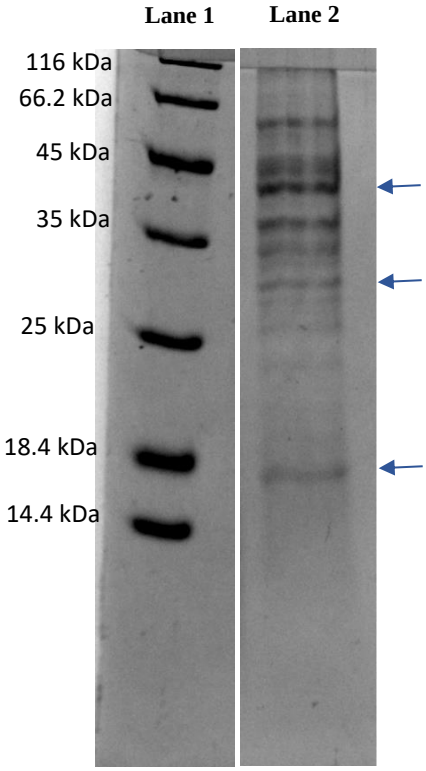
Lane 1
Lane 2
116 kDa
66.2 kDa
45 kDa
35 kDa
25 kDa
18.4 kDa
14.4 kDa

(C)

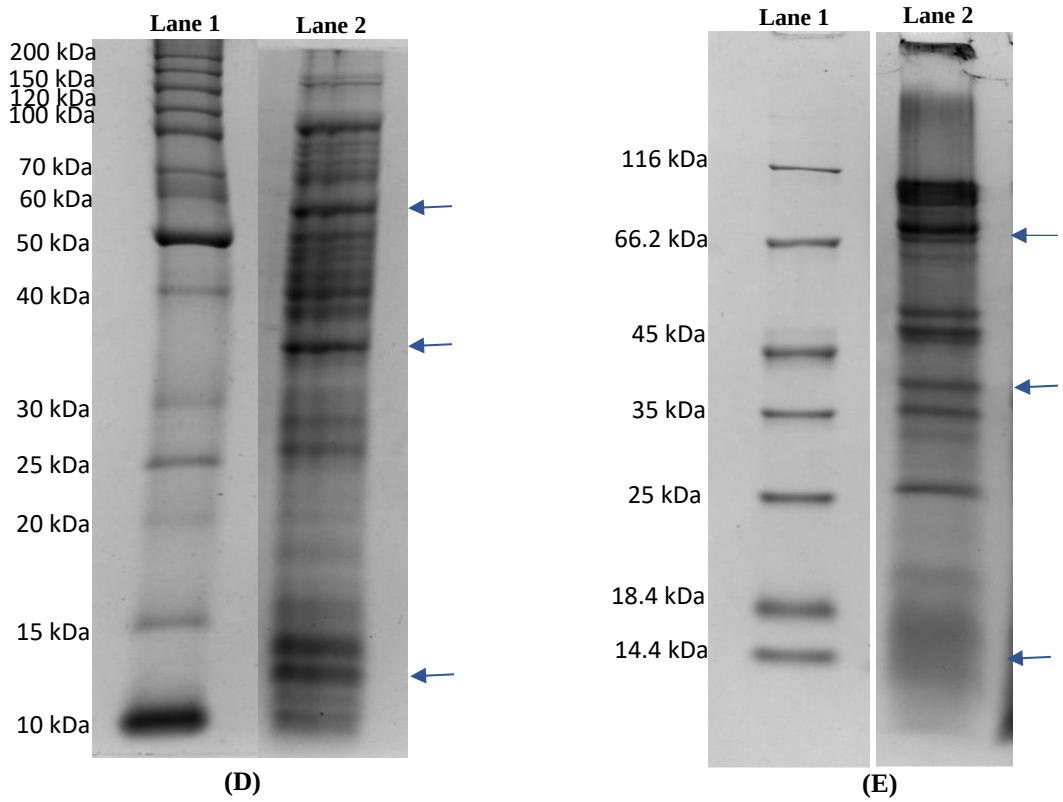

Figure 4.16 SDS-PAGE analysis of extracellular proteins secreted from *C. dactyloctenicola* VJP08 incubated in MSM+3% dextrose (A) and MSM+1% PSS incubated at different exposure duration at day 10 (B), 15 (C), 20 (D) and 30 (E). Lane 1 represents molecular size marker and lane 2 represents fungal extracellular protein sample.

4.5 Conclusion

The present study divulges the potential of phylloplane fungi of xerophytic plants towards myco-transformation of PSS, which is a structural analogue of PS. Out of 20 fungal isolates, *C. dactyloctenicola* VJP08 showed highest growth increase (~52%) in the fungal biomass FW after 30 days' exposure to PSS as sole carbon source which indicated its potency to utilize carbon from the aromatic structure of PSS. Further, independent variables, viz. exposure duration, temperature, and pH were set in the range of 5-30 days, 15-40°C, and 5-8 pH, respectively to evaluate the fungal response towards PSS myco-transformation by monitoring the change in biomass FW, chemical & myco-transformation compounds composition, and protein expression. The obtained results suggested that 28 °C temperature, pH 7.0, and exposure duration between 15 to 20 days were optimum for PSS myco-transformation. The higher concentration of total extracellular proteins in the MSM+1% PSS treatment in comparison to control (only MSM) illustrated their possible role in the myco-transformation of PSS. The extracellular protein profile showed varied band pattern at different exposure durations. The present study depicts 3 major aspects: (i) the phylloplanes of xerophytic plants harbour phytopathogenic fungi of exceptional potential to myco-transform recalcitrant compounds including PSS; (ii) the increase in fungal biomass FW in presence of PSS as sole carbon source could be correlated to successful utilization of PSS by fungus for its growth and metabolism; (iii) presence of high amount of aliphatic and cyclic alkanes, along with their respective alcohol and fatty acid derivatives indicated that their generation was due to transformation of PSS by *C. dactylocteniola* VJP08.

Further, these organic compounds were incorporated into the central pathways of cellular catabolism, which supports the fungal growth. Moreover, the observed correlation between these compounds strongly indicated that the fungus possesses highly sensitive protein system capable of utilizing PSS as sole carbon source for maintaining its biochemical activities. In addition to the metabolomics approach discussed in the present chapter, detailed proteomics profile of extracellular fungal proteins was performed to further explore and identify the functional moieties behind myco-transformation of PSS.

Chapter 5

Proteomics Analysis Reveals Putative Proteins in the Secretome of *Curvularia dactyloctenicola* VJP08 Involved in PSS Transformation

5.1 Introduction

PS is one of the most persistent and recalcitrant plastics due to its aromatic structure and tightly packed C-C atoms. Although, few studies have discussed the possibility of PS biodegradation, the enzymes involved and their mechanistic aspects are largely unexplored [Danso et al. 2019]. The PlasticDB (a database of plastic degrading enzymes) display only one entry for PS degrading enzyme namely alkane-1 monooxygenase which has been reported to break the aliphatic chain of PS, however the enzymes behind the cleavage of aromatic PS ring are unknown till date [Kim et al. 2021; Gambarini et al. 2022]. A wide biodiversity of microorganisms have adapted to metabolize aromatic hydrocarbons of diverse degradation pathways and become a central interest for researchers [van Hamme et al. 2003]. Few enzyme families viz. oxidoreductases and hydrolases have been reported as potential PS degraders based on the *in silico* studies [Hou and Majumder, 2021].

As discussed in Chapter 4, among various phylloplanic fungi screened, *C. dactyloctenicola* VJP08 displayed the highest capacity for PSS transformation. Further, the optimization of various process parameters revealed that 28℃ temperature, pH 7.0, and exposure duration of 15-20 days were the most suited parameters for PSS myco-transformation. The SDS-PAGE profile of extracellular proteins in MSM+1% PSS treatment at different exposure durations revealed diverse band patterns indicating the involvement of various proteins and potential enzyme(s) in PSS myco-transformation [Figure 4.6]. The critical analysis showed that PSS transformation was slowed down after day 20 due to the degradation of extracellular proteins. Hence, the quantitative proteomics analysis was performed for the selected extracellular protein samples (from day 5 to day 20) in order to clearly identify and evaluate the participating protein(s) in PSS myco-transformation.

The proteomics-based approach directly detects and quantifies protein expression and has proven its huge potential in mining new enzymes from a broad repertoire of microbial sources [Bers et al. 2011; Sturmberger et al. 2016]. Exoproteome is the principal target while screening potential plastic-degrading enzymes. As to introduce initial break-down of the rigid structure, the microbial enzymes engaged in depolymerization are usually secreted extracellularly [Urbanek et al. 2020]. Therefore, this chapter discusses the quantitative proteomics profiling of *C. dactyloctenicola* VJP08 exposed to MSM+3% dextrose (for 5 days) and MSM+1% PSS (for 5, 10, 15 and 20 days), in order to comparatively evaluate the key participating proteins involved in PSS myco-transformation.

5.2 Materials and Methods

5.2.1 Materials

All chemicals used for the preparation of protein samples were of analytical grade and purchased from Sigma Aldrich (India) unless otherwise stated. Milli-Q water was acquired from a Milli-Q Biocel water purification system manufactured by Merck Millipore (Merck KGaA, Darmstadt, Germany).

5.2.2 Sample Preparation and Peptide fractionation

To analyse the extracellular fungal proteins involved in the myco-transformation of PSS, the extracellular proteins present in the fungal cell-free filtrate of the experimental flasks (including control i.e. MSM+ 3% dextrose) were precipitated using modified TCA/acetone precipitation method, as discussed in Chapter 4.

The purified and dialyzed extracellular protein samples (50 ug) were reduced using 5 mM Tris (2-carboxyethyl) phosphine hydrochloride (TCEP) at 56℃ for 30 min (which results in the opening of cysteine linkages), followed by subsequent alkylation with 50 mM iodoacetamide at 23℃ for 30 min under dark conditions (which prevents the reformation of disulfide linkages in a random manner). The protein samples were further subjected to digestion using trypsin (1:50, trypsin/lysate ratio) at 37°C for 16 h. The protein digests were cleaned using a C18 silica cartridge in order to remove salts, followed by drying using vacuum centrifuge. The obtained dried pellet was re-suspended in buffer A containing 2% acetonitrile, 0.1% formic acid.

5.2.3 LC-MS/MS Analysis

The gel-free proteomics analysis was performed using EASY-nLC-1000 UHPLC system coupled with an Orbitrap Exploris Mass Spectrometer (Thermo Fisher Scientific). One microgram of each of the peptide samples was loaded on C18 LC column (3.0 µm particle size, 0.075 mm diameter, 150 mm length) (Acclaim^{TM} PepMap^{TM}; Thermo Fisher Scientific). Peptides were separated with a linear gradient from 0-40% gradient buffer B (80% acetonitrile and 0.1% formic acid) at a flow rate of 300 nl min^{-1} for 60 min and injected for MS analysis. MS1 spectra were acquired in the Orbitrap (R= 60k; AGQ target= 300%; Max IT= 25 ms; RF Lens = 70%; mass range = 375-1500; Profile data). Dynamic exclusion was employed for 30s excluding all charge states for a given precursor. MS2 spectra (R= 15k; AGC target 200%; Max IT= 22ms) were collected for top 12 peptides.

5.2.4 Data Analysis for Protein Identification

The generated RAW data files for all the samples were searched against the Uniprot database with Proteome Discoverer (v2.5) (Thermo Fisher Scientific). For dual SEQUEST^{TM} and MSAmanda search, the precursor mass tolerance was set to 10 ppm and the fragment ion tolerance was set to 0.02 Da. The enzyme specificity was set for trypsin/P with allowed cleavage at the C terminus of "K/R: unless followed by "P". Carbamidomethyl on cysteine as fixed modification and oxidation of methionine and N-terminal acetylation were considered as variable modifications for the database search. Both peptide spectrum match and protein false discovery rate were set to False discovery rate (FDR) of 0.01%. The obtained data was analysed to calculate fold changes (FC) followed by $\log_2$ transformation. The proteins with the $\log_2$-fold change value between ≥ 0.25 and ≤ -0.25 were considered to be upregulated and down-regulated, respectively [Massafra et al. 2017; Zhou et al. 2021].

5.2.5 *In silico* characterization

Secondary Structure Prediction and Physio-chemical Properties of Protein

In the absence of three-dimensional structure, secondary structure prediction is an intermediate step facilitating structural understanding of proteins. Secondary structure of selected differential/overexpressed protein(s) was generated using PSIPRED server to find out the total number of α-helices and β-sheets present and to depict the conformation of amino acid residues.

Molecular modelling and ligand preparation

I-TASSER server was used to generate the 3D structure of cerato-platanin and laccase, [Yang and Zhang, 2015]. The model was then subjected to overall structural refinement and energy minimization to generate a model close to native form in terms of H-bonding, backbone topology and side chains positioning. Model refinement was done using ModRefiner [Xu and Zhang, 2011]. The refined model was validated for various parameters viz. the covalent bond distances and angles, stereochemical validation and atom nomenclature using the Structural Analysis and Verification Server 6 (SAVES6) server [Laskowski et al., 1993; Hooft et al., 1996].

Additionally, the 3D structure of PSS was downloaded from PubChem database (PubChem CID: 75905) in SDF format. Open Babel software was used to convert the SDF file to PDB file [O'Boyle et al. 2011].

Molecular docking studies

Protein-Protein docking is useful to predict the binding extent between protein complexes of biological relevance. In order to predict the binding between cerato-platanin and laccase proteins, ClusPro 2.0 server was used. The protein-protein docking was performed by uploading prepared PDB files of cerato-platanin and laccase into server, followed by job submission using default parameters [Kozakov et al. 2013; 2017; Vajda et al. 2017; Desta et al. 2020]. Blind molecular docking studies were performed using AutoDock 4.2.6 program to understand the interactions of selected protein with styrene sulfonate monomer [Morris et al. 2009]. The ligand was kept in flexible condition when interacting with macromolecules which was kept in rigid conditions. ADT files were used for running grid coordinates and subsequent docking. Kollman charges and polar hydrogen atoms were included in the protein structure and the prepared file was saved in the .PDBQT format. Ligand-binding affinities were predicted as negative Gibbs free energy (ΔG) scores (kcal mol^{-1}). Post-docking analyses were visualized using AutoDock 4.2.6, LigPlot+ and PyMol [Morris et al. 2009; Laskowski and Swindells, 2011]. Subsequently, binding poses of the complex were observed, and the best and most energetically favourable conformation was selected.

5.3 Results and Discussion

The extracellular protein profile of *C. dactyloctenicola* VJP08 exposed to MSM+3% dextrose (for 5 days) and to MSM+1% PSS (for 5, 10, 15 and 20 days) was carried out to comparatively evaluate the key proteins involved in PSS transformation. The obtained results showed that 109 proteins in total were common among all the treatments. In MSM+3% dextrose (control), 16 proteins showed differential expression, while in MSM+1% PSS, the differentially expressed proteins were seen to gradually rise from 2 (at day 5), 6 (at day 10), 20 (at day 15) to 22 (at day 20) [Figure 5.1 a].

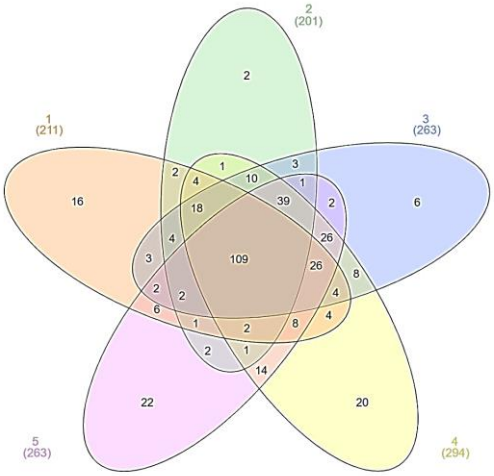
2
(201)
1
(211)
3
(263)
5
(263)
4
(294)
2
16
6
22
20
109
18
39
10
26
14

(a)

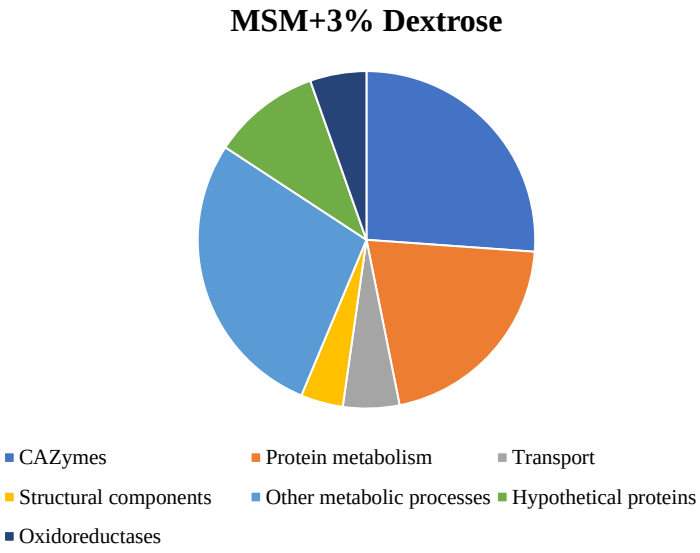
MSM+3% Dextrose
CAZymes
Protein metabolism
Transport
Structural components
Other metabolic processes
Hypothetical proteins
Oxidoreductases

(b)

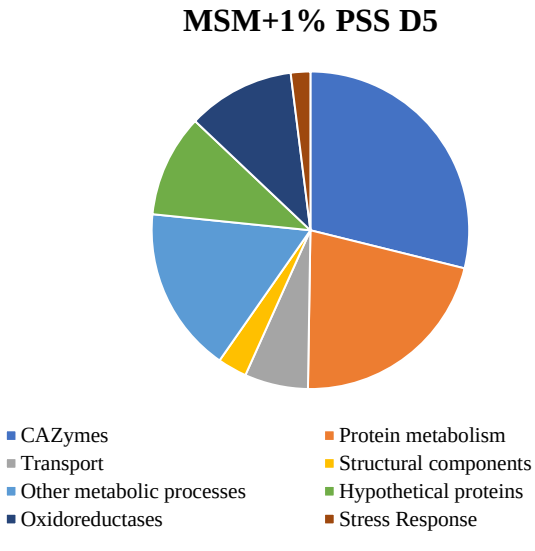
MSM+1% PSS D5
CAZymes
Protein metabolism
Transport
Structural components
Other metabolic processes
Hypothetical proteins
Oxidoreductases
Stress Response

(c)

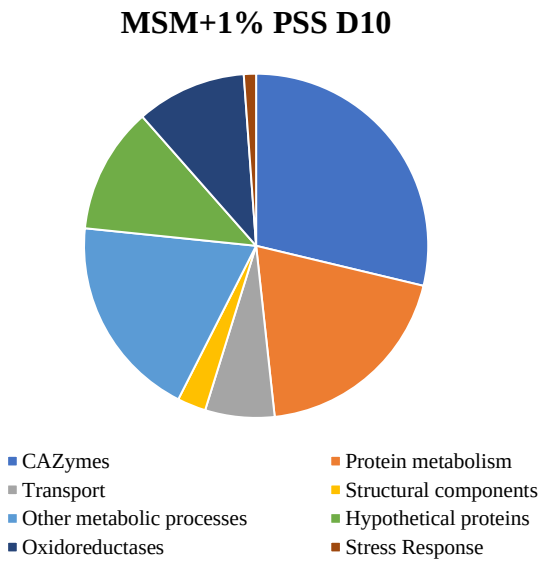
MSM+1% PSS D10
CAZymes
Protein metabolism
Transport
Structural components
Other metabolic processes
Hypothetical proteins
Oxidoreductases
Stress Response

(d)

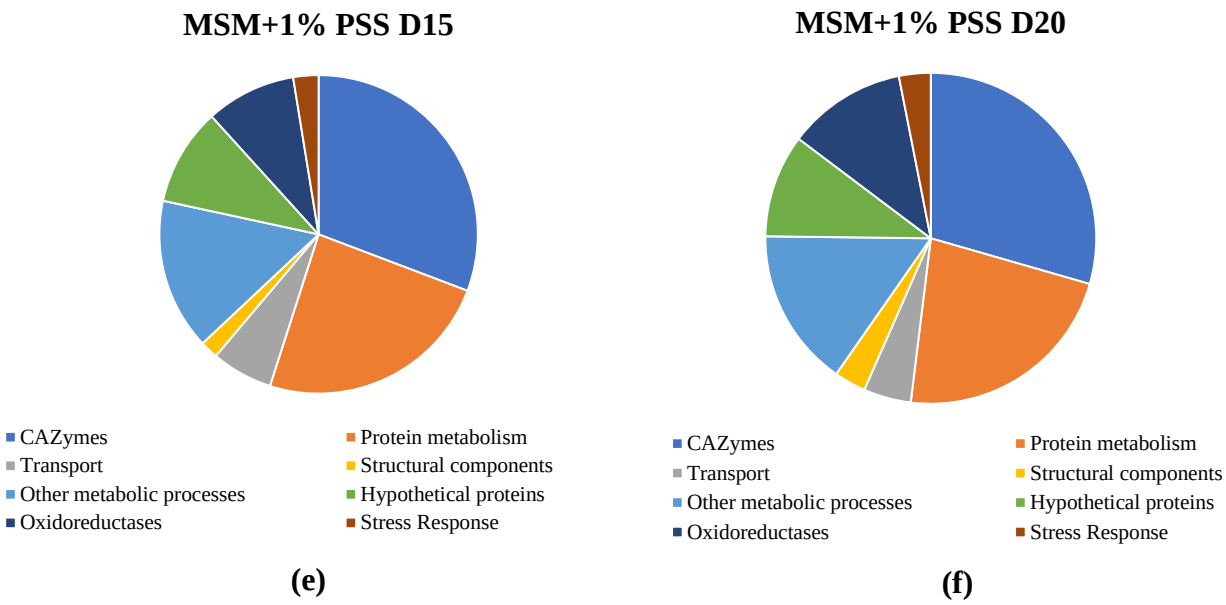

Figure 5.1 Proteomic analysis of extracellular protein extracted from control and tested samples: (a) Venn diagram showing shared and unique proteins in the protein extracts, where 1 represents MSM+3% dextrose and 2-5 represent MSM+1% PSS at exposure duration from day 5-20 with 5-day interval; (b-f) Pie diagram representing the relative abundance of proteins related to different molecular functions during different treatment conditions.

The proteomics analysis revealed proteins involved in various molecular functions viz. carbohydrate-active enzymes (CAZymes), protein metabolism, structural proteins, transport proteins, hypothetical proteins, oxidoreductases and proteins involved in stress response and metabolic processes. Among these, the proteins associated with basic cellular functions i.e. carbohydrate and protein metabolism were found to be the most abundant in all treatment conditions. Noteworthy, MSM+1% PSS treatment displayed expression of some additional proteins related in stress response which were not expressed in case of MSM+3% dextrose [Figure 5 b-f]. These stress-responsive proteins play an important role in promoting microbial adaptation to the nutrient challenging environment [Seo et al. 2009]. Careful analysis data suggests that two categories of proteins are of central importance, (i) the oxidoreductases that would mediate the PSS break-down in order to extract the carbon from its structure, and (ii) CAZymes which assist in carbon assimilation by mediating the conversion of PSS-derived carbon into more utilizable form to support fungal growth and energy metabolism [Ene et al. 2014; Goulet and Saville, 2017; Mohanan et al. 2020]. Therefore, these two protein categories were expressed in all treatment conditions [Figure 5.2]. Oxidoreductases have also been known to be involved in fungal housekeeping functions, hence their expression in case of MSM+3%

dextrose (control) sample is justified [Sützl et al. 2019]. The most dominating oxidoreductases in MSM+3% dextrose sample were GMC (glucose-methanol-choline) oxidoreductases which assist the activity of other CAZymes including glucose dehydrogenase, glucose oxidase, pyranose dehydrogenase, etc [Sützl et al. 2018]. In addition, different subclasses of oxidoreductases reported to be involved in biodegradation of organic pollutants were also identified in the protein profile of MSM+1% PSS extracts. Highest expression of CAZymes was observed to be highest at day 15 of exposure duration in MSM+1% PSS sample. Oxidoreductases were observed to be significantly higher in MSM+1% PSS samples in comparison to MSM+3% dextrose. During day 10 through day 20, presence of high concentration of oxidoreductases indicates active fungal-mediated metabolism of PSS which was the sole carbon source.

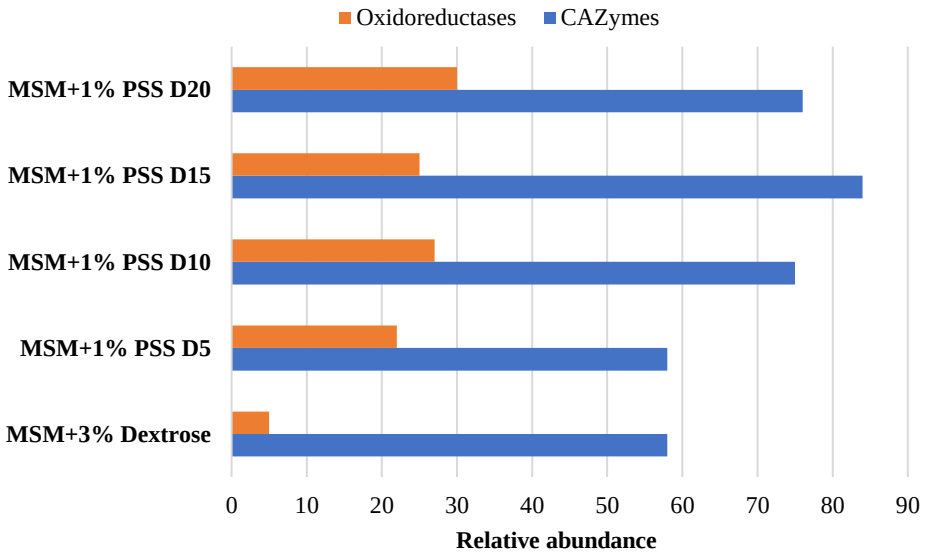

Figure 5.2 Bar diagram depicting relative abundance of oxidoreductases and CAZymes in different treatment conditions.

5.3.1 Log_2-Fold Change Analysis

The log_2-fold change values were generated to track and measure the protein expression from day 5 to 20 in order to determine the ideal exposure time. A total number of 25, 49, 74 and 64 proteins were found to be upregulated in MSM+1% PSS samples on day 5, 10, 15 and 20, respectively. Majority of the upregulated proteins were found to be common at different days. Highest upregulation of proteins was observed at day 15 which confirms the PSS transformation results in Chapter 4. Oxidoreductases, particularly bilirubin oxidase, FAD-binding PCMH-type, laccase, and multicopper oxidase were found to be highly expressed at

day 15 of exposure duration. Considering the higher number of proteins and higher log_2 fold-change values observed at day 15, we concentrated on thorough and meticulous analysis of protein expression data at day 15.

Based on the log_2-fold change, a total of 74 proteins were found to be upregulated and 14 proteins were found to be downregulated at day 15 as depicted in Tables 5.1 and 5.2, respectively. The majority of upregulated proteins (23) belonged to CAZymes, which were followed by the proteins involved in fungal protein metabolism (16), transporter proteins (4), fatty acid biosynthesis (1), and other metabolic processes (12), such as maintaining cell homeostasis, lipid metabolism, etc. Various oxidoreductases (10) were also found to be upregulated. A surface-active biosurfactant protein, namely cerato-platanin, which is only secreted by fungus was also found to be upregulated.

Fungi have a wide range of intracellular and extracellular enzymes which can catalyse a variety of reactions making them highly efficient for the degradation of pollutants such as petroleum-based polymers [Olicón-Hernández et al. 2017]. These enzymes include various oxidoreductases with unique characteristics and ability to attack a wide variety of recalcitrant substrates. Among them, laccases, tyrosinases, peroxidases and monooxygenases, are important for the fungal-mediated metabolism of organic pollutants [Harms et al. 2011]. These enzymes transfer carry out oxidation-reduction reactions using H_2O_2 as an electron accepting co-substrate, as well as additional reactions including epoxidation, aromatic preoxygenation and sulfoxidation, to transport electrons from organic pollutants to molecular oxygen [Karich et al. 2017]. Moreover, previous reports on the fungal-mediated plastic degradation suggest that oxidoreductases trigger the C-C bond scission, activating key metabolic pathways that result in the production of alkanes, fatty acids, alcohols, and other compounds that were also demonstrated in Chapter 4 [Francesc et al. 2005; Balserio-Romero et al. 2017; Ghosal et al. 2017]. Upregulation of oxidoreductases viz. laccases, multi-copper oxidases, copper radical oxidases, peroxidases and FAD binding PCMH-type domain containing proteins in the MSM+1% PSS treatment in comparison to control at day 15 showed their involvement in transformation of PSS structure. The observed upregulation of cerato-platanin is due to its functions as a surface-active self-assembling protein which is known to mediate the attachment of fungal hyphae to the hydrophobic PSS polymer [Sánchez, 2020]. The upregulation of various transport proteins indicates their involvement in the uptake of PSS myco-transformed products for further intracellular utilization. Zhang et al. (2022) also reported upregulation of various enzymes associated with bacterial PVC biodegradation (extracellular catalase-

peroxidase), and subsequent transport of small organic molecules and fatty acids (ABC transporter, porins), and intracellular metabolism (ATP synthase, Glucose-6-phosphate, etc) to support growth. Similarly, Nzila et al. (2018) reported upregulation of proteins involved in cell homeostasis, and chemical stress during pyrene biodegradation by *Achromobacter xylosoxidans*. However, the bacterial proteomics data of both the above-mentioned studies lack the presence of key oxidoreductases i.e. laccases, monooxygenases, etc which might be involved in the cleavage of C-C bond of aromatic ring/PVC. The present study revealed the upregulation of multiple oxidoreductases indicating that fungi have superior potential to degrade recalcitrant substances in comparison to the bacteria [Harms et al. 2011]. Moreover, the expression profile of *C. dactyloctenicola* VJP08 extracellular protein revealed concurrent involvement of various enzymes in PSS myco-transformation.

The total number of downregulated proteins (15) were found to be lesser in comparison to the upregulated proteins [Table 5.2]. It includes proteins related to CAZymes, protein metabolism, and some hypothetical proteins. Among these, some other isoforms of CAZymes were also found to be upregulated [Table 5.1]. To maximize the utilization of different carbon sources, fungi secrete different isoforms within a protein family, for instance, different isoforms of glycoside hydrolase family were largely upregulated [Table 5.1]. None of the oxidoreductases were found to be downregulated in the extracellular proteins of *C. dactyloctenicola* VJP08 in MSM+1% PSS treatment. Although, a few studies have emerged which discuss the proteomics-based mechanism of plastic biodegradation by marine bacteria [Meyer-Cifuentes et al. 2020; Zadjelovic et al. 2022], the present study first time reports the role of extracellular fungal proteins in PSS transformation.

Table 5.1 List of extracellular proteins identified as upregulated from the expression profile of *C. dactyloctenicola* VJP08 in MSM+1% PSS treatment at 15 days of incubation.

S.No.	Protein Name	Accession no. of isomers*
CAZymes		
1	Carbohydrate-binding module family 18 protein	*W6Z4Z3*
2	Carbohydrate esterase family 4 protein	*W7EEQ1, W7F3Q0*
3	Chitinase	*A0A8H5ZK68, M2SUE9*
4	beta-Galactosidase	*W6XSF9*
5	beta-Glucosidase	*W6ZVR3*

6	Galactose mutarotase-like protein	*W6Y6M3*
7	Glycoside hydrolase family 2 protein	*M2UAT3*
8	Glycoside hydrolase family 3 protein	*W6YDY2, W6ZPH6*
9	Glycoside hydrolase family 5 protein	*W6ZTN5*
10	Glycoside hydrolase family 30 protein	*W7EMS5*
11	Glycoside hydrolase family 36 protein	*W7F0E5*
12	Glycoside hydrolase family 38 protein	*W7EIT4*
13	Glycoside hydrolase family 55 protein	*M2TRM0*
14	Glycoside hydrolase family 93 protein	*N4XN89, N4WMU7*
15	Glycoside hydrolase family 105 protein	*W6YBN9*
16	Glycoside hydrolase family 125 protein	*N4X945*
17	Probable alpha/beta-glucosidase agdC	*N4XPU0*
18	beta-Xylanase	*W6YT31*
19	Oxalate decarboxylase oxdC	*W7E0Q9*
Protein Metabolism		
1	Carboxypeptidase	*W7EVT4, W6YV41, M2U894*
2	Dipeptidyl-peptidase V	*A0A8H6DVX7*
3	Glutaminase GtaA	*W6XUG2*
4	Peptide hydrolase	*W6YRA6*
5	Peptidase A1 domain-containing protein	*W6ZHW7*
6	Peptidase M14 domain	*N4X3P3, M2RZW3, W6Z7U9*
7	Peptidase_S9 domain-containing protein	*W6Y890*
8	Sialidase domain-containing protein	*M2S7I2*
9	Subtilisin-like serine protease-like protein	*M2TG45, M2V0Q8, W6ZLN6*
10	Succinylglutamate desuccinylase/aspartoacylase	*A0A8H6DVF5*
Transporter Proteins		
1	ABC transporter domain-containing protein	*W7E781*
2	Plasma membrane ATPase	*W6XUR4*

3	Phosphatidylglycerol/phosphatidylinositol transfer protein	*W6Y2V1*
4	MFS domain-containing protein (sugar transport)	*W7ECZ7*
Fatty acid Biosynthesis		
1	ATP citrate synthase	*W6ZJD3*
Other Metabolic Processes		
1	Alkaline phosphatase	*N4XS65*
2	Carboxylic ester hydrolase	*N4XE860, A0A8H5ZMQ8*
3	COesterase domain-containing protein	*N4WWG3*
4	Hypothetical NAD binding oxidoreductase	*W7EQ31*
5	GP-PDE domain-containing protein	*W6ZU26*
6	Glutathione hydrolase	*A0A8H5ZK14*
7	Heme_Haloperoxidase domain-containing protein	*M2TGH4*
8	PHD-type domain-containing protein	*W6ZUQ8*
9	Phosphorylcholine phosphatase	*W7EUJ8*
10	Pyridoxamine 5'-phosphate oxidase-domain-containing protein	*N4XX09*
11	WD40 repeat-like protein	*M2T321*
Oxidoreductases		
1	Bilirubin oxidase	*N4XVC2*
2	Copper radical oxidase	*A0A8H5ZFZ8*
3	FAD-binding PCMH-type domain-containing protein	*M2UGF4, N4XQY9, W6YQQ1, W6Z9D3, W7ENE7*
4	Laccase	*M2TBI3*
5	Multicopper oxidase	*W7EKA0*
6	Secreted protein (Lignin/Versatile/MnP peroxidases)	*W6YQY4*
Biosurfactant		
1	Cerato-platanin	*W6YTX3*
Structural		
1	ADF-H domain-containing protein	*N4X2Z7*

Hypothetical Proteins		
1	Apple domain-containing protein	*M2RJ61*
2	FAS1 domain-containing protein	*W7F128*
3	Lactamase_B domain-containing protein	*W7E4N5*
4	MARVEL domain-containing protein	*M2TEL5*
5	Ovule protein	*N4X6U1*
6	Uncharacterized protein	*W6XKI0*

*The accession no. are from UniProt.

Table 5.2 List of extracellular proteins identified as downregulated from the expression profile of *C. dactyloctenicola* VJP08 in MSM+1% PSS treatment at 15 days of incubation.

S.No.	Protein Name	Accession no. of isoforms*
CAZymes		
1	Glucan endo-1,3-beta-glucosidase btgC	*A0A8H5ZFU3*
2	Glucose-6-phosphate isomerase	*N4WP77*
3	Glycoside hydrolase family 43 protein	*M2U0R6, W7F9D4*
4	Glycoside hydrolase family 55 protein	*N4X5Q9*
5	Glucanase	*A0A8H6E0Q6*
6	1,3-beta-Glucanosyltransferase	*W6Y5Y5*
7	alpha,alpha-Trehalase	*W6YHE0*
Protein Metabolism		
1	Carboxypeptidase	*A0A8H5ZNS3*
2	Peptide hydrolase	*W7A2V0*
Other Metabolic Processes		
1	Oxoglutarate dehydrogenase (succinyl-transferring)	*W7EFL6*
Hypothetical Proteins		
1	Extracellular serine-rich protein	*W6YV56*
2	NmrA domain-containing protein	*W7E6X0*
3	Secreted protein (Fragment)	*N4X2I2*
4	SurE domain-containing protein	*N4X3H3*

*The accession no. are from UniProt.

5.3.2 Differentially Expressed and Potential Proteins Involved in PSS Myco-transformation

The differentially expressed proteins in the MSM+1% PSS treatment at 15 days of exposure duration were identified in comparison to MSM+3% dextrose treatment. The obtained data revealed that a total of 20 proteins were differentially regulated, which majorly belonged to the two main protein categories (oxidoreductases and CAZymes) associated with PSS myco-transformation [Table 5.3]. It is apparent that both the upregulated and differentially expressed proteins combinedly participate in PSS myco-transformation. Based on the proteomics analysis, it is proposed that a total of 17 different oxidoreductases (from upregulated and differentially regulated proteins) participate in PSS transformation, in addition to other enzymes that lead to the utilization of cleaved PSS products and their subsequent conversion into simpler organic metabolites which are easily utilized by fungus. Table 5.4 depicts the location and proposed function of these 17 oxidoreductases with suitable references.

Table 5.3 List of differentially expressed proteins identified from the expression profile of *C. dactyloctenicola* VJP08 in MSM+1% PSS in comparison to MSM+3% dextrose (control) at 15 days of incubation.

S.No.	Protein Name	Accession no. of isoforms*
Carbohydrate Metabolism		
1	Chitinase	*M2SUE9*
2	Glutaminase Gta A	*M2UIE0*
3	Glycoside Hydrolase family 3	*W7ES27*, *W7ESF5*
4	Glycoside Hydrolase family 43	*W6YLR9*
5	Glycoside Hydrolase family 105	*M2UUH3*
Protein Metabolism		
1	Alpha-1,2-Mannosidose	*M2UQX6*
2	Peptidase_M14 domain	*A0A8H6DZ70*
3	Peptidase_S9 domain	*A0A8H5Z924*
4	Indoleamine2,3-dioxygenase	*W6Y5B3*
Oxidoreductases		
1	BH4_2 domain	*W6Y3P4*
2	Enoyl reductase	*M2V7N5*
3	FAD_binding_3 domain	*M2ST41*

4	FAD binding PCMH-type	*W6XSB5*
5	Flavodoxin-like domain	*M2T268*
6	Tyrosinase Cu-bd domain	*N4X430*
7	Vanadium chloroperoxidase	*M2UKA1*
Other Metabolic Processes		
1	elF-5a domain Translation elongation	*W7EZK6*
Hypothetical Proteins		
1	DUF4331 domain	*N4X1U3*
2	GCR1_C domain	*W6ZDU6*

*The accession no. are from UniProt.

Since PSS is comprised of aromatic ring structure, many studies indicated that enzymes capable to cleave the associated aromatic compounds would also be functional against PSS. For example, enzymes such as ring-hydroxylating dioxygenase and biphenyl dioxygenase, benzoate 1,2-dioxygenase which have been reported to cleave the related aromatic compounds namely, benz[a]anthracene, biphenyl, and benzoate, respectively, would also be applicable in PS/PSS biodegradation [Patrauchan et al. 2008; Fu et al. 2018; Peng et al. 2018]. Further, oxidoreductases and lipases have also been proposed by other researchers to be involved in PS-degrading pathways. For instance, P450 monooxygenases and alkane hydroxylases probably play a role to break the main-chain C-C bonds of PS [Hou and Majumder, 2021]. Additionally, biochemical analysis of PS degradation had also indicated the probable role of depolymerases in its degradation [Mohan et al. 2016]. However, the clear involvement of these enzymes in PS biodegradation has not been identified yet.

Table 5.4 Combined list of upregulated and differentially expressed oxidoreductases identified from the expression profile of *C. dactyloctenicola* VJP08 in MSM+1% PSS at 15 days of incubation.

S.No	Protein Name	Accession no. of isoforms*	Cellular Location	Proposed Function	Reference
1	Bilirubin oxidase	*N4XVC2*	Extracellular	Unrecognised function	Messerschmidt and Huber, 1990

2	BH4_2 domain	*W6Y3P4*	Intracellular	aromatic ring cleavage	Fujii et al. 1988
3	Copper radical oxidase (Glyoxal oxidase)	*A0A8H5ZFZ8*	Intracellular	aldehydes to carboxylic acids	Whittaker et al. 1999
4	Enoyl reductase	*M2V7N5*	Intracellular	Alcohol dehydrogenases	Jörnvall et al. 1987
5	FAD_binding_3 domain	*M2ST41*	Intracellular	Aromatic ring cleavage	Schreuder et al. 1992
6	FAD-binding PCMH-type	*M2UGF4, W6YQQ1, W6Z9D3, W7ENE7*	Extracellular	Vanillyl alcohol oxidase-like activity	Fraaije et al. 2000
7	FAD binding PCMH-type	*W6XSB5, N4XQY9*	Intracellular	Dehydrogenase activity	Condon et al. 2013
8	Flavodoxin-like domain	*M2T268*	Intracellular	NAD(P)H dehydrogenase	Wang et al. 1997
9	Laccase	*M2TBI3*	Extracellular	Ring cleavage of organic compounds	Kumar and Chandra, 2020
10	Multicopper oxidase	*W7EKA0*	Extracellular	Phenolic substrates	Messerschmidt and Huber, 1990
11	Secreted protein (Lignin/Versatile/ MnP peroxidases)	*W6YQY4*	Extracellular	Phenolic and non-phenolic substrates	Sellami et al. 2022
12	Tyrosinase Cu-bd domain	*N4X430*	Extracellular	Hydroxylation of phenols	Halaouli et al. 2006
13	Vanadium chloroperoxidase	*M2UKA1*	Intracellular	Sulfoxidation of organic sulfides	ten Brink et al. 2000

*The accession no. are from UniProt.

5.3.3 Predicted PSS Myco-transformation Pathways

In the present study, the oxidoreductases identified as upregulated and differentially regulated must have a crucial role in PSS transformation processes. However, since a total number of 16 oxidoreductases were identified in both the analysis, it was necessary to short-list these enzymes by identifying their target substrates [Table 5.4]. The analysis revealed that there were 9 extracellular and 8 intracellular oxidoreductases indicating that the intracellular enzymes would have released in the cell-free filtrate during fungal life cycle (including replication and cell death). However, the presence of these enzymes widened the PSS myco-transformation pathway visualization spectrum. Based on the combined analysis of proteomics data with respect to the reported functional mechanism of probable enzymes, we propose the following mechanism for PSS myco-transformation by *C. dactyloctenicola* VJP08:

Common Step: In order to depolymerize the hydrophobic aromatic ring of PSS, its accessibility for catalysis is an essential step. The extracellular and intracellular degradation of PS has not yet been evaluated explicitly [Hou and Majumder, 2021]. Based on our study, we propose that transformation pathway of PSS involves several steps. The amphiphilic biosurfactant 'cerato-platanin' is hypothesised to function as the 'interaction bridge' (between PSS and catalytic enzyme) for the initial cleavage of polymeric PSS into its monomeric form SS (styrene sulfonate). It is possible that either chitinase, laccase or both participate in the cleavage of PS main chain. Essentially, the extracellular oxidation of SS can be mediated by laccases or peroxidases resulting in either aromatic ring fission, hydroxylation or quinoid production. The metabolites generated during extracellular oxidation may be subject to intracellular catabolism. The initial transformation may occur intracellularly by the action of monooxygenases, followed by further catabolism and metabolite secretion [Harms et al. 2011]. A recent study demonstrated that the known depolymerizing enzymes (mainly acting on polymers with aromatic residues and long-chain alkane groups), like leucine arylamidase, β-glucuronidase, β-galactosidase, phosphatases, chitinase, etc., exhibited higher activities in the gut microbiome of *T. molitor* larvae when it was fed with cellulose, PE and PS waste [Przemieniecki et al., 2020].

Extracellular PSS transformation: The key participating extracellular enzymes proposed to be crucial for PSS myco-transformation are laccases, peroxidases, tyrosinases and multicopper oxidases. All these enzymes have been reported to be involved in the degradation of aromatic pollutants via ring cleavage [Harms et al. 2011]. Among these, laccases were found

to be the most abundant enzymes, followed by multicopper oxidase (64% lesser than laccases), and bilirubin oxidase (73% lesser than laccases). As all the three enzymes belong to a common family of multicopper oxidase, they are capable in catalysing one-electron oxidation of a broad range of compounds including substituted phenols, arylamines and aromatic thiols to the corresponding radicals. [Reiss et al. 2013]. Interestingly, the enzyme intradiol dioxygenase was also present at day 15 of exposure duration, however, it was neither upregulated nor downregulated in comparison to control. Since intradiol dioxygenase play a crucial role in ring cleavage, its functional relevance can also be considered in PSS myco-transformation. Considering the presence of reported enzymes in the secretome of *C. dactyloctenicola* VJP08, the PSS myco-transformation may take place through various probable pathways occurring through side-chain or aromatic ring cleavage [Figure 5.3].

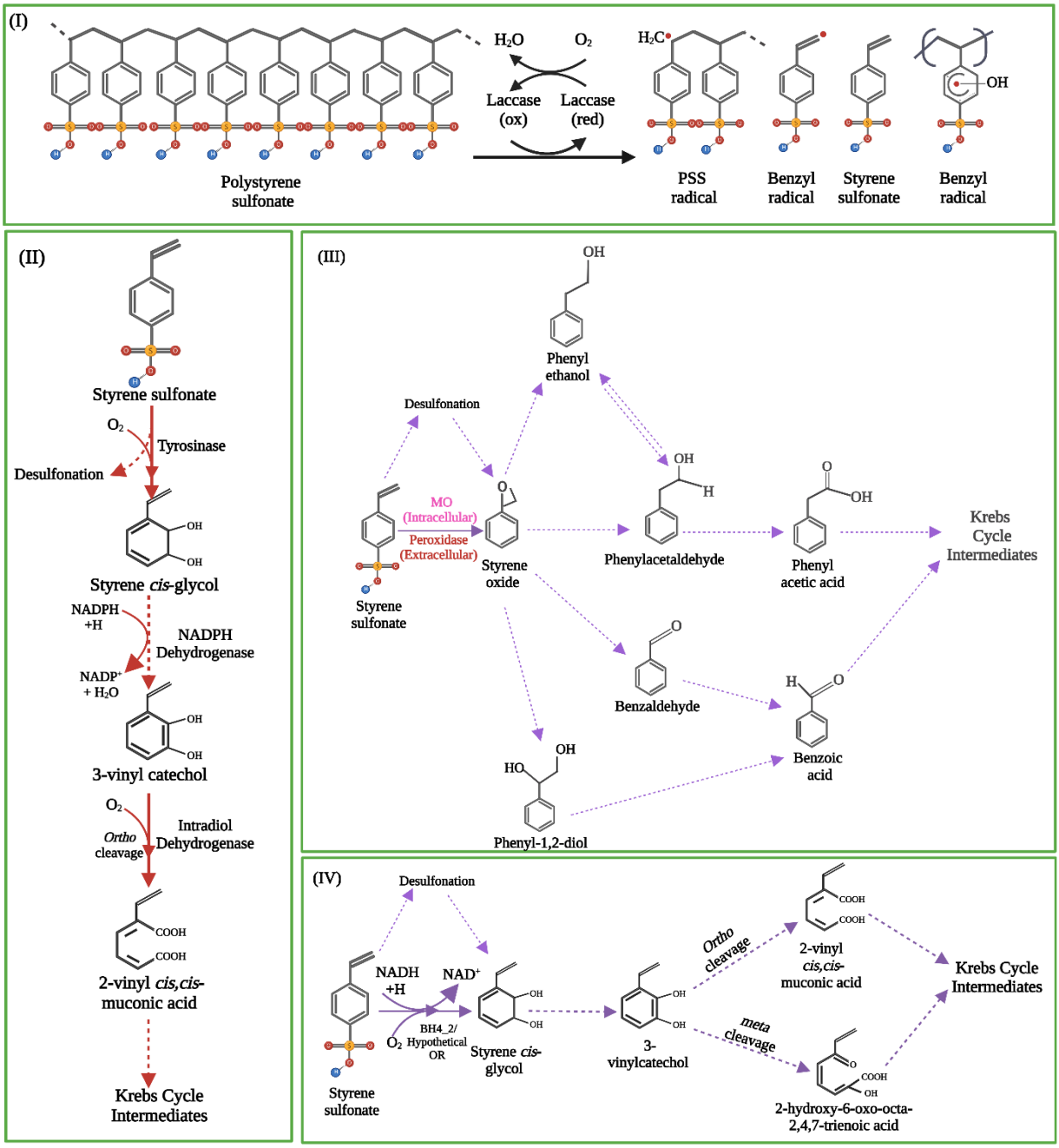

Figure 5.3 Predicted extracellular and intracellular events of PSS myco-transformation by *C. dactyloctenicola* VJP08. Dotted arrows represent the most probable series of events where the participating biomacromolecule have not been identified in proteomics study. The reactions in different sections indicate: (I) extracellular PSS depolymerization, (II) extracellular SS transformation via aromatic ring cleavage, (III) common extracellular and intracellular transformation via side-chain cleavage and (IV) intracellular aromatic ring cleavage of SS.

In the first and the most probable pathway, laccases act on PSS and introduces cleavage in its polymeric main-chain via radical chain scission mechanism, leading to the formation of primary free radicals due to the bond rupture of PSS backbone. The secondary radicals formed at the vinyl side-chain or by direct ring-cleavage forming peroxyl radical of styrene [Fordyce et al. 1984; Gubler et al. 2011]. Since laccase is a high redox potential enzyme capable of oxidizing the subsequent substrates, it is predicted that the generated radicals are subsequently oxidized by laccase leading to the generation of metabolites including alcohols, aldehydes and carboxylic acids (also observed in Chapter 4). Using *in silico* studies, Santacruz-Juárez et al. (2021), also predicted hydrophobin (biosurfactant) HFBII-assisted laccase-mediated degradation of PE caused the oxidation of PE due to its oxidation and subsequent generation of alcohols, aldehydes and carboxylic acids which were reported to enter the Krebs cycle to be mineralized into CO_2 and H_2O. Moreover, PS has been reported to be depolymerized by two laccases AbiLac1 and AbiLac2 from white-rot fungi *Abortiporus biennis* via aromatic ring cleavage. These enzymes have high affinity towards the degraded products including hydroxybenzoles, methoxybenzoles, hydroxybenzoic acids and catechol. These findings suggest that laccases are capable of converting PS into compounds that can beconsumed by cells on their own [Zerva et al. 2023]. In contrast to the present study, the commercial laccase from *Trichoderma versicolor* did not show any evidence of PSS degradation [Krueger et al., 2015]. It should be noted that the redox potential of laccases plays a key role in the degradation of polymers, hence the extent of degradation may vary.

Other pathways predicted to occur extracellularly include peroxidases mediated side-chain oxidation of styrene monomer to form styrene oxide (SO), which can also be metabolised intracellularly [Maurya et al. 2007]. This SO may be sequentially oxidated extracellularly into phenylacetaldehyde or benzoic acid which are then supplied into the Krebs cycle [Tsochatzis et al. 2021]. The metabolomic study of the treatment extract in the present study (Chapter 4) also revealed the production of benzoic acid, demonstrating that PSS is simultaneously metabolised by various pathways. Moreover, tyrosinases can also add OH groups to the aromatic ring of styrene monomer forming diphenolic structure, which is eventually dehydrogenated (by NADPH dehydrogenase) to form 3-vinyl catechol [Figure 5.3 II]. This modified aromatic ring (catechol) is cleaved by the action of intradiol dioxygenase, which cleaves the aromatic ring at ortho position (ring opening reaction) leading to synthesis of 2-vinyl *cis, cis* muconic acid which is ultimately fed into Krebs cycle [Guzik et al. 2013]. Similar results were observed in case of *Marinobacter* HA2 which secretes intradiol dioxygenase to

degrade phenol by ortho-ring cleavage [Abbas et al. 2022]. It has been reported that many aromatic compounds are biodegraded by being converted into intermediates such as protocatechuate or catechol which are then processed into Krebs cycle intermediates through the β-ketoadipate pathway [Harwood and Parales, 1996]. Also, it's possible that catechol undergoes extracellular metabolic conversion to form alkanes, alcohols and carboxylic acids, extracellularly, which are subsequently transported inside the cell via ABC transporters.

Intracellular PSS metabolism: The SS monomer generated due to depolymerization of PSS by laccase occurs as a common step. The fungal cells may allow either the SS monomers, or any of the laccase generated intermediates such as styrene sulfonate oxide (SSO), phenylacetic acid or benzoic acid to enter and be further metabolised. The SS monomers that enter the cell may be oxidised into SSO by the action of FAD_binding_3 domain or Flavodoxin-like monooxygenases (MO), which exhibit SMO-like activity [Figure 5.3 III]. This oxidised SSO may be further metabolised into Krebs cycle intermediates by enoyl reductase which exhibit alcohol dehydrogenase activity and facilitate production of aldehydes from alcohol, and copper radical oxidase which exhibit glyoxal oxidase activity and mediates the conversion of aldehydes to carboxylic acids. However, the understanding of the specific substrates for enoyl reductase and copper radical oxidase in the PSS transformation pathway are lacking and might be clearly predicted by studies specifically targeting intracellular transformation of PSS.

Additionally, the aromatic ring cleavage of SS monomer can occur by the action of BH4_2 domain like protein and Hypothetical NAD binding oxidoreductase (domains similar to benzene dioxygenase), resulting in its conversion into catechol, which is ultimately fed into the Krebs cycle [Figure 5.3 IV]. However, as the present study did not focus on intracellular PSS myco-transformation, hence, the proposed pathways are solely based on the proteomics data. Since biological systems are quite dynamic, there is a great possibility that other enzymes may also be involved and that the stated enzymes may catalyse other reactions. Furthermore, there is also a possibility that some of the intermediate enzymes were proteolyzed by the enzymes that breakdown extracellular proteins.

In summation, the experimental findings indicate the involvement of various enzymes involved in PSS myco-transformation via side-chain and aromatic ring cleavage mechanisms, as schematically represented in Figure 5.4. Here, it may be hypothesized that the presence of PSS in the surrounding environment is sensed by an unkown protein, which induces fungal cell

to synthesise different proteins required for its cellular utilization. Since the aromatic ring structure is hydrophobic in nature, biosurfactant: cerato-platanin assists the laccase in binding and catalysing the depolymerization of PSS into its subsequent monomers. Moreover, laccases are self-sufficient enzymes for PSS myco-transformation via generation of radical monomers and oligomers, which undergo subsequent transformations. The generated SS monomer may either enter the fungal cell via diffusion or get further transformed extracellularly by the fungal secretome. Both extra- and/or intra-cellular transformations of SS occur via two pathways: aromatic ring cleavage and/or side-chain cleavage. In case of extracellular transformation, the intermediates or generated metabolites finally enter the cell through ABC transporters and fed into the Krebs cycle.

It has been reported that some oxidative enzymes such as vanillyl-alcohol oxidase, act as auxiliary enzymes in synergy with the primary degrading enzymes (laccases) [Gygli et al. 2018]. Notably, H_2O_2 is produced by the majority of enzymes categorised as oxidoreductases. Extracellular H_2O_2 is necessary for the production of oxygen radicals, peroxidase activity, and laccase [Shah and Nerud, 2002]. Among H_2O_2-generating enzymes, aryl alcohol oxidase and glyoxal oxidase are most important enzymes [Kersten and Cullen, 2007]. Interestingly, auxiliary enzymes like vanillyl-alcohol oxidase and glyoxal oxidase observed in the current study suggest their potential role in PSS myco-transformation.

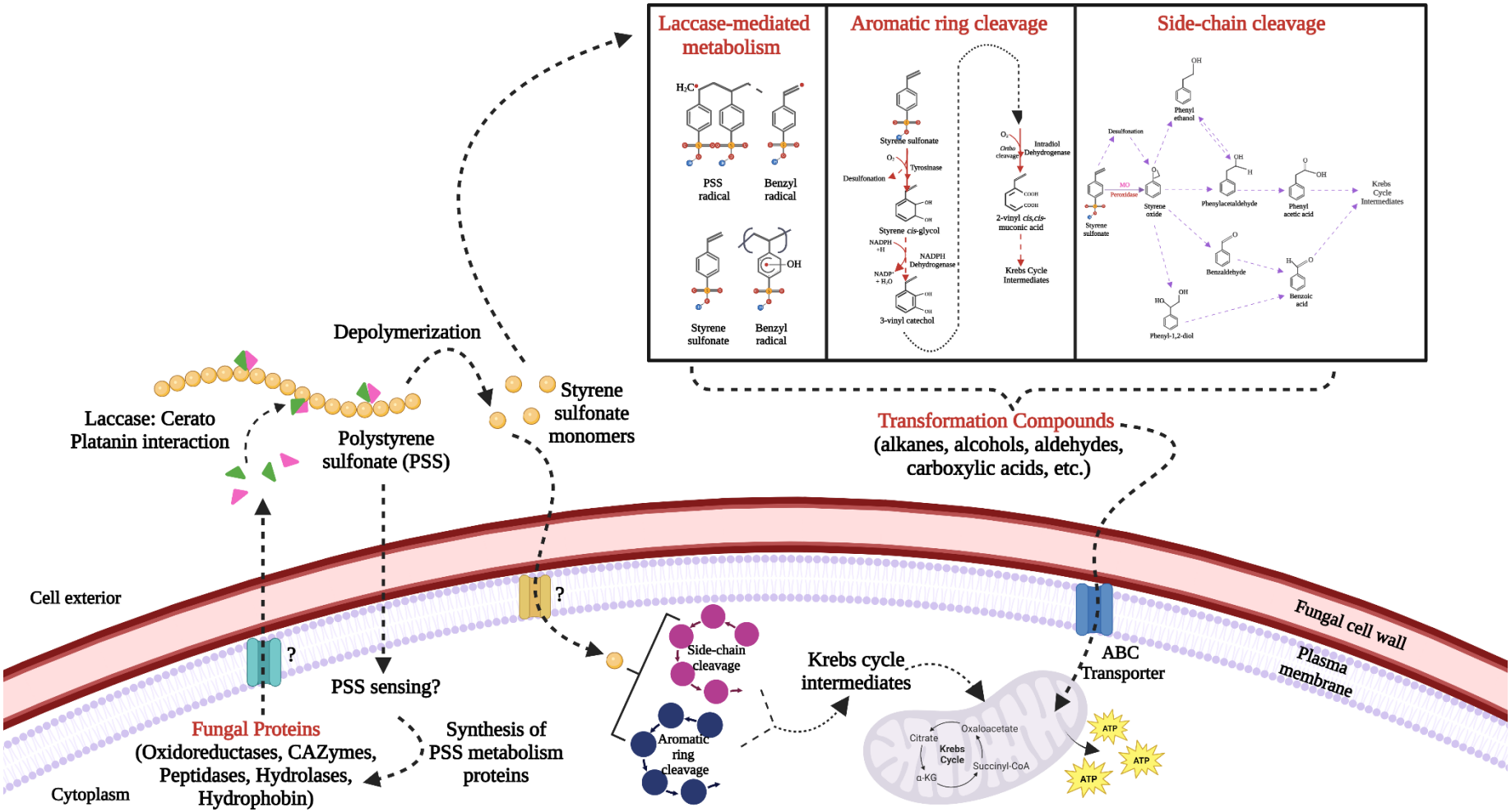

Figure 5.4 Schematic representation of the predicted series of events behind different PSS myco-transformation mechanisms by *C. dactyloctenicola* VJP08. Dotted arrows represent the hypothetical series of events where the participating biomacromolecule is unknown.

5.3.4 *In silico* Characterization

Structural analysis and physio-chemical properties

The secondary structure of cerato-platanin (14.3 kDa; 138 amino acids) and laccase (66.2 kDa; 601 amino acids) were generated using online server PSIPRED [Buchan and Jones, 2019]. The obtained results indicated that cerato-platanin protein consisted of 4 α-helices (H) and 5 β-strands (E) joined by a total 11 coils (C) [Figure 5.5 a]. Cerato-platanin was found to be majorly comprised of non-polar (43.47%), hydrophobic (21.01%), and aromatic cysteine residues (13.04%) indicating that the protein is mainly dominated by hydrophobic forces, although the presence of polar residues (22.46%) imparts an amphiphilic nature [Figure 5.5 b].

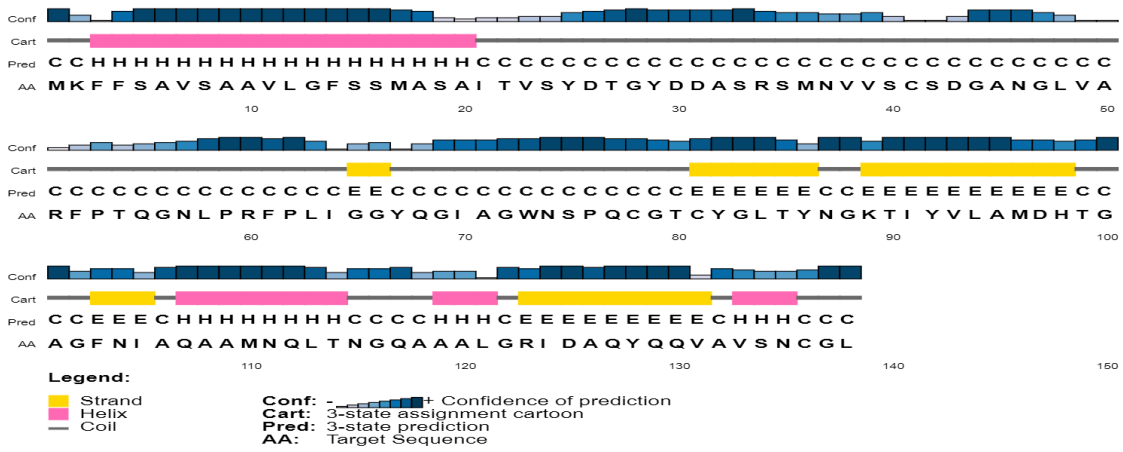

(a)

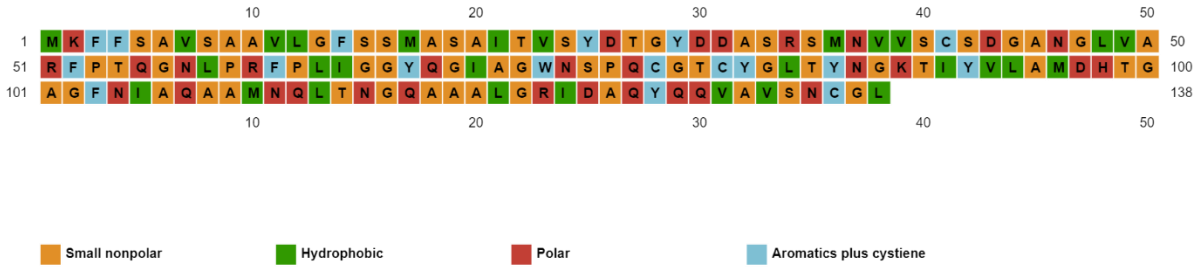

(b)

Figure 5.5 Structural analysis of cerato-platanin (a) predicted secondary structural elements (b) hydropathy profile indicating the polarity of the amino acid sequence.

For laccase, the obtained results showed that it protein consisted of 8 α-helices (H) and 31 β-strands (E) joined by a total 39 coils (C) [Figure 5.6 a]. Laccase was found to be majorly comprised of non-polar (36.27%), hydrophobic (21.79%), aromatic cysteine residues (11.31%) and polar (30.63%) residues [Figure 5.6 b].

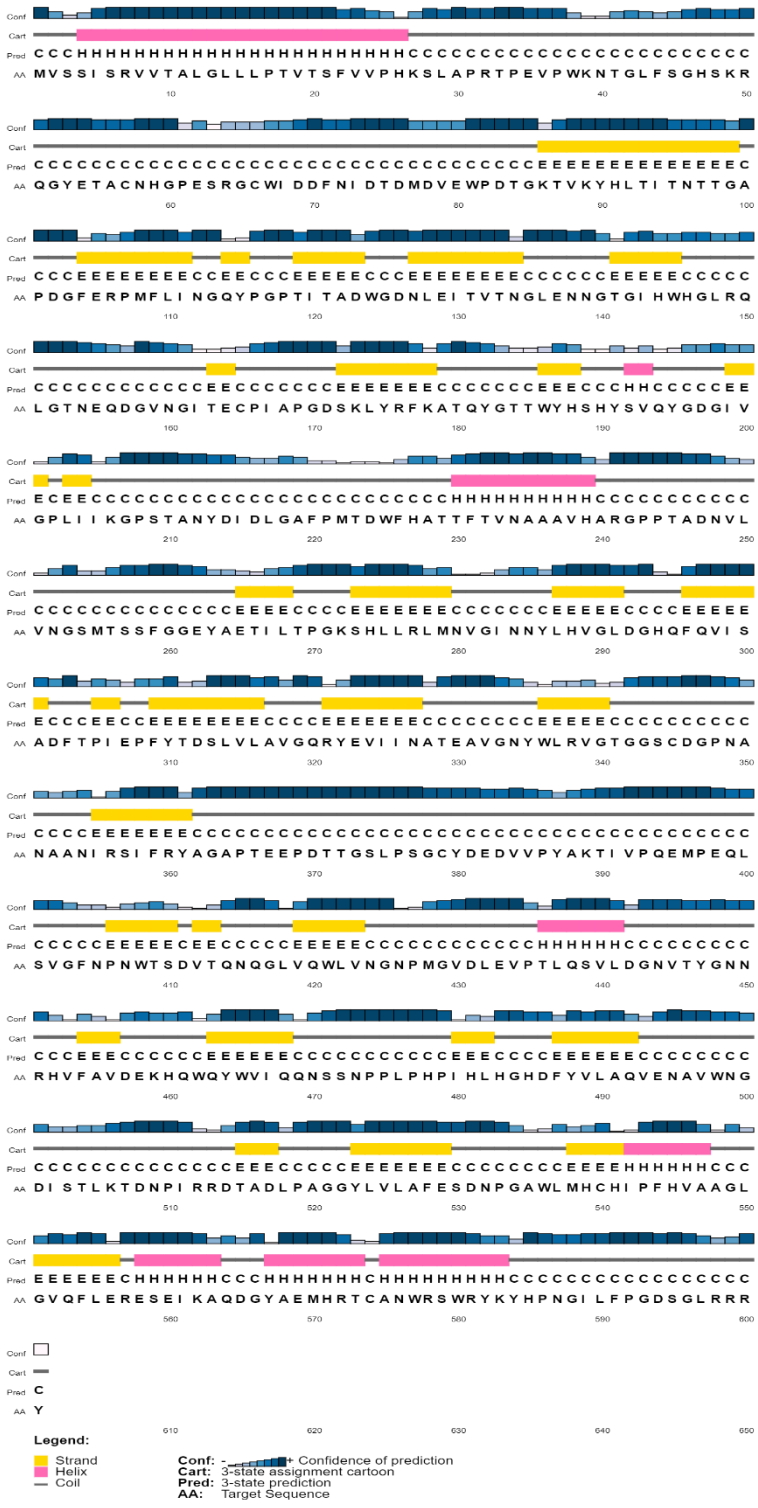

(a)

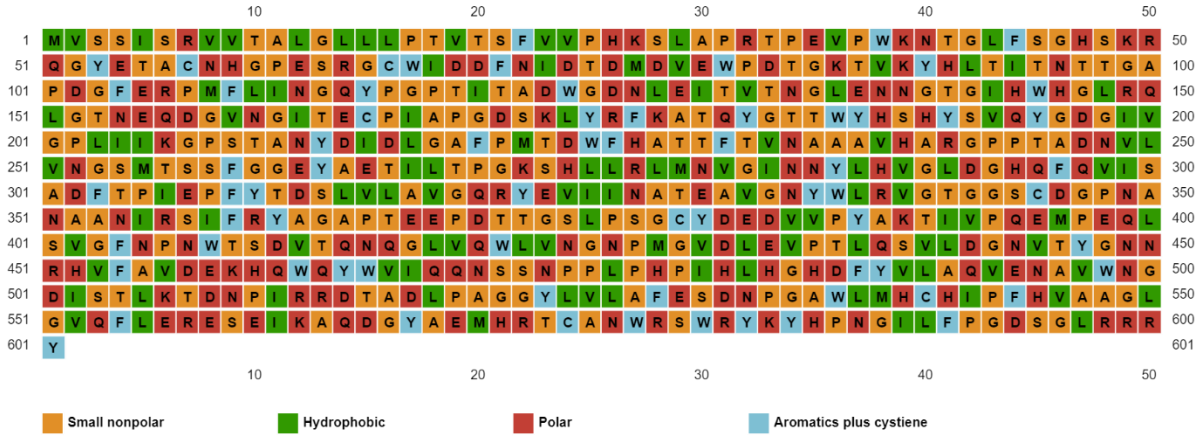

(b)

Figure 5.6 Structural analysis of laccase (a) Predicted secondary structural elements (b) hydropathy profile indicating the polarity of the amino acid sequence.

Further, the GRAVY values for both cerato-platanin and laccase were observed to be 0.131 and -0.27 indicating that the former is slightly hydrophobic in nature while the latter is hydrophilic in nature [Chang and Yang, 2013].

Molecular modelling, model refinement and validation

The FASTA sequences of cerato-platanin (Accession no. EUC40798) and laccase (Accession no. EMD66227) were extracted from NCBI and submitted to I-TASSER for model generation. Since, the protein models were generated through threading, its necessary to minimize the model energy in order to determine the most stable and energetically favourable molecular conformation [Elton et al., 2019]. Hence, the generated models were refined using ModRefiner. Further, both the models were validated using Ramachandran Plot [Figure 5.7 a and b]. In case of cerato-platanin, the Ramachandran plot analysis showed that 78 residues (67.8%) were in favourable region, 36 residues (31.3%) were in allowed region and only 1 residue (0.9%) was found in the disallowed region. The overall existence of 99.1% residues in favoured and allowed regions showed that the model is good and free from stearic hindrance. Additionally, the model had a C-score of -0.27 and TM-score of 0.68±0.12. For laccase, the Ramachandran plot analysis revealed that 380 (76.3%) residues were in favourable region, 100 (22.3%) residues were in allowed region, and 7 (1.4%) residues were in disallowed region. These results indicate that this protein model is also good and free from stearic hinderance. Additionally, the model had a C-score of -1.39 and TM-score of 0.54±0.15. The model having

a C-score value >−1.5 and TM-score value >0.5 is considered to have a correct fold [Xu and Zhang, 2010; Yang and Zhang, 2015].

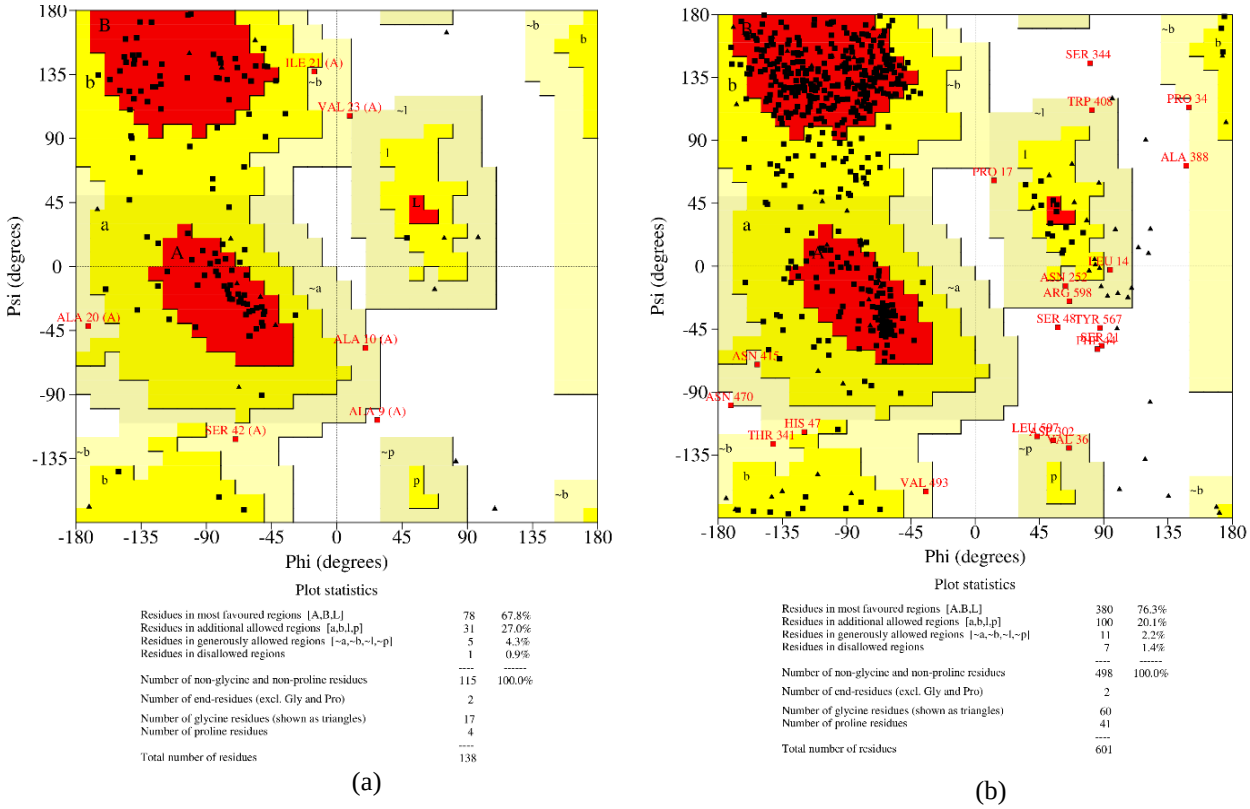

Figure 5.7 Ramachandran plot assessment for (a) Cerato-platanin and (b) Laccase.

Cerato-platanin-Laccase docking using ClusPro 2.0

Docking analysis by ClusPro 2.0 revealed that both cerato-platanin and laccases have a strong binding capacity. ClusPro protein–protein docking displayed 10 best-docked confirmations, of which the top ranked model from balanced coefficient module was downloaded in PDB format and used for analysis. The individual model of laccase and docked proteins have been depicted Figure 5.8. Cerato-platanin and laccases exhibited binding energy value of – 897.3 kcal mol^{-1}. Protein-protein docking is a common approach used to understand the vaccine designing, amyloid aggregation and peptide designing against diseases [Kowalsman and Eisenstein 2007; Cui et al. 2010]. However, protein-protein docking to study biodegradation mechanism is rare. Hence, in order to evaluate the binding energies, the above-mentioned reports were considered for comparison. For instance, docking of a human toll-like receptor with a vaccine model showed the energy score of -1311.5 kcal mol^{-1} which was suggested to be good binding affinity [Yang et al. 2021]. The observed binding between cerato-

platanin and laccase supported our predicted hypothesis that both these proteins interact during PSS myco-transformation.

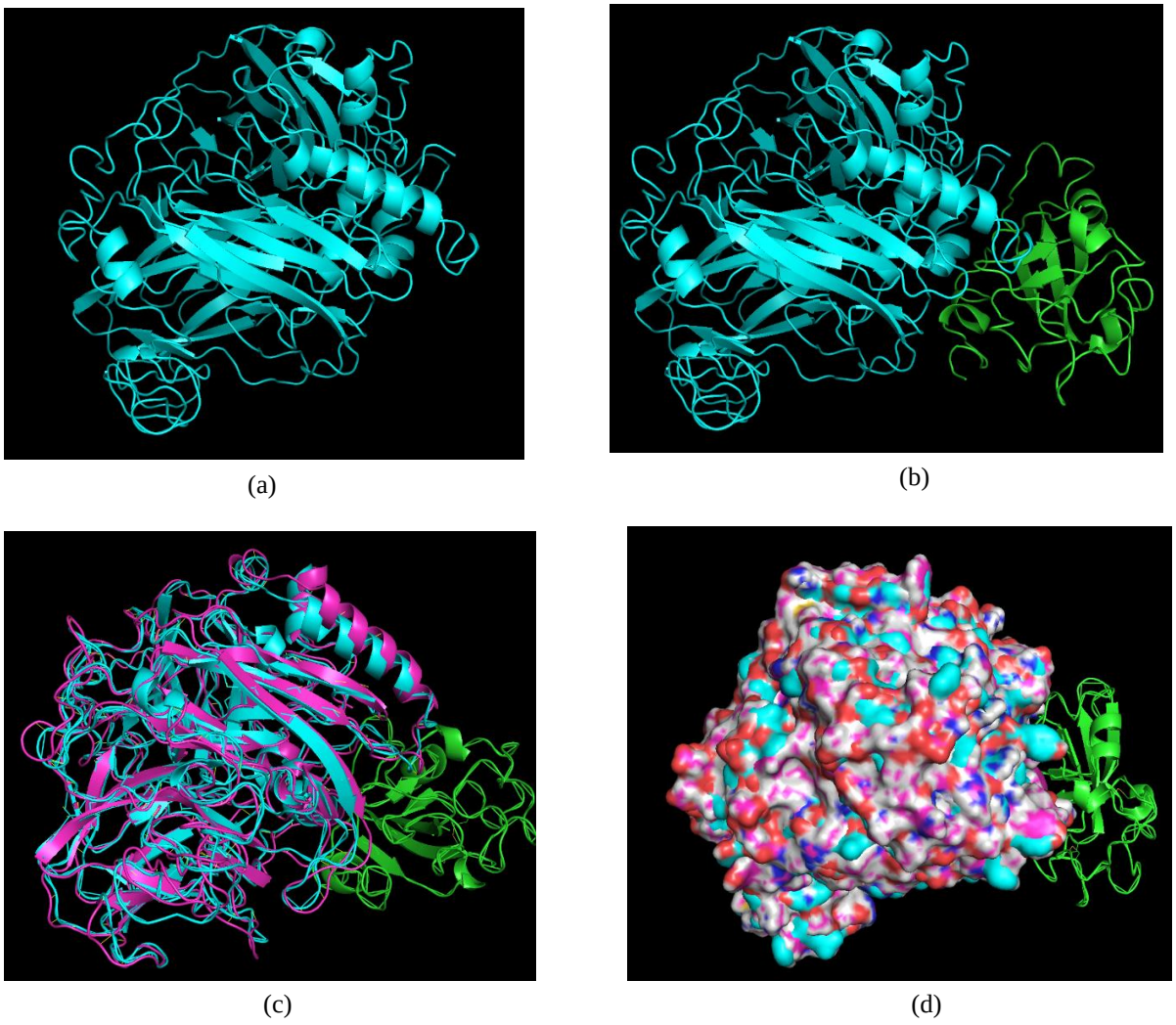

Figure 5.8 *In silico* docking analysis of binding interactions between cerato-platanin and laccase (a) Laccase only, (b) Cerato-platanin (green) and laccase (cyan) docked complex, (c) Overlapped structure of laccase over docked complex, and (d) Surface representation of laccase with cerato-platanin.

Cerato-platanin-Styrene sulfonate complex analysis by molecular docking

Based on the above-mentioned results, it is clear that cerato-platanin and laccase displayed strong interaction potential and may also function together for PSS myco-transformation. Hence, it is important to individually understand their interaction with SS. The docking analysis between cerato-platanin and SS highlighted that the protein pocket interacting with SS is mainly comprised of 7 hydrophobic residues namely Ala10, Gly69, Gly102, Ile21, Phe14, Tyr67 and Val11and 2 polar residues namely, Gln68 and Thr22. The aromatic ring

mainly interacts with the hydrophobic patch, whereas two hydrogen bonds (indicated in green) of length 3.04 Å and 2.67 Å were observed between the oxygen atom of the SS and Thr22 [Figure 5.9 a]. These hydrophobic residues form a hydrophobic-ligand binding pocket for SS [Figure 5.9 b]. Additionally, all the 7 hydrophobic residues interact via hydrophobic interactions (indicated in red) with the oxygen, sulfur and ring (C1-C6) and side-chain carbon of SS, indicating strong interaction between the residues of cerato-platanin and SS.

The binding energy of the cerato-platanin and SS complex was found to be -5.55 kcal mol^{-1}. The binding energy of a complex is important for defining the strength of the protein-ligand interactions and is considered as the most important aspect for estimating the complex stability [Bitencourt-Ferreria et al. 2019]. Cerato-platanin family is a relatively newly discovered protein family of unique fungal proteins with overlapping and closly related attributes to hydrophobins [Bonazza et al. 2015]. However, cerato-platanins are better in solubility than hydrophobins [Gaderer et al. 2014]. Cerato-platanins are commonly found in phytopathogenic fungi and promote their hyphal adherence to the cuticle. These proteins self-assemble in the form amphipathic membrane at the hydrophobic/hydrophilic interfaces, thereby forming a protective surface coating of fungal structures and aiding in their adherence to the surfaces [Baccelli, 2015]. Therefore, the basic focus of the cerato-platanin studies are mainly related to plant sciences, and lack docking studies.

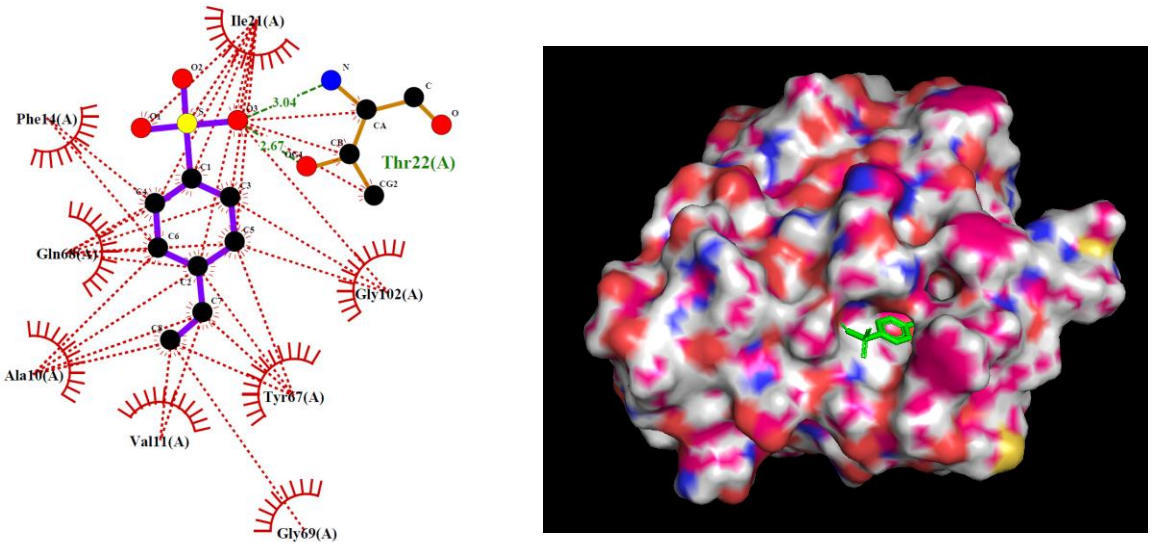

Figure 5.9 *In silico* molecular docking analysis of binding interactions between cerato-platanin with SS (a) Schematic 2D representation of the identified hydrogen bonding and hydrophobic interacting residues in the protein domain. (b) representation of the binding cavity showing the interaction of SS with cerato-platanin.

Laccase-Styrene sulfonate complex analysis by molecular docking

The docking analysis of laccase with SS revealed that both the moieties interact via hydrogen and hydrophobic interactions. There are mainly 4 hydrophobic residues Arg176, Glu129, Lys173 and Tyr175 which interact with the sulfur, oxygen & ring (C1-C6), and side-chain carbon of SS via hydrophobic interactions (shown in red). Further, Leu174 forms 2 hydrogen bonds (shown in green) of length 3.18 Å and 3.28 Å with SS; while Gln156 forms 2 hydrogen bonds of length 2.72 Å and 3.08 Å with SS indicating that the binding is quite strong between two interacting moieties.

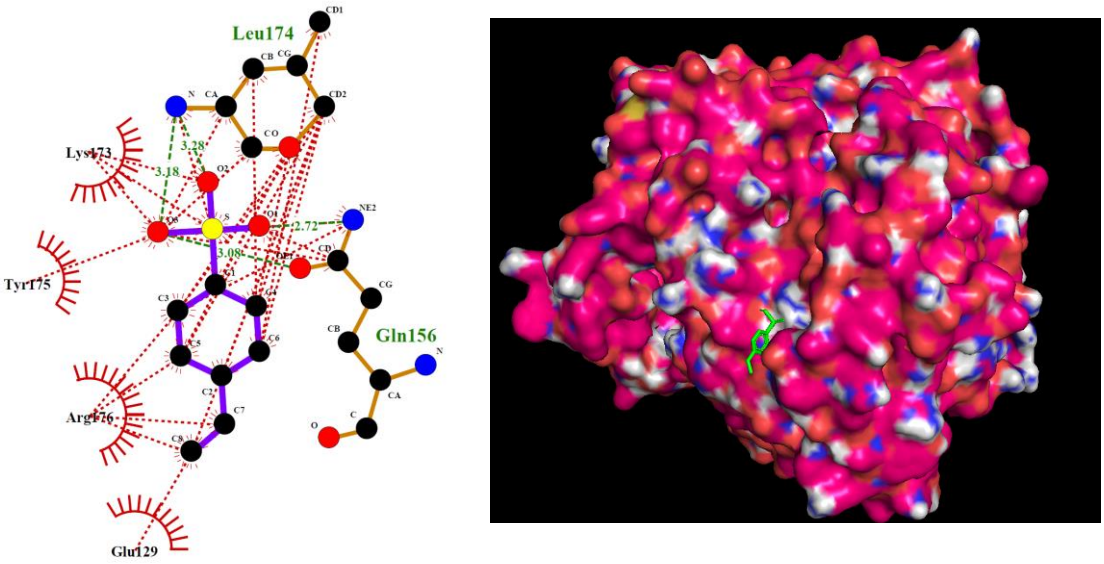

(a) (b)

Figure 5.10 *In silico* molecular docking analysis of binding interactions between laccase with SS (a) Schematic 2D representation of the identified hydrogen bonding and hydrophobic interacting residues in the protein domain. (b) representation of the binding cavity showing the interaction of the SS with laccase.

Further, the binding energy of the docked complex was observed to be -5.41 kcal mol^{-1}. Interestingly, both cerato-platanin and laccase exhibited similar extent of binding energies towards SS. The negative binding energy reflects that process is spontaneous. The lower binding energy between enzyme and substrate makes it more favourable for the enzyme to combine with the substrate, and subsequently ease degradation of pollutants can be degraded [Hongyan et al. 2019]. The binding energy between laccase and SS were found to be comparable with the published reports. The binding energy between laccase and PE was observed to be -6.0 kcal mol^{-1}, and laccase was found to be crucial in polyethylene degradation

[Santacruz-Juárez et a. 2021]. The binding free energy between bisphenol A and laccase was calculated to be -7.25 kcal mol^{-1} [Hongyan et al. 2019]. Binding energy of -7.19 kcal mol^{-1} was observed during molecular docking of laccase and azo dyes [Sridharan et al. 2021]. Majority of the above-mentioned studies used the experimentally derived laccase structures, whereas the structure of *C. dactyloctenicola* VJP08 laccase was derived by threading. So, it is possible that the structural interactions established through experiments will indicate stronger binding energy with SS. In summation, the proximity of the above discussed binding energies to the binding energy found in the present study suggests that laccase has a great potential for PSS myco-transformation.

5.4 Conclusion

The extracellular proteomic analysis revealed that *C. dactyloctenicola* VJP08 secretes a huge array of depolymerization enzymes. These enzymes include oxidoreductases essential for PSS myco-transformation, CAZymes important for utilizing the generated metabolites, stress-response and homeostasis proteins, energy generation proteins and surface-active cerato-platanin protein crucial for mediating interaction between laccase and PSS. Together, these proteins support the utilization of PSS as the sole carbon source to enable fungal metabolism and growth. The proteomics analysis also identified various fungal-mediated extra- and intra-cellular fungal-mediated PSS metabolising pathways that function via aromatic or side-chain cleavage. These findings were further validated by *in silico* studies which exhibited preliminary indication that the two functionally complementing proteins, namely cerato-platanin (biosurfactant) and laccase (catalytic) necessary for PSS myco-transformation have significant binding forces. Both these proteins independently exhibited similar binding energies towards SS monomer suggesting their capability to interact with SS. The results support the conclusion that cerato-platanin interact with hydrophobic SS as biosurfactant and aides in catalytic enzymes ability to depolymerize it. Together, these findings have important environmental significance as they can deepen our understanding on the molecular mechanism underlying proteins that degrade plastics. These findings can shed light on putative mechanisms behind the myco-transformation pathways, which would assist in functional predictions and future validations on the identified proteins. These findings also raise intriguing questions on the selection process of microbes used for plastic biodegradation. The present study suggests that phytopathogenic fungi are an excellent source of depolymerization proteins and enzymes. Since phytopathogenic fungi have evolved to penetrate and infect hydrophobic plant barriers, by degrading natural polymers, such as cutin, the extracellular enzyme arsenal of these fungi

functionally relevant to metabolize structurally related compounds like plastics. The present study identified that phytopathogenic fungus *C. dactylocteniola* VJP08 releases a variety of oxidoreductases including Laccase, Multicopper oxidase, Tyrosinase Cu-bd domain, FAD_binding_3 domain, Flavodoxin-like domain, which have the ability to cleave aromatic rings and long chain carbons by oxidation, which otherwise is a challenging problem in plastic biodegradation. The oxidation and cleavage of PSS makes the polymer more hydrophilic, after carboxylic group synthesis, and facilitates its interactions with other extracellular enzymes (e.g., lipase and esterase). These enzymes were also observed to be upregulated in the proteomics data. Last but not least, the proteomics data revealed significant expression of several transporters, which play a key role in absorption of generated myco-transformation products by fungal cells.

Chapter 6

Phylloplane Fungus *Curvularia dactyloctenicola* VJP08 Effectively Degrades Commercially Available PS Products

6.1 Introduction

Industrial, economic and population expansion has led to the over-exploitation of fossils fuels for generation of energy, chemicals, and commodity products raising three majorly inter-connected global challenges i.e., climate change, loss of biodiversity, and chemical pollution [Demeneix et al. 2020; Raj et al. 2022]. One of the key contributing factors to the environmental deterioration is plastic pollution. Invented about 110 years ago, plastics are now the most widely used man-made substances with excellent properties such as durability, resistance to erosion, ease of processing and economic feasibility leading to its mass applicability in medical supplies, packaging, disposable cutlery, automobiles, clothing, and construction materials [Wong et al. 2015]. Global production of plastics had drastically increased over the decade, and it is expected to reach up to 589 Mt by the year of 2050 [Garside, 2020]. The increase in plastic demand has consequently led to the generation and accumulation of larger amount of plastic waste being released into the environment. About 50% of the total plastic manufacturing is inclined towards single-use products and only ~20% is used for long-term applications [Geyer et al.2017]. Despite their mass production, effective strategies in response to the plastic waste disposal issues lack implementation [Kedzierski et al. 2020]. Furthermore, current strategies such as recycling, incineration and landfilling are practically inadequate to reduce the impact of waste on the environment [Turner, 2018]. Serious health effects have been observed in workers involved in plastic manufacturing and recycling industries [Meeker et al. 2009; Zhigui et al. 2015].

Polystyrene (PS) is a single-use thermoplastic composed of aromatic styrene monomers. Presently, PS dominates the market with applications in everyday disposable cutlery such as clamshell containers, ready-to-consume food packaging, take-away drinking cups, lids, etc [Thakur et al. 2018]. Therefore, a large portion of PS waste ends up in landfills/ oceans that ultimately cause the leaching out of harmful additives as well as its micro-/nano-forms into the environment [Avio et al. 2016; Syranidou et al. 2017]. The adverse consequences of ingestion of PS/ PS derived micro- and nano-plastics have also been investigated to induce various molecular, biochemical, and cellular alterations such as induction of oxidative stress, neurotoxicity, DNA damage, and impaired organ formation [Xiao et al. 2020; Dimitriadi et al. 2021; Teng et al. 2022].

The PS biodegradation studies have discussed various approaches including culture enrichment, pre-treatments, and carbon-labelling to monitor the degradation process, however, lower degradation rate is a major concern [Zhang et al. 2022]. The reason behind this could be that PS structure is extensively formed by the C-C skeleton which requires high bond dissociation energy (BDE) making it a less preferential carbon source for the microbes [Blanksby and Ellison, 2003]. Some microorganisms, such as bacteria (*Bacillus* sp., *Pseudomonas* sp., *Rhodococcus* sp., *Microbacterium* sp., etc) and fungi (*Aspergillus* sp., *Alternaria* sp., *Curvularia* sp., *Cephalosporium* sp., *Mucor* sp., etc) can form biofilm on PS, and can partially change the chemical properties of PS [Zhang et al. 2022]. However, majority of the studies on PS degradation focus on its pre-treatment by exposing PS to various chemicals and/ or radiations causing its structure to be susceptible for the microbial action prior to exposing it to microorganisms [Galgali et al. 2004; Motta et al. 2009; Chaudhary et al. 2021].

The mineralization of polymers is a complex process and can be accomplished by the microbial species having functional complementarity and adaptability [Syranidou et al. 2019]. As established in previous chapters, phylloplane fungus *Curvularia dactyloctenicola* VJP08 demonstrated characteristic ability towards utilization of polystyrene sulfonate (PSS), which is a structural analogue to PS. The present study highlights the efficiency of *C. dactyloctenicola* VJP08 towards its ability to utilize and colonize over the commercially used PS products. The fungal response was estimated in terms of its growth, microscopic investigations, mechanical properties of PS and predicted metabolites generated during treatment duration.

6.2 Materials and Methods

6.2.1 PS sample collection

The PS lids were collected from the food vendors at the Chhatrapati Shivaji Maharaj International airport (coordinates: 19.0904°N, 72.8628°E). The lids clearly bearing the PS identification symbol were collected. The procured samples were cleaned with sterile distilled water and then aseptically cut into smaller pieces of 5mm*5mm size. These samples were surface sterilized using 70% ethanol solution prior to incubation with fungi.

6.2.2 PS Myco-degradation Studies

Microbial degradation of PS samples was studied using *C. dactyloctenicola* VJP08. The stock culture of fungal isolate was maintained by regular sub-culturing on PDA plates (pH 5.6±0.2) at 28℃. From an actively growing culture, a loopful of spores was inoculated in

circular fashion on the surface of mineral salt agar (MSA) plates containing NH_4NO_3 3 g L^{-1}; KH_2PO_4 & $K_2HPO_4 \cdot 3H_2O$ 0.5 g L^{-1} each; $MgSO_4 \cdot 7H_2O$ 0.008 g L^{-1}; $CuSO_4 \cdot 5H_2O$, $MnSO_4 \cdot H_2O$, $FeSO_4 \cdot 7H_2O$ & $CaCl_2 \cdot 2H_2O$ 0.002 g L^{-1} each; and agar 20 g L^{-1}; pH 5.6±0.2. Total 8 PS sample pieces (5mm×5mm size) as the sole carbon source were firmly placed at almost equal distance on the fungal inoculum circle in the MSA plates and incubated at 28℃ under dark conditions for 30 days. MSA plates inoculated with fungal spores (without PS pieces) as negative control and MSA plates with 1% dextrose (without PS sample pieces) as positive control were also incubated simultaneously along with experimental plates in three replicates.

6.2.3 Assessment of PS Myco-degradation

6.2.3.1 Surface Morphology and Chemical Characterisation of PS Samples

The morphological changes in the PS samples before and after fungal exposure were investigated using Field Emission-Scanning Electron Microscope (FE-SEM). The PS samples with and without fungal exposure were fixed on aluminium stubs using a double-sided carbon tape and sputter coated with gold palladium for 60-120 s at 40 mA (Quorum Q150T ES Plus, United Kingdom), and visualized under FE-SEM (ApreoS FEI/ FESEM, Thermo Fischer, USA) at different magnifications. A voltage of 10 kV was maintained while imaging the samples. Additionally, the critical elemental composition of PS samples was determined using Energy Dispersive spectroscopy (EDS), in order to evaluate the extent of degradation of the PS samples.

6.2.3.2 Determination of Percent Weight Loss

For the myco-degradation study, the initial weight of PS sample pieces were recorded prior to their placement on the MSA plates. After completion of incubation period (30d), the PS sample pieces were aseptically taken out and washed properly with aqueous sodium dodecyl sulfate (2% v/v) solution [Sivan et al., 2006]. After washing, the final weight of the air-dried PS sample pieces was recorded, and the percent weight loss was calculated using the following formula:

$$\% \text{ weight loss} = \frac{W_i - W_f}{W_i} \times 100$$

Where, W_i: initial weight; W_f: final weight

6.2.3.3 Determination of Percent Change in Thickness of PS samples

The initial and final thickness of PS sample pieces were measured at five distinct locations using a micrometer screw gauge (Fisher Scientific). The average thickness and standard deviation were calculated for each piece. The percent change in the thickness was calculated using the following formula:

$$\%\ \text{change in thickness} = \frac{T_i - T_f}{T_i} \times 100$$

Where, T_i: initial thickness; T_f: final thickness

6.2.3.4 Differential Scanning Calorimetry (DSC) Analysis

In order to understand the molecular changes in the control and test PS samples, differential scanning calorimetry (DSC) analysis was carried out using DSC-4000 system (Perkin Elmer, USA). The temperature ranges from 20 to 110 °C with a heating rate of 10 °C/min was used in a nitrogen atmosphere for the first and second heating and cooling cycles.

6.2.3.5 GC-MS/MS Analysis

After completion of incubation period (30 days), the degraded products of PS sample pieces were identified by the GC-MS/MS analysis. For this, the treated PS samples were washed (as described in section 6.2.3.2) and individually mixed in 10 mL chloroform followed by ultrasonication for 2 h at 55°C. The chloroform was evaporated at room temperature, and the samples were re-suspended in 2 mL chloroform followed by filteration using 0.2 μm PTFE syringe filter. The filtered samples were analysed by GC-MS/MS using helium as carrier gas (head pressure 72.5 kPa; flow rate 1.0 mL/min). Rtx-5 capillary column having 0.10 μm film thickness, 0.25 mm i.d., and 30 m length was used. The oven temperature was initially held at 60 °C for 2 min and then increased at a rate of 5 °C min^{-1} to a final temperature of 220 °C. The injector temperature was set to 250 °C. Electron impact mass spectra were collected at 70 eV over the range of 30–300 *m*/*z*. The ion source and analyser temperatures were set to 250 and 230 °C, respectively. Identification of the degradation products was performed by comparing their mass spectra with the NIST16 Mass Spectral Library.

6.3 Results and Discussion

6.3.1 Myco-degradation of PS

In nature, fungi are the major decomposers and predominantly responsible for the degradation of naturally occurring polymers such as lignocelluloses. The lignocelluloses form a very complex and stable conglomerate of different structural units including polysaccharides linked to aromatic lignin imparting strength to the whole structure [Nishimura et al. 2018]. Lignin is a complex aromatic biopolymer and have methyl ester and C-C bonds. The bond-dissociation energy (BDE) of C-C bonds (240-425 KJ mol^{-1}) in lignin is comparable to the BDE of C-C bonds (330-370 KJ mol^{-1}) present in the plastics such as PS [Daly et al. 2021]. Besides possessing slightly higher BDE range, lignin is susceptible to fungal action, while plastics are not readily utilized by the fungi. Since the adaptability of fungus towards lignin degradation dates to the Palaeozoic era, fungi have not yet evolved active enzymes adapted to attack the comparatively 'recently' discovered and introduced plastics in the environment [Floudas et al. 2012]. However, there are reports which support that pathogenic fungi have dominant prevalence and degradative relevance towards plastic degradation [Danso et al. 2019]. Mechanistically, the prevalence of pathogens in plastic degradation may be reasoned by the production of invasive structures (e.g., appressoria), biofilm formation, mucilage secretion and thigmotropism [Gkoutselis et al. 2021]. Hence, the potential of phytopathogenic fungi may be explored towards their ability to attack plastics. In the present study, the ability of phylloplane fungus *C. dactyloctenicola* VJP08 towards utilization of commercially available PS as nutrition source was tested. As expected, substantial mycelial growth was observed in MSA plates (without PS sample pieces) containing 1% dextrose as carbon source at day 2 of incubation [Figure 6.1 a]. However, no growth was observed at day 2 in the negative control MSA plates as they did not contain any carbon source [Figure 6.1 b]. Interestingly, the fungal hyphae began to develop around the PS sample pieces within 2 days of incubation, and gradually lead to dense growth on the PS samples over an incubation period of 30 days [Figure 6.1 c & d].

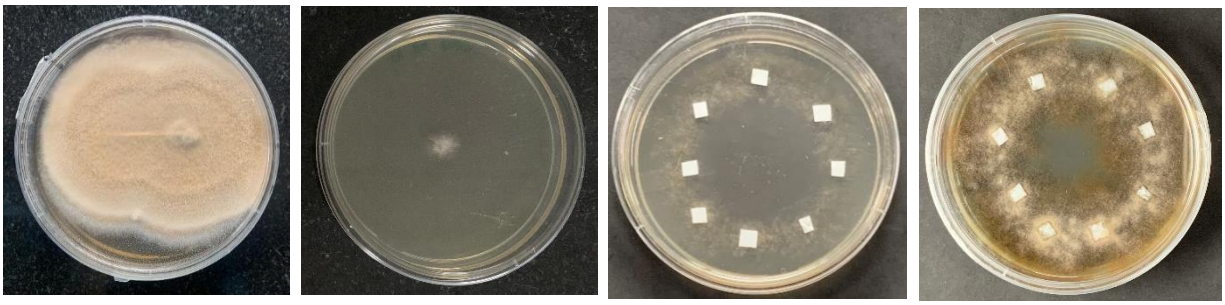

(a) (b) (c) (d)

Figure 6.1. Representative images depicting the growth of *C. dactyloctenicola* VJP08 on (a) MSA+ 1% dextrose (at day 4), (b) only MSA (at day 4); and around & on the PS sample pieces firmly placed on MSA plates (c) at day 2 (d) at day 30 of incubation.

6.3.2 Surface morphology and chemical characterisation of PS samples

The visual and physical appearance of specimens provides a first clue about the occurrence of polymer degradation during the biodegradation process [Karimi-Avargani et al. 2020]. The degradation of plastics begins with the attachment of fungal hyphae followed by the mycelial growth and colonization on the plastic surface and disturbing the molecular arrangement within plastics by altering the physical and mechanical properties [Bhanot et al. 2020; Chaudhary et al. 2021]. During the present study, a gradual increase in the fungal growth on the PS sample pieces was clearly observed visually during the incubation period [Figure 6.1]. In order to minutely visualise the physical changes on the PS surface, SEM analysis of different PS sample was performed [Figure 6.2]. SEM micrographs showcased a relatively smooth and homogeneous solid surface in the untreated control PS samples [Figure 6.2 a and b]. In contrast, the PS samples incubated with *C. dactyloctenicola* VJP08 showed dense colonization by the fungal mycelia [Figure 6.2 c and d]. The presence of dense hyphal network of *C. dactyloctenicola* VJP08 on the PS surface suggested the possible utilization of PS as carbon source during the growth and development of fungal mycelia [Figure 6.2 c and d].

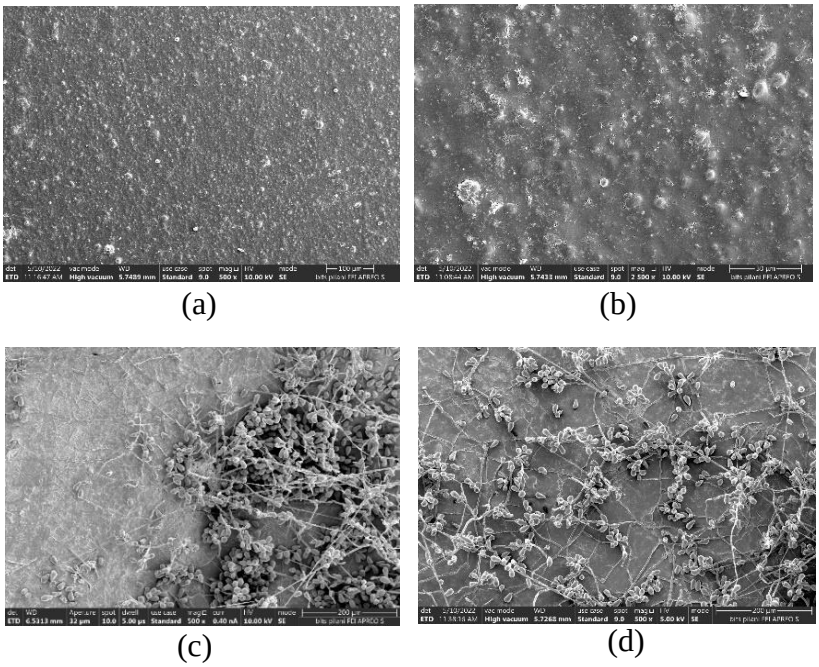

Figure 6.2. Representative SEM micrographs of PS sample pieces. (a) and (b): control; (c) and (d): mycelial network on the surface of PS samples inoculated with *C. dactyloctenicola* VJP08 after 30 days of incubation. Scale bar in a = 100 μm; b = 30 μm; c and d = 20 μm

Higher resolution (HR) SEM micrographs depicted the presence of overlapped and densely intertwined hyphae presumably considered as the sites for the release of higher amount of extracellular matrix (proteins, enzymes and polysaccharides) mediating the PS degradation [Figure 6.3 a, b, d]. The formation of pores, fractures and corrosions over the PS surface were clearly visualised at the immediate proximity of the hyphal meshwork indicating the breakdown of PS by fungal enzymes [Figure 6.3 c and d]. Noteworthy, after hyphal growth, the fungi developed reproductive conidia [Figure 6.3 a, b, c]. Gkoutselis et al. (2021) also reported the presence of similar fungal structures (hyphae and conidia) and fungal secreted mucilage on the microplastic polymer matrix. During degradation, the formation of the void structures such as pores, corrosion or cracks over the plastic surface are known to facilitate the penetration of fungal hyphae resulting in diffusion of enzymes further deeper into the plastic matrix, thereby decrease its thickness [Karimi-Avargani et al. 2020]. It is noteworthy that solid hydrophobic surfaces such as PS films, are also known to induce morphological differentiation and formation of invasive structures in pathogenic fungi [Kumamoto, 2008]. Nonetheless, the presence of putatively germinating spores and a conidiogeneous hypha further confirmed the reproduction and propagation of fungus as a result of PS degradation.

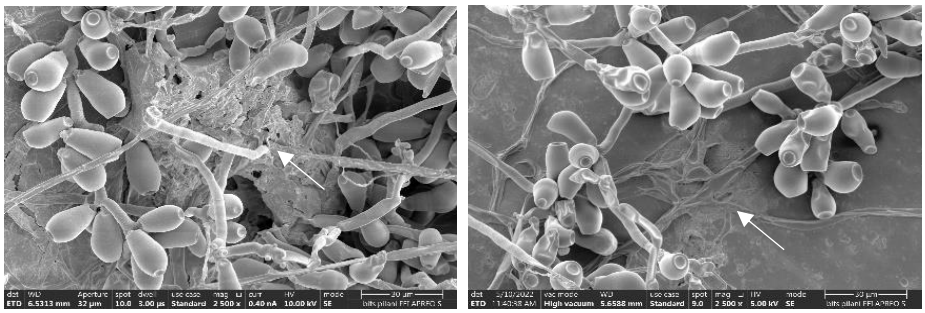

(a) (b)

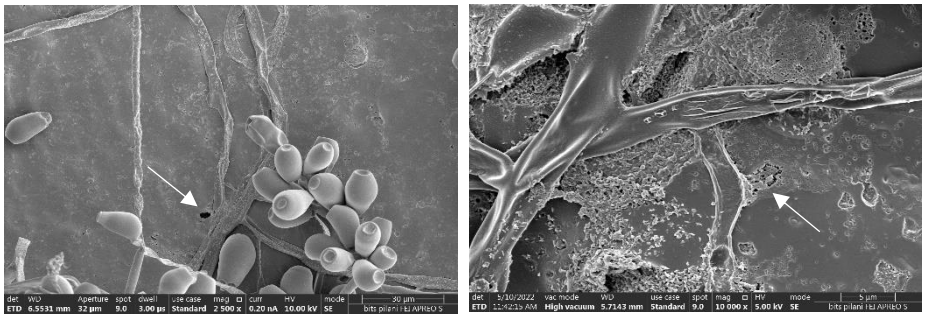

(c) (d)

Figure 6.3. HR-SEM micrographs showing fungal colonization on PS and its surface degradation artifacts. (a) and (b): dense intertwined hyphae and conidia, with extracellular matrix (indicated by white arrows); (c) and (d): pores and cracks (indicated by white arrows) on the PS surface.

The EDS analysis of the untreated and treated PS samples further confirmed the degradation of PS when inoculated with *C. dactyloctenicola* VJP08 for 30 days [Figure 6.4]. In comparison to the untreated samples, the fungal-treated samples showed 3% decrease in the carbon content, indicating the extraction of carbon from the PS to support the fungal growth and metabolism. Moreover, ~3% increase in the oxygen content of the treated samples also confirmed the PS degradation. Canopoli et al. (2020) also reported alterations in the surface morphology and increased amount of oxygen by SEM-EDS analysis which were considered as indicators for the plastic degradation.

(a)

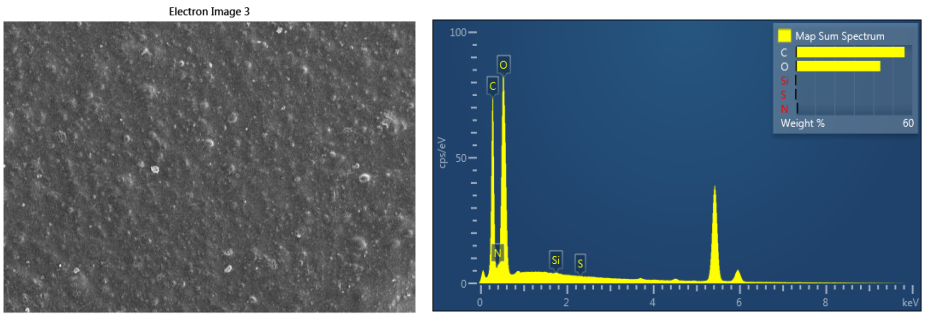

Map sum spectrum	Atomic %
Carbon	63.04
Nitrogen	0.00
Oxygen	36.81
Silicon	0.11
Sulfur	0.03
Total	100.00

(b)

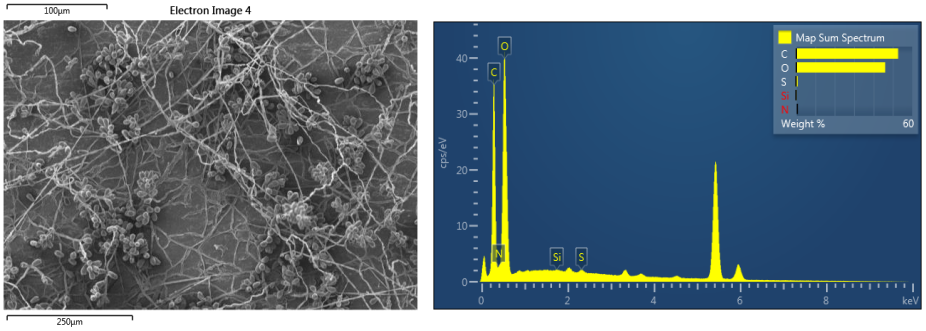

Map sum spectrum	Atomic %
Carbon	60.06
Nitrogen	0.00
Oxygen	39.41
Silicon	0.12
Sulfur	0.41
Total	100.00

Figure 6.4. SEM-EDS spectra and elemental composition of PS samples (a) control and (b) PS samples inoculated with *C. dactyloctenicola* VJP08 after 30 days of incubation.

6.3.3 Percent Weight Loss in PS Sample Pieces

Microbial growth on the plastic surfaces is considered as the initial step implicating its biodegradation. The extent of biodegradation can be confirmed by performing the gravimetric analysis of the degraded plastic samples [Syranidou et al. 2019]. One of the fundamental method to determine the degradation of polymers is measurement of its weight loss. Several studies have reported weight reduction in the plastic samples due to the activity of various microbes [Balasubramanian et al. 2010; Das and Kumar, 2015]. Before placing the PS sample pieces on the MSA plates inoculated with *C. dactyloctenicola* VJP08, the initial average weight of the PS pieces was recorded to be 0.0114±0.0012 g. After 30 days of incubation, the average final weight was recorded to be 0.0107±0.0016 g. The observed weight reduction of 3.57% in the PS samples confirmed the capability of *C. dactyloctenicola* VJP08 to degrade PS and showed its potential to survive on the surface of PS as the sole carbon source.

Previous reports of fungal-mediated degradation of pure PS samples observed 2.17% and 1.81% weight reduction when incubated for 8 weeks with *Cephalosporium* sp. and *Mucor* sp., respectively [Chaudhary and Vijayakumar, 2020]. Moreover, the fungal-mediated degradation of PS and PS-linked with different carbohydrates revealed that pure PS was resistant to degradation by fungi including *Aspergillus niger* NCIM 1025, *Penicillium ochrocloron* NCIM 1219, *Pullularia pullalans* NCIM 1049 and *Trichoderma* sp. NCIM 1297,

while PS-linked lactose, PS-linked glucose and PS-linked sucrose were susceptible to fungal degradation showing a maximum % weight reduction of 12%, 20.4% and 19.6%, respectively [Galgali et al. 2004]. However, the reason behind this partial degradation could be the selective utilization of carbohydrate source by the fungi. In another study, chemically oxidised PS was reported to be susceptible for colonization and degradation by *Curvularia* sp. however this study only focused on microscopic analysis of fungal adherence and lacked % weight reduction analysis [Motta et al. 2009]. Nonetheless, majority of the studies monitor the degradation of pre-treated PS samples [Johnston et al 2018; Du et al. 2022], which are inherently more susceptible to the microbial attack.

6.3.4 Percent Change in Thickness of PS Samples

Since fungal hyphae breach the substrate for nutrition, the fungal mediated degradation of PS can also be evaluated by measuring the change in thickness of treated samples. The average initial thickness of all the PS samples was recorded to be 0.317±0.018 mm. After 30 days of incubation with tested fungal species, the average thickness of treated PS sample pieces was recorded to be 0.289±0.018 mm. The decrease of 8.8% in the thickness of PS sample pieces indicated that *C. dactyloctenicola* VJP08 successfully penetrated and utilized PS sample for carbon acquisition and growth.

Earlier studies also reported that fungal degradation of different plastic types is accompanied by the decrease in thickness of tested samples. For instance, 52% decrease in the thickness was observed when polylactic acid (PLA) was incubated with *Aspergillus flavus* CCUG 28296 for a period of 6 months [Karimi-Avargani et al. 2020]. Another study reported 16.6% decrease in the film thickness of polyhydroxybutyrate and hydroxyvalerate (PHBV) when landfilled for a period of 120 days [Ishigaki et al. 2004]. Although, various studies have been published which report the % change in the weight of PS samples, the present study first time report fungal induced % change in the thickness of PS samples.

6.3.5 DSC Analysis

The influence of *C. dactyloctenicola* VJP08 colonisation on the thermal properties of PS was studied by DSC that measures the heat flow into a sample. During DSC measurement, the glass transition temperature (T_g) of the control PS sample was recorded to be 97.28℃, which was found to decrease to 95.23℃ in case of PS sample exposed to *C. dactylocteniola* VJP08 for 30 days [Figure 6.5]. The reduction in T_g occurred due to the alterations in the physical and mechanical properties of polymer by fungal degradation, causing higher degree

of freedom of molecular motility in presence of heat [Lu and Jiang, 1991]. Thermal stability or decomposition onset temperature is directly related to its mean molecular weight, such that lower molecular weight results in lower thermal stability of the polymer [Shojaeiarani et al. 2019]. Since, T_g is inversely proportion to the molar mass of the polymer, the decrease in T_g indicated decrease in the molar mass of PS.

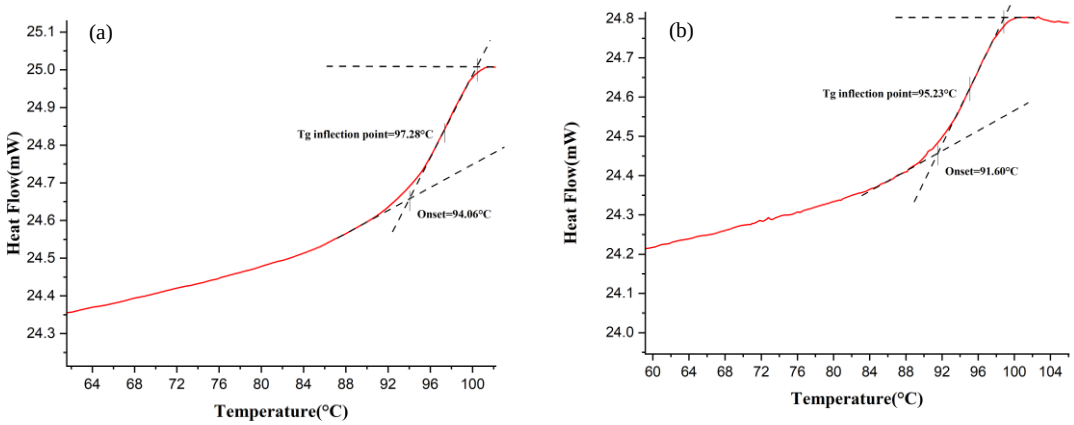

Figure 6.5. DSC thermograms of PS film: (a) control; (b) PS sample inoculated with *C. dactyloctenicola* VJP08 after 30 days of incubation.

Similar results were observed by Karimi-Avargani et al. (2020), who reported a decrease in the T_g of fungal treated PLA from 61.5°C to 60.5°C after six months of incubation. Various other studies have also reported the application of DSC to identify the structural changes in different plastics indicating the decrease in crystallinity and T_g as a result of their degradation [Volke-Sepúlveda et al. 2001; Tatai et al. 2007; Houchin and Topp, 2009; Osman et al. 2017].

6.3.6 GC-MS/MS Analysis

To further explore the details of PS degradation by *C. dactyloctenicola* VJP08, the degradation products were analysed by GC-MS/MS [Figure 6.6 a and b]. The untreated control and fungal treated PS samples were analysed for the presence of various PS monomers, oligomers, plastic additives and various aromatic derivatives such as benzene, 2, 4 Di-tert-butylphenol (2,4-DTBP), Diethyl phthalate, 1,2 -diphenyl cyclobutane and (2,3-diphenylcyclopropyl) methylsulfanylbenzene (2,3-DCMSB). After 30 days of incubation with *C. dactyloctenicola* VJP08, these compounds were observed to be either partially or completely utilized by the fungus. A significant decrease of 73.6% in the peak area of benzene was observed, which is a key monomer of the PS structure, which suggest that the major proportion of carbon was extracted from the PS skeleton by its degradation. Additionally, diethyl

phthalate, which is a plastic additive, was found to be completely utilized by the fungus, along with significant reduction in the concentrations of aromatic derivatives including 2,3-DCMSB after incubation period. These results are in accordance with the previous studies, where similar PS-derived compounds have been detected during PS myco-degradation. For instance, 2,4-DTBP and aromatic derivative namely, 1,3,5-triphenylcyclohexane and 2,4,6-triphenylcyclohexene were identified in the PS samples treated with *Tenebrio molitor* larvae [Tsochatzis et al. 2020]. Similarly, compounds such as benzene, cyclobutane, and phenyl derivatives were identified during the PS myco-degradation by fungal isolates and mealworm larvae [Oelschlägel et al. 2018; Chaudhary and Vijayakumar, 2020; Tsochatzis et al. 2021]. Furthermore, Diethyl 2-(p-tolyl) malonate and Dodecanamide were the newly generated compounds hypothesized to be the degradation by-products of PS. Noteworthy, as observed in the treated samples, earlier reports also observed generation of benzene associated amides- , methyl-, methoxy-, and sulfoxide groups during the microbial degradation of styrene [Oelschlägel et al. 2018]. The obtained results clearly indicated that the tested fungal isolate VJP08 could significantly colonize and utilized PS which was the sole carbon source in MSA plate.

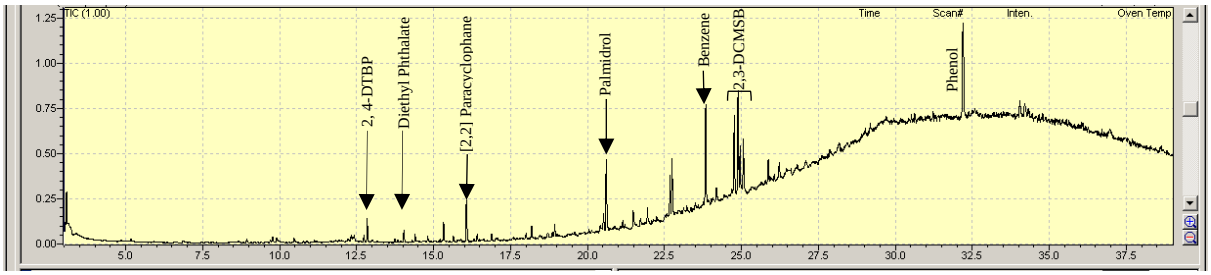

(a)

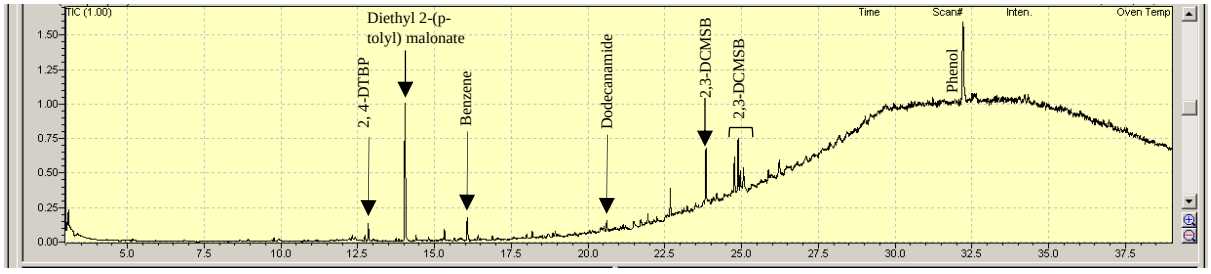

(b)

Figure 6.6. Representative GC-MS/MS chromatogram of PS degradation products (a) control containing PS extract in chloroform; (b) treatment containing PS samples exposed to *C. dactyloctenicola* VJP08.

6.4 Conclusion

As discussed in chapter 1 and 3, owing to the similarities between the naturally occurring lignocelluloses and synthetic plastics, the phytopathogenic fungi emerged as better candidates adapted to utilize plastics. The present study revealed the functional potential of phylloplane fungus *C. dactyloctenicola* VJP08 (reportedly a phytopathogen) towards its ability to colonize and degrade the commercially available PS products. The PS myco-degradation was systematically evaluated by different characterization techniques. The visual and SEM analysis revealed the surface profile of PS samples displaying dense fungal colonisation, propagation and mycelial invasion for carbon extraction causing cracks and holes on its surface. The EDS analysis revealed that PS was utilized by the fungi via oxidation leading to 3% reduction in the atomic carbon concentration. The weight and thickness of PS samples were reduced by 3.57% and 8.8% respectively, indicating its degradation and utilization by fungus for the growth and metabolism. The altered mechanical strength of PS was confirmed by the DSC analysis, which revealed a decrease in T_g in treated samples. Furthermore, GC-MS/MS analysis showed a significant reduction in the concentration of benzene and related aromatic derivatives due to the fungal action, which was fully consistent with the above-mentioned analysis. These findings establish a clear cross-assessment of the phylloplane fungi which may have the ability to breach the plant cuticle to be analyzed for their potential application in development of degradation strategies of synthetic plastics.

Chapter 7

Unveiling the Potential of *Lichtheimia ramosa* AJP11 towards PSS Myco-transformation

Part of the work presented in this chapter has been published as per the following details:

- Bhanot et al. (2023) *Journal of Environmental Management* 325, 116579

7.1. Introduction

Biodegradation of pollutants is a complex process facilitated by the action of various microbial enzymes and subsequent utilization of degraded products as the nutrient source [Srikanth et al. 2022]. The extent of biodegradation is facilitated by a strong enzymatic arsenal and robust microbial growth. Among various microbes, fungi have an enormous extracellular and intracellular enzymatic system that work together to support the fungal growth under different environmental conditions [Shin et al. 2018]. In addition, fungi also have the ability to modify their mycelial structure for optimal nutrient acquisition. The mycelial network undergoes continuous remodelling which makes it highly dynamic towards adapting to different nutrient conditions [Davidson and Olsson, 2000]. For instance, in response to defence against frugivorous nematodes, *Coprinopsis cinerea* undergoes a novel type of hyphal differentiation and communication within a fungal mycelium facilitating faster and more efficient redistribution of nutrients and signals within the hyphal network in comparison to simple diffusion [Schmieder et al. 2019]. Similarly, for utilization of nutrients from rigid solid polymers, fungi spread their mycelia to grow through the solid substrate and dig into the substrate using extracellular enzymes [Naranjo-Ortiz and Gabaldón, 2019]. Fungi have a well-developed secretome that allows them to extract nutrients, even from highly polymerized and often very hydrophobic compounds, such as cutin and/ or lignin, which is very difficult for other microbes [Hiscox et al. 2018]. In secretome, there are certain surface-active fungal proteins namely hydrophobins (hydrophobic surface-binding proteins) which has the ability to bind to hydrophobic surfaces. Although these proteins do not possess catalytic activity, they play a major assistive role during degradation of hydrophobic compounds.

The present study aimed to investigate (i) the ability of fungi isolated from the rhizosphere of plants growing in heavy metal rich sites to myco-transform the synthetic polymer polystyrene sulfonate (PSS) and, (ii) highlight the probable myco-transformation mechanism and identify the putative biomacromolecule(s) involved in myco-transformation of PSS.

7.2. Materials and Methods

7.2.1 Chemicals and Reagents

All chemicals (analytical grade) and solvents (GC grade) used were procured from Sigma Aldrich (India) or Merck (India) unless otherwise stated. All culture media used were purchased from HiMedia (India). Poly(sodium 4-styrenesulfonate) (PSS; M_w ~70,000 Da) was used as the source of PS. Standard protein molecular weight marker (26610) was obtained from Thermo Fischer, USA. For ultrafiltration of proteins, a 12 kDa cut-off nitrocellulose membrane (Merck) was used.

7.2.2 Screening and Shortlisting of Fungal Isolates with PSS Mycotransformation Ability

The metal-tolerant fungal isolates (AJP02-AJP11) used in the present study were isolated from the rhizosphere of the plants growing in iron rich sites. The complete details of their isolation and molecular characterization can be seen in the previous report of our lab [Bhargava et al. 2016]. The individual fungal isolates were revived from the glycerol stocks by streaking on the potato dextrose agar (PDA) media plates followed by incubation at 28°C for 3-4 days, and subsequent sub-culturing. The pure cultures of all the 10 fungal isolates (AJP02-AJP11) were screened to check their ability towards PSS myco-transformation as per the protocol described in Chapter IV (section 4.2.2). The fungal isolates showing maximum increase in their fresh weight biomass was selected for further studies.

7.2.3 PSS Myco-transformation Studies

Three different treatment conditions were used for analysing the PSS myco-transformation potential of short-listed fungal isolate. For this, freshly grown 20 g fungal biomass was resuspended in 200 mL of MSM containing 1% (v/v) PSS in 500 mL Erlenmeyer flask and incubated at 28°C for 30 days on a shaker (150 rpm) under dark conditions in triplicate. Simultaneously, 20 g fungal biomass was also resuspended in only MSM (negative control) and in MSM+3% dextrose (positive control) and incubated at 28°C for 30 days and 4 days, respectively in triplicates. All the experimental flasks were tightly sealed using cotton plugs. After incubation, the fungal biomass was separated by centrifugation (2500 rpm, 10 min, 4°C) and evaluated for the percent change in its fresh weight. The obtained supernatant was vacuum filtrated using Whatman filter paper no. 1 and the fungal cell-free filtrate (CFF) containing extracellular fungal metabolites was collected for further analysis [Jain et al. 2014].

7.2.3.1 Determination of Fungal Biomass and Viability

After incubation, the separated biomass was washed thrice with the autoclaved Mili-Q water. The percent change in the fresh weight of biomass was measured by comparing it with the initial weight of fungal biomass inoculated at day zero of the experiment. The increase in fungal biomass would be indicative of utilization of PSS as sole carbon source for sustaining fungal metabolism. The data points represent the mean of independent measurements, and the uncertainties were represented as standard error.

The viability of fungal cells after exposure to PSS for 30 days was determined by inoculating the exposed fungal mycelia on fresh PDA (pH 5.6) plates. The inoculated plates were incubated at 28˚C for 4 days under dark conditions [Jain et al. 2013]. Since the method indicating the direct utilization of PSS for fungal growth are lacking, the increase in the fungal biomass (in presence of PSS as sole carbon source) and fungal viability after 30 days' exposure to PSS were found to be the most reliable indicators to check the capability of fungi towards utilization of PSS.

7.2.3.2 GC-MS/MS Analysis

Chromatographic analyses were performed following the method described by Krueger et al. [2015] as per the details given in Chapter 4 (section 4.2.4.2).

7.2.4 Mechanistic Studies

7.2.4.1 Protein Precipitation and One-dimensional Gel Electrophoresis

To find out active role of extracellular fungal proteins in PSS myco-transformation, the extracellular proteins in fungal CFF from experimental flasks (including controls) were precipitated, quantified and stained for visualisation as per the details given in Chapter 4 (section 4.2.5).

7.2.4.2 Peptide Mass Fingerprinting

The over-expressed protein bands obtained by SDS-PAGE were subjected to in-gel digestion overnight at 37°C with 10 ng μL^{-1} of trypsin [Shevchenko et al. 1996]. The resulting peptides were mixed with α-Cyano-4-hydroxycinnamic acid (HCCA) matrix in 1:1 ratio and 2 µl sample was spotted onto MALDI plate. After air drying the sample, it was analyzed on the MALDI TOF/TOF Ultraflex III instrument. FLEX analysis software was used for obtaining

the peptide mass fingerprint and the obtained mass spectra were submitted for MASCOT search in "CONCERNED" database for identification of protein [Jain et al. 2014].

7.2.4.3 *In silico* Characterization

***Secondary Structure Prediction* and Physio-chemical Properties of Protein**

Secondary structure prediction was done as per the details given in Chapter 5 (section 5.2.5).

Physico-chemical properties such as amino acid composition, molecular weight, theoretical isoelectric point (pI), extinction coefficient, instability index, aliphatic index, grand average of hydropathicity (GRAVY), the total number of positively and negatively charged residues of the selected protein(s) were identified using Protparam server [Gasteiger et al. 2005].

Molecular Modelling, Ligand Preparation and Molecular Docking Studies

Molecular modelling, ligand preparation and molecular docking were performed as per the details given in Chapter 5 (section 5.2.5).

7.3 Results and Discussion

7.3.1 Screening and Shortlisting of Fungal Isolates

All the 10 fungal isolates (AJP02-AJP11) were screened for their PSS utilization ability. Out of which, *Lichtheimia ramose* AJP11 showed maximum biomass increase (see section 7.3.2.1) by utilizing PSS as the sole carbon source in comparison to all the other fungal isolates (data not shown) and hence, it was short-listed for further studies.

7.3.2 PSS Myco-transformation Studies

7.3.2.1 Effect of PSS on Fungal Biomass and Viability of *L. ramosa* AJP11

As heterotrophs, fungi obtain nutrition from surrounding environment by secreting extracellular enzymes, which breakdown the complex organic compounds. Carbon is major and an essential compound for sustaining all the metabolic processes and maintaining cellular integrity. Hence, it needs to be extracted by the fungi from the surrounding environment in considerable amount. In the present study, utilization of PSS as possible carbon source was tested by incorporating it in MSM for the growth of *L. ramosa* AJP11. The increase in fungal biomass in MSM+1% PSS would indicate the utilization of PSS present as the sole carbon

source in medium towards the growth and metabolic activities of fungal hyphae. Figure 7.1 shows comparative fungal biomass growth at day zero (a) and day 30 (b) in Erlenmeyer flask containing MSM+1% PSS. The fresh weight of fungal biomass at day 30 was recorded to be 28.3±1.8 g. Since the initial fresh weight of fungal biomass inoculated at day zero of experiment was 20 g, the increase (41.6%) in the fungal biomass could positively correlate and indicate utilization/transformation of PSS by the fungal isolate. However, in case of only MSM, since no carbon source was present in the media, the fungus showed significant decrease (22.2%) in the fresh weight biomass. As dextrose is an easily extractable and preferred carbon source, *L. ramosa* AJP11 showed enhanced fresh weight biomass (52±1.5 g) in MSM+3% dextrose (positive control) after 4 days. The fungus incubated in only MSM displayed considerably low revival rate with minimized growth intensity [Figure 7.1 c]. However, the fungus could appreciably maintain its normal growth rate as it showed significant growth on PDA plates even after 30 days exposure to PSS as the sole carbon source [Figure 7.1 d].

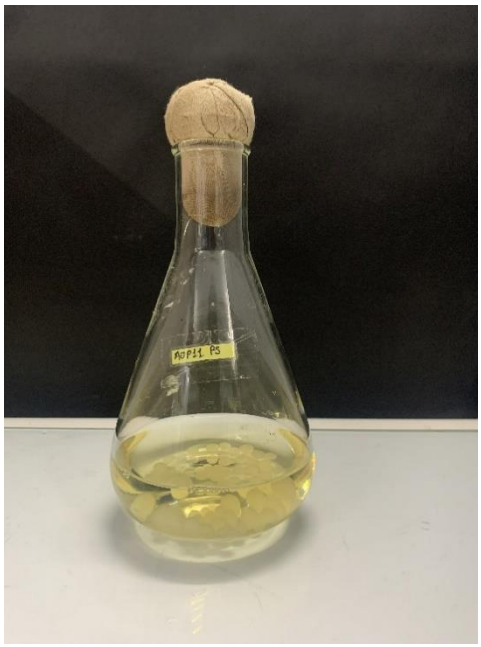

(a)

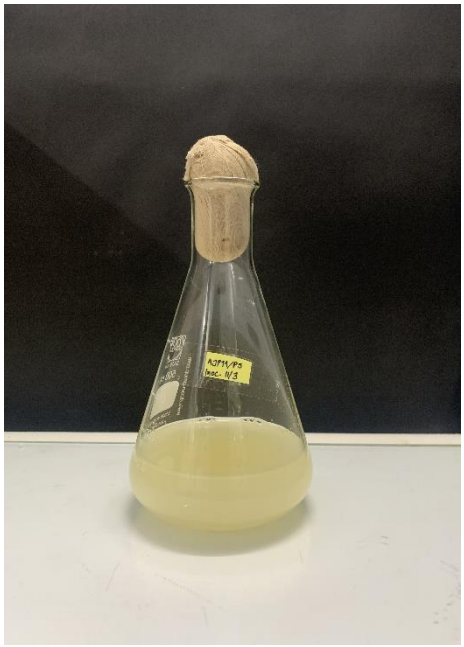

(b)

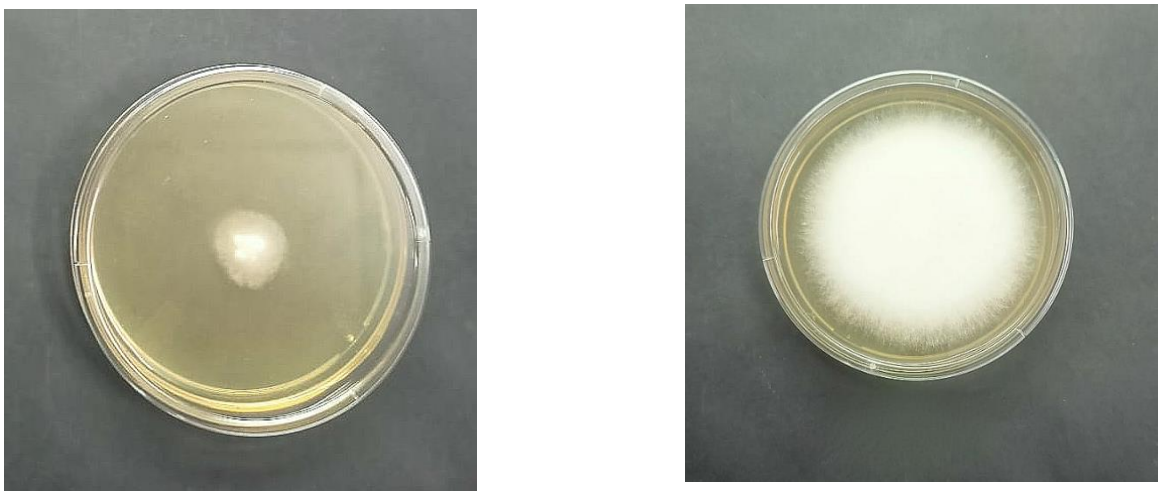

(c) (d)

Figure 7.1 Visual representation of the comparative biomass growth (a) at zero day of incubation (b) at 30 day of incubation; growth of fungi after 30 days exposure to (c) only MSM (d) PSS as sole carbon source.

7.3.2.2 GC-MS/MS Analysis

In fungi, the carbon source utilization is regulated via finely tuned system that allows utilization of various complex sources. Potential of fungi to degrade various organic pollutants viz. polyhydroxy aromatic and aliphatic hydrocarbons, recalcitrant dyes, persistent organic pollutants and complex polymers (plastics) is widely studied [Bhargava et al. 2016; Carstens et al. 2020; Li et al. 2020; Grelska and Noszczyńska, 2020]. Various reports have demonstrated the degradation potential of fungal enzymes namely, esterases, cutinases and lipases against various plastic types such as PE, PU and PET [Ali et al. 2021]. However, reports discussing fungal-mediated degradation of PS are limited. Interestingly, pre-treatment of PS by chemicals and UV-radiations has been observed to make it susceptible to the action of fungi such as *Cephalosporium* sp. and *Penicillium variabile* [Tian et al. 2017; Chaudhary et al. 2021, 2022]. However, all these studies involved harsh pre-treatment conditions, prolonged incubation period (8-16 weeks) and lacked focus on the molecular mechanism behind the PS degradation. As plastics are composed of long-chain carbon atoms attached via covalent bonds, their fungal-mediated catabolism would result in the generation of various by-products that can provide insight into the overall plastic utilization metabolism.

In the present investigation, the by-products generated during the exposure of *L. ramosa* AJP11 to PSS in comparison to the tested controls implied about the previously unestablished modes of PSS utilization [Table 7.1]. On the basis of GC-MS/MS analysis, following three major findings were acknowledged, (i) disappearance of benzene and [1,1'-biphenyl]-2,3'diol in the PSS fungal treated sample [Figure 7.2 a & b] indicated the depolymerization of PSS by fungal enzyme(s) since benzene is the structural unit of PS and biphenyl is a popular persistent organic plastic additive; (ii) formation of PS oligomers such as cyclohexane and 2,4-DTBP indicated myco-transformation of PSS for carbon utilization; (iii) the alkanes such as pentadecane, hexadecane, heptadecane, octacosane, nonadecane, etc., released as by-products of PS degradation, may undergo oxidation to their subsequent alcohol, aldehyde and carboxylic acid forms. Moreover, they can further react with Coenzyme A to undergo β-oxidation resulting in formation of acetyl-CoA units which subsequently enters in the Krebs cycle. The bioactive compounds such as free fatty acids and alkanes formed due to the significant enzymatic and biochemical activity that occurred during myco-transformation of PSS. However, the origin of triethyl phosphate (TEP) observed during GC-MS/MS analysis is debateable since it's an organophosphate plasticizer of anthropogenic origin but has also been reported to serve as a source of phosphate under stress conditions with lesser-known effects on the microbial growth [Story and Brigmon, 2017].

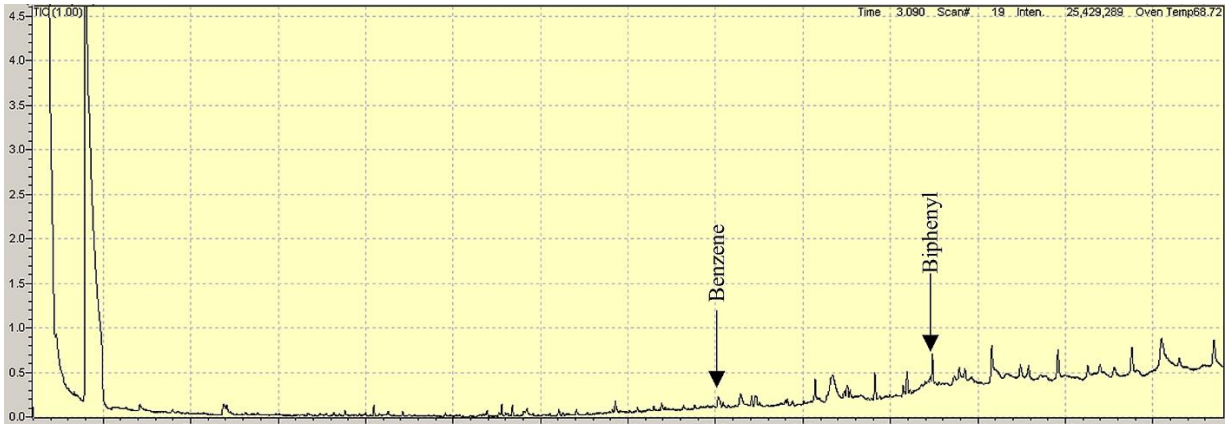

(a)

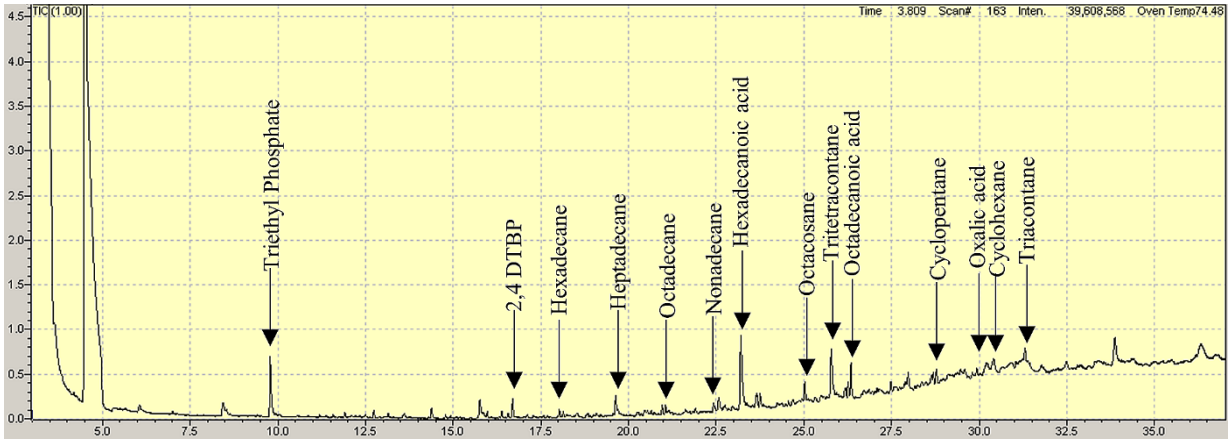

(b)

Figure 7.2 Representative GC-MS/MS chromatogram of PSS myco-transformation products (a) control containing MSM+1% PSS (without fungal biomass); (b) treatment containing MSM+1% PSS with fungal biomass.

Earlier reports also referred to the release/generation of organic compounds including alkanes, carboxylic acids and keto carbonyls due to plastic degradation by the action of microbial enzymes [Shahnawaz et al. 2016; Sangale et al. 2019]. The key components generated in the treatment containing MSM+1% PSS with fungal biomass (Table 7.1) were found to be consistent with Tsochatzis et al. [2021] who reported depolymerization of PS into oligomers such as acetophenone, 2,4-DTBP and cyclohexane in the gut of mealworm. Moreover, utilization of complex plastic source such as PP by yeast also generated fatty acids namely, oleic acid, palmitic acid and stearic acid [Mihreteab et al. 2019]. Balasubramanian et al. [2014] reported the release of similar alkanes and carboxylic acids as a consequence of myco-transformation of high-density polyethylene (HDPE), and hypothesized their further oxidation and activation into fatty acetyl-CoA subsequently entering the Krebs cycle. Additionally, Sangale et al. [2019] reported the release of similar organic compounds as major by-products of fungal treated PE. Oxalic acid, octadecanoic acid and acetic acid found in the treatment extract can serve as crucial intermediates at the junction of anabolic and catabolic biochemical pathways including Krebs cycle, amino acid and fatty acid metabolism and can act as substrates for the acetyl-CoA synthetase to form acetyl-CoA [Patel and Walt, 1987; Starai and Escalante-Semerena 2004]. The obtained results suggest that emergence of organic products/intermediates resulted due to the myco-transformation of PSS. Apart from these intermediates, exact fate of other by-products needs to be further explored due to limited knowledge of biological and ecological relevance of individual organic compounds and their mixtures w.r.t fungal biochemistry [Bitas et al. 2013; Guo et al. 2020]. Interestingly, *n*-alkanes

have also been reported to induce certain enzymes capable of catalysing oxidization reactions and facilitating hydrocarbon assimilation in fungi [Huarte-Bonnet, 2018]. Consequently, it may be hypothesized that certain recorded *n*-alkanes might be inducing the enzymes involved in oxidation of a complex hydrocarbon source, PSS.

Table 7.1 Key compounds generated in the treatment extract containing in MSM+1% PSS with fungal biomass.

Analyte	Retention Time	Molecular Formula	Molecular Mass (Da)
2,4-Di-tert butyl-phenol (DTBP)	16.694	$C_{14}H_{22}O$	206.32
Pentadecane	16.568	$C_{15}H_{32}$	212.41
Hexadecane	18.137	$C_{16}H_{34}$	226.41
Heptadecane	19.634	$C_{17}H_{36}$	240.5
Octadecane	21.056	$C_{18}H_{38}$	254.494
Nonadecane	22.426	$C_{19}H_{40}$	268.518
Octacosane	25.024	$C_{28}H_{58}$	394.80
Hexadecanoic acid (Palmitic acid)	23.206	$C_{16}H_{32}O_2$	256.42
Octadecanoic acid (Stearic acid)	25.777	$C_{18}H_{36}O_2$	284.50
Acetic acid	26.345	CH_3COOH	60.052
Cyclopentane	28.630	C_5H_{10}	70.135
Oxalic acid	29.805	$C_2H_2O_4$	90.034
Cyclohexane	30.105	C_6H_{12}	84.160
Triacontane	31.301	$C_{30}H_{62}$	422.81

7.3.3 Mechanism behind PSS degradation

7.3.3.1 Characterization of Fungal Extracellular Protein

Out of the wide range of extracellular metabolites (exo-polysaccharides, organic acids, fatty acids, phenols, quinones and proteins), the major component of the fungal secretome are enzymes (proteins) which possess various absorptive, hydrolytic and biosurfactant properties and have ability to extract carbon from plastics as energy source for cellular metabolism [Pareek et al. 2020; Sánchez, 2020]. Since fungal enzymes are functionally involved in catalysing various reactions, it is justified to study their expression during different treatment conditions in order to identify the relevant candidate(s) of PSS myco-transformation. Previously, Krueger et al. (2017) studied that the action of Fenton chemistry driven oxidation of PSS, however, no specific proteins in the process of oxidation were discussed.

The fungal extracellular proteins under different treatment conditions were precipitated by modified TCA/acetone method and dialysed using 12-kDa cut off cellulose membrane to analyse and understand their involvement in PSS degradation. The concentration of total extracellular proteins was found to be highest in treatment with MSM+1% PSS (74.75 μg mL^{-1}), followed by MSM+3% dextrose (70.57 μg mL^{-1}), whereas lowest concentration was found for only MSM (61.62 μg mL^{-1}). In order to completely transform PSS into utilizable organic compounds, fungus could secrete more number/amount of extracellular proteins (enzymes) when exposed to PSS. Whereas, comparatively lesser amount of proteins in case of only MSM signifies that in absence of any energy source, fungus metabolised few secreted proteins during treatment duration.

The total extracellular protein profile revealed the presence of varied band patterns across different treatments. For instance, the treatment MSM+3% dextrose showed eleven protein bands ranging from molecular weight of 16.8 kDa to 85.5 kDa [Figure 7.3, Lane 2]; while in case of treatment with only MSM, nine bands ranging from 15.6 kDa to 105.2 kDa of comparatively lower intensity were observed [Figure 7.3, Lane 3]. Eleven discrete protein bands with a molecular weight of 14.4 kDa (a), 20 kDa (b), 22.6 kDa (c), 26.5 kDa (d), 38.4 kDa (e), 40.4 kDa (f), 43.8 kDa (g), 46.8 kDa (h), 60 kDa (i) and 107.9 kDa (j) were present in the treatment containing MSM+1% PSS [Figure 7.3, Lane 4]. Out of which, protein bands at 14.4 kDa, 46.8 kDa and 107.9 kDa were exclusively overexpressed in MSM+1% PSS treatment, while bands such as (b), (c), (d), (f), (g) and (j) were consistently expressed in all the three treatments indicating their housekeeping role in the fungal metabolism. Noteworthy,

the protein band at 14.4 kDa (indicated by the arrow) was found to be significantly intense in comparison to other bands/treatments indicating its possible role in PSS myco-transformation.

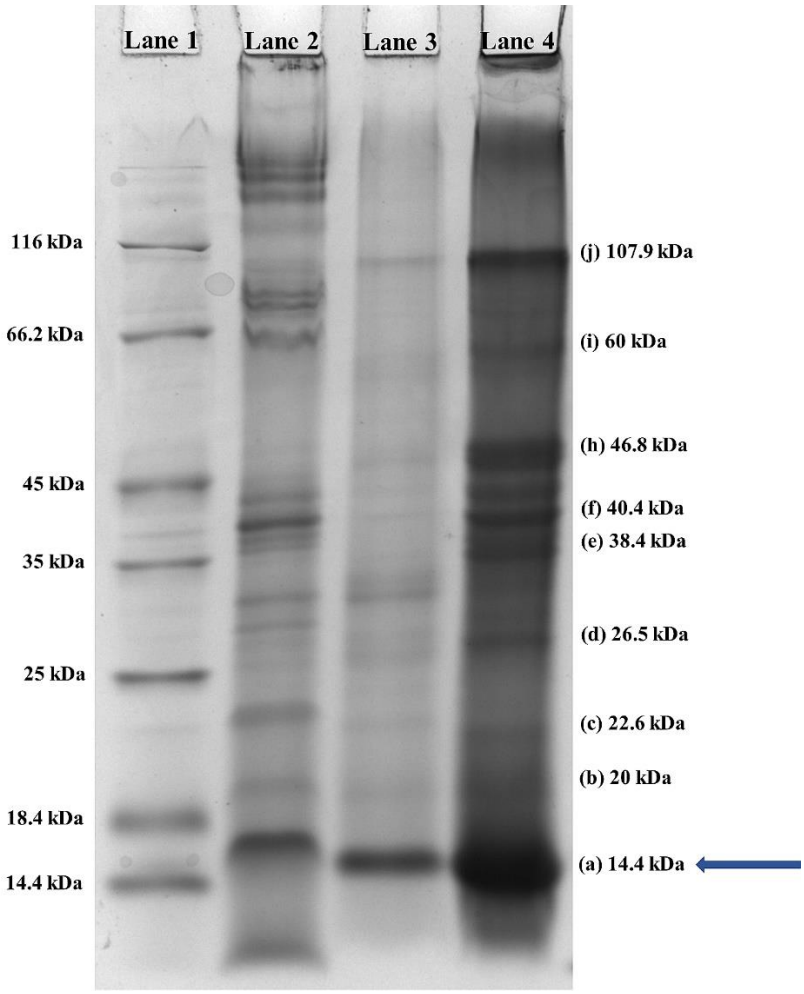

Figure 7.3 One-dimensional SDS-PAGE analysis of extracellular proteins secreted from *L. ramosa* AJP11. Lane 1: molecular size marker ranging from 14.4 to 116 kDa; Lane 2: fungal extracellular proteins in MSM+3% Dextrose; Lane 3: fungal extracellular proteins in only MSM and Lane 4: fungal extracellular proteins in MSM+1% PSS.

7.3.3.2 Peptide Mass Fingerprinting

To characterize the overexpressed proteins at 14.4 kDa, 46.8 kDa and 107.9 kDa and to elucidate their role in PSS myco-transformation, they were analysed by MALDI-TOF/TOF mass spectroscopy and the obtained sequences were searched for sequence homologies using MASCOT server against NCBI protein database. The obtained results indicated that these proteins belong to very different protein families namely, universal stress protein (Usp; 46.8 kDa) (Accession no. CDS03339.1) [Figure 7.4] and PRP-1 splicing factor (107.9 kDa) (Accession no. CDS07580.1) [Figure 7.5], and hydrophobic surface binding protein (Hsb;14.4

kDa) (Accession no. CDS02765.1) [Figure 7.6]. Noteworthy, Usp and PRP-1 splicing factor are intracellular proteins [Urushiyama et al. 1997; Chi et al. 2019]. Presence of these proteins in the extracellular cell free filtrate may be due to the disruption of few fungal cells during long exposure duration under PSS stress condition.

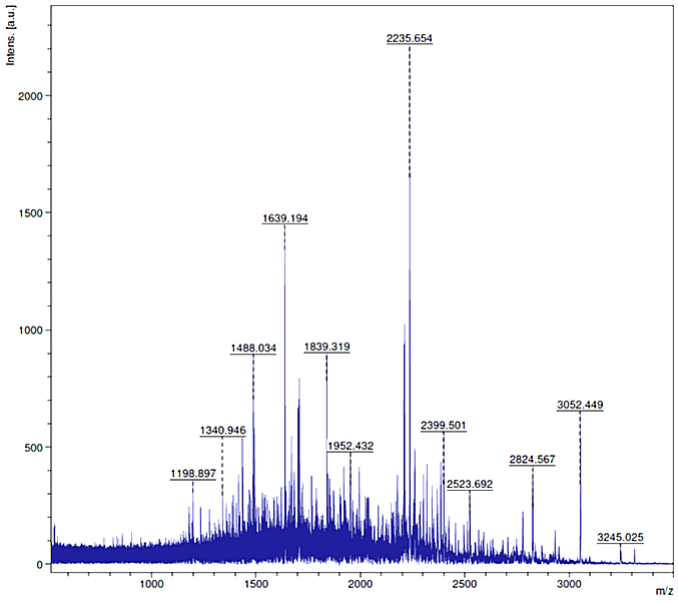

(a)

Start – End	Observed	Mr(expt)	Mr(calc)	Delta	M	Peptide
19 – 31	1708.1339	1707.1266	1707.8230	-0.6963	1	R.RQLFDHFHTHNEK.S
32 – 53	2499.5010	2498.4937	2499.3221	-0.8284	2	K.SEKPHYDLPKVTVTDTSKVDIK.D
42 – 66	2776.8086	2775.8014	2776.4131	-0.6117	2	K.VTVTDTSKVDIKDPVEAQSFQDLNK.V
54 – 66	1489.9342	1488.9269	1489.7049	-0.7780	0	K.DPVEAQSFQDLNK.V
99 – 112	1637.1937	1636.1864	1636.7072	-0.5208	1	K.GAEMLEDDMEKNQK.L
99 – 112	1670.2162	1669.2089	1668.6971	0.5118	1	K.GAEMLEDDMEKNQK.L + 2 Oxidation (M)
110 – 117	1029.6982	1028.6909	1028.5363	0.1546	1	K.NQKLDQQR.Q
110 – 127	2259.5686	2258.5613	2258.0523	0.5091	2	K.NQKLDQQRQNEEEEEVSR.V
141 – 154	1702.1904	1701.1832	1701.8977	-0.7146	1	K.YIPYIEPQPETPKK.K
158 – 169	1435.0350	1434.0278	1433.6874	0.3403	0	K.HPHLGFDEPVMR.I
195 – 222	3311.5022	3310.4949	3311.4906	-0.9956	1	R.KPRVYMVACDFSSESVNAIEWTMGTMMR.D + Oxidation (M)
198 – 222	2932.3811	2931.3738	2930.2417	1.1321	0	R.VYMVACDFSSESVNAIEWTMGTMMR.D + Oxidation (M)
266 – 280	1839.3193	1838.3121	1838.0059	0.3062	1	K.HMLLYDIKMVVHAIR.G
285 – 306	2523.6924	2522.6851	2522.3059	0.3792	1	K.EVLISMIYELPLTMVVCGSRGR.S
346 – 357	1234.9285	1233.9212	1233.6466	0.2747	0	K.AAHPAPLSESVR.T

(b)

1 MDYHQSPHPHRHHHHHYRRQLFDHFHTHNEKSEKPHYDLPKVTVTDTSKVDIKDPVEAQSFQDLNKVDAQ
71 DAAVPPAEIVNPEPVQNVIDKQDPMYYKGAEMLEDDMEKNQKLDQQRQNEEEEEVSRVSEELRRTTEQNK
141 YIPYIEPQPETPKKKKKHPHLGFDEPVMRILPDRVVITQLYGHQPVSEMQQAKRKPRVYMVACDFSSESV
211 NAIEWTMGTMMRDRDEVHILTVVPPDDSSSQGSSPANQLQGTSISLCDKARDILKHMLLYDIKMVVHAIR
281 GHVKEVLISMIYELPLTMVVCGSRGRSGMKGLLVGSISNYLIQKSPVPVSVIRKPKTKSKVKKTKAAHPA
351 PLSESVRTGQLVVDELGSKSKHER

(c)

Figure 7.4 (a) MALDI-TOF/TOF MS Spectrum of the tryptic digests of Universal Stress Protein (46.8 kDa) from *Lichtheimia ramosa* AJP11 (b) List of identical peptide sequences with their relative molecular masses and position in protein sequence (c) Complete amino acid sequence deduced from MASCOT analysis using NCBI database.

Based on the obtained results, it may be hypothesized that sensing of PSS in the outer environment of fungal cells triggers a series of events inside the cell that allow the uptake of PSS. For instance, it is well known that the Usp(s) play a crucial role in reprogramming the cell to withstand different stress conditions by largely unknown mechanisms [Tkaczuk et al. 2013]. Some of the reported mechanisms in bacteria and plants suggest their function in increasing the transcript turnover, and/or modulating the metabolic pathway [Lee et al. 2006; Chi et al. 2019]. However, in fungi, their function during stress conditions is least explored. Apart from the Usp, another identified protein belongs to the family of splicing factors. Fungal splicing factors have been studied to be particularly involved during the unfavourable conditions [Grützmann et al. 2014].

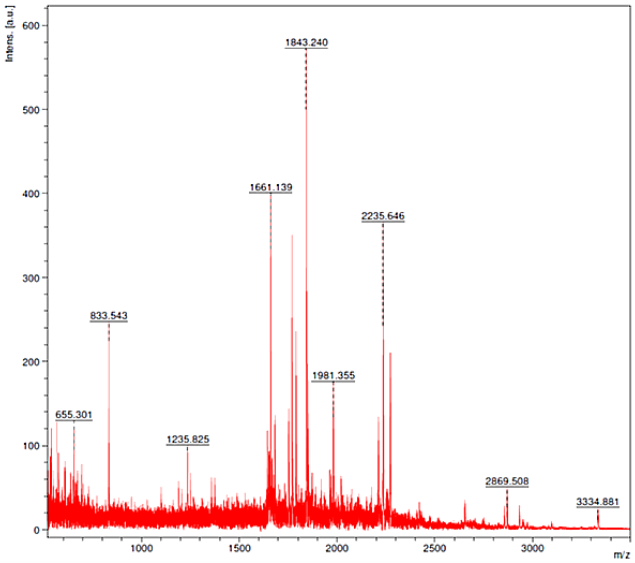

(a)

Start – End	Observed	Mr(expt)	Mr(calc)	Delta	M	Peptide
1 – 6	654.4790	653.4717	653.3207	0.1510	0	-.MFGATK.D
7 – 23	1771.7490	1770.7417	1770.9417	-0.2000	0	K.DFIGKPAPPNYVAGLGR.G
32 – 54	2205.1216	2204.1143	2204.0458	0.0685	2	R.SDIGPARESGDFGADAKQGAAGK.E
89 – 101	1650.5749	1649.5676	1649.8018	-0.2342	2	R.VWAMIDTKMDERR.K
89 – 101	1666.7490	1665.7417	1665.7967	-0.0550	2	R.VWAMIDTKMDERR.K + Oxidation (M)
97 – 102	834.5874	833.5802	833.4177	0.1624	2	K.MDERRK.A
118 – 131	1687.3699	1686.3626	1686.9053	-0.5427	1	R.QERPKISQQFADLK.R
118 – 132	1844.1790	1843.1717	1843.0064	0.1653	2	R.QERPKISQQFADLKR.Q
133 – 156	2655.8327	2654.8254	2654.3187	0.5066	1	R.QLSSIDEEEWAAIPEVGDLVGKNR.K
222 – 238	1789.4893	1788.4820	1788.8742	-0.3921	0	K.LDQVSDSVSGQTTIDPK.G
239 – 259	2236.5708	2235.5635	2235.1634	0.4001	1	K.GYLTDLNSVVVKSDAEIGDIK.K
342 – 357	1855.5880	1854.5807	1854.0251	0.5556	2	K.IWLKAVDLETDPKAQK.R
359 – 372	1641.8426	1640.8353	1640.9726	-0.1373	2	R.VLRRALEFIPNSVK.L
376 – 393	1971.3555	1970.3482	1970.9731	-0.6249	1	R.AAVNMEENPDDAKVLLSR.A
420 – 440	2274.4829	2273.4757	2273.2756	0.2000	2	K.VLNKARAAVPTSHEIWIAAAR.L
461 – 471	1160.1969	1159.1896	1159.6197	-0.4301	0	R.ALSQTGTVLDR.D
619 – 628	1241.6987	1240.6915	1240.5207	0.1707	0	K.VESESNEYER.A
645 – 648	563.2149	562.2076	562.2937	-0.0862	0	R.VWMK.S

(b)

1 MFGATKDFIGKPAPPNYVAGLGRGATGFTTRSDIGPARESGDFGADAKQGAAGKEGGDDDDERFQDPDNE
71 VGLFSGAPYEEDDEEADRVWAMIDTKMDERRKARREAREREELARYRQERPKISQQFADLKRQLSSIDEE
141 EWAAIPEVGDLVGKNRKRNKMPERYTPMTDTILAAARDKTGYDTTLNEQEQKLGGVTTPADGMMTNFREI
211 GQARDKVLGLKLDQVSDSVSGQTTIDPKGYLTDLNSVVVKSDAEIGDIKKARLLLNSVITTNPKHAPGWI
281 AAARLEEVAGRPVQARNIIAKGCEQCPKSEDVWLESARLNTVDNAKIILANAVRQLPQSVKIWLKAVDLE
351 TDPKAQKRVLRRALEFIPNSVKLWRAAVNMEENPDDAKVLLSRAVELVPLSVELWLALARLESYENAQKV
421 LNKARAAVPTSHEIWIAAARLEEQHGKPHMVDRIIQLAARALSQTGTVLDRDQWLKEAEKCEKNGSVLTC
491 QAIVRATIGLGVEEEDQKATWMEDAESCIAHGSIETARAIYAHALKVFPGRKSIWMAAAYLEKGHGTPQS
561 LEELLQRAVRYCPQAEVLWLMGAKEKWLADDVQGARAILEEAFRANPNSEKIWLAAVKVESESNEYERAR
631 KLLELARKESGTDRVWMKSAMLERQLKNYDGCLQLLEEGLQRYPTFDKLWAIKGQVEDEALNNSSKARET
701 YNKAVKNCPKSTLLWILLAKLEEKMGMVTKARSTLEKARYTNPKTPELWVEGIRIEVRAKNQSVAKSMSA
771 KALQECPTSGAIWREVIFLEARPQRKARSVDALKKCEHDPIVVTTVALLFWTDRKIEKARNWFQKAVQID
841 PDQGDSFAWWYKFELQHGTEEQQEAVVKRCVASEPRHGERWTAVAKDMANIGKRTADILKLCAAKLEPIK

(c)

Figure 7.5 (a) MALDI-TOF/TOF MS Spectrum of the tryptic digests of PRP-1 Splicing protein (107.9 kDa) from *Lichtheimia ramosa* AJP11 (b) List of identical peptide sequences with their relative molecular masses and position in protein sequence (c) Complete amino acid sequence deduced from MASCOT analysis using NCBI database.

Splicing factors play crucial role in mediating fungal response during the stress conditions by regulating a wide range of cellular functions related to enzyme activation and the binding affinities of proteins [Sieber et al. 2018]. These functions allow the fungi to survive under unfavourable scenarios. According to previous findings, PRP-19 associated splicing proteins are functionally involved in regulating the depolymerization of plant cuticle (hydrophobic in nature) for promoting fungal pathogenicity [Liu et al. 2021]. Here, it is hypothesized that the overexpressed PRP-1 splicing factor indicated the increased translational efficiency of the fungal biomass for the synthesis of various potential protein(s), one of which could be the third over-expressed protein, Hsb, in order to combat stress conditions and facilitating the myco-transformation of PSS.

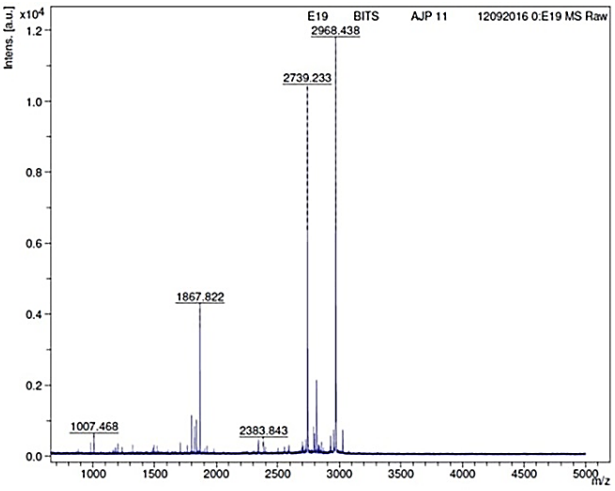

(a)

Mr(expt)	Mr(calc)	ppm	Start	End	Miss	Ions	Peptide
979.4674	979.4975	-30.69	51 -	60	0	---	K.VSDGYAGALK.V
1006.4610	1006.4832	-22.01	156 -	164	0	---	K.DQANAYVAR.I
1866.8145	1866.9211	-57.10	61 -	76	1	153	K.VQTEETKLENYLDSAK.S
2738.2260	2738.3511	-45.69	139 -	164	1	---	K.TDALDNALLSATPASYKDQANAYVAR.I
2790.2588	2790.3957	-49.07	77 -	103	0	---	K.SACTISGTVSDTDAQTILAQVDTLVPK.V
2967.4312	2967.4937	-21.07	137 -	164	2	---	K.TKTDALDNALLSATPASYKDQANAYVAR.I

(b)

1 MKFTAIIALV AFTAVNALTL DRRGVPECAA GLTTVQNQLD VVTTGVNNWK VSDGYAGALK
61 VQTEETKLEN YLDSAKSACT ISGTVSDTDA QTILAQVDTL VPKVESALSS IVTKKPDFDK
121 VLLVTALVTK DIKNLKTKTD ALDNALLSAT PASYKDQANA YVARINKAFA DAYTAYGI

(c)

Figure 7.6 (a) MALDI-TOF/TOF MS Spectrum of the tryptic digests of hypothetical protein (14.4 kDa) from *Lichtheimia ramosa* AJP11 (b) List of identical peptide sequences with their relative molecular masses and position in protein sequence (c) Complete amino acid sequence deduced from MASCOT analysis using NCBI database.

The Hsb proteins belong to the small-secreted proteins (SSPs) secretome of fungi that contain a signal peptide having sequence less than 300 amino acids. Only few of them have been functionally characterized, specifically belonging to fungal genera *Aspergillus* [Valette et al. 2017]. The SSPs are reported to be involved in strategies developed by fungi to resist the associated stress that could be due to toxicity of some aromatic compounds or reactive oxygen species released during degradation. Thus far the only known fungal hydrophobic surface binding protein (HsbA; 14.5 kDa) is reported to be produced by *Aspergillus oryzae* RIB40 [Ohtaki et al. 2006]. Different orthologs/paralogs of HsbA have been identified in other fungal

species. Hydrophobic surface binding proteins have functional similarities to hydrophobins, a class of surface-active fungal proteins with the ability to bind hydrophobic surfaces [Sunde et al. 2017]. Although these proteins do not possess catalytic activity, they play a major assistive role during degradation of hydrophobic compounds. The Hsb proteins have the ability to interact and adsorb to the hydrophobic moieties such as plastic surfaces and potentially enhances the recruitment of lytic enzymes to promote the depolymerization of the plastic [Ohtaki et al. 2006]. It may be hypothesized that Hsb might also have a role in initially sensing the hydrophobic surfaces in the environment.

However, the exact molecular mechanism behind the interaction of Hsb(s) to the hydrophobic polymer is unexplored. Hence, *in silico* studies were performed to further understand the mechanism behind the functioning of this unique hypothetical protein of *L. ramose* AJP11 in mediating PSS transformation.

7.3.3.3 *In silico* Characterization

Structural Analysis and Physio-chemical Properties

The secondary structure of the selected overexpressed protein (14.4 kDa; hypothetical) of *L. ramosa* AJP11 was generated using online server PSIPRED [Buchan and Jones, 2019]. The obtained results showed that it consisted of 7 α-helices (H) joined with the help of total 8 coils (C), with no β-strands in protein structure [Figure 7.7 a]. The protein was found to be majorly comprised of hydrophobic (25%) and non-polar (38%) residues, while polar (29%) and cysteine residues (8%) were present in moderate proportion, giving it an amphiphilic understanding [Figure 7.7 b]. Since cysteine side-chain hydrophobicity has been a matter of ambiguity, their occurrence imparts both hydrophilic and hydrophobic attribute [Marino and Gladyshev, 2010; Iyer and Mahalakshmi, 2019]. Sulfhydryl (-SH) group of cysteine imparts non-polar nature restricting formation of hydrogen bonds with water, however, the involvement of sulfhydryl group also allows covalent bond formation, thus modifying residue properties to greater extent [Poole, 2015].

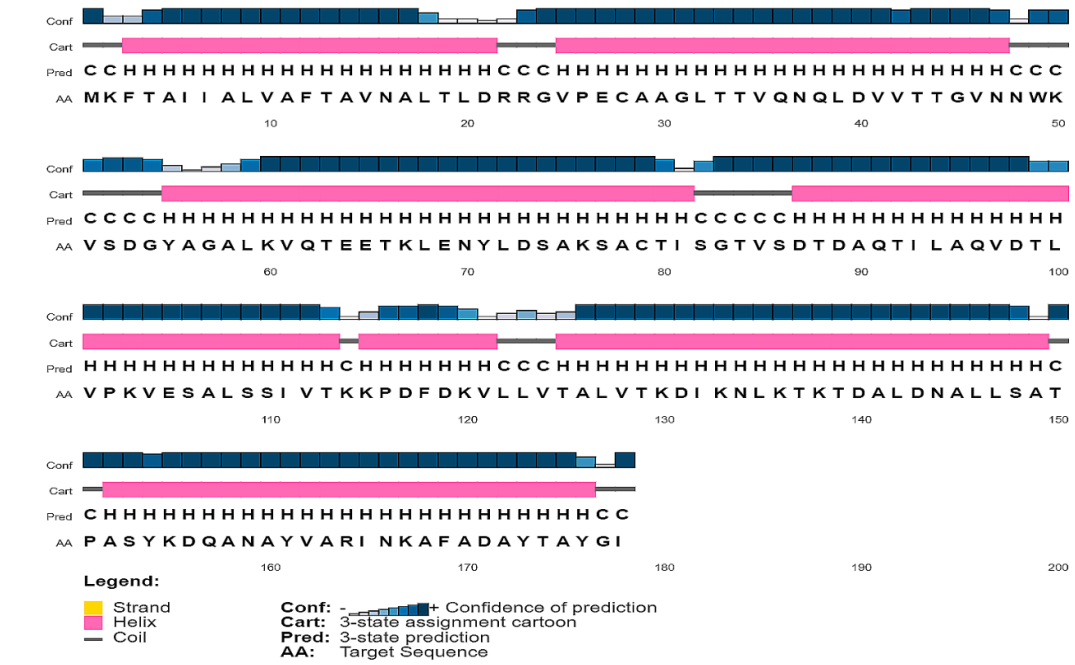

(a)

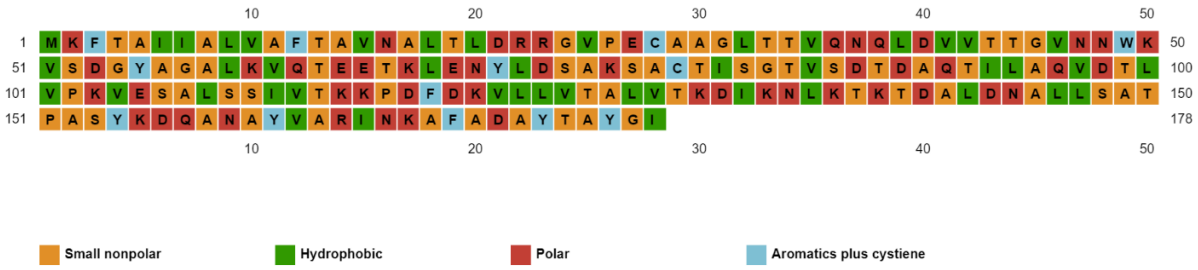

(b)

Figure 7.7 Structural analysis of hypothetical protein of *L. ramosa* AJP11 (a) Predicted secondary structure showing α-helices as the main structural elements joined by coils (b) hydropathy profile indicating the polarity of the amino acid sequence.

Further, physicochemical properties of the hypothetical protein were identified using online servers PSIPRED and ProtParam [Table 7.2] [Gasteiger et al. 2005]. The instability index is an estimation of the stability of a protein, where a value smaller than 40 is considered stable [Guruprasad et al. 1990]. Since the instability index value for the hypothetical protein was found to be 18.12, it can be regarded as a stable protein. The aliphatic index of protein is defined as the relative volume occupied by the aliphatic side chains [alanine (Ala), valine (Val), isoleucine (Ile), and leucine (Leu)] and is correlated with the thermostability of protein [Ikai, 1980]. The high aliphatic index (100.90) of hypothetical protein indicated its stability under wide temperature range. The GRAVY is calculated by adding the hydropathy value of all residues divided by the number of residues in polypeptide

[Kyte and Doolittle, 1982]. Positive GRAVY values indicate hydrophobic, whereas negative values mean hydrophilic [Chang and Yang, 2013]. Since the GRAVY value of the tested protein was 0.075, it could be understood that the protein has amphiphilic attribute.

Table 7.2 Characteristic features of hypothetical protein of *L. ramosa* AJP11.

Characteristic features	**Value**
Molar extinction coefficient	13370.00
Molecular weight	18909.57
Isoelectric point	5.23
Charge	-0.97
Instability index	18.12
Aliphatic index	100.90
Grand average of hydropathicity (GRAVY)	0.075

Additionally, the 2D topology of the protein was predicted using the PROTTER software which showed presence of a 17 residues long signal peptide at the N-terminal of protein [Figure 7.8]. The presence of a signal peptide on hypothetical protein further confirms that the protein is a fungal SSP. No possible sites for post-translational modifications such as phosphorylation/glycosylation were observed.

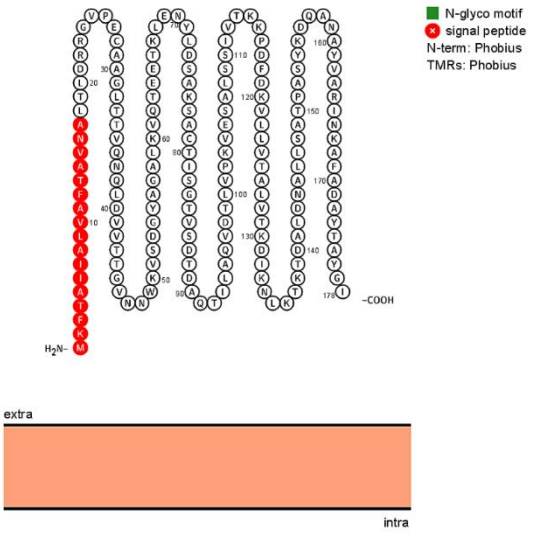

Figure 7.8 Two-dimension topology of the hypothetical protein of *L. ramose* AJP11 with the predicted signal peptide shown in red colour.

These results were in coherence with the previously reported HsbA and HsbB proteins (Accession no. BAE53453 and BAE53530) of *Aspergillus oryzae* [Table 7.3; Ohtaki et al. 2006]. The obtained results suggest that although these proteins belong to same superfamily of Hsb proteins and have similar sequence length, molecular weight and 2D topologies, there is rather low percent identity between the sequences indicating that these proteins cannot be identified based on sequence alignment and share low sequence conservancy.

Table 7.3 BLAST analysis of the FASTA sequences of hypothetical protein of *L. ramosa* AJP11 with its orthologs/paralogs of *A. oryzae* [Ohtaki et al. 2006].

Proteins	Hypothetical protein and HsbA	Hypothetical protein and HsbB	HsbA and HsbB
Percent identity	26.16%	29.21%	29.75%

Molecular Modelling, Model refinement and Validation

The FASTA sequence of the 14.4 kDa protein (178 amino acid residues) was extracted from NCBI and submitted to I-TASSER. It resulted in generation of five protein models, out of which, the first model was selected based on the given C- score and estimated local accuracy. The selected model comprised of α-helices and had a C-score of 0.53 and TM-score of

0.65±0.13 [Figure 7.9 a]. It is well known that the model having a C-score value >−1.5 and TM-score value >0.5 is considered to have a correct fold [Xu and Zhang, 2010; Yang and Zhang, 2015]. Additionally, binding ligands were predicted by COACH server (in-built in i-TASSER program) by matching the target model with the BioLip database which showed that compounds containing long chain hydrocarbons and benzene could be possible ligands for the protein [Yang et al. 2013a, b].

Since, the model was generated through threading, its necessary to minimize the model energy in order to determine the most stable and energetically favourable molecular conformation [Elton et al. 2019]. Hence, the model was refined using ModRefiner. The obtained results showed ERRAT score of 100 indicating that the generated model is of high quality. Additionally, the model was validated using Ramachandran Plot which showed that 161 residues (97.6%) were in favourable region. Only 1 residue (0.6%) was in allowed region and 3 residues (1.8%) were found in the dissallowed region. The overall existence of 98.2% residues in favoured and allowed regions showed that the model is good and free from stearic hinderance [Figure 7.9 b & c].

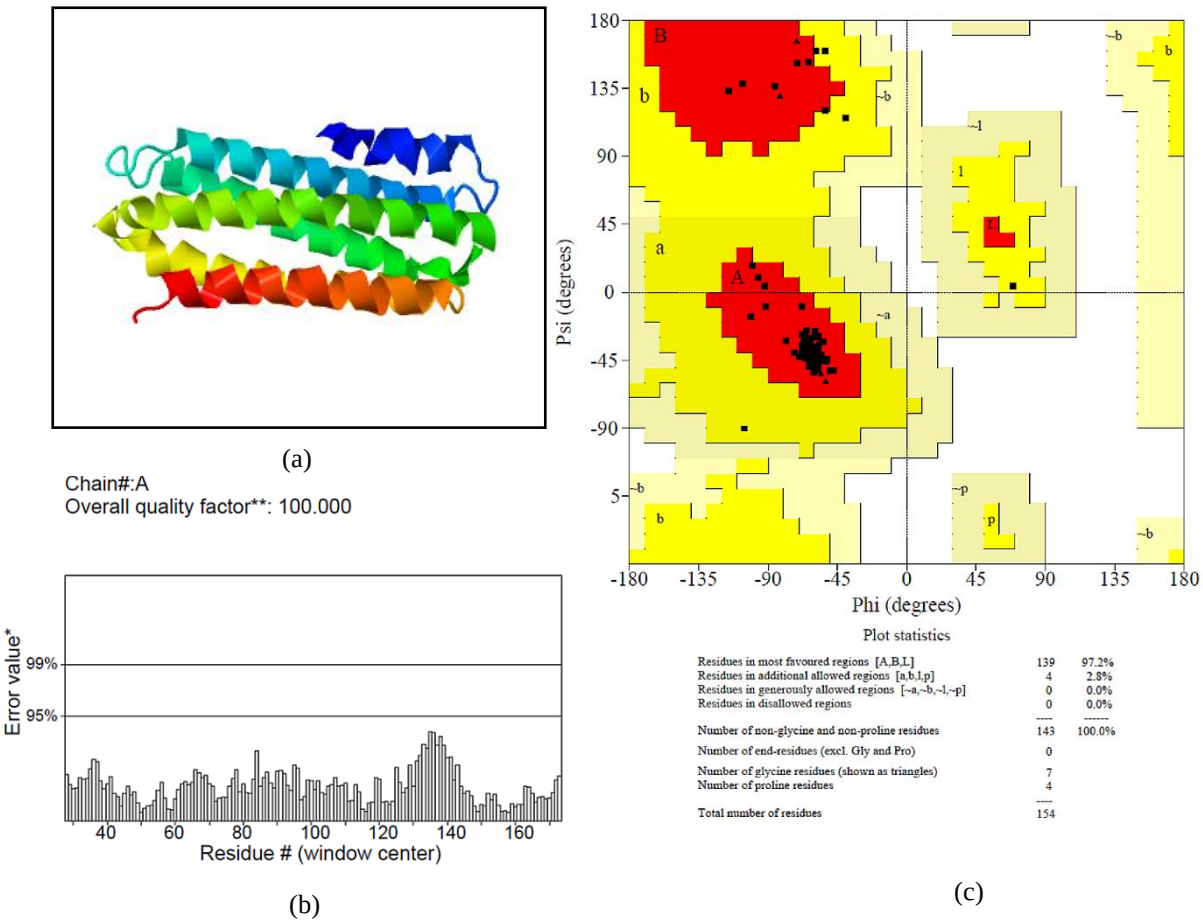

Figure 7.9 (a) Predicted 3-D structure of hypothetical protein of *L. ramosa* AJP11 (b) Ramachandran plot assessment and; (c) ERRAT validation of refined 3-D structure.

Hypothetical Protein-Styrene Sulfonate Complex Analysis by Molecular Docking

Beyond experimental and structural validation, it was also interesting to understand the interactions between the 14.4 kDa protein and monomeric styrene sulfonate (SS). The protein pocket interacting with SS comprised of four amino acid residues namely, Lys50, Lys 60, Gly45 and Val51. The docking analysis revealed that SS interacts with protein via two types of bonds, i.e. hydrogen and hydrophobic bonds. The docking analysis revealed the sizes and locations of binding sites, hydrogen-bond interactions, hydrophobic interactions, and bonding distances from the position of the docked ligand. The oxygen atoms in styrene structure forms two hydrogen bonds (indicated in green) of length 2.77 Å and 2.80 Å with the Lys60 and one hydrogen bond of length 2.64 Å with Lys50 [Figure 7.10 a]. Additionally, lysine also forms four hydrophobic interactions (indicated in red) with the oxygen, sulfur and carbon (C1 and C3) of SS, indicating lysine as a crucial residue capable of interacting with the ligand via different bonds [Figure 7.10 a]. Owing to its amphipathicity, lysine residues have been reported to frequently occur in the active/binding sites of the proteins and also known to form hydrogen

bonds with ligand molecules [Betts and Russell, 2007]. Along with lysine, neighbouring neutral and hydrophobic residues viz. Gly45 and Val51 also exhibited hydrophobic interactions with carbon atoms comprising the styrene ring as well as the vinyl chain. Similarly, Liu et al. [2018] reported the interactions between hydrophobic amino acids of PETase, namely, methionine, tyrosine, tryptophan and isoleucine providing ready-to-bind structural base against the hydrohobic PET facilitating its degradation. The hydrophobic interactions significantly manifest the adhesion between two moeities including the self-assembly of proteins [Yoon et al. 1999; Meyer et al. 2006; Ohtaki et al. 2006]. Since, the Hsb proteins show similar functional assemblages over plastic surfaces, the presence of these interactions could also function in between the protein and SS interaction. Consequently, ligand binding cavity was found to be largely consisting of hydrophobic patches surrounding the vinyl side chain and aromatic ring of SS, whereas polar sulfonate group interacts with the hydrophilic patch [Figure 7.10 b]. Here, it is hypothesized that the proposed protein can adsorb over the hydrophobic surface of SS by the virtue of hydrogen and hydrophobic interactions enabling its biotransformaion into intermediates of the central metabolic pathways (as shown in GC-MS/MS analysis). Since the bulky aromatic ring of styrene obstructs the binding of PS polymers within the active site of the catalytic enzymes, the interactions of Hsb proteins with the hydrophobic moieties facilitates the action of catalytic enzymes [Ohtaki et al. 2006; Zhang et al. 2022].

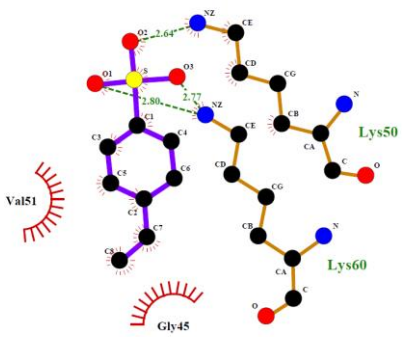

(a)

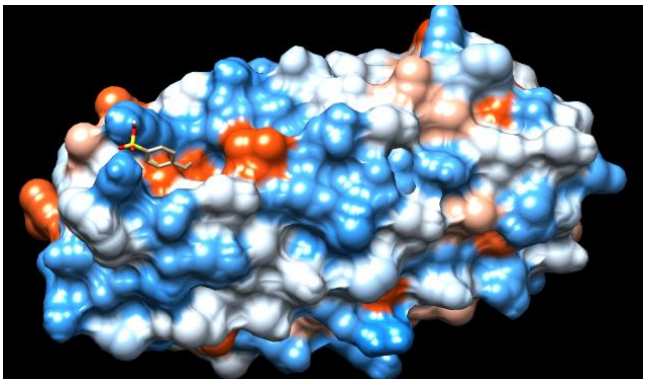

(b)

Figure 7.10 *In silico* molecular docking analysis of binding interactions between hypothetical protein of *L. ramosa* AJP11 with SS (a) Schematic 2D representation of the identified hydrogen bonding and hydrophobic interacting residuesin the protein domain. The Lys50 and Lys60 form hydrogen bonds with the sulfonate group of the SS; while Gly45 and Val51 participate in hydrophobic interactions (b) representation of the binding cavity showing the interaction of the vinyl chain of SS with the hydrophobic (red) surface cavity of the protein.

Further, the binding energy between the hypothetical protein and SS monomer was found to be -5.02 kcal mol^{-1}. Similarly, the hydrolases capable of degrading different forms of phthalates had binding energy of -5.01 and -4.4 kcal mol^{-1} for mono-hexyl phthalate and mono-ethyl-hexyl phthalate, respectively [Singh et al. 2017]. The binding energy of PETase-like enzyme against PCL was found to be ≤ -5.0 kcal mol^{-1} [Almeida et al. 2019]. Additionally, the binding energies for fungal lignonlytic enzymes against PE were reported to range between -6.09 to -5.5 kcal mol^{-1} [Santacruz-Juárez et al. 2021]. The propinquity of the above-reported binding energy scores for protein-mediated biodegradation of different organo-pollutants indicated that it is an efficient value for degradation approximation.

7.4 Conclusion

The exponential demand and production of various plastic goods has lead to the over-accumulation of plastic waste that requires a sustainable solution. The present study unviel the potential of *L. ramosa* AJP11 for myco-transformation of PSS which is a structural analogue of PS. Upon 30 days exposure to PSS as the sole carbon source, the observed increase (41.6%) in the fungal biomass indicated utilization of carbon from the aromatic structure of PSS. Further analysis revealed formation of various organic intermediates viz. alkanes and fatty acids which are involved in energy generation and cellular metabolism. The higher concentration of total extracellular proteins in the MSM+1% PSS treatment in comparison to only MSM treatment portrays the possible role of extracellular proteins (enzymes) in the myco-transformation of PSS. The extracellular fungal protein profile showed considerable overexpression of Hsb protein (14.4 kDa). *In silico* analysis of Hsb protein sequence explorated that it is α-helical protein that showed involvement of hydrophobic amino acids pivotal in forming hydrophobic interactions with PSS. Although, bacterial-based enzyme systems for PS degradation have been reported, this is the first report introducing the involvment of Usp, Prp-1 splicing factor and Hsb protein in mediating PSS myco-transformation by monitoring the fungal response to different treatment conditions. Based on the experimental findings, a schematic representation of the series of events occuring during the myco-transformation of PSS have been depicted in Figure 7.11. Here, it may be hypothesized that the presence of PSS in the surrounding environement is sensed by an unkown protein, which induces the *Usp* gene in nucleus resulting in maximizing cellular transcript level (by PRP-1 splicing protein) in order to utilize PSS. The various transcripts synthesize different proteins including extracellular Hsb which adheres to the hydrophobic PSS assiting its myco-trasnformation into organic compounds, which are later used by fungal cells for growth. Moreover, there is a strong possibility that catalysing enzyme

plays collaborative role with Hsb in mediating metabolic-conducive biotransformation of PSS. Further, the application of Hsb in a cell-free way or in a cellular engineered system under controlled reactor conditions may offer an accelerated and sustainable platform for PS waste disposal. The obtained results represent the binding attributes of Hsb protein with hydrophobic material which can be further explored for depolymerization of other hydrophobic pollutants. Alongside, subsequent efforts must be made to imporve the plastic recyling and waste management strategies. Currently, the laws and policies against plastic pollution are strictly territorial resulting in the accumulation of plastic waste over international waters. Hence, the global response must be holistic and dynamic, requiring coordinated action by diverse stakeholders at the national, regional, and international levels.

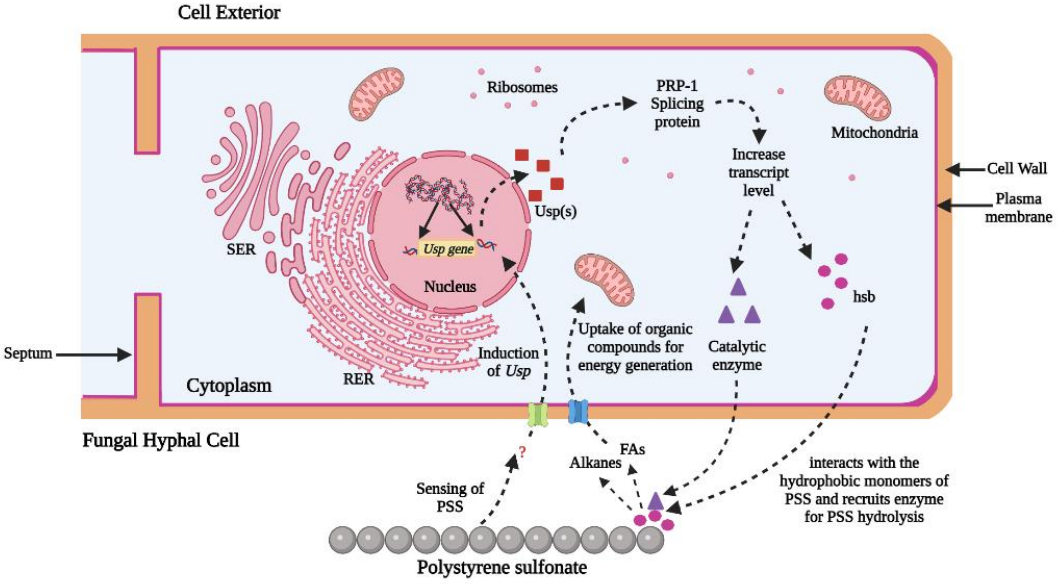

Figure 7.11 Schematic representation of the fungal mycelial cell showing the predicted series of events behind the myco-transformation of PSS by cellular proteins. Abbreviations: USP: Universal Stress Proteins; FAs: Fatty acids; SER: Smooth Endoplasmic Reticulum; RER: Rough Endoplasmic Reticulum; Hsb: Hydrophobic Surface Binding Proteins. Dotted lines represent the hypothetical series of events where the participating biomacromolecule is unknown.

Chapter 8

Summary and Future Prospects

8.1 Summary of the Work

The plastic crisis is a global burden that requires immediate solution, particularly for the plastics' end-of-life fate. Plastics can withstand harsh climatic conditions and can remain durable for decades, becoming widely distributed in the environment. These distributed plastic fractions can travel across continents and act as vectors for undesired microflora and hazardous chemicals, which either leach into the soil and enter groundwater system and/or are ingested by invertebrates causing their introduction into the food chain. Therefore, land and water act as final sink for the discarded plastic which results in ecosystem destabilization. Ongoing attempts to mitigate the hazardous effects of plastic waste include development of waste disposal strategies, recycling, and their replacement with biodegradable (bio)plastics, however, a lot of challenges exist in their implementation. In the past decade, various studies have reported the microbe-mediated utilization of plastics as a non-toxic sustainable solution. It is mediated by utilization of plastic as a carbon source and its conversion into cellular metabolites. Additionally, during microbial transformation, the plastic sources are upcycled into valuable products such as bioplastics and biosurfactants. However, to commercially achieve these valuable by-products, it is essential to understand the microbial enzymes and associated pathways involved in plastic-transformation. It would help to develop sustainable strategies to mitigate the plastics waste problem.

The present work is based on the rationale focuses on the similarities of the hydrophobic recalcitrant plant cuticle & its associated components with plastics. Since the phytopathogenic fungi are capable of breaching the hydrophobic cuticle, their functional attributes were evaluated towards their applicability in plastic degradation. Since xerophytic plants possess thicker cuticle to preserve water loss from transpiration, the infected xerophytic leaves were collected in different seasons, and phylloplanic fungi were isolated via agar plate imprinting method. A total of 20 different fungal species were isolated and evaluated for the ability to utilize polystyrene sulfonate (PSS) as the sole carbon source on the basis of change in fresh weight of the fungal biomass in MSM+1% PSS treatment. Fungal genera such as *Aspergillus*, *Alternaria*, *Cladosporium* and *Curvularia* showed ability to utilize PSS. *Curvularia dactylotenicola* VJP08, showed maximum efficiency with an increase of ~52% in the final fungal biomass (FW). Hence, *C. dactyloctenicola* VJP08 was selected for further optimization of process parameters viz. exposure duration (5,10, 15, 20 and 30 days), temperature (15℃, 28℃ and 40℃) and pH (5.0, 5.5, 6.0, 6.5, 7.0 and 8.0). The results were evaluated by monitoring the change in FW of fungal biomass, Raman spectroscopy, GC-MS/MS, and

protein profiling. The obtained results suggested that 28 °C temperature, pH 7.0, and exposure duration between 15 to 20 days were optimum for PSS myco-transformation. Further, the exometabolites generated during the PSS myco-transformation process indicated the utilization of PSS (as a sole carbon source) into cellular metabolites which supported the fungal growth and metabolism.

The proteomics analysis of the secretome of *C. dactyloctenicola* VJP08 exposed to MSM+1% PSS for different exposure durations (day 5, 10, 15 and 20) revealed that maximum upregulation of extracellular proteins occurred at day 15. The upregulated proteins included a wide arsenal of depolymerization proteins, including oxidoreductases (essential for PSS myco-transformation), CAZymes (important for utilizing the generated metabolites), stress-response and homeostasis proteins, energy generation proteins and surface-active cerato-platanin protein (crucial for mediating interaction between laccase and PSS). Protein such as fad_binding_3 domain, flavodoxin-like domain, laccase, multicopper oxidase, tyrosinase Cu-bd domain were found to be critical in PSS myco-transformation. The experimental findings indicated involvement of various enzymes in PSS myco-transformation via aromatic ring cleavage and/or side-chain cleavage of PSS, and its subsequent conversion into alcohols, ketones and aldehydes which can be directly fed into Krebs cycle [Figure 5.4]. The *in silico* study of two primarily participating proteins namely, laccase and cerato-platanin revealed a strong association between these proteins confined our hypothesis that, both these proteins work in collaboration to transform PSS. Additionally, both the proteins individually displayed strong binding energies with SS, indicating their involvement in its transformation.

Furthermore, the real-time potential of *C. dactyloctenicola* VJP08 towards polystyrene (PS) depolymerization was confirmed by checking its ability to colonize and degrade the commercially available PS products. Different characterization techniques such as SEM, EDS, DSC and GC-MS/MS revealed that upon exposure to *C. dactyloctenicola* VJP08, the surface profile of PS pieces displayed dense fungal colonisation, propagation and mycelial invasion for carbon extraction causing cracks and holes on its surface. The fungal colonization also led to alter various in properties such as reduction in weight (3.57%), thickness (8.8%), and T_g of PS treated samples. Additionally, GC-MS/MS analysis confirmed significant decrease in the concentration of benzene and related aromatic derivatives as a result of fungal action. Combinedly, all the above-mentioned analysis strongly indicated phytopathogenic fungus *C. dactyloctenicola* VJP08 to be a powerful contender for plastic depolymerization.

Considering the fact that different fungi employ unique biomolecules to adapt under varied environmental conditions, the present study also evaluated the potential of fungus *Lichtheimia ramosa* AJP11 isolated from the rhizosphere of plants growing in heavy metal rich sites towards PSS myco-transformation and its underlying mechanism. *L. ramosa* AJP11 was observed to display increased biomass (~41%) in the presence of MSM+1% PSS as sole carbon source. GC-MS/MS analysis revealed the formation of various organic intermediates viz. alkanes and fatty acids which were involved in energy generation and cellular metabolism. The extracellular protein profile indicated over-expression of three proteins (14.4 kDa, 46.8 kDa and 107.9 kDa), identified to be hydrophobic surface binding protein, universal stress protein and PRP-1 splicing factor, respectively. *In silico* analysis of Hsb indicated its involvement as an assistive protein crucial for mediating the interactions between hydrophobic PSS and catalysing enzyme. Based on the obtained results, the series of events occurring during myco-transformation of PSS have been identified [Figure 7.11].

Overall, the present study suggests that phytopathogenic fungi are interesting candidates for the myco-transformation of PSS (and related plastics). Since phytopathogenic fungi have evolved to attack and depolymerize hydrophobic and rigid plant cuticle, their extracellular protein profile represents a huge array of enzymes which are capable to depolymerize plastics. Interestingly, the study also highlighted that different fungi employ different proteins in metabolizing same organic pollutant. To the best of our knowledge, this is the first report which combinedly present the metabolic proteomic and *in silico* analysis of PSS myco-transformation by *C. dactyloctenicola* VJP08.

8.2 Future Prospects

In the present-day scenario, concerns regarding increasing environmental issues, particularly plastic pollution, has gained much attention. Although, the implementation of possible solutions of plastic waste management is a futuristic idea, the development of a workable strategy is a current requirement. Microbial treatment of plastic waste is a persuasive option that uses plastic as a carbon source leading to its transformation into value-added products. Although, studies primarily focusing on biodegradation of plastic have been a focus for researchers, limited progress has been made into studying the participating biomolecules and mechanisms behind its microbial utilization. The present work opens interesting gateways to progress in the arena of plastic biodegradation. Various oxidoreductases such as laccases, multicopper oxidases, tyrosinases, intradiol dioxygenase and biosurfactants cerato-platanin and hydrophobic surface-binding (Hsb) protein have been found to be transforming PSS. Since the

structure of PSS is comprised of extensive C-C bonds, the above-mentioned enzymes may also be applicable towards transformation of related plastics such as PE, PP and PVC. However, much more work at molecular level is still required for its successful implementation. Here we present the following recommendations for future experiments:

1. Whole-genome sequencing and functional gene annotation of *C. dactyloctenicola* VJP08.

   It will reveal the genetic basis of the proteins involved in the degradation of plastics and other xenobiotic pollutants. The annotation of genes responsible for plastic degradation is critical to identify target proteins which are functionally relevant in understanding the potential degradation cascades and production of commercially valuable products.

2. Real-time PCR and transcriptomic analysis to reveal highly functional genes in plastic biodegradation.

   It will reveal the potential biomolecules involved in plastic sensing mechanism(s) and channel proteins that allow the intake of plastic oligomers/monomers into the cell. Identification of such biomolecules would be helpful in speeding up the process of plastic biodegradation.

3. Structural analysis of biosurfactants viz. cerato-platanin, Hsb and catalytic proteins including laccases, multicopper oxidases, tyrosinases, intradiol dioxygenase by X-ray crystallography/ Nuclear magnetic resonance.

   Studying the structural biology of proteins will provide the molecular basis of biological processes. The resolved 3D structures would be helpful in experimental validation of protein reactivity, substrate specificity and thermostability. It will help to understand the involvement of structural components important for plastic biodegradation.

4. Real-time analysis of adsorption kinetics between biosurfactants and catalytic enzymes.

   In the present study, both biosurfactants and enzymes have been predicted to co-localise onto the hydrophobic plastic surface to mediate its degradation. Hence, their real-time interactions can be validated by quartz crystal microbalance (QCM), circular dichroism and fluorescence recovery after photobleaching (FRAP) analysis. The QCM analysis would reveal whether the biosurfactant and catalytic proteins establish direct contact with each other over the plastic surface. Circular dichroism would provide the extent of their attachment onto the plastic surface and FRAP analysis would reveal the real-time mobility of these proteins over the plastic surface.

5. Assessment of enzyme kinetics of the participating proteins.

   Understanding of the kinetic parameters for enzymes involved in both, degradation and upcycling processes would be crucial for formulating and establishing a methodology for designing batch biodegradation reactors. This would not only allow the large-scale degradation of plastic waste but would also facilitate the recovery of commercially important secondary metabolites released as by-products during the biodegradation process.

Considering the demand for sustainable, economical feasible and tailor-made technologies for handling the over-accumulating plastic (and other xenobiotic pollutant) waste, the present study provides a strong foundation and various possibilities of translating the powerful fungal enzyme system into ecology-based technologies.

References

Abbas, N.H., Elsayed, A., Hassan, H.A., El-Sabbagh, S., Elbaz, A.F. and Khalil, H. (2022) Characterization and expression analysis of extradiol and intradiol dioxygenase of phenol-degrading haloalkaliphilic bacterial isolates. *Current Microbiology*, 79, 294.

Agrawal, N., Barapatre, A., Shahi, M.P. and Shahi, S.K. (2021) Biodegradation pathway of polycyclic aromatic hydrocarbons by ligninolytic fungi *Podoscypha elegans* strain FTG4 and phytotoxicity evaluation of their metabolites. *Environmental Processes*, 8, 1307-1335.

Alawlaqi, M.M. and Alharbi, A.A. (2020) Exo- and endoglucanase production by *Curvularia affinis* using bean (*Phaseolus vulgaris* L.) waste biomass. *Bioresources and Bioprocessing*, 7, 1-11.

Aleklett, K. and Boddy, L. (2021) Fungal behaviour: a new frontier in behavioural ecology. *Trends in Ecology & Evolution*, 36, 787-796.

Ali, H.E. and Ghaffar, A.M.A. (2017) Preparation and effect of gamma radiation on the properties and biodegradability of poly (styrene/starch) blends. *Radiation Physics and Chemistry*, 130, 411-420.

Ali, S.S., Elsamahy, T., Koutra, E., Kornaros, M., El-Sheekh, M., Abdelkarim, E., Zhu, D. and Sun, J. (2021) Degradation of conventional plastic wastes in the environment. A review on current status of knowledge and future perspectives of disposal. *Science of the Total Environment*, 144719.

Almeida, E.L., Rincón, A.F.C., Jackson, S.A. and Dobson, A.D.W. (2019) In silico screening and heterologous expression of a polyethylene terephthalate hydrolase (PETase)-like enzyme (SM14est) with the polycaprolactone (PCL)-degrading activity, from the marine sponge derived strain *Streptomyces* sp. SM14. *Frontiers in Microbiology*, 10, 2187.

Amaral-Zettler, L.A., Zettler, E.R. and Mincer, T.J. (2020) Ecology of the plastisphere. *Nature Reviews Microbiology*, 18, 139-151.

Amobonye, A., Bhagwat, P., Singh, S. and Pillai, S. (2021) Plastic Biodegradation: frontline microbes and their enzymes. *Science of the Total Environment*, 759, 143536.

Andlar, M., Rezić, T., Marđetko, N., Kracher, D., Ludwig, R. and Šantek, B. (2018) Lignocellulose degradation: an overview of fungi and fungal enzymes involved in lignocellulose degradation. *Engineering in Life Sciences*, 18, 768-778.

Andrady, A.L. and Neal, M.A. (2009) Applications and societal benefits of plastics. *Philosophical Transactions of the Royal Society B: Biological Sciences*, 364, 1977-1984.

Andrady, A.L. (2011) Microplastics in the marine environment. *Marine Pollution Bulletin*, 62, 1596-1605.

Appels, F.V.W., Dijksterhuis, J., Lukasiewicz, C.E., Jansen, K.M.B., Wösten, H.A.B. and Krijgsheld, P. (2018) Hydrophobin gene deletion and environmental growth conditions impact mechanical properties of mycelium by affecting the density of the material. *Scientific Reports*, 8, 4703.

Aragón, W., Reina-Pinto, J.J. and Serrano M. (2017) The intimate talk between plants and microorganisms at the leaf surface. *Journal of Experimental Botany*, 68, 5339-5350.

Atlas, R.M. (1975) Effects of temperature and crude oil composition on petroleum biodegradation. *Applied Microbiology*, 30, 396-403.

Avio, C.G., Gorbi, S. and Regoli, F. (2016) Plastics and microplastics in the oceans: from emerging pollutants to emerge threat. *Marine Environmental Research*, 128, 2-11.

Baccelli, I. (2015) Cerato-platanin family proteins: one function for multiple biological roles? *Frontiers in Plant Science*, 5, 769.

Balasubramanian, V., Natarajan, K., Rajeshkannan, V. and Perumal, P. (2014) Enhancement of in vitro high-density polyethylene (HDPE) degradation by physical, chemical and biological treatments. *Environmental Science and Pollution Research*, 21, 12549-12562.

Balserio-Romero, M., Gkorezis, P., Kidd, P.S., Van Hamme, J., Weyens, N., Monterroso, C. and Vangronsveld, J. (2017) Characterization and degradation potential of diesel-degrading bacterial strains for application in bioremediation. *International Journal of Phytoremediation*, 19, 955-963.

Baral, D., Thapa, S. and Saha, J. (2022) First report of *Curvularia alcornii* as a plant pathogen causing post-harvest rot of tomatoes. *New Disease Reports*, 45, e12078.

Barnes, D.K.A., Galgani, F., Thompson, R.C. and Barlaz, M. (2009) Accumulation and fragmentation of plastic debris in global environments. *Philosophical Transactions of the Royal Society B: Biological Sciences*, 364, 1985-1998.

Barthlott, W., Neinhuis, C., Cutler, D., Ditsch, F., Meusel, I., Theisen, I. and Wilhelmi, H. (1998) Classification and terminology of plant epicuticular waxes. *Botanical Journal of the Linnean Society*, 126, 237-260.

Bayry, J., Aimanianda, V., Guijarro, J.I., Sunde, M. and Latgé, J.P. (2012) Hydrophobins-unique fungal proteins. *PLoS Pathogens*, 8, 6-9.

Benguenab, A. and Chibani, A. (2021) Biodegradation of petroleum hydrocarbons by filamentous fungi (*Aspergillus ustus* and *Purpureocillium lilacinum*) isolated from used engine oil contaminated soil. *Acta Ecologica Sinica*, 41, 416-423.

Bers, K. Leroy, B., Breugelmans, P., Albers, P., Lavigne, R., Sørensen, S.R., Aamand, J., De Mot, R., Wattiez, R. and Springael, D. (2011) A novel hydrolase identified by genomic-proteomic analysis of Phenylurea herbicide mineralization by *Variovorax* sp. strain SRS16. *Applied and Environmental Microbiology*, 77, 8754-8764.

Berg, G., Grube, M., Schloter, M. and Smalla, K. (2014) The plant microbiome and its importance for plant and human health. Frontiers in Microbiology, 5, 491.

Berger, B.W. and Sallada, N.D. (2019) Hydrophobins: multifunctional biosurfactants for interface engineering. *Journal of Biological Engineering*, 13, 10.

Betts, M.J. and Russell, R.B. (2007) Amino-acid properties and consequences of substitutions In: *Bioinformatics for Geneticists: A Bioinformatics Primer for the Analysis of Genetic Data*, 2nd Edition, Barnes, M.R. (Ed.), John Wiley and Sons Ltd., Chichester, U.K., p. 311-342.

Bhanot, V., Pareek, V., Fadanavis, SV. and Panwar, J.P. (2020) Myco-degradation of plastics. In: *New and Future Developments in Microbial Biotechnology and Bioengineering*, Singh, J. and Gehlot, P. (Eds.), Elsevier, Amsterdam, Netherlands, pp. 25-34.

Bhanot, V., Fadanavis, S.V. and Panwar, J. (2021) Revisiting the architecture, biosynthesis and functional aspects of the plant cuticle: there is more scope. *Environmental and Experimental Botany*, 183, 104364.

Bhanot, V., Shobham., Mamta. and Panwar, J. (2023) Unveiling the potential of *Lichtheimia ramosa* AJP11 for myco-transformation of polystyrene sulfonate and its driving molecular mechanism. *Journal of Environmental Management*, 325, 116579.

Bhargava, A., Jain, N., Khan, M.A., Pareek, V., Dilip, R.V. and Panwar, J. (2016) Utilization of metal tolerance potential of soil fungus for efficient synthesis of gold nanoparticle synthesis with superior catalytic activity for degradation of rhodamine B. *Journal of Environmental Management*, 183, 22-32.

Bhatt, J.K., Ghevariya, C.M., Dudhagara, D.R., Rajpara, R.K. and Dave, B.P. (2014) Application response surface methodology for rapid chrysene biodegradation by newly isolated marine-derived fungus *Cochliobolus lunatus* strain CHR4D. *Journal of Microbiology*, 52, 908-917.

Bitas, V., Kim, H.S., Bennett, J.W., and Kang, S. (2013) Sniffing on microbes: diverse roles of microbial volatile compounds in plant health. *Molecular Plant-Microbe Interactions*, 26, 835-843.

Bitencourt-Ferreira, G., Veit-Acosta, M. and de Azevedo Jr W.F. (2019) Electrostatic energy in protein-ligand complexes. Methods in Molecular Biology, 2053, 67-77.

Blanksby, S.J. and Ellison, G.B. (2003) Bond dissociation energies of organic molecules. *Account of Chemical Research*, 36, 255-263.

Boanares, D., Bueno, A., de Souza, A.X., Kozovits, A.R., Sousa, H.C., Pimenta, L.P.S., Isaias, R.M.S. and França, M.G.C. (2021) Cuticular wax composition contributes to different strategies of foliar water uptake in six plant species from foggy rupestrian grassland in tropical mountains. *Phytochemistry*, 190, 112894.

Bonazza, K., Gaderer, R., Neudl, S., Pezylucka, A., Allmaier, G., Druzhinina, I.S., Grothe, H., Friedbacher, G. and Seidl-Seiboth, V. (2015) The fungal cerato-platanin protein EPL1 forms highly ordered layers at hydrophobic/hydrophilic interfaces. *Soft Matter*, 11, 1723-1732.

Bonomo, R.P., Cennamo, G., Purrello, R., Santoro, A.M. and Zappalá, R. (2001) Comparison of three fungal laccases from *Rigidoporus lignosus* and *Pleurotus ostreatus*: correlation between conformation changes and catalytic activity. *Journal of Inorganic Biochemistry*, 83, 67-75.

Borisjuk, N., Peterson, A.A., Lv, J., Qu, G., Luo, Q., Shi, L., Chen, G., Kishchenko, O., Zhou, Y. and Shi, J. (2018) Structural and biochemical properties of Duckweed surface cuticle. *Frontiers in Chemistry*, 6, 317.

Brandon, A.M., Garcia, A.M., Khlystov, N.A., Wu, W-M. and Criddle, C.S. (2021) Enhanced bioavailability and microbial biodegradation of PS in an enrichment derived from the gut microbiome of *Tenebrio molitor* (mealworm larvae). *Environmental Science & Technology*, 55, 2027-2036.

Buchan, D.W.A. and Jones, D.T. (2019) The PSIPRED protein analysis workbench: 20 years on. *Nucleic Acid Research*, 47, W402-W407.

Buda, G.J., Isaacson, T., Matas, A.J., Paolillo, D.J. and Rose, J.K.C. (2009) Three-dimensional imaging of plant cuticle architecture using confocal scanning laser microscopy. *The Plant Journal*, 60, 378-385.

Cárdenas, P.D., Almeida, A. and Bak, S. (2019) Evolution of structural diversity of triterpenoids. *Frontiers in Plant Science*, 10, 1523.

Canopoli, L., Coulon, F. and Wagland, S.T. (2020) Degradation of excavated polyethylene and polypropylene waste from landfill. *Science of the Total Environment*, 698, 134125.

Carpenter, E.J., Anderson, S.J., Harvey, G.R., Miklas, H.P. and Bradford B. (1972) Polystyrene spherules in coastal waters. *Science*, 178, 749-750.

Carstens, L., Cowan, A.R., Seiwert, B. and Schlosser, D. (2020) Biotransformation of phthalate plasticizers and bisphenol A by marine-derived, freshwater, and terrestrial fungi. *Frontiers in Microbiology*, 11, 317.

Ceci, A., Pinzari, F., Russo, F., Persiani, A.M. and Gadd, G.M. (2019) Roles of saprophytic fungi in biodegradation or transformation of organic and inorganic pollutants in co-contaminated sites. *Applied Microbiology and Biotechnology*, 103, 53-68.

Chai, Y., Li, A., Wai, S.C., Song, C., Zhao, Y., Duan, Y., Zhang, B. and Lin, Q. (2020) Cuticular wax composition changes of 10 apple cultivars during postharvest storage. *Food Chemistry*, 324, 126903.

Chamas, A., Moon, H., Zheng, J., Qiu, Y., Tabassum, T., Hang, J.H., Abu-Omar, M., Scott, S.L. and Suh, S. (2020) Degradation rates of plastics in the environment. *ACS Sustainable Chemistry & Engineering*, 8, 3494-3511.

Chang, K.Y. and Yang, J-R. (2013) Analysis and prediction of highly effective antiviral peptides based on random forests. *PLoS ONE*, 8, e70166.

Chaudhary, A.K., Chaitanya, K. and Vijayakumar, R.P. (2021) Synergistic effect of UV and chemical treatment of biological degradation of polystyrene by *Cephalosporium* strain NCIM 1251. *Archives of Microbiology*, 203, 2183-2191.

Chaudhary, A.K., Chitriv, S.P. and Vijayakumar, R.P. (2022) Influence of nitric acid on biodegradation of polystyrene and low-density polyethylene by *Cephalosporium* species. *Archives of Microbiology*, 204, 489.

Chen, S., Su,L., Chen, J. and Wu, J (2013) Cutinase: characteristics, preparation, and application. *Biotechnology Advances*, 31, 1754-1767.

Chen, A.J., Frisvad, J.C., Sun, B.D., Varga, J., Kocsube, S., Dijksterhuis, J., Kim, D.H., Hong, S.B., Houbraken, J. and Samson, R.A. (2016) *Aspergillus* section *Nidulantes* (formerly *Emericella*): polyphasic taxonomy, chemistry and biology. *Studies in Mycology*, 84, 1-118.

Chen, C.-C., Dai, L., Ma, L. and Guo, R.-T. (2020) Enzymatic degradation of plant biomass and synthetic polymers. *Nature Reviews Chemistry*, 4, 114-126.

Chi, Y.H., Koo, S.S., Oh, H.T., Lee, E.S., Park, J.H., Phan, K.A.T., Wi, S.D., Bae, S.B., Paeng, S.K., Chae, H.B., Kang, C.H., Kim, M.G., Kim, W.-Y., Yun, D.-J. and Lee, S.Y. (2019) The physiological functions of universal stress proteins and their molecular mechanism to protect plants from environmental stresses. *Frontiers in Plant Sciences*, 10, 750.

Chiba, S., Saito, H., Fletcher, R., Yogi, T., Kayo, M., Miyagi, S., Ogido, M. and Fujikura, K. (2018) Human footprint in the abyss: 30 year records of deep-sea plastic debris. *Marine Policy*, 96, 204-212.

Cheng, Q., Thomas, S.M. and Rouvière, P. (2002) Biological conversion of cyclic alkanes and cyclic alcohols into dicarboxylic acids: biochemical and molecular basis. *Applied Microbiology and Biotechnology*, 58, 704-711.

Condon, B.J., Leng, Y., Wu, D., Bushley, K.E., Ohm, R.A., Otillar, R., Martin, J., Schackwitz, W., Grimwood, J., MohdZainudin, N., Xue, C., Wang, R., Manning, V.A., Dhillon, B., Tu, Z.J., Steffenson, B.J., Salamov, A., Sun, H., Lowry, S., LaButti, K., Han, J., Copeland, A., Lindquist, E., Barry, K., Schmutz, J., Baker, S.E., Ciuffetti, L.M., Grigoriev, I.V., Zhong, S. and Turgeon, B.G. (2013) Comparative genome structure, secondary metabolite, and effector coding capacity across *Cochliobolus* pathogens. *PloS Genetics*, 9, e1003233.

Corcoran, P.L. and Jazvac, K. (2020) The consequence that is plastiglomerate. *Nature Reviews Earth & Environment*, 1, 6-7.

Crabo, A.G., Singh, B., Nguyen, T., Emami, S., Gassner, G.T. and Sazinsky, M.H. (2017) Structure and biochemistry of phenylacetaldehyde dehydrogenase from *Pseudomonas putida* S12 styrene catabolic pathway. *Archives of Biochemistry and Biophysics*, 616, 47-58.

Cui, W., Wei, Z., Chen, Q., Cheng, Y., Geng, L., Zhang, J., Chen, J., Hou, T. and Ji, M. (2010) Structure-based design of peptides against G3BP with cytotoxicity on tumor cells. *Journal of Chemical Information and Modeling*, 50, 380-387.

Dahabiyeh, L.A., Malkawi, A.K., Wang, X., Colak, D., Mujamammi, A.H., Sabi, E.M., Li, L., Dasouki, M. and Rahman, A.M.A. (2020) Dexamethasone-induced perturbations in tissue metabolomics revealed by chemical isotope labeling LC-MS analysis. *Metabolites*, 10, 42.

Daly, P., Cai, F., Kubicek, C.P., Jiang, S., Grucij, M., Rahimi, M.J., Sheteiwvy, M.S., Giles, R., Riaz, A., de Vries, R.P., Akcapinar, G.B., Wei, L. and Druzhinina, I.S. (2021) From

lignocelluloses to plastics: knowledge transfer on the degradation approaches by fungi. *Biotechnology Advances*, 50, 107770.

Danso, D., Chow, J. and Streit, W.R. (2019) Plastics: environmental and biotechnological perspectives on microbial degradation. *Applied and Environmental Microbiology*, 85: e01095-19.

Das, M.P. and Kumar, S. (2015) An approach to low-density polyethylene biodegradation by *Bacillus amyloliquefaciens*. *3 Biotech*, 5, 81-86.

Davidson, F.A. and Olsson, S. (2000) Translocation induced outgrowth of fungi in nutrient-free environment. *Journal of Theoretical Biology*, 205, 73-84.

de Sousa, F.D.B. (2021) Plastics and its consequences during the COVID-19 pandemic. *Environmental Science and Pollution Research*, 28, 46067-46078.

Demeneix, B.A. (2020) How fossil fuel-derived pesticides and plastics harm health, biodiversity, and the climate. *The Lancet Diabetes and Endocrinology*, 8, 462-464.

Desta, I.T., Porter, K.A., Xia, B., Kozakov, D. and Vajda, S. (2020) Performance and its limits in rigid body protein-protein docking. *Structure*, 28, 1071-1081.

Dimitriadi, A., Papaefthimiou, C., Genizegkini, E., Sampsonidis, I., Kalogiannis, S., Feidantsis, K., Bobori, D.C., Kastrinaki, G., Koumoundouros, G., Lambropoulou, D.A., Kyzas, G.Z. and Bikiaris, D.N. (2021) Adverse effects of polystyrene microplastics exert on zebrafish heart-molecular to individual level. *Journal of Hazardous Materials*, 416, 125969.

Ding, S., Zhang, J., Wang, R., Ou, S. and Shan, Y. (2018) Changes in cuticle compositions and crystal structure of 'Bingtang' sweet orange fruits (*Citrus sinensis*) during storage. *International Journal of Food Properties*, 21, 2411-2427.

do Val Siqueira, L., Arias, C.I.L.F., Maniglia, B.C. and Tadini, C.C. (2021) Starch based-biodegradable plastics: methods of production, challenges and future perspectives. *Current Opinion in Food Science*, 38, 122-130.

Domínguez, E., Cuatero, J. and Heredia, A. (2011) An overview on plant cuticle biomechanics. *Plant Science*, 181, 77-84.

Dong, C-D., Chen, C-W., Chen, Y-C., Chen, H-H., Lee, J-S. and Lin, C-H. (2020) Polystyrene microplastic particles: in vitro pulmonary toxicity assessment. *Journal of Hazardous Materials*, 385, 121575.

dos Santos, P.R.P., Leão, E.U., de Souza Aguiar, R.W., de Melo, M.P. and dos Santos, G.R. (2018) Morphological and molecular characterization of *Curvularia lunata* pathogenic to Anddropogon grass. *Plant protection*, 77, 326-332.

Du, Y., Yao, C., Dou, M., Wu, J., Su, L. and Xia, W. (2022) Oxidative degradation of pre-oxidated polystyrene plastics by dye decolorizing peroxidases from *Thermomonospora curvata* and *Nostocaceae*. *Journal of Hazardous Materials*, 436, 129265.

Edwards, H.G.M., Brown, D.R., Dale, J.A. and Plant, S. (2000) Raman spectroscopy of sulfonated polystyrene resins. *Vibrational Spectroscopy*, 24, 213-224.

Eigenbrode, S.D., Espelie, K.E. and Shelton, A.M. (1991) Behavior neonate diamondback moth larvae [*Plutella xylosrella* (l.)] on leaves and on extracted leaf waxes of resistant and susceptible cabbages. *Journal of Chemical Ecology*, 17, 1691-1704.

El-Aziz, A.R.M., Al-Othman, M.R., Hisham, S.M. and Shehata, S.M. (2021) Evaluation of crude oil biodegradation using mixed fungal cultures. *PLoS ONE*, 16, e0256376.

El- Gendi, H., Saleh, A.K., Badierah, R., Redwan, E.M., El-Maradny, Y.A. and El-Fakharay, E.M. (2022) A comprehensive insights into fungal enzymes: structure, classification, and their role in mankind's challenges. *Journal of Fungi*, 8, 23.

Elton, D.C., Boukouvalas, Z., Fuge, M.D. and Chung, P.W. (2019) Deep learning for molecular design- a review of the state of the art. *Molecular Systems Design & Engineering*, 4, 828-849.

Ene, I.V., Brunke, S., Brown, A.J.P. and Hube, B. (2014) Metabolism in fungal pathogens. *Cold Springer Harbor Perspectives in Medicine*, 4, a019695.

Ensikat, H.J., Ditsche-Kuru, P., Neinhuis, C. and Barthlott, W. (2011) Superhydrophibicity in perfection: the outstanding properties of the lotus leaf. *Beilstein Journal of Nanotechnology*, 2, 152-161.

Endeshaw, A., Birhanu, G., Zerihun, T. and Misganaw, W. (2017) Application of microorganisms in bioremediation-review. *Environmental Microbiology*, 1, 2-9.

Engqvist, M.K.M. (2018) Correlating enzyme annotations with a large set of microbial growth temperatures reveals metabolic adaptations to growth at diverse temperatures. *BMC Microbiology*, 18, 177.

Eyerer, P. (2010) Plastics: classification, characterization, and economic data. Polymers-opportunities and risks I. In: *The Handbook of Environmental Chemistry*, Bercelo, D., Kostianoy, A. (Eds.), Springer, Berlin, pp. 1-17.

Fraaije, M.W., van Den Heuvel, R.H., van Berkel, W.J. and Mattevi, A. (2000) Structural analysis of flavinylation in vanillyl-alcohol oxidase. *Journal of Biological Chemistry*, 275, 38654-8

Francesc, X., Boldú, P., Summerbell, R. and de Hoog, G.S. (2005) Fungi growing on aromatic hydrocarbons: biotechnology's unexpected encounter with biohazard? *FEMS Microbiology Reviews*, 30, 109-130.

Fecker, T., Galaz-Davison, P., Engelberger, F., Narui, Y., Sotomayer, M., Parra, L.P. and Ramírez-Sarmiento, C.A. (2018) Active site flexibility as hallmark for efficient PET degradation by *I. sakaiensis* PETase. *Biophysical Journal*, 114, 1302-1312.

Ferguson, B.A., Dreisbach, T.A., Parks, C.G., Filip, G.M. and Schmitt, C.L. (2003) Coarse-scale population structure of pathogenic Armillaria species in a mixed-conifer forest in the Blue Mountains of northeast Oregon. *Canadian Journal of Forest Research*, 33, 612-623.

Fester, T, Geibler, J., Wick, L.Y., Schlosser, D., Kästner, M. (2014) Plant-microbe interactions as drivers of ecosystem functions relevant for the biodegradation of organic contaminants. *Current Opinion in Biotechnology*, 27, 168-175.

Floudas, D., Binder, M., Riley, R., Barry, K., Blanchette, R.A., Henrissat, B., Martínez, A.T., Otillar, R., Spatafora, J.W., Yadav, J.S. et al. (2012) The paleozoic origin of enzymatic lignin decomposition reconstructed from 31 fungal genomes. *Science*, 336, 1715-1719.

Fordyce, M., Devries, K.L. and Fanconi, B.M. (1984) Chain scission and mechanical degradation of polystyrene. *Polymer Engineering and Science*, 24, 421-427.

Fricker, M.D., Lee, J.A., Bebber, D.P., Tlalka, M., Hynes, J., Darrah, P.R., Watkinson, S.C. and Boddy, L. (2008) Imaging complex nutrient dynamics in mycelial networks. *Journal of Microscopy*, 231, 317-331.

Frisvad, J.C., Hubka, V., Ezekiel, C.N., Hong, S.-B., Nováková, A., Chen, A.J., Arzanlou, M., Larsen, T.O., Sklenář, F., Mahakarnchanakul, W., Samson, R.A. and Houbraken, J. (2019) Taxonomy of *Aspergillus* section *Flavi* and their production of aflatoxins, ochratoxins and other mycotoxins. *Studies in Mycology*, 93, 1-63.

Fu, B., Xu, T., Cui, Z., Ng, H.L., Wang, K., Li, J. and Li, Q.X. (2018) Mutation of phenylalanine-223 to leucine enhances transformation of benzo[a]pyrene by ring-hydroxylating dioxygenase of *Sphingobium* sp. FB3by increasing accessibility of the catalytic site. *Journal of Agricultural and Food Chemistry*, 66, 1026-1213.

Fujii, I., Ebizuka, Y. and Sankawa, U. (1988) A novel anthraquinone ring cleavage enzyme of *Aspergillus terreus. Journal of Biochemistry*, 103, 878-883.

Furukawa, M., kawakami, N., Tomizawa, A. and Miyamoto, K. (2019) Efficient degradation of poly(ethylene terephthalate) with *Thermobifida fusca* cutinase exhibiting improved catalytic activity generated using mutagenesis and additive-based approaches. *Scientific Reports*, 9, 16038.

Galgali, P., Puntambekar, U.S., Gokhale, D.V. and Varma, A.J. (2004) Fungal degradation of carbohydrate-linked polystyrenes. *Carbohydrate Polymers*, 55, 393-399.

Gaderer, R., Bonazza, K. and Seidl-Seiboth, V. (2014) Cerato-platanins: a fungal protein family with intriguing properties and application potential. *Applied Microbiology and Biotechnology*, 98, 4795-4803.

Gambarini, V., Pantos, O., Kingsburry, J.M., Weaver, L., Handley, K.M. and Lear, G. (2022) PlasticDB: a database of microorganisms and proteins linked to plastic biodegradation. *Database*, 2022, 1-12. (Accessed on February 2, 2023)

Ganesan, S., Maradudin, A. and Oitmaa, J. (1970) A lattice theory of morphed effects in crystal and diamond structure. *Annals of Physics*, 56, 556-594.

Garside, M. (2020) Plastics industry-statistics & facts. https://www.statista.com/topics/5266/plastics-industry/ Accessed 9 November 2022.

Gasteiger, E., Hoogland, C., Gattiker, A., Duvaud, S., Wilkins, M., Appel, R. and Bairoch, A. (2005) Protein identification and analysis tools on the ExPASy server Nucleic Acids Research. In: *The Proteomics Protocols Handbook*, Walker, J.M., Totowa, N.J. (Eds.), Humana Press, Totowa, New Jersey, p. 571-607.

Germain, J., Raveton, M., Binet, M.-N. and Mouhamadou, B. (2021) Potentiality of native Ascomycete strains in bioremediation of highly polychlorinated biphenyl contaminated soils. *Microorganisms*, 9, 612.

Geyer, R., Jambeck, J.R. and Law, K.L. (2017) Production, use and fate of all plastics ever made. *Science Advances*, 3, e1700782.

Ghosal, D., Ghosh, S., Dutta, T.K. and Ahn, Y. (2017) Current state of knowledge in microbial degradation of polycyclic aromatic hydrocarbons (PAHs): a review. Frontiers in Microbiology, 7, 1369.

Gkoutselis, G., Rohrbach, S., Harjes, J., Obst, M., Brachmann, A., Horn, M.A. and Rambold, G. (2021) Microplastics accumulate fungal pathogens in terrestrial ecosystems. *Scientific Reports*, 11, 13214.

Goldman, G.H. (2020) New opportunities for modern fungal biology. *Frontiers in Fungal Biology*, 1, 596090.

Gómez-Patiño, M.B., Estrada-Reyes, R., Vargas-Diaz, M.E. and Arrieta-Baez, D. (2020) Cutin from *Solanum myriacanthum* danul and *Solanum aculeatissimum* jacq. as a potential raw material for biopolymers. *Polymers*, 12, 1945.

González-Abradelo, D., Pérez-Llano, Y., Peidro-Guzmán, H., Sánchez-Carbente, M.R., Folch-Mallol, J.L., Aranda, E., Vaidyanathan, V.K., Cabana, H., Gunde-Cimerman, N. and Batista-Garcia, R.A. (2019) First demonstration that ascomycetous halophilic fungi (*Aspergillus sydowii* and *Aspergillus destruens*) are useful in xenobiotic mycoremediation under high salinity conditions. *Bioresource Technology*, 279, 287-296.

Goulet, K.M. and Saville, B.J. (2017) Carbon acquisition and metabolism changes during fungal biotrophic plant pathogenesis: insights from *Ustilago maydis*. *Canadian Journal of Plant Physiology*, 39, 247-266.

Grelska, A. and Noszczyńska, M. (2020) White rot fungi can be promising tool for removal of bisphenol A, bisphenol S, and nonylphenol from wastewater. *Environmental Science and Pollution Research*, 27, 39958-39976.

Grützmann, K., Szafranski, K., Pohl, M., Voigt, K., Petzold, A. and Schuster, S. (2014) Fungal alternative splicing is associated with multicellular complexity and virulence: a genome-wide multi-species study. *DNA Research*, 21, 27-39.

Gubler, L., Dockheer, S.M. and Koppenol, W.H. (2011) Radical ($HO^{\bullet}$, $H^{\bullet}$ and $HOO^{\bullet}$) formation and ionomer degradation in polymer electrolyte fuel cells. *Journal of The Electrochemical Society*, 158, B755-B769.

Guignard, G. (2019) Thirty-three years (1986-2019) of fossil plant cuticle studies using transmission electron microscopy: a review. *Review of Palaeobotany and Palynology*, 271, 104097.

Guo, Y., Jud, W., Ghirardo, A., Antritter, F., Benz, P., Schnitzler, J-P. and Rosenkranz, M. (2020) Sniffing fungi: phenotyping of volatile chemical diversity in *Trichoderma* species. *New Phytologist*, 227, 244-259.

Gupta, V.K., Kubicek, C.P., Berrin, J.-G., Wilson, D.W., Couturier, M., Berlin, A., Filho, E.X.F. and Ezeji, T. (2016) Fungal enzymes for bio-products from sustainable and waste biomass. *Trends in Biochemical Sciences*, 41, 633-645.

Guruprasad, K., Reddy, B.V. and Pandit, M.W. (1990) Correlation between stability of a protein and its dipeptide composition: a novel approach for predicting in vivo stability of a protein from its primary sequence. *Protein Engineering*, 4, 155-161.

Guzik, U., Hupert-Kocurek, K. and Wojcieszynska, D. (2013) Intradiol Dioxygenase-The key enzymes in xenobiotic degradation, In: Rolando Chamy (Ed.) *Biodegradation of Hazardous and Special Products*. InTech, pp. 131-157.

Guzmán-Puyol, S., Heredia, A., Heredia-Guerrero, J.A. and Benítez, J. J. (2010) Cutin-inspired polymers and plant cuticle-like composites as sustainable food packaging materials. In: *Sustainable Food Packaging Technology*, Athanassiou, A. (Ed.), Wiley-Vch GmbH, pp. 161-198.

Gygli, G., de Vries, R.P. and van Berkel, W.J.H. (2018) On the origin of vanillyl alcohol oxidase. *Fungal Genetics and Biology*, 116, 24-32.

Hahladakis, J.N., Velis, C.A., Weber, R., Lacovidou, E. and Purnell, P. (2018) An overview of chemical additives present in plastics: migration, release, fate and environmental impact during their use, disposal and recycling. *Journal of Hazardous Materials*, 344, 179-199.

Halaouli, S., Asther, M., Sigoillot, J. C., Hamdi, M. and Lomascolo, A. (2006) Fungal tyrosinases: new prospects in molecular characteristics, bioengineering and biotechnological applications. *Journal of Applied Microbiology*, 100, 219-232.

Hamad, A.A., Moubasher, H.A., Moustafa, Y.M. and Mohamed, N.H. (2021) Petroleum hydrocarbon bioremediation using native fungal isolates and consortia. *The Scientific World Journal*, 6641533.

Han, X., Liu, W., Huang, J.W., Ma, J., Zheng, Y., Ko, T.P., Xu, L., Cheng, Y.S., ChengC.C. and Guo, R.T. (2017) Structural insight into catalytic mechanism of PET hydrolase. *Nature Communications*, 8, 2106.

Handbook for institutional Biosafety Committee (IBSC) (2020). (http://ibkp.dbtindia.gov.in/).

Harms, H., Schlosser, D. and Wick, L.Y. (2011) Untapped potential: exploiting fungi in bioremediation of hazardous chemicals. *Nature Reviews Microbiology*, 9, 177-192.

Harwood, C.S. and Parales, R.E. (1996) The beta-ketoadipate pathway and the biology of self-identity. *Annual Reviews in Microbiology*, 50, 553-590.

Haugland, R.A., Varma, M., Wymer, L.J. and Vesper, S.J. (2004) Quantitative PCR analysis of selected *Aspergillus*, *Penicillium* and *Paecilomyces* species. *Systematic and Applied Microbiology*, 27, 198-210.

Hennig, S., Rödel, G. and Ostermann, K. (2016) Hydrophobin based surface engineering for sensitive and robust quantification of yeast pheromones. *Sensors (Basel)*, 16, 602.

Henry, T., Iwen, P.C. and Hinrichs, S.H. (2000) Identification of *Aspergillus* species using internal transcribed spacer region 1 and 2. *Journal of Clinical Microbiology*, 38, 1510-1515.

Hiscox, J., O'Leary, J. and Boddy. L. (2018) Fungus wars: basidiomycete battles in wood decay. *Studies in Mycology*, 89, 117-124.

Ho, B.T., Roberts, T.K. and Lucas, S. (2018) An overview on biodegradation of polystyrene and modified polystyrene: the microbial approach. *Critical Reviews in Biotechnology*, 38, 308-320.

Hongyan, L., Zexiong, Z., Shiwei, X., He, X., Yinian, Z., Haiyun, L. and Zhongsheng, Y. (2019) Study on transformation and degradation of bisphenol A by *Trametes versicolor* laccase and simulation of molecular docking. *Chemosphere*, 224, 743-750.

Hooft, R.W., Vriend, G., Sander, C. and Abola, E.E. (1996) Errors in protein structures. *Nature*, 381, 272.

Hou, L. and Majumder, E.L.-W. (2021) Potential for and distribution of enzymatic biodegradation of polystyrene by environmental microorganisms. *Materials (Basel)*, 14, 503.

Houbraken, J.A.M.P., Frisvad, J.C. and Samson, R.A. (2010) Taxonomy of *Penicillium citrinum* and related species. *Fungal Diversity*, 44, 117-133.

Hou, L. and Majumder, E.L.-W. (2021) Potential for and distribution of enzymatic biodegradation of polystyrene of environmental microorganisms. *Materials*, 14, 503.

Houchin, M.L. and Topp, E.M. (2009) Physical properties of PLGA films during polymer degradation. *Journal of Applied Polymer Science*, 114, 2848-2854.

Huang, M., Sanchez-Moreiras, A.M., Abel, C., Sohrabi, R., Lee, S., Gershenzon, J. and Tholl, D. (2012) The major volatile organic compound emitted from *Arabidopsis thaliana* flowers, the sesquiterpene (E)-β-caryophyllene, is a defense against a bacterial pathogen. *New Phytologist*, 193, 997-1008.

Huarte-Bonnet, C., Kumar, S., Saparrat, M.C.N., Girotti, J.R., Santana, M., Halssworth, J.E. and Pedrini, N. (2018) Insights into the hydrocarbon assimilation by eurotialean and hypocrealean fungi: roles of CYP52 and CYP53 clans of cytochrome P450 genes. *Applied Biochemistry and Biotechnology*, 184, 1047-1060.

Ikai, A. (1980) Thermostability and aliphatic index of globular proteins. *The Journal of Biochemistry*, 88, 1895-1898.

Ishigaki, T., Sugano, W., Nakanishi, A., Tateda, M., Ike, M. and Fujita, M. (2004) The degradability of biodegradable plastics in aerobic and anaerobic waste landfill model reactors. *Chemosphere*, 54, 225-233.

Iturrieta-González, I., Gené, J., Wiederhold, N. and García, D. (2020) Three new *Curvularia* species from clinical and environmental sources. *Mycokeys*, 68, 1-21.

Iyer, B.R. and Mahalakshmi, R. (2019) Hydrophobic characteristic is energetically preferred for cysteine in a model membrane protein. *Biophysical Journal*, 117, 25-35.

Jain, N., Bhargava, A., Tarafdar, J.C., Singh, S.K. and Panwar, J. (2013) A biomimetic approach towards synthesis of zinc oxide nanoparticles. *Applied Microbiology and Biotechnology*, 97, 859-869.

Jain, N., Bhargava, A., Sabat, D. and Panwar, J. (2014) Unveiling the potential of metal-tolerant fungi for efficient enzyme production. *Process Biochemistry*, 49, 1858-1866.

Jayawardena, R.S., Hyde, K.D., de Farias, A.R.G., Bhunjun, C.S., Ferdinandez, H.S., Manamgoda, D.S., Udayanga, D., Herath, I.S., Thambugala, K.M., Manawasinghe, I.S., Gajanayake, A.J., Samarakoon, B.C., Bundhun, D., Gomdola, D., Huanraluek, N., Sun, Y.-R., Tang, X., Promputtha, I. and Thines, M. (2021) What is a species in fungal plant pathogens? *Fungal Diversity*, 109, 239-266.

Jensen, B.G., Anderson, M.R., Pederson, M.H., Frisvad, J. and Søndergaard, I. (2010) Hydrophobins from *Aspergillus* species cannot be clearly divided into two classes. *BMC Research Notes*, 3, 344.

Jeyakumar, D., Christeen, J. and Doble, M. (2013) Synergistic effect of pretreatment and blending on fungi mediated biodegradation of polypropylenes. *Bioresource Technology*, 148, 78-85.

Ji, Y., Mao, G., Wang, Y., Bartlam, M. (2013) Structural insights into diversity and n-alkane biodegradation mechanisms of alkane hydroxylases. *Frontiers in Microbiology*, 4, 1-13.

Jin, Y., Lu, L., Tu, W., Luo, T. and Fu, Z. (2019) Impacts of polystyrene microplastic on the gut barrier, microbiota and metabolism of mice. *Science of the Total Environment*, 649, 308-317.

Jindrová, E., Chocová, M., Demnerová, K. and Brenner, V. (2002) Bacterial aerobic degradation of benzene, toluene, ethylbenzene and xylene. *Folia Microbiologica*, 47, 83-93.

Joel, F.R. (1995) Introduction in polymer science In: *Polymer Science and Technology*, 3rd Ed, Prentice Hall, Upper Saddle River, New Jersey, USA, pp. 4-9.

Johnston, B., Radecka, I., Hill, D., Chiellini, E., Ilieva, V.I., Sikorsa, W., Musioł, M., Zięba, M., Marek, A.A., Keddie, D., Mendrek, B., Darbar, S., Adamus, G. and Kowalczuk, M. (2018) The microbial production of polyhydroxyalkanoates from aste polystyrene fragments attained using oxidative degradation. *Polymers*, 10, 957.

Joo, S., Cho, I.J., Seo, H., Son H.F., Sagong, H.Y., Shin, T.J., Choi, S.Y., Lee, S.Y. and Kim, K.J. (2018) Structural insight into the molecular mechanism of poly(ethylene terephthalate) degradation. *Nature Communications*, 9, 382.

Joo, S.H., Liang, Y., Kim, M., Byun, J. and Choi, H. (2021) Microplastics with adsorbed contaminants: mechanisms and treatment. *Environmental Challenges*, 3, 100042.

Jörnvall, H., Persson, B. and Jeffery, J. (1987) Characteristics of alcohol/polyol dehydrogenase. *European Journal of Biochemistry*, 167, 195-201.

Jukes, T.H. and Cantor, C.R. (1969) Evolution of Protein Molecules, In: *Mammalian Protein Metabolism*, Vol. III, Munro, H.N. (Ed.) Academic Press, New York, pp. 21–131.

Kalia, V.C., Patel, S.K.S., Shanmugam, R. and Lee, J.-K. (2021) Polyhydroxyalkanoates: trends and advances toward biotechnological applications. *Bioresource Technology*, 326, 124737.

Kamtsikakis, A., Baales, J., Zeisler-Diehl. V.V., Vanhecke, D., Zoppe, J.O., Schreiber, L. and Weder, C. (2021) Asymmetric water transport in dense leaf cuticles and cuticle-inspired compositionally graded membranes. *Nature Communication*, 12, 1267.

Karich, A., Ullrich, R., Scheibner, K. and Hofrichter, M. (2017) Fungal unspecific peroxygenases oxidize the majority of organic EPA priority pollutants. *Frontiers in Microbiology*, 8, 1463.

Karimi-Avargani, M., Bazooyar, F., Biria, D., Zamani, A. and Skrifvars, M. (2020) The special effect of the *Aspergillus flavus* and its enzymes on biological deterioration of polylactic acid (PLA) and PLA-jute composite. *Polymer Degradation and Stability*, 179, 109295.

Kedzierski, M., Frère, D., Maguer, G.L. and Bruzaud, S. (2020) Why is there plastic packaging in the natural environment? Understanding the roots of our individual plastic waste management behaviours. *Science of the Total Environment*, 740, 139985.

Kersten, P. and Cullen, D. (2007) Extracellular oxidative systems of the lignin-degrading Basidiomycete *Phanerochaete chrysosporium*. *Fungal Genetics and Biology*, 44, 77-87.

Khanal, B.P. and Knoche, M. (2017) Mechanical properties of cuticles and their primary determinants. *Journal of Experimental Botany*, 68, 5351-5367.

Kik, K., Bukowska, B. and Sicińska, P. (2020) Polystyrene nanoparticles: sources, occurrence in the environment, distribution in tissues, accumulation and toxicity to various organisms. *Environmental Pollution*, 262, 114297.

Kim, H.-W., Jo, J.H., Kim, Y.-B., Le, T.-K., Cho, C.-W., Yun, C.-H., Chi, W.S. and Yeom, S.-J. (2021) Biodegradation of polystyrene by bacteria from the soil in common environments. *Journal of Hazardous Materials*, 416, 126239.

Kim, K.S., Park, S. H. and Jenks, M. A. (2007) Changes in leaf cuticular waxes of sesame (*Sesamum indicum* L.) plants exposed to water deficit. *Journal of Plant Physiology*, 164, 1134-1143.

Kirk, W.W., Wharton, P.S., Schafer, R.L., Tumbalam, P., Poindexter, S., Guza, C., Fogg, R., Schlatter, T., Stewart, J., Hubbell, L. and Ruppal, D. (2008) Optimizing fungicide timing for the control of *Rhizoctonia* root and crown root of sugar beet using soil temperature and plant growth stages. *Plant Disease*, 92, 1091-1098.

Kiss, N., Homa, M., Manikandan, P., Mythili, A., Krizsán, K., Revathi, R., Varga, M., Papp, T., Vágvölgyi, C., Kredics, L. and Kocsubé. (2019) New species of the genus *Curvularia: C. tamilnaduensis* and *C. coimbatorensis* from Fungal keratitis cases in South India. *Pathogens*, 20, 9.

Klisińska-Kopacz, A., Łydżba-Kopczyńska, B., Czarnecka, M., Koźlecki, T., del Hoyo-Melèndez, J.M., Mendys-Frodyma, A., Kłosowska-Klechowska, A., Obarzanowski, M. and Frączek, P. (2018) Raman spectroscopy as a powerful technique for the identification of polymers used in cast sculptures from museum collections. *Journal of Raman Spectroscopy*, 50, 1-9.

Koch, K. and Barthlott, W. (2006a) Plant epicuticular waxes: chemistry, form, self-assembly and function. *Natural Product Communications*, 1,1067-1072.

Koch, K., Barthlott, W., Koch, S., Hommes, A., Wandelt, K., Mamdouh, W., De-Feyter, S. and Broekmann, P. (2006b) Structural analysis of wheat max (*Triticum aestivum*, c.v 'Naturastar' L.) from the molecular level to three dimensional crystals. *Planta*, 223, 258-270.

Koch, K. and Ensikat, H.-J. (2008) The hydrophobic coating of plant surfaces: epicuticular wax crystals and their morphologies, crystallinity and molecular self-assembly. *Micron*, 39, 759-772.

Kowalsman, N. and Eisenstein, M. (2007) Inherent limitations in protein-protein docking proedures. *Bioinformatics*, 23, 421-426.

Kozakov, D., Beglov, D., Bohnuud, T., Mottarella, S., Xia, B., Hall, D.R. and Vajda, S. (2013) How good is automated protein docking? *Proteins: Structure, Function and Bioinformatics*, 81, 2159-2166.

Kozakov, D., Hall, D.R., Xia, B., Porter, K.A., Padhorny, D., Yueh, C., Beglov, D. and Vajda, S. (2017) The ClusPro web server for protein-protein docking. *Nature Protocols*, 12, 255-278.

Krueger, M.C., Hofmann, U., Moeder, M. and Schlosser, D. (2015) Potential of wood-rotting fungi to attack polystyrene sulfonate and its depolymerization by *Gloeophyllum trabeum* via hydroquinone-driven fenton chemistry. *PLoS ONE*, 10, e0131773.

Krueger, M.C., Seiwert, B., Prager, A., Zhang, S., Abel, B., Harms, H. and Schlosser, D. (2017) Degradation of polystyrene and selected analogues by biological Fenton chemistry approaches: opportunities and limitations. *Chemosphere*, 173, 520-528.

Kumamoto, C.A. (2008) Molecular mechanisms of mechanosensing and their roles in fungal contact. *Nature Reviews Microbiology*, 6, 667-673.

Kumar, A. and Chandra, R. (2020) Ligninolytic enzymes and its mechanisms for degradation of lignocellulosic waste in environment. *Heliyon*, 6, e03170.

Kyte, J. and Doolittle, R.F. (1982) A simple method for displaying the hydropathic character of a protein. *Journal of Molecular Biology*, 157, 105-132.

Laemmli, U.K. (1970) Cleavage of structural proteins during the assembly of the head of bacteriophage T4. *Nature*, 227, 680-685.

Landraud, P., Chuzeville, S., Billon-Grande, G., Poussereau, N. and Bruel, C. (2013) Adaptation to pH and role of PacC in the rice blast fungus *Magnaporthe oryzae*. *PLoS ONE* 8, e69236.

Laskowski, R.A., MacArthur, M.W., Moss, D.S. and Thornton, J.M. (1993) PROCHECK: a program to check the stereochemical quality of protein structures. *Journal of Applied Crystallography*, 26, 283-291.

Laskowski, R.A. and Swindells, M.B. (2011) LigPlot+: multiple ligand-protein interaction diagrams for drug discovery. *Journal of Chemical Information and Modeling*, 51, 2778-2786.

Lee, B.-H., Kapoor, A., Zhu, J. and Zhu, J.-K. (2006) STABILIZED1, a stress-upregulated nuclear protein, is required for pre-mRNA splicing, mRNA turnover, and stress tolerance in *Arabidopsis*. *The Plant Cell*, 18, 1736-1749.

Leger, R.J.S., Joshi, L. and Roberts, D. (1998) Ambient pH is a major determinant in the expression of cuticle-degrading enzymes and hydrophobin by *Metarhizium anisophilae*. *Applied Microbiology and Biotechnology*, 64, 709-713.

Lebreton, L. and Andrady, A (2019) Future scenarios of global plastic waste generation and disposal. *Palgrave Communications*, 5, 6.

Li, S., Deng, Y., Lian, S., Dai, C., Ma, Q. and Qu, Y. (2022) Succession of diversity, functions, and interactions of the fungal community in activated sludge under aromatic hydrocarbon stress. *Environmental Research*, 204, 112143.

Li, Y., Wadsö, L. and Larsson, L. (2009) Impact of temperature on growth and metabolic efficiency of *Penicillium roqueforti*-correlation between produced heat, ergosterol content and biomass. *Journal of Applied Microbiology*, 106, 1494-1501.

Li, Q., Liu, J. and Gadd, G.M. (2020) Fungal bioremediation of soil co-contaminated with petroleum hydrocarbons and toxic metals. *Applied Microbiology and Biotechnology*, 104, 8999-9008.

Liang, Y., Ran, S.-F., Bhat, J., Hyde, K.D., Wang, Y. and Zhao, D.G. (2018) *Curvularia microspore* sp. nov. associated with leaf diseases of *Hippeastrum striatum* in China. *Mycokeys*, 29, 49-61.

Lienemann, M., Gandier, J.A., Joensuu, J.J., Iwanaga, A., Takatsuji, Y., Haruyama, T., Master, E., Tenkanen, M. and Linder, M.B. (2013) Structure-function relationships in hydrophobins:

probing the role of charges side chains. *Applied Environmental Microbiology*, 79, 5533-5538.

Liers, C., Arnstadt, T., Ullrich, R. and Hofrichter, M. (2011) Patterns of lignin degradation and oxidative enzyme secretion by different wood- and litter- colonizing basidiomycetes and ascomycetes grown on beech-wood. *FEMS Microbiology Reviews*, 78, 91-102.

Linder, M.B., Szilvay, G.R., Nakari-Setälä, T. and Penttilä, M.E. (2005) Hydrophobins: the protein-amphiphiles of filamentous fungi. *FEMS Microbiology Reviews*, 29, 877-896.

Liu, B., He, L., Wang, L., Li, T.,Li, C., Liu, H., Luo, Y. And Bao, R. (2018) Protein crystallography and site-directed mutagenesis analysis of the poly(ethylene terephthalate) hydrolase PETase from *Ideonella sakaiensis*. *ChemBioChem*, 19, 1471-1475.

Liu, M., Zhang, T., Long, L., Zhang, R. and Ding, S. (2019) Efficient enzymatic degradation of poly(ε-caprolactone) by an engineered bifunctional lipase-cutinase. *Polymer Degradation and Stability*, 160, 120-125.

Liu, S.-H., Zeng, G.-M., Niu, Q.-Y., Liu, Y., Zhou, L., Jiang, L.-H., Tan, X., Xu, P., Zhang, C. and Cheng, M. (2017) Bioremediation mechanisms of combined pollution of PAHs and heavy metals by bacteria and fungi: a mini review. *Bioresource Technology*, 224, 25-33.

Liu, X., Pan, X., Chen, D., Yin, C., Peng, J., Shi, W., Qi, L., Wang, R., Zhao, W., Zhang, Z., Yang, J. and Peng, Y.-L. (2021) Pep-19 associated splicing factor Cwf15 regulates fungal virulence and development in the rice blast fungus. *Environmental Microbiology*, 23, 5901-5916.

Luangsa-Ard, J., Houbraken, J., van Doorn, T., Hong, S.-B., Borman, A.M., Hywel-Jones, N.L. and Samson, R.A. (2011) Purpureocillium, a new genus for the medically important *Paecilomyces lilacinus*. *FEMS Microbiology Letters*, 321, 141-149.

Lu, X. and Jiang, B. (1991) Glass transition temperature and molecular parameters of polymer. *Polymer*, 32, 471-478.

Lu, X., Zhang, J., Brown, B., Li, R., Rodríguez-Romero, J., Berasategui, A., Liu, B., Xu, M., Luo, D., Pan, Z., Baerosn, S.R., Gershenzon, J., Li, Z., Sesma, A., Yang, B. and Peters, R.J. (2018) Inferring roles in defense from metabolic allocation of rice diterpenoids. *Plant Cell*, 30, 1119-1131.

Lux, A., Morita, S., Abe, J. And Ito, K. (2005) An improved method for cleaning and staining free-hand sections and whole-mount samples. *Annals of Botany*, 96, 989-996.

Ma, Y., Yao, M., Li, B., Ding, M., He, B., Chen, S., Zhou, X. and Yuan, Y. (2018) Enhanced poly(ethylene terephthalate) hydrolase activity by protein engineering. *Engineering*, 4, 888-893.

Madrid, H., da Cunha, K.C., Gene, J., Dijksterhuis, J., Cano, J., Sutton, D.A., Guarro, J. and Crous, P.W. (2014) Novel *Curvularia* species from clinical specimens. *Persoonia*, 33, 48-60.

Manteau, S., Abouna, S., Lambert, B. and Legendre, L. (2003) Differential regulation by ambient pH of putative virulence factor secretion by the phytopathogenic fungus *Botrytis cinerea*. *FEMS Microbiology*, 43, 359-366.

Mariano, S., Tacconi, S., Fidaleo, M., Rossi, M. and Dini, L. (2021) Micro and nanoplastics identification: classic methods and innovative detection techniques. *Frontiers in Toxicology*, 3, 636640.

Marichevlam, M.K., Jawaid, M. and Asim, M. (2019) Corn and rice starch-based bio-plastics as alternative packaging materials. *Fibers*, 7, 32.

Marin-Felix, Y., Senwanna, C., Cheewangkoon, R. and Crous, P.W. (2017) New species and records of *Bipolaris* and *Curvularia* from Thailand. *Mycosphere*, 8, 1555-1573.

Marin-Felix, Y., Groenewald, J.Z., Cai, L., Chen, Q., Marincowitz, S., Barnes, I., Bensch, K., Braun, U., Camporesi, E., Damm, U. et al. (2017) Genera of phytopathogenic fungi: GOPHY1. *Studies in Mycology*, 86, 99-216.

Marin-Felix, Y., Hernández-Restrepo, M. and Crous, P.W. (2020) Multi-locus phylogeny of the genus *Curvularia* and description of ten new species. *Mycological Progress*, 19, 59-588.

Marino, S.M. and Gladyshev, V.N. (2010) Cysteine function governs its conservation and degeneration and restricts its utilization on protein surfaces. *Journal of Molecular Biology*, 404, 902-916.

Martens, P. (1933) Recherches sur la cuticule. III. Structure, origine at signification du relief cuticulaire. *Protoplasma*, 20, 483-515.

Massafra, V., Milona, A., Vos, H.R., Burgering, B.M.T. and van Mil, S.W.C. (2017) Quantitative liver proteomics identifies FGF19 targets that couple metabolism and proliferation. *PLoS One*, 12, e0171185.

Maurya, M.R., Chandrakar, A.K. and Chand, S. (2007) Oxidation of phenol, styrene and methyl phenyl sulfide with H_2O_2 catalysed dioxovanadium (V) and copper (II) complexes of 2-aminomethylbenzimidazole-based ligand encapsulated in zeolite -Y. *Journal of Molecular Catalysis A: Chemical*, 263, 227-237.

Meeker, J.D., Sathyanarayana, S. and Swan, S.H. (2009) Pthalates and other additives in plastics: human exposure and associated health outcomes. *Philosophical Transactions of the Royal Society, B: Biological Sciences*, 364, 2097-2113.

Mehta, T., Meena, M. and Nagda, A. (2022) Bioactive compounds of *Curvularia* species as a source of various biological activities and biotechnological applications. *Frontiers in Microbiology*, 13, 1069095.

Mei, W., Chen, G., Bao, J., Song, M., Li, Y. And Luo, C. (2020) Interactions between MPs and organic compounds in aquatic environments: a mini review. *Science of the Total Environment*, 736, 139472.

Meijner, M., Houbraken, J.A.M.P., Dalhujisen, S., Samson, R.A. and de Vries, R.P. (2011) Growth and hydrolase profiles can be used as a characteristics to distinguish *Aspergillus niger* and other black aspergilli. *Studies in Mycology*, 69, 19-30.

Messerschmidt, A. and Huber, R. (1990) The blue oxidases, ascorbate oxidase, laccase and ceruloplasmin modelling and structural relationships. *European Journal of Biochemistry*, 187, 341-352.

Meyer-Cifuentes, I.E., Werner, J., Jehmlich, N., Will, S.E., Neumann-Schaal, M. and Öztürk, B. (2020) Synergistic biodegradation of aromatic-aliphatic copolyester plastic by a marine microbial consortium. *Nature Communications*, 11, 5790.

Meyer, E.E., Rosenberg, K.J. and Israelachvili, J. (2006) Recent progress in understanding hydrophobic interactions. *Proceedings of the National Academy of Sciences of the United States of America*, 103, 15739-15746.

Meyer, M. (1937) Die submikroskopische struktur der kutinislerten zellmembranen. *Protoplasma*, 29, 552-586.

Mihreteab, M., Stubblefield, B.A. and Gilbert, E.S. (2019) Microbial bioconversion of thermally depolymerized polypropylene by *Yarrowia lipolytica* for fatty acid production. *Applied Microbiology and Biochemistry*, 103, 7729-7740.

Mohan, A.J., Sekhar, V.C., Bhaskar, T. and Nampoothiri, K.M. (2016) Microbial assisted high impact polystyrene (HIPS) degradation. *Bioresource Technology*, 213, 204-207.

Mohanan, N., Montazer, Z., Sharma, P.K. and Levin, D.B. (2020) Microbial and enzymatic degradation of synthetic plastics. *Frontiers in Microbiology*, 11, 580709.

Morris, G.M., Huey, R., Lindstrom, W., Sanner, M.F., Belew, R.K., Goodsell, D.S. and Olson, A.J. (2009) AutoDock 4 and AutoDockTools4: automated docking with selective receptor flexibility. *Journal of Computational Chemistry*, 16, 2785-2791.

Morrison, E., Kantz, A., Gassner, G.T. and Sazinsky, M.H. (2013) Structure and mechanism of styrene monooxygenase reductase: new insight into the FAD-transfer reaction. *Biochemistry*, 52, 6063-6075.

Motta, O., Proto, A., De carlo, F., De caro, F., Santoro, E., Brunetti, L. and Capunzo, M. (2009) Utilization of chemically oxidized polystyrene as co-substrate by filamentous fungi. *International Journal of Hygiene and Environmental Health*, 212, 61-66.

Mukherjee, S., Chaudhuri, U.R. and Kunda, P.P. (2017) Biodegradation of polyethylene via complete solubilization by the action of *Pseudomonas fluorescens*, biosurfactant produced by *Bacillus licheniformis* and anionic surfactant. *Journal of Chemical Technology & Biotechnology*, 93, 1300-1311.

Murphy, K.M. and Zerbe, P. (2020) Specialized diterpenoid metabolism in monocot crops: biosynthesis and chemical diversity. *Phytochemistry*, 172, 112289.

Myeling, N.V. and Eilenberg, J. (2006) Isolation and characterization of *Beauveria bassiana* isolates from phylloplanes of hedgerow vegetation. *Mycological Research*, 110, 188-195.

Nawrath, C. (2006) Unraveling the complex network of cuticular structure and function. *Current Opinion in Plant Biology*, 9, 281-287.

Naranjo-Ortiz, M.A. and Gabaldón, T. (2019) Fungal evolution: major ecological adaptations and evolutionary transitions. *Biological Reviews of the Cambridge Philosophical Society*, 94, 1443-1476.

Nava, V., Frezzotti, M.L. and Leoni, B. (2021) Raman spectroscopy for the analysis of microplastics in aquatic systems. *Applied Spectroscopy*, 75, 1341-1357.

Nishimura, H., Kamiya, A., Nagata, T., Katahira, M., Watanabe, T. (2018) Direct evidence of α ether linkage between lignin and carbohydrates in wood cell walls. *Scientific Reports*, 8, 6538.

Niu, L., Zhang, H., Wu, Z., Wang, Y., Liu, H., Wu, X. and Wang, W. (2018) Modified TCA/acetone precipitation of plant proteins for proteomics analysis. *PLoS ONE*, 14, e0211612.

Numoto, N., Kamiya, N., Bekker, G-J., Yamagami, Y., Inaba, S., Ishii, K., Uchiyama, S., Kawai, F., Ito, N. and Oda, M. (2018) Structural dynamics of the PET-degrading cutinase-like enzyme from *Sachharomonospora viridis* AHK190 in substrate-bound states elucidates Ca^{2+}-driven catalytic cycle. *Biochemistry*, 57, 5289-5300.

Nzila, A., Ramirez, C.O., Musa, M.M., Sankara, S., Basheer, C. and Li, Q.X. (2018) Pyrene biodegradation and proteomics analysis in *Achromobacter xylosoxidans*, PY4 strain. *International Biodeterioration & Biodegradation*, 130, 40-47.

O'Boyle, N.M., Banck, M., James, C.A., Morley, Vandermeersch, T. and Hutchison, G.R. (2011) Open Babel: An open chemical toolbox. *Journal of Cheminformatics*, 3, 33.

Obande, W., Mamalis, D., Ray, D., Yang, L. and Brádaigh, C.M.Ó. (2019) Mechanical and thermomechanical characterization of vacuum-infused thermoplastic-and thermoset-based composites. *Materials & Design*, 175, 107828.

Oelschlägel, M., Zimmerling, J. and Tischler, D. (2018) A review: the styrene metabolizing cascade of side-chain oxygenation as biotechnological basis to gain various valuable compounds. *Frontiers in Microbiology*, 9, 490.

Ohtaki, S., Maeda, H., Takahashi, T., Yamagata, Y., Hasegawa, F., Gomi, K., Nakajima, T. and Abe, K. (2006) Novel hydrophobic surface binding protein, HsbA, produced by *Aspergillus oryzae*. *Applied and Environmental Microbiology*, 72, 2407-2413.

Olicón-Hernández, D.R., González-López, J. and Aranda, E. (2017) Overview on the biochemical potential of filamentous fungi to degrade pharmaceutical compounds. *Frontiers in Microbiology*, 8, 1792.

Osman, M., Satti, S.M., Luqman, A., Hasan, F., Shah, Z. and Shah, A.A. (2018) Degradation of polyester polyurethane by *Aspergillus* sp. strain S45 isolated from soil. *Journal of Polymers and the Environment*, 26, 301-310.

Othman, A.R., Ismail, N.S., Abdullah, S.R.S., Hasan, H.A., Kurniawan, S.B., Sharuddin, S.S.N. and Ismail, N.I. (2022) Potential of indigenous biosurfactant-producing fungi from real crude oil sludge in total petroleum hydrocarbon degradation and its future research prospects. *Journal of Environmental Chemical Engineering*, 10, 107621.

Pareek, V., Bhargava, A. and Panwar, J. (2020) Biomimetic approach for multifarious synthesis of nanoparticles using metal tolerant fungi: a mechanistic perspective. *Materials Science & Engineering B*, 262, 114771.

Patel, S.S. and Walt, D.R. (1987) Substrate specificity of acetyl coenzyme A synthetase. *Journal of Biological Chemistry*, 262, 7132-7134.

Pathan, A.K., Bond, J. and Gaskin, R.E. (2008) Sample preparation for scanning electron microscopy of plant tissues-horses for courses. *Micron*, 39, 1049-1061.

Patrauchan, M.A., Florizone, C., Eapen, C., Gómez-Gil, L., Sethuraman, B., Fukuda, M., Davies, J., Mohn, W.W. and Eltis, L.D. (2008) Roles of ring-hydroxylating dioxygenases in styrene and benzene catabolism in *Rhodococcus jostii* RHA1. *Journal of Bacteriology*, 190, 37-47.

Pang, Z., Chong, J., Zhou, G., Morais, D.A.L., Chang, L., Barrette, M., Gauthier, C., Jacques, P.-È., Li, S. and Xia, J. (2021) MetaboAnalyst 5.0: narrowing the gap between raw spectra and functional insights. *Nucleic Acids Research*, 49, W388-W396.

Peel, M.C., Finlayson, B.L. and McMahon, T.A. (2007) Updated world map of Köppen-Geiger climate classification. *Hydrology and Earth System Sciences*, 11, 1633-1644.

Peiponen, K. E., Räty, J., Ishaq, U., Pélisset, S. and Ali, R. (2019) Outlook on optical identification of micro- and nanoplastics in aquatic environments. *Chemosphere*, 214, 424-429.

Peng, T., Luo, A., Kan, J., Liang, L., Huang, T. and Hu, Z. (2018) Identification of a ring-hydroxylating dioxygenases capable of anthracene and benzo[a]pyrene by rig-hydroxylating oxidation from *Rhodococcus* sp. P14. *Journal of Molecular Microbiology and Biotechnology*, 28, 183-189.

Peterson, S.W. (2008) Phylogenetic analysis of *Aspergillus* species using DNA sequences from four loci. *Mycologia*, 100, 205-226.

Peterson, S.W. and Horn, B.W. (2009) *Penicillium parvulum* and *Penicillium georgiense*, sp. nov., isolated from conidial heads of *Aspergillus* species. *Mycologia*, 101, 71-83.

Pettersen, E.F., Goddard, T.D., Huang, C.C., Couch, G.S., Greenblatt, D.M., Meng, E.C. and Ferrin, T.E. (2004) UCSF Chimera--a visualization system for exploratory, research and analysis. *Journal of Computational Chemistry*, 25, 1605-1612.

Pham., C.L.L., de Francisco, B.R., Valsecchi, I., Dazzoni, R., Pillé, A., Lo, V., Ball, S.R., Cappai, R., Wein, F., Kwan, A.H., Guijarro, J.I. and Sunde, M. (2018) Probing structural changes

during self-assembly of surface-active hydrophobin proteins that form functional amyloids in fungi. *Journal of Molecular Biology*, 430, 3784-3801.

Pilevar, Z., Bahrami, A., Beikzadeh, S., Hosseini, H. and Jafari, S.M. (2019) Migration of styrene monomers from polystyrene packaging materials into foods: characterization and safety evaluation. *Trends in Food Science & Technology*, 91, 248-261.

Plastics Europe. (2020). Plastics-The Facts 2020: An Analysis of European Plastics Production, Demand and Waste Data 2020. Brussels: Plastics Europe.

Pointing, S.B. (2001) Feasibility of bioremediation by white-rot fungi. *Applied Microbiology and Microbiology*, 57, 20-33.

Poole, L.B. (2015) The basics of thiols and cysteines in redox biology and chemistry. *Free Radical Biology and Medicine*, 80, 148-157.

Pryor, B.M. and Bigleow, D.M. (2003) Molecular characterization of *Embellisia* and *Nimbya* species and their relationship to *Alternaria*, *Ulocladium* and *Stemphylium*. *Mycologia*, 95, 1141-1154.

Przemienniecki, S.W., Kosewska, A., Ciesielski, S. and Kosewska, O. (2020) Changes in the gut microbiome and enzymatic profile of *Tenebrio molitor* larvae biodegrading cellulose, polyethylene and polystyrene waste. *Environmental Pollution*, 256, 113265.

Puspitasari, N., Tsai, S.L. and Lee, C-K. (2021) Fungal hydrophobin RolA enhanced PETase hydrolysis of polyethylene terephthalate. *Applied Biochemistry & Biotechnology*, 193, 1284-1295.

Raj, T., Chandrasekhar, K., Kumar, A.N. and Kim, S.-H. (2022) Lignocellulosic biomass as renewable feedstock for biodegradable and recyclable plastics production: a sustainable approach. *Renewable and Sustainable Energy Reviews*, 158, 112130.

Rakeman, J.L., Bui, U., Lafe, K., Chen, Y.C., Honeycutt, R.J. and Cookson, B.T. (2005) Multilocus DNA sequence comparisons rapidly identify pathogenic molds. *Journal of Clinical Microbiology*, 43, 3324-3333.

Rasmussen, H.T. and Huang, K. (2012) Chromatographic Separations and Analysis: Chromatographic Separations and Analysis of Enantiomers, In: Carreira, E.M. and Yamamoto, H. (Eds.) *Comprehensive Chirality* Eds., Elsevier, pp. 96-114.

Rehner, S.A. and Buckley, E. (2005) A *Beauveria* phylogeny inferred from nuclear ITS and EF1-α sequences: evidence for cryptic diversification and links to *Cordyceps* teleomorphs. Mycologia, 97, 84-98.

Reiss, R., Ihssen, J., Richter, M., Eichhorn, E., Schilling, B. and Thöny-Meyer, L. (2013) Laccase versus laccase-like multicopper oxidase: a comparative study of similar enzymes with diverse substrate spectra. *PLoS One*, 8, e65633.

Riederer, M. and Müller, C. (2006) Biology of the Plant Cuticle. Blackwell, Oxford, pp. 1-11.

Reisser, J., Slat, B., Noble, K., du Pessis, K., Epp, M., Proeitti, M., de Sonneville, J., Becker, T. and Pattiaratchi, C. (2015) The vertical distribution of buoyant plastic sea: an observational study in the North Atlantic Gyre. *Biogeosciences*, 12, 1249-1256.

Rhodes, C.J. (2018) Plastic pollution and potential solutions. *Science Progress*, 101, 207-260.

Riglet, L., Gatti, S. and Moyroud, E. (2021) Sculpting the surface: structural patterning of plant epidermis. *iScience*, 24, 103346.

Rogowska, A. and Szakiel, A. (2020) The role of sterols in plant response to abiotic stress. *Phytochemistry Reviews*, 19, 1525-1538.

Roma, L.P. and Santos, D.Y.A.C. (2021) A comprehensive review of the chemical composition and epicuticular wax morphology of the cuticle in Sapindales. *Brazilian Journal of Botany*, 45, 5-14.

Roy, P.K., Titus, S., Surekha, P., Tulsi, E., Deshmukh, C and Rajagopal, C. (2008) Degradation of abiotically aged LDPE films containing pro-oxidant by bacterial consortium. *Polymer Degradation and Stability*, 93, 1917-1922.

Ru, J., Huo, Y. and Yang, Y. (2020) Microbial degradation and valorization of plastic wastes. *Frontiers in Microbiology*, 11, 442.

Samson, R.A., Visagie, C.M., Houbraken, J., Hong, S.-B., Hubka, V., Klaassen, C.H.W., Perrone, G., Seifert, K.A., Susca, A., Tanney, J.B., Varga, J., Kocsubé, S., Szigeti, G., Yaguchi, T. and Frisvad, J.C. (2014) Phylogeny, identification and nomenclature of genus Aspergillus. *Studies in Mycology*, 78, 141-173.

Sánchez, C. (2020) Fungal potential for the degradation of petroleum-based polymers: an overview of macro- and microplastics biodegradation. *Biotechnology Advances*, 40, 107501.

Sandhibigraha, S., Mandal, S., Awasthi, M., Bandyopadhyay, T.K. and Bhunia, B. (2020) Optimization of various process parameters for biodegradation of 4-chlorophenol using Taguchi methodology. *Biocatalysis and Agricultural Biotechnology*, 24, 101568.

Sandoval-Denis, M., Sutton, D.A., Gene, J., Cano-Lira, J.F., Martin, A., Wiederhold, N.P. and Guarro, J. (2015) *Cladosporium* species recovered from clinical samples in the United States. *Journal of Clinical Microbiology*, 53, 1-35.

Sangale, M.K., Shahnawaz, M. and Ade, A.B. (2019) Gas chromatography-mass spectra analysis and deleterious potential of fungal based polythene-degradation products. *Scientific Reports*, 9, 1599.

Santacruz-Juárez, E., Buendia-Corona, R.E., Ramírez, R.E. and Sánchez, C. (2021) Fungal enzymes for the degradation of polyethylene: molecular docking simulation and biodegradation pathway proposal. *Journal of Hazardous Materials*, 411, 125118.

Sargent, C. (1976) The occurrence of a secondary cuticle in *Libertia elegans* (Iridaceae). *Annals of Botany*, 40, 355-359.

Schoch, C.L., Robbertse, B., Robert, V., Vu, D., Cardinali, G., Irinyi, L., Meyer, W., Nilsson, R.H., Hughes, K., Miller, A.N. et al. (2014) Finding needles in haystacks: linking scientific names, reference specimens and molecular data for fungi. *Database (Oxford)*, 2014, bau061.

Schreiber, L. and Schönherr, J. (2009) Water and solute permeability of plant cuticles: measurement and data analysis. Berlin Germany: Springer Verlag.

Schubert, K., Greslebin, A., Groenewald, J.Z. and Crous, P.W. (2009) New foliicolous species of *Cladosporium* from South America. *Persoonia*, 22, 111-122.

Schmieder, S.S., Stanley, C.E., Rzepiela, A., van Swaay, D., Sabotiĉ, J., Nørrelykke, S.F., deMello, A.J., Aebi, M. and Künzer, M. (2019) Bidirectional propagation of signals and nutrients in fungal networks via specialized hyphae. *Current Biology*, 29, 217-228.

Schreuder, H.A., van der Laan, J.M., Swarte, M.B., Kalk, K.H., Hol, W.G. and Drenth, J. (1992) Crystal structure of the reduced form of p-hydroxybenzoate hydroxylase refined at 2.3 A resolution. *Proteins*, 14, 178-90.

Seay, J., Chen, W. and Ternes, M.E. (2020) Waste plastic: challenges and opportunities for the chemical industry. *Chemical Engineering Progress*, 116, 22-29.

Sellami, K., Couvert, A., Nasrallah, N., Maachi, R., Abouseoud, M. and Amrane, A. (2022) Peroxidase enzymes as green catalysts for bioremediation and biotechnological applications: a review. *Science of the Total Environment*, 806, 150500.

Seo, J.S., Keum, Y.S. and Li, Q.X. (2009) Bacterial degradation of aromatic compounds. *International Journal of Environmental Research and Public Health*, 6, 278-309.

Shah, V. and Nerud, F. (2002) Lignin degrading system of white-rot fungi and its exploitation for dye decolorization. *Canadian Journal of Microbiology*, 48, 857-880.

Shahnawaz, M., Sangale, M.K. and Ade, A.B. (2016) Bacteria-based polythene degradation products: GC-MS analysis and toxicity testing. *Environmental Science and Pollution Research*, 23, 10733-10741.

Sharma, P., Madhyastha, H., Madhyastha, R., Nakajima, Y., Maruyama, M., Verma, K.S., Verma, S., Prasad, J., Kothari, S.L. and Gour, V.S. (2019) An appraisal of cuticular wax of *Calotropis procera* (Ait.) R. Br.: Extraction, chemical composition, biosafety and application *Journal of Hazardous Materials*, 368, 397-403.

Sharma, S. and Malaviya, P. (2016) Bioremediation of tannery wastewater by chromium resistant novel fungal consortium. *Ecological Engineering*, 91, 419-425.

Sharma, R., Prakash, O., Sonawane, M.S., Nimonkar, Y., Golellu, P.B. and Sharma, R. (2016) Diversity and distribution of phenol oxidase producing fungi from Salt Lake and description of *Curvularia lonarensis* sp. nov. *Frontiers in Microbiology*, 7, 1847.

Shepherd, T., Robertson, G.W., Griffiths, D.W. and Birch, A.N.E. (1999) Epicuticular wax composition in relation to aphid infestation and resistance in red raspberry (*Rubus idaeus* L.). *Phytochemistry*, 52, 1239-1254.

Sherwood, M.H., Greenway, A.R. and Griffiths, D.C. (1981) responses of *Myzus persica* (Sulzer) (Hemiptera: Aphididae) to plants treated with fatty acids. *Bulletin of Entomological Research*, 71, 133-136.

Shevchenko, A., Wilm, M., Vorm, O. and Mann, M. (1996) Mass spectrometric sequencing of proteins silver-stained polyacrylamide gels. *Analytical Chemistry*, 68, 850-858.

Shi, K., Su, T. and Wang, Z. (2019) Comparison of poly(butyele succinate)biodegradation by *Fusarium solani* cutinase and *Candida antactica* lipase. Polymer Degradation and Stability, 164, 55-60.

Shi, K., Jing, J., Song, L., Su., T. and Wang, Z. (2020) Enzymatic hydrolysis of polyester: degradation of poly(ε-caprolactone) by *Candida antarctica* lipase and *Fusarium solani* cutinase. International Journal of Biological Macromolecules, 144, 183-189.

Shin, J., Kim, JE., Lee, Y.W. and Son, H. (2018) Fungal cytochrome P450s and the P450 complement (CYPome) of *Fusarium graminearum*. *Toxins*, 10, 112.

Shirke, A.N., White, C., Englaender, J.A., Zwarycz, A., Butterfoss, G.L., Linhardt, R.J. and Gross R.A. (2018) Stabilizing leaf and branch compost cutinase (LCC) with glycosylation: mechanism and effect on PET hydrolysis. *Biochemistry*, 57, 1190-1200.

Shojaeiarani, J., Bajwa, D.S., Rehovsky, C., Bajwa, S.G. and Vahidi, G. (2019) Deterioration in the physico-mechanical and thermal properties of biopolymers due to reprocessing. *Polymer*, 11, 58.

Siddiqui, S.A., Agrawal, S., Brahmbhatt, H. and Rathore, M.S. (2022) Metabolite expression changes in *Kappaphycus alvarezzi* (a red algae) under hypo- and hyper-saline conditions. *Algal Research*, 63, 102650.

Sieber, P., Voigt, K., Kämmer, P., Brunke, S., Schuster, S. and Linde, J. (2018) Comparative study on alternate splicing in human fungal pathogens suggests its involvement during host invasion. *Frontiers in Microbiology*, 9, 2313.

Simonin, A., Palma-Guerrero, J., Fricker, M. and Glass, N.L. (2012) Physiological significance of networks organization in fungi. *Eukaryotic Cell*, 11, 1345-1352.

Singh, B. and Sharma, N. (2008) Mechanistic implications of plastic degradation. *Polymer Degradation and Stability*, 93, 561-584.

Singh, N., Dalal, V., Mahto, J.K. and Kumar, P. (2017) Biodegradation of phthalic acid esters (PAEs) and in silico structural characterization of mono-2-ethylhexyl phthalate (MEHP) hydrolase on the basis of close structural homolog. *Journal of Hazardous Materials*, 338, 11-22.

Singh, Y., Nair, A.M. and Verma, P.K. (2021) Surviving the odds: from perception to survival of fungal phytopathogens under host-generated oxidative burst. *Plant Communications*, 2, 100142.

Singha, S., Gowda, V. and Hedenqvist, M.S. (2021) Plant cuticle-inspired polyesters as promising green and sustainable polymer materials. *ACS Applied Polymer Materials*, 3, 4088-4100.

Sivan, A. (2011) New perspectives in plastic biodegradation. *Current Opinion in Biotechnology*, 22, 422-426.

Sivan, A. and Szanto, M. and Pavlov, V. (2006) Biofilm development of the polyethylene-degrading bacterium *Rhodococcus ruber*. *Applied Microbiology and Biotechnology*, 72, 346-352.

Sjøholm, K.K., Birch, H., Hammershøj, R., Saunders, D.M.V., Dechesne, A., Loibner, A.P. and Mayer, P. (2021) Determining the temperature dependency biodegradation kinetics for 34 hydrocarbons while avoiding chemical and microbial confounding factors. *Environmental Science & Technology*, 55, 11091-11101.

Song, Y, Qui, R., Hu, J., Li, X., Zhang, X., Chen, X., Wu, W.-M. and He, D. (2020) Biodegradation and disintegration of expanded polystyrene by land snails *Achatina fulca*. *Science of the Total Environment*, 746, 141289.

Sridharan, B., Krishnaswamy, V.G., Archana, K.M., Rajagopal, R., Kumar, D.T. and Doss, C.G.P. (2021) Integrated approach on azo dyes degradation using laccase enzyme and Cul nanoparticle. *SN Applied Sciences*, 3, 370.

Srikanth, M., Sandeep, T.S.R.S., Sucharitha, K. and Godi, S. (2022) Biodegradation of plastic polymers by fungi: a brief review. *Bioresources and Bioprocessing*, 9, 42.

Stajich, J.E., Berbee, M.L., Blackwell, M., Hibbett, D.S., James, T.Y., Spatafora, J.W. and Taylor, J.W. (2009) The fungi. *Current Biology*, 19, R840-R845.

Starai, V.J. and Escalante-Semerena, J.C. (2004) Acetyl-coenzyme A synthetase (AMP formimg). *Cellular and Molecular Life Sciences*, 61, 2020-2030.

Story, S. and Brigmon, R.L. (2017) Influence of triethyl phosphate on phosphatase activity in shooting range soil: isolation of a zinc-resistant bacterium with an acid phosphatase. *Ecotoxicology and Environmental Safety*, 137, 165-171.

Sturmberger, L., Wallace, P.W., Glieder, A. and Birner-Gruenberger, R. (2011) Synergism of proteomics and mRNA sequencing for enzyme discovery. *Journal of Biotechnology*, 235, 132-138.

Su, A., Kiokekli, S., Naviwala, M., Shirke, A.N., Pavlidis, I.V. and Gross, R.A. (2020) Cutinases as stereoselective catalysts: specific activity and enantioselectivity of cutinases and lipases for methanol and its analogs. *Enzyme and Microbial Technology*, 133, 109467.

Sunde, M., Kwan, A.H.Y., Templeton, M.D., Beever, R.E. and Mackay, J.P. (2008) Structural analysis of hydrophobins. *Micron*, 39, 773-784.

Sunde, M., Pham, C.L.L. and Kwan, A.H. (2017) Molecular characteristics and biological functions of surface-active and surfactant proteins. *Annual Reviews of Biochemistry*, 86, 585-605.

Sützl, L., Laurent, C., Abrera, A.T., Schütz, G., Ludwig, R., Haltrich, D. (2018) Multliplicity of enzymatic functions in the CAZy AA3 family. *Applied Microbiology and Biotechnology*, 102, 2477-2492.

Sützl, L., Foley, G., Gillam, E.M.J., Bodèn, M. and Haltrich, D. (2019) The GMC superfamily of oxidoreductases revisited: analysis and evolution of fungal GMC oxidoredutases. *Biotechnology of Biofuels and Bioproducts*, 12, 118.

Syberg, K., Khan, F.R., Selck, H., Palmqvist, A., Banta, G.T., Daley, J., Sano, L. and Duhaime, M.B. (2015) MPs: addressing ecological risk through lessons learned. *Environmental Toxicology and Chemistry*, 34, 945-953.

Syranidou, E., Karkanorachaki, K., Amorotti, F., Franchini, M., Repouskou, E., Kaliva, M., Vamvakaki, M., Kolvenbach, B., Fava, F., Corvini, P.X.-F. and Kalogerakis, N. (2017) Biodegradation of weathered polystyrene films in seawater microcosms. *Scientific Reports*, 7, 17991.

Syranidou, E., Karkanorachaki, K., Amorotti, F., Avgeropoulos, A., Kolvenbach, B., Zhou, N.-Y., Fava, F., Corvini, P.F.-X. and and Kalogerakis, N. (2019) Biodegradation of mixture of plastic films by tailored marine consortia. *Journal of Hazardous Materials*, 375, 33-42.

Takahashi, T., Maeda, H., Yoneda, S., Ohtaki, S., Yamagata, Y., Hasegawa, F., Gomi, K., Nakajima, T. and Abe, K. (2005) The fungal hydrophobin RolA recruits polyesterase and laterally moves on hydrophobic surfaces. *Molecular Microbiology*, 57, 1780-1796.

Tamura, K., Stecher, G. and Kumar, S. (2021) MEGA11: Molecular Evolutionary Genetics Analysis Version 11. *Molecular Biology and Evolution*, 38, 3022-3027.

Tan, Y.P., Crous, P.W. and Shivas, R.G. (2018) Cryptic species of *Curvularia* in the culture collection of the Queensland Plant Pathology Herbarium. *MycoKeys*, 35, 1-25.

Tan, Y., Henehan, G.T., Kinsella, G.K. and Ryan, B.J. (2021) An extracellular lipase from *Amycolatopsis mediterannei* is a cutinase with plastic degradation activity. *Computational and Structural Biotechnology Journal*,19, 869-879.

Tatai, L., Moore, T.G., Adhikari, R., Malherbe, F., Jayasekara, R., Griffiths, I. and Gunatillake, P.A. (2017) Thermoplastic biodegradable polyurethanes: the effect of chain extender structure on properties and *in-vitro* degradation. *Biomaterials*, 28, 5407-5417.

ten Brink, H.B., Dekker, H.L., Schoemaker, H.E. and Wever, R. (2000) Oxidation reactions catalyzed by vanadium chloroperoxidase from *Curvularia inaequalis. Journal of Inorganic Biochemistry*, 80, 91-98.

Teng, M., Zhao, X., Wu, F., Wang, C., Wang, C., White, J.C., Zhao, W., Zhou, L., Yang, S. and Tian, S. (2022) Charge-specific adverse effects of polystyrene nanoplastics on zebrafish (*Danio rerio*) development and behaviour. *Environment International*, 163, 107154.

Thakur, S., Verma, A., Sharma, B., Chaudhary, J., Tamulevicius, S. and Thakur, V.K. (2018) Recent developments in recycling of polystyrene based plastics. *Current Opinion in Green and Sustainable Chemistry*, 13, 32-38.

Thompson J.D., Higgins, D.G. and Gibson T.J. (1994) CLUSTAL W: improving the sensitivity of progressive multiple sequence alignment through sequence weighting, position-specific gap penalties and weight matrix choice. *Nucleic Acids Research*, 22, 4673-4680.

Tian, L., Kolvenbach, B., Corvini, N., Wang, S., Tavanaie, N., Wang, L., Ma, Y., Scheu, S., Corvini, P.F.-X. and Ji, R. (2017) Mineralization of 14C-labelled polystyrene plastics by *Penicillium variabile* after ozonation pre-treatment. *New Biotechnology*, 38, 101-105.

Tilton Jr, R.F. and Dewan, J.C. and Petsko, G.A. (1992) Effects of temperature on protein structure and dynamics: x-ray crystallographic studies of the protein ribonuclease-A at nine different temperatures from 98 to 320 K. *Biochemistry*, 31, 2469-2481.

Tischler, D., Eulberg, D., Lakner, S., Kaschabek, S.R., van Berkel W.J.H. and Schlomann, M. (2009) Identification of novel self-sufficient styrene monooxygenase from *Rhodococcus opacus* 1CP. *Journal of Bacteriology*, 191, 4996-5009.

Tiso, T., Winter, B., Wei, R., Hee, J., de Witt, J., Wierckx, N., Quicker, P., Bornscheuer, U.T., Bardow, A., Nogales, J. and Blank, L.M. (2022) The metabolic potential of plastics as biotechnological carbon sources- review and targets for the future. *Metabolic Engineering*, 71, 77-98.

Tkaczuk, K.L., Shumilin, I.A., Chruszcz, M., Evdokimova, E., Savchenko, A. and Minor, W. (2013) Structural and functional insight into the universal stress protein family. *Evolutionary Applications*, 6, 434-449.

Tournier, V., Topham, C.M., Gilles, A., David, B., Folgoas, C., Moya-Leclair, E., Kamionka, E., Desrousseaux, M.L., Texier, H., Gavalda, S., Cot, M., Guémard, E., Dalibey, M., Nomme, J., Cioci, G., Barbe, S., Chateau, M., André, I., Duquesne, S. and Marty, A. (2020) An engineered PET depolymerase to break down and recycle plastic bottles. *Nature*, 580, 216-219.

Trivedi, P., Nguyen, N., Klavins, L., Kviesis, J., Heinonen, E., Remes, J., Jokipii-Lukkari, S., Klavins, M., Karppinen, K., Jaakola, L. and Häggman, H. (2021) Analysis of composition,

morphology, and biosynthesis of cuticular wax in wild type bilberry (*Vaccinium myrtillus* L.) and its glossy mutant. *Food Chemistry*, 354, 129517.

Tsochatzis, E., Berggreen, I.E., Tedeschi, F., Ntrallou, K., Gika, H. and Corredig, M. (2021) Gut microbiome and degradation product fermentation during biodegradation of expanded polystyrene by mealworm larvae under different feeding strategies. *Molecules*, 26, 7568.

Tsochatzis, E., Lopes, J.A., Gika, H. and Theodoridis, G. (2021) Polystyrene biodegradation by *Tenebrio molitor* larvae: identification of generated substances using GC-MS untargeted screening method. *Polymers*, 13, 17.

Tsochatzis, E.D., Berggreen, I.E., Nørgaard, J.V., Theodoridis, G. and Dalsgaard, T.K. (2021) Biodegradation of expanded polystyrene by mealworm larvae under different feeding strategies evaluated by metabolic profiling using GC-TOF-MS. *Chemosphere*, 281, 130840.

Turner, A. (2018) Black plastics: Linear and circular economies, hazardous additives and marine pollution. *Environment International*, 117, 308-318.

Ueda, H., Tabata, J., Seshime, Y., Masaki, K., Sameshima-Yamashita, Y. and Kitamoto, H. (2021) Cutinase-like biodegradable plastic-degrading enzymes from phylloplane yeasts have cutinase activity. *Bioscience, Biotechnology, and Biochemistry*, 85, 1890-1898.

Urbanek, A.K., Mirończuk, A.M., García-Martín, A., Saborido, A., de la Mata, I. and Arroyo, M. (2020) Biochemical properties and biotechnological applications of microbial enzymes involved in the degradation of polyester-type plastics. *Biochimica et Biophysics Acta-Proteins and Proteomics*, 1868, 140315.

Urushiyama, S., Tani, T. and Ohshima, Y. (2019) The *prp1+* gene required for pre-mRNA splicing in *Schizosaccharomyces pombe* encodes a protein that contains TPR motifs and is similar to Prp6p of budding yeast. *Genetics*, 147, 101-115.

Vajda, S., Yueh, C., Beglov, D., Bohnuud, T., Mottarella, S.E., Xia, B., Hall, D.R., Kozakov, D. (2017) New additions to the ClusPro server motivated by CAPRI. *Proteins: Structure, Function and Bioinformatics*, 85, 435-444.

Valenzuela-Lopez, N.M.A., Stchigel, A.M., Cano-Lira, J.F., Guarro, J., Crous, P. and Sutton, D.A. (2017) *Coelomyectous Dothideomycetes* with emphasis on the families *Cucurbitariaceae* and *Didymellaceae*. *Studies in Mycology*, 90, 1-69.

Valette, N., Benoit-Gelber, I., Di Falco, M., Wiebenga, A., de Vries, R.P., Gelhaye, E. and Morel-Rouhier, M. (2017) Secretion of small proteins is specie specific within *Aspergillus* sp. *Microbial Biotechnology*, 10, 323-329.

Valitova, J.N., Sulkarnayeva, A.G. and Minibayeva, F.V. (2016) Plant Sterols: diversity, biosynthesis, and physiological functions. *Biochemistry (Moscow)*, 81, 819-834.

van den Berg, R., Hoefsloot, H.C.J, Westerhuis, J.A., Smilde, A.K. and van der Werf, M. J. (2006) Centering, scaling, and transformations: improving the biological information content of metabolomics data. *BMC Genomics*, 7, 142.

Van Hamme, J.D., Singh, A. and Ward, O.P. (2003) Recent advances in petroleum microbiology. *Microbiology and Molecular Biology Reviews*, 67, 503-549.

Venkatachalam, M., Gèrard, L., Milhau, C., Vinale, F., Dufossè, L. and Fouillaud, M. (2019) Salinity and temperature influence growth and pigment production in the marine-derived fungal strain *Talaromyces albobiverticillius* 30548. *Microorganism*s, 7, 10.

Verma, R., Vinoda, K.S., Papireddy, M. and Gowda, A.N.S. (2016) Toxic pollutants from plastic waste. *Procedia Environmental Sciences*, 35, 701-708.

Vipotnik, Z., Michelin, M. and Tavares, T. (2021) Ligninolytic enzymes production during polycyclic aromatic hydrocarbons degradation: effect of soil pH, soil amendments and fungus co-cultivation. *Biodegradation*, 32, 193-215.

Volke-Sepúlveda, T., Saucedo-Castañedo, G., Gutiérrez-Rojas, M., Manzur, A. and Favela-Torres, E. (2001) Thermally treated low density polyethylene biodegradation by *Penicillium pinophilum* and *Aspergillus niger*. *Journal of Applied Polymer Science*, 83, 305-314.

Vu, D., Groenewald, M., de Vries, M., Gehrmann, T., Stielow, B., Eberhardt, U., Al-Hatmi, A., Groenewald, J. Z., Cardinali, G., Houbraken, J., Boekhout, T., Crous, P.W., Robert, V. and Verkley, G.J.M. (2019) Large-scale generation and analysis of filamentous fungal DNA barcodes boosts coverage for kingdom fungi and reveals thresholds for fungal species and higher taxon delimitation. *Studies in Mycology*, 92, 135-154.

Vylkova S. (2017) Environmental pH modulation by pathogenic fungi as a strategy to conquer the host. *PLoS Pathogens*, 13, e1006149.

Wagner, G.J., Wang, E. and Shepherd, R.W. (2004) New approaches for studying and exploiting an old protuberance, the plant trichome. *Annals of Botany*, 93, 3-11.

Wang, M., Roberts, D.L., Paschke, R., Shea, T.M., Masters, B.S. and Kim, J.J. (1997) Three-dimensional structure of NADPH-cytochrome P450 reductase: prototype for FMN- and FAD-containing enzymes. *Proceeding of the National Academy of Sciences USA*, 94, 8411-8416.

Wang, Z., Xin, X., Shi X. and Zhang, Y. (2020) A polystyrene-degrading Acinetobacter bacterium isolated from the larvae of *Tribolium castaneum*. *Science of the Total Environment*, 726, 138564.

Wang, Y., Mao, H., Lv, Y., Chen, G. and Jiang, Y. (2021) Comparative analysis of total wax content, chemical composition and crystal morphology of cuticular wax in Korla pear under different relative humidity of storage. *Food Chemistry*, 339, 128097.

Warner, G.R. and Flaws, J.A. (2019) Bisphenol A and phthalates: how environmental chemicals are reshaping toxicology. *Toxicological Sciences*, 166, 246-249.

Whittaker, M.M., Kersten, P.J., Cullen, D., Whittaker, J.W. (1999) Identification of catalytic residues in glyoxal oxidase by targeted mutagenesis. *Journal of Biological Chemistry*, 274, 36226-36232.

White, T.J., Bruns, T., Lee, S. and Taylor, J. (1990) Amplification and direct sequencing of fungal ribosomal RNA genes for phylogenetics. In: Innis, M.A., Gelfand, D.H., Sninsky, J.J. and White, T.J. (Eds.) PCR Protocols a guide to methods and applications. Academic Press, San Diego, pp. 315-322.

Worm, B., Lotze, H.K., Jubinville, I., Wilcox, C. and Jambeck, J. (2017) Plastic as a persistent marine pollutant. *Annual Reviews of Environment and Resources*, 42, 1-26.

Wösten, H.A.B. and Scholtmeijer, K. (2015) Applications of hydrophobins: current state and perspectives. *Applied Microbiology and Biotechnology*, 99, 1587-1597.

Wong, S.L., Ngadi, N., Abdullah, T.A.T., Inuwa, I.M. (2015) Current state and future prospects of plastic waste as source of fuel: a review. *Renewable and Sustainable Energy Reviews*, 50, 1167-1180.

Wright, S.L. and Kelly, F.J. (2017) Plastic and human health: a micro issue? *Environmental Science & Technology*, 51, 6634-6647.

Wrzosek, M., Ruszkiewicz-Michalska, M., Sikora, K., Damszel, M. and Sierota, Z. (2017) The plasticity of fungal interactions. *Mycological Progress*, 16, 101-108.

Wu, X., Yin, H., Chen, Y., Li, L., Wang, Y., Hao, P., Cao, P., Qi, K. and Zhang, S. (2017) Chemical composition, crystal morphology and key gene expression of cuticular waxes of Asian pears at harvest and after storage. *Postharvest Biology and Technology*, 132, 71-80.

Wu, X. Yin, H., Shi, Z., Chen, Y., Qi, K., Qiao, X., Wang, G., Cao, P. and Zhang, S. (2018) Chemical composition and crystal morphology of epicuticular wax in mature fruits of 35 Pear (*Pyrus* spp.) cultivars. *Frontiers in Plant Science*, 9, 679.

Xia, J.G. and Wishart, D.S. (2011) Web-based inference of biological patterns, functions and pathways from metabolomic data using MetaboAnalyst. *Nature Protocols*, 6, 743-760.

Xiao, Y., Jiang, X., Liao, Y., Zhao, W., Zhao, P. and Li, M. (2020) Adverse physiological and molecular level effects of polystyrene microplastics on freshwater microalgae. *Chemosphere*, 255, 126914.

Xu, D. and Zhang, Y. (2011) Improving the physical realism and structural accuracy of protein models by a two-step atomic-level energy minimization. *Biophysical Journal*, 101, 2525-2534.

Xu, J and Zhang, Y. (2010) How significant is a protein structure similarity with TM score=0.5? *Bioinformatics*, 26, 889-895.

Xu, X., Xiao, L., Feng, J., Chen, N., Chen, Y., Song, B., Xue, K., Shi, S., Zhou, Y. and jenks, M.A. (2016) Cuticle lipids on heteromorphic leaves of *Populus euphratica* Oliv. growing in riparian habitats differing in available soil moisture. *Physiology Plantarum*, 158, 318-330.

Xu, X., Chen, N., Feng, J., Zhou, M., He, J., Zou, Y., Shi, S., Zhou, Y. and Jenks, M.A. (2020) Comparative analyses of leaf cuticular lipids of two succulent xerophytes of the Ordos

Plateau (Gobi Desert), *Tetraena mongolica* maxim and *Zygophyllum xanthoxylum* (Bunge) Engl. *Environmental and Experimental Botany*, 177, 104129.

Yadav, B.K., Shrestha, S.R. and Hassainzadeh, S.M. (2012) Biodegradation of toluene under seasonal and diurnal fluctuations of soil-water temperature. *Water, Air, & Soil Pollution*, 223, 3597-3588.

Yadav, G. and Meena, M. (2021) Bioprospecting of endophytes in medicinal plants of Thar desert: an attractive resource for biopharmaceuticals. *Biotechnology Reports*, 30, e00629.

Yang, F., Wang, S. and Zhang, Y. (2020) Effects of laser power and substrate on Raman shift of carbon-nanotube papers. *Carbon Trends*, 1, 100009.

Yang, J., Roy A and Zhang, Y. (2013a) Protein-ligand binding site recognition using complementary binding-specific substructure comparison and sequence profile alignment. Bioinformatics, 29, 2588-2595.

Yang, J., Roy A and Zhang, Y. (2013b) BioLiP: A semi-manually curated database for biologically relevant ligand-protein interactions. Nucleic Acids Research, 41, 1096-1103.

Yang, J. and Zhang, Y. (2015) Protein structure and function prediction using I-TASSER. *Current Protocols in Bioinformatics*, 52, 5.8.1-5.8.15.

Yang, Y-F., Chen, C-Y., Lu, T-H. and Liao, C-M. (2019) Toxicity-based toxicokinetic/toxicodynamic assessment for bioaccumulation of polystyrene microplastics in mice. *Journal of Hazardous Materials*, 366, 703-713.

Yang, Y., Wang, J. and Xia, M. (2020) Biodegradation and mineralization of polystyrene by plastic-eating superworms *Zophobas atratus*. *Science of the Total Environment*, 708, 135233.

Yang, Z., Bogdan, P. and Nazarian, S. (2021) An *in silico* deep learning approach to multi-epitome vaccine design: a SARS CoV-2 case study. *Scientific Reports*, 11, 3238.

Yang, Z., Lu, F., Zhang, H., Wang, W., Shao, L., Ye, J. and He, P. (2021) Is incineration the terminator of plastics and microplastics? *Journal of Hazardous Materials*, 401, 123429.

Yaradoddi, J.S., Banapurmath, N.R., Ganachari, S.V., Soudagar, M.E.M., Hallad, S., Hugar, S. and Fayaz, H. (2020) Biodegradable carboxymethyl cellulose based material for sustainable packaging application. *Scientific Reports*, 10, 21960.

Yeats, T.H. and Rose, J.K.C. (2013) The formation and function of plant cuticles. *Plant Physiology*, 163, 5-20.

Yoon, J-Y., Kim, W.S. and Kim, J.H. (1999) The relationship of the interaction forces in the protein adsorption onto polymeric microspheres. *Colloids and Surfaces A: Physiochemical and Engineering Aspects*, 153, 413-419.

Yuniarto, K., Purwanto, Y.A., Purwanto, S., Welt, B.A., Purwadaria, H.K. and Sunarti, T.C. (2016) Infrared and Raman studies on polylactide acid and polyethylene glycol-400 blend. *AIP Conference Proceedings*, 1725, 020101.

Zadjelovic, V., Erni-Cassola, G., Obrador-Viel, T., Lester, D., Eley, Y., Gibson, M.I., Dorador, C., Golyshin, P.N., Black, S., Wellington, E.M.H. and Christie-Oleza, J.A. (2022) A mechanistic understanding of polyethylene biodegradation by the marine bacterium *Alcanivorax*. *Journal of Hazardous Materials*, 436, 129278.

Zeisler-Diehl, V.V., Barthlott, W. and Schreiber, L. (2018) Plant Cuticular waxes: composition, function, and interactions with microorganisms. In: Wilkes, H. (Eds.) *Hydrocarbons, oils, and lipids: diversity, origin, chemistry and fate. Handbook of hydrocarbon and lipid microbiology*, Springer, Cham, pp. 1-16.

Zerva, A., Siaperas, R., Taxeidis, G., Kyriakidi, M., Vouyiouka, S., Zervakis, G.I. and Topakas, E. (2023) Investigation of *Abortiporus biennis* lignocellulolytic toolbox, and the role of laccases in polystyrene degradation. *Chemosphere*, 312, 137338.

Zettler, E.R., Mincer, T.J. and Amaral-Zettler, L.A. (2013) Life in the 'Plastisphere': microbial communities on plastic marine debris. *Environmental Science & Technology*, 47, 7137-7146.

Zhang, Y., Du, Z., Han, Y., Chen, X., Kong, X., Sun, W., Chen, C. and Chen, M. (2021) Plasticity of the cuticular transpiration barrier in response to water shortage and resupply in *Camellia sinensis*: a role of cuticular waxes. *Frontiers in Plant Science*, 11, 600069.

Zhang, Y., Pedersen, J.N., Eser, B.E. and Guo, Z. (2022) Biodegradation of polyethylene and polystyrene: from microbial deterioration to enzyme discovery. *Biotechnology Advances*, 60, 107991.

Zhang, Z., Peng, H., Yang, D., Zhang, G., Zhang, J. and Ju, F. (2022) Polyvinyl chloride degradation by a bacterium isolated from the gut of insect larvae. *Nature Communications*, 13, 5360.

Zhao, Z., Shao, S., Liu, N., Liu, Q., Jacquemyn, H. and Xing, X. (2021) Extracellular enzyme activities and carbon/nitrogen utilization in mycorrhizal fungi isolated from epiphytic and terrestrial orchids. *Frontiers in Microbiology*, 12, 787820.

Zheng, J. and Suh, S. (2019) Strategies to reduce the global carbon footprint of plastics. *Nature Climate Change*, 9, 374-378.

Zhigui, H., Li, G., Chen, J., Huang, Y., An, T. Zhang, C. (2015) Pollution characteristics and health risk assessment of volatile organic compounds emitted from different plastic solid waste recycling workshops. *Environmental International*, 77, 85-94.

Zhou, J., Wu, J., Zheng, S., Chen, X.,Zhou, D. and Shentu, X. (2018) Integrated transcriptomic and proteomic analysis reveal up-regulation of apoptosis and small heat shock proteins in lens of rats under low temperature. *Frontiers in Physiology*, 12, 683056.

Zhu, X., Zhang, Y., Du, Z., Chen, X., Zhou, X., Kong, X., Sun, W., Chen, Z., Chen, C. and Chen, M. (2018) Tender leaf and fully-expanded leaf exhibited distinct cuticle structure and wax lipid composition in *Camellia sinensis cv Fuyun 6*. *Scientific Reports*, 14944.

Ziv, C., Zhao, Z., Gao, Y.G. and Xia, Y. (2018) Multifunctional roles of plant cuticle during plant-pathogen interactions. *Frontiers in Plant Science*, 9, 1088.

Appendices

List of Publications

Research papers and Book Chapters

1. **Bhanot, V**., Shobham, Mamta and Panwar, J. 2023. Unveiling the potential of *Lichtheimia ramosa* AJP11 for myco-transformation of polystyrene sulfonate and its driving molecular mechanism. *Journal of Environmental Management*, 325, 116579.
2. **Bhanot, V**., Fadanavis, S.V. and Panwar, J. 2021. Revisiting the architecture, biosynthesis and functional aspects of the plant cuticle: there is more scope. *Environmental and Experimental Botany*, 183, 104364.
3. **Bhanot, V**., Pareek, V. Fadanvis, S.V. and Panwar, J. 2020. Myco-degradation of plastics. In: *New and Future Developments in Microbial Biotechnology and Bioengineering*, Singh, J. and Gehlot, P. (Eds.), Elsevier, Amesterdam, Netherlands, pp. 25-34.

Research Papers under communication

1. **Bhanot, V.**, Fadanavis, S.V., Mamta, Shobham and Panwar, J. 2023. Temporal variations in the surface micromorphology and chemical composition of cuticular wax in xerophytic plants. In "*Plant Physiology and Biochemistry*".
2. **Bhanot, V.**, Mamta, Gupta, S. and Panwar, J. 2023. Phylloplane fungus *Curvularia dactyloctenicola* VJP08 effectively degrades commercially available PS product. In "*Journal of Environmental Management*".

Research Papers from additional work during Ph.D. tenure

1. **Bhanot, V.**, Pali, S. and Panwar, J. 2022. Understanding the *in silico* aspects of bacterial catabolic cascade for styrene degradation. *Proteins: Structure, Function and Bioinformatics*, 1-10.
2. Pareek, V., Bhargava, A., **Vishalakshi**, Gupta, R., Jain, N. and Panwar, J. 2018. Formation and characterization of protein corona around nanoparticles: A review. *Journal of Nanoscience and Nanotechnology*, 18: 6653-6670.

Conference Abstracts

1. **Bhanot, V** and **Panwar, J.** 2022. Understanding the surface micromorphology and chemical composition of the epicuticular wax over the leaves of xerophytes. In: *FEMS*

Conference on Microbiology, June 30-July 02, 2022, Belgrade, Serbia, p. 910 (Virtual mode).

2. **Bhanot, V.**, Fadanavis, S.V., Shobham. and Panwar, J. 2020. Can similarities between plastics and cuticular wax facilitate myco-degradation of plastics. In: *ASM Microbe 2020*, June18-20, 2020 Chicago, Illinois, USA (Virtual mode).
3. **Bhanot, V.**, Fadanavis, S.V. and Panwar, J. 2019. Fungal-mediated degradation of polystyrene. In: *60th Annual Conference of Association of Microbiologists of India* (AMI-2019) and *International Symposium on "Microbial Technologies in Sustainable Development of Energy, Environment Agriculture and Health"*. November 15-18, 2019, Central University of Haryana, Mahendragarh, p. 183-184.

BIOGRAPHY

Prof. Jitendra Panwar

Prof. Jitendra Panwar completed his Master's degree in Botany with specialization in Microbiology in year 1997 and Doctoral degree in the area of Mycorrhizal Biotechnology in year 2000 from Jai Narain Vyas University, Jodhpur. After Ph.D., he moved to Division of Soil-Water-Plant Relationship, Central Arid Zone Research Institute (ICAR), Jodhpur for Post-Doctoral studies (June 2000 to January 2003), where he worked in the area of Microbiology, Plant Physiology and Soil Fertility. Subsequently, he executed DST Young Scientist Project awarded to him by Department of Science and Technology, Govt. of India, New Delhi, India during February 2003 to September 2005. He joined Department of Biological Sciences, BITS Pilani, Pilani campus as Lecturer in October 2005, became Assistant Professor in January 2006, Associate Professor in February 2013 and Professor in July 2018. He served as Head of the Department during September 2012 to August 2014. He worked as Associate Dean, Academic - Graduate Studies and Research Division (AGSRD), BITS Pilani, Pilani Campus during August 2018 to August 2022. He has total 25 years of teaching and research experience as in the year 2023.

Prof. Panwar is recipient of prestigious Visiting Professor Fellowship award by Indian National Science Academy (INSA) for the year 2011 as well as 2016. He has successfully implemented several research projects in the field of Microbial Biotechnology and Nanobiotechnology, funded by DST, New delhi; ICAR-NAIP, New Delhi; Aditya Birla Group, Mumbai; UGC, New Delhi; DST-Nano Mission; Aditya Birla Science & Technology Company Pvt. Ltd. (ABSTCPL), Mumbai; DST-ASACODER and DBT, New Delhi. So far, he has published 68 research papers in various journals and 17 chapters in the books of international repute. In addition, he has presented papers and delivered lectures in several National & International conferences and organizations. The current ongoing research work in his lab focuses on fugal mediated degradation of xenobiotic pollutants; myco-remediation of industrial waste water; enhancement of bioplastic production by extremophiles utilizing rice straw; and to elucidate the underlying mechanism.

BIOGRAPHY

Vishalakshi Bhanot

Ms. Vishalakshi Bhanot did her Integrated Graduation in Master of Science (M.Sc. Hons.) with specialization in Microbiology and sub-specialization in Biochemistry from Punjab Agricultural University, Ludhiana, Punjab. To pursue her doctoral research, she joined the research group of Prof. Jitendra Panwar at Department of Biological Sciences, Birla Institute of Technology and Science, Pilani, Pilani Campus, India in August 2017. She received "Institute Fellowship" during the Ph.D. tenure.

She has presented her research work at several national and international conferences hosted by American Society for Microbiology (ASM) and Federation of European Microbiological Societies (FEMS). She has also participated in different scientific workshops focusing on Molecular Docking & Drug Delivery. She has also participated in the organizing and conducting International Conference on Life Science and its interface with Engineering and allied sciences held from November 12-14, 2020 at BITS Pilani, Pilani Campus. She has published 5 research articles in journals of international repute till now. She has also been consistently involved in the teaching programme at Department of Biological Sciences, BITS Pilani, Pilani Campus.

Representative GC-MS/MS Chromatograms (Chapter 4)

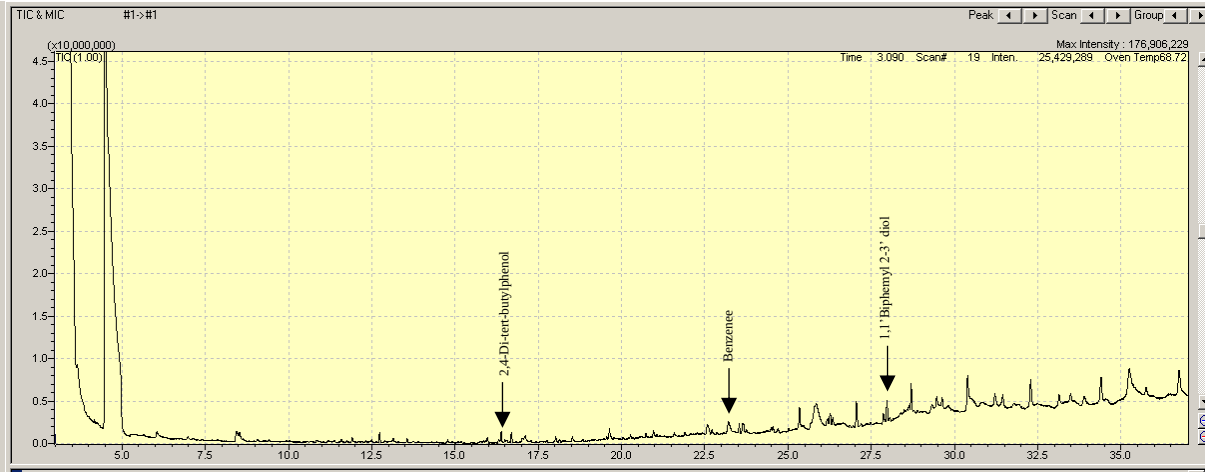

Figure 1. Representative GC-MS/MS chromatogram of untreated MSM+1% PSS.

Effect of Exposure Duration on PSS Myco-transformation Potency (Chapter 4)

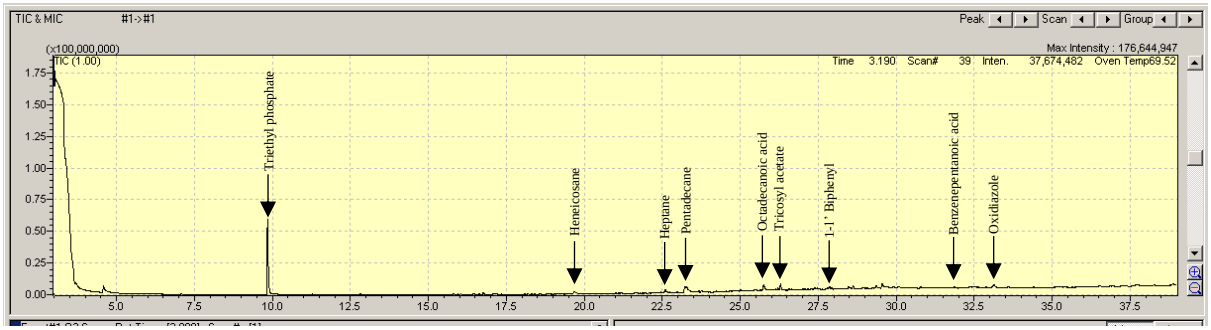

(a)

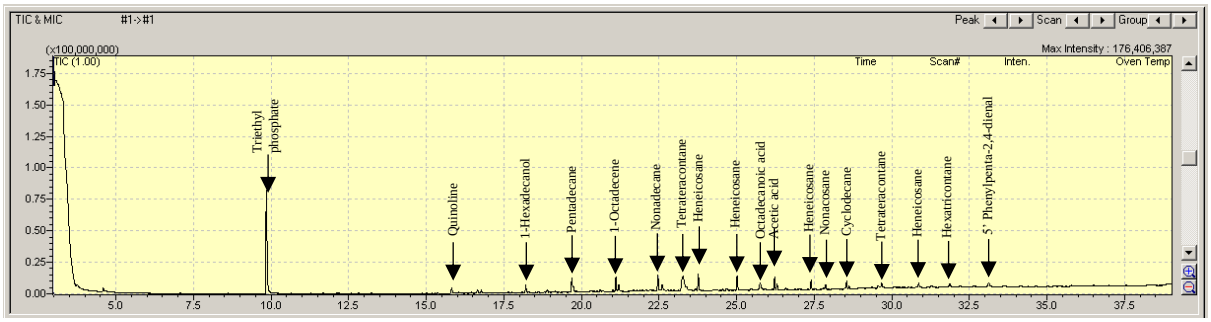

(b)

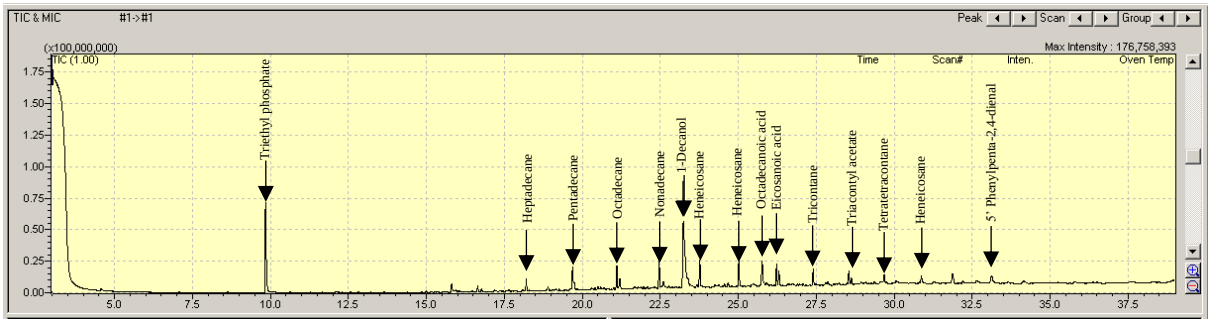

(c)

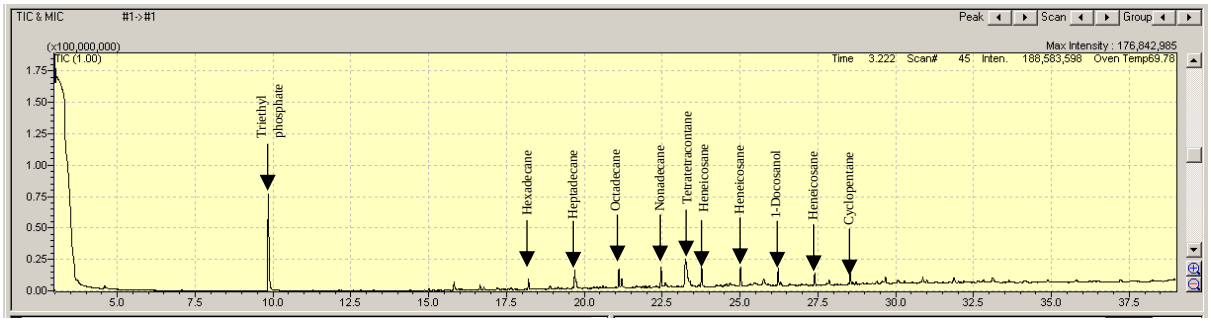

(d)

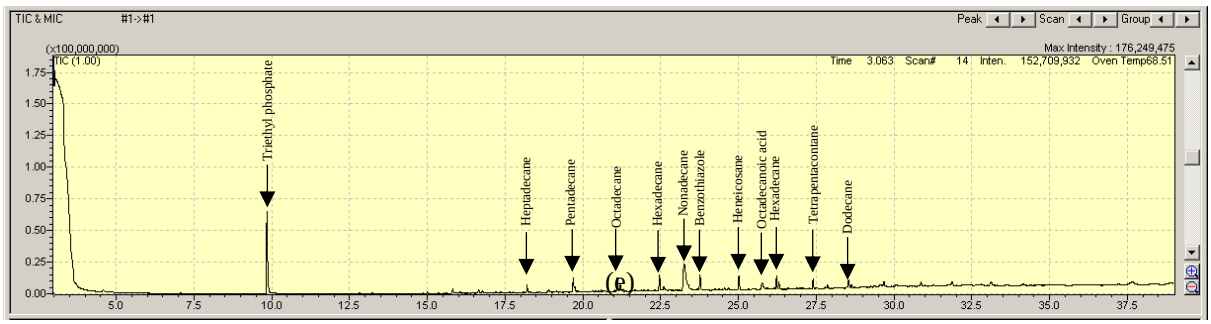

Figure 2. Representative GC-MS/MS chromatogram of PSS myco-transformation products in treatments containing MSM+1% PSS exposed to *C. dactyloctenicola* VJP08 for different exposure duration; (a) Day 5; (b) Day 10; (c) Day 15; (d) Day 20 and (e) Day 30.

Effect of Temperature on PSS Myco-transformation Potency (Chapter 4)

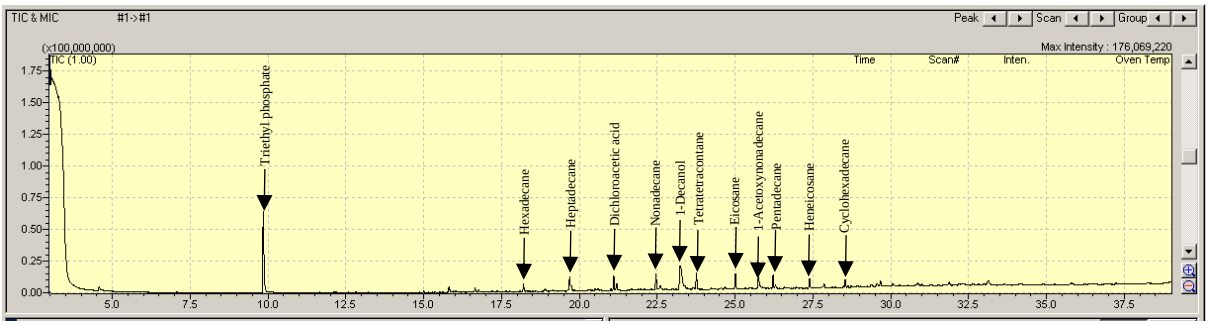

(a)

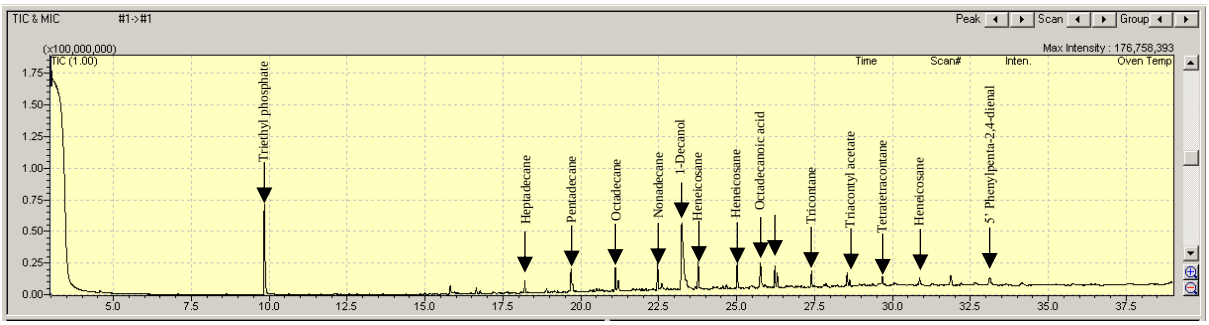

(b)

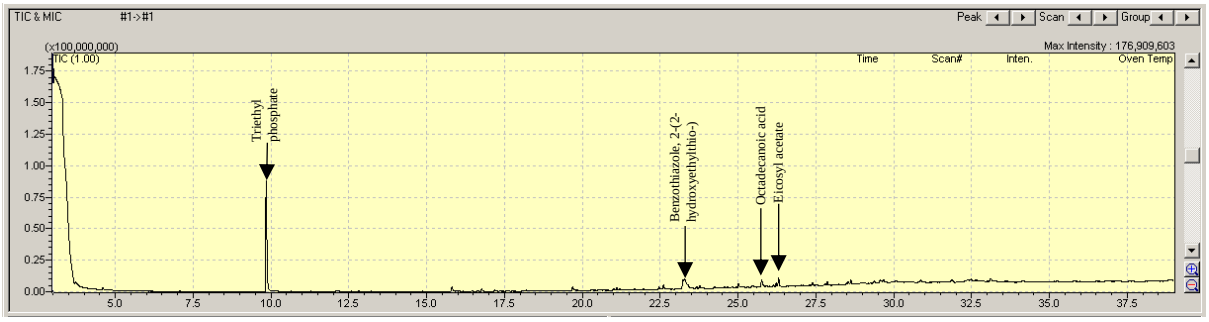

(c)

Figure 3. Representative GC-MS/MS chromatogram of PSS myco-transformation products in treatments containing MSM+1% PSS exposed to *C. dactyloctenicola* VJP08 at different temperatures; (a) 15℃; (b) 28℃ and (c) 40℃.

Effect of pH on PSS Myco-transformation Potency (Chapter 4)

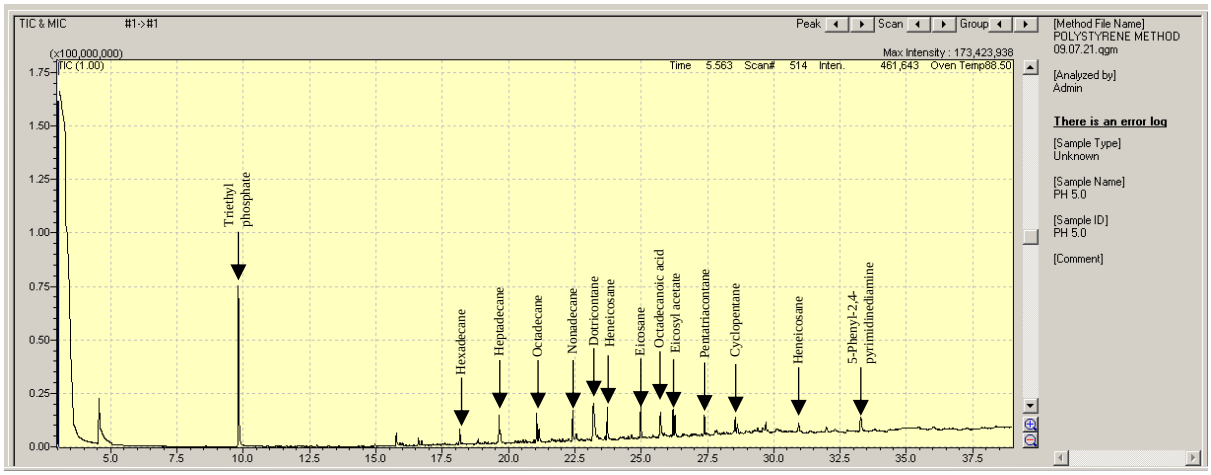

(a)

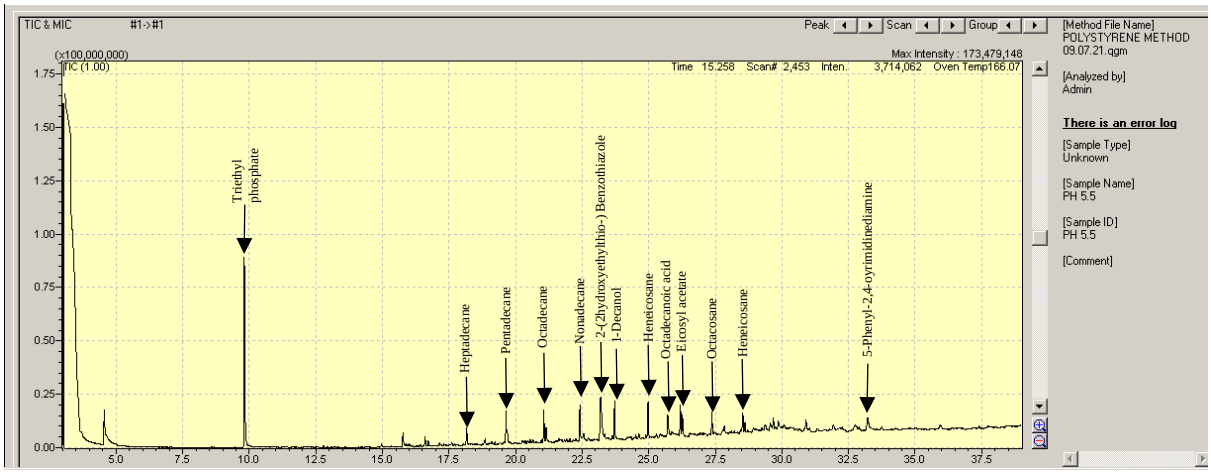

(b)

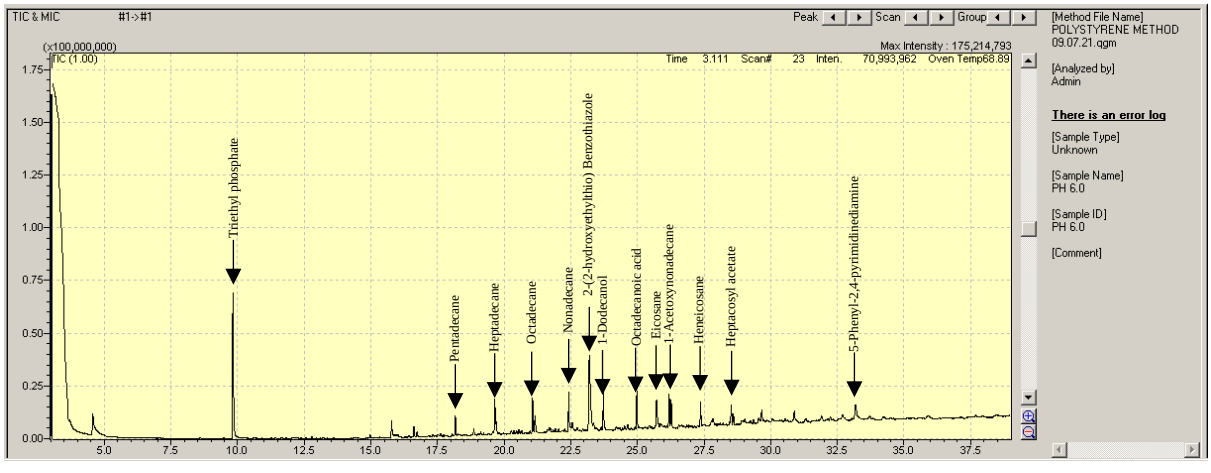

(c)

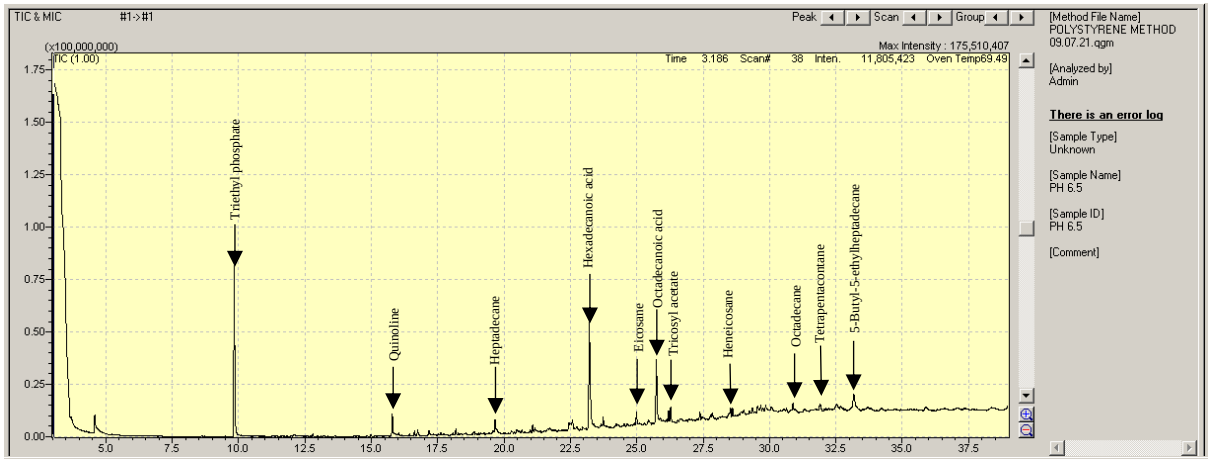

(d)

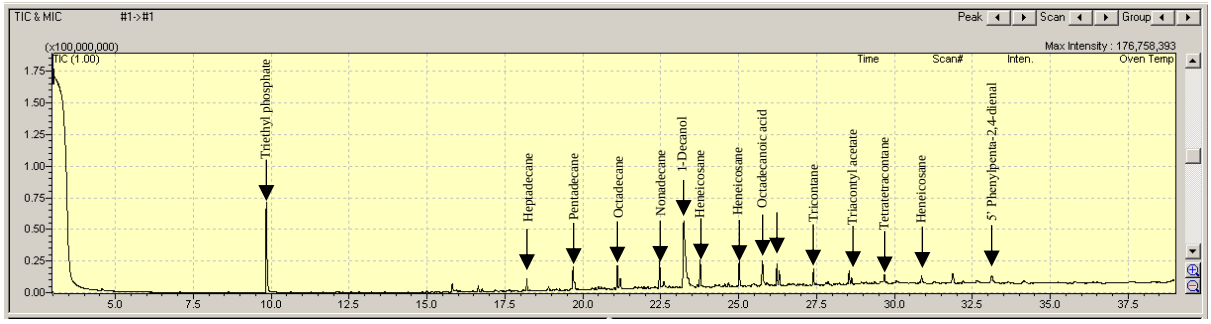

(e)

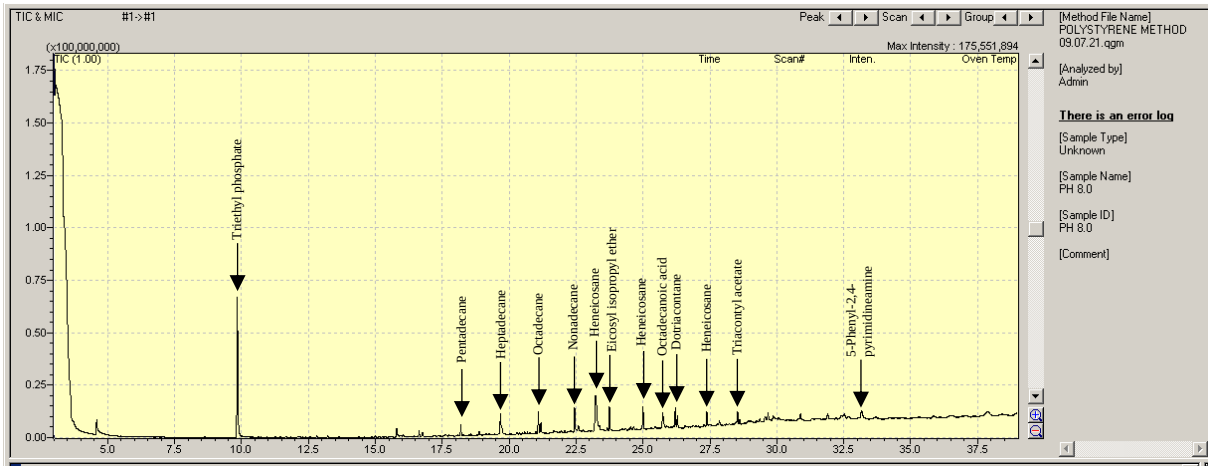

(f)

Figure 4. Representative GC-MS/MS chromatogram of PSS myco-transformation products in treatments containing MSM+1% PSS exposed to *C. dactyloctenicola* VJP08 at different pH; (a) pH 5.0; (b) pH 5.5; (c) pH 6.0; (d) pH 6.5; (e) pH 7.0 and (f) pH 8.

Re-print of Publications

CHAPTER

3

Myco-degradation of plastics

*Vishalakshi Bhanot, Vikram Pareek, Shreya Vivek Fadanavis, Jitendra Panwar**

Department of Biological Sciences, Birla Institute of Technology and Sciences, Pilani, Rajasthan, India

***Corresponding author. E-mail: drjitendrapanwar@yahoo.co.in**

3.1 Introduction

The word plastic is derived from the Greek word "plastikos," which means "capable of being molded or shaped" (Joel, 1995). Plastics are manmade, long-chain polymeric molecules of carbon and hydrogen atoms as the backbone to which oxygen, sulfur, or nitrogen atoms may be attached. The majority of plastic monomers such as ethylene and propylene are derived from fossil hydrocarbons, which are extracted from oil, coal, and natural gas (Sheldrick and Vogl, 1976). Plastics are robust, light, odorless, chemically resistant, and last for hundreds of years. Plastics have replaced paper, glass, and metals in most manufactured goods. Plastics have become omnipresent in our daily lives, and a world without plastics seems unimaginable today. Polyethylene (PE), polypropylene (PP), polystyrene (PS), polyvinyl chloride (PVC), polyethylene terephthalate (PET), and polyurethane (PUR) are the main types of plastics that correspond to more than 80% of total demand (Geyer et al., 2017).

However, the success, dominance, and longevity of plastic have led to serious global environmental concerns due to its recalcitrant nature and negligible decomposition. The majority of plastics are notably resistant to degradation under natural environmental conditions and therefore tend to last long in the environment (Andrady, 2015; Prieto, 2016). Hence, plastics concentrate rather than decompose in landfills and the natural environment. Over the past 70 years, plastics' production and its waste have dramatically increased due to rapid urbanization, resulting in increased production of "throw-away" products. In the year 2010 alone, ~ 4 to 12 million metric tons (Mt) of plastic waste generated on land had entered the marine environment, and this amount is expected to grow steadily (Jambeck et al., 2015). As of 2015, ~ 6300 Mt of plastic waste has been generated worldwide. Of this waste, around 9% has been recycled, 12% has been incinerated, and 79% has been dumped into landfills or the natural environment. With the concomitant increase in "white pollution" around the world, it is estimated that by 2050 around 12,000 Mt of plastic will be dumped in the natural environment and will be a major threat to life on Earth (Geyer et al., 2017).

3.2 Plastic types and their structures

There are multiple types of plastics with different chemical composition and properties, such as strength, weather resistance, melting point, thermal and moisture resistance, and so on. These properties make plastics suitable for various uses in domestic, industrial, and nonindustrial industries. Variation in plastic types contributes majorly to the world's economy and infrastructure as they have applications in telecommunications, wire-coatings, pipes, packaging, healthcare, construction, and most importantly, agriculture.

Plastics are of two types, namely, synthetic and biodegradable plastics. Synthetic plastics are derived from nonrenewable sources such as coal, petroleum, or natural gas, and are mostly nondegradable in the environment. A few examples are PE, PP, PVC, and PS. According to ASTM International (formerly known as the American Society for Testing and Materials), a biodegradable plastic is one in which the degradation results from the action of naturally occurring microorganisms such as bacteria, fungi, and algae, such as polyhydroxyalkanoates (PHA) and polybutylene succinate (PBS) (ASTM, 1999). Table 3.1 represents different plastic types and their respective chemical structures.

https://doi.org/10.1016/B978-0-12-821007-9.00003-6

Environmental and Experimental Botany 183 (2021) 104364

Contents lists available at ScienceDirect

Environmental and Experimental Botany

journal homepage: www.elsevier.com/locate/envexpbot

Revisiting the architecture, biosynthesis and functional aspects of the plant cuticle: There is more scope

Vishalakshi Bhanot, Shreya Vivek Fadanavis, Jitendra Panwar *

Department of Biological Sciences, Birla Institute of Technology and Sciences, Pilani, 333031, Rajasthan, India

ARTICLE INFO

Keywords:
Cuticle
Cutin
Wax
Cutan
Biosynthesis
Plant health
Abiotic and biotic factors

ABSTRACT

Having evolutionary significance in establishing colonization of terrestrial plants, cuticle occurs to act as a continuous shield over the plant epidermal cells, facilitating multifunctional communication passage between the plant and outer environment. Cuticle is a hydrophobic layer acting as a fencing between the aerial plant parts viz. primary stem, leaves, trichomes, flowers and fruits, and their external environment. The chemical nature and structure of cuticle may vary during various developmental and growth stages, as well as between various organs, genotypes, and species, depending on the environmental conditions. It is majorly composed of cutin and epicuticular wax depositions. In-depth understanding of the mechanism behind the cuticle biosynthesis remains to be unveiled. This review systematically discusses and sheds light on the structure and composition of cuticle, various genes, transcription factors and molecular pathways involved in the biosynthesis of cuticle, and how their regulation affect the plant health. Moreover, various functions of cuticle in terms of plant protection have been discussed.

1. Introduction

The occurrence of plants in the terrestrial ecosystem was marked around 470–500 million years ago in mid-Palaeozoic era, when Charophycean green algae evolved to their new form, the embryophytes [Waters, 2003; Niklas and Kutschera, 2010]. Transition of these algae from the aquatic ecosystem to their new home, the terrestrial ecosystem, required a lot of modifications to support their survival and successful colonization. Factors such as UV exposure, winds, temperature extremes, desiccation due to heat, etc. required development of various physiological and morphological advancements. The development of cuticle coating on the various aerial parts of the plants has been one of the most important adaptations. *Klebsormidium flaccidum*, a transitional link between the green algae and terrestrial plants shows the presence of a cuticle-like matrix which is made up of a lipid polymer and waxes [Kondo et al., 2016]. Cuticle works as an interface between the plants and their outer environment. The presence of cuticle on aerial surfaces has been supported by fossil evidences [Edwards, 1993]. It is found to be present among a wide range of all embryophytes [Budke et al., 2012]. It provides protection to the plants against high intensity UV-radiations, temperature, mechanical and chemical damage by various phytopathogens, prevent evaporation of water and penetration of pollutants [Yeats and Rose, 2013; Heredia-Guerrero et al., 2018].

Cuticle is a hydrophobic layer composed of two lipophilic moieties namely, cuticular wax and cutin. The cuticular waxes can be extracted using organic solvents such as chloroform, acetone, ethyl acetate, hexane and methanol whereas, the cross-linked polymeric network and lack of melting point of cutin makes it insoluble and difficult to extract [Nawrath, 2006; Kumar et al., 2018]. The cutin majorly constitutes a network of esterified and oxygenated aliphatic C16-C18 ω-hydroxy fatty acids, glycerol, polysaccharides (cellulose, hemicelluloses, pectin), waxes and small amounts of terpenoids, flavonoids and phenyl propanoids [Heredia, 2003; Heredia-Guerrero et al., 2014]. Plant biopolymers such as suberin and sporopollenin are the structural and functional homologues of cutin, known to play significant roles in transportation of water, protection from high temperature, UV radiations and external injuries by working as an insulator for the plants [Scott, 1994; Scott et al., 2004]. Like cuticle, both suberin and sporopollenin are extracellular biopolymers that protect the plants from various physical, chemical or mechanical stress. Suberin, and associated waxes are deposited on the root epidermal cells, cork and casparian strips [Karahara et al., 2004; Thomas et al., 2007]. Suberin is primarily composed of ω-hydroxy fatty acids (C16-C18), fatty α,ω-diacids (C16-C26), very long chain fatty acids (VLCFA), alcohols [Kolattukudy,

* Corresponding author.
E-mail addresses: jpanwar@pilani.bits-pilani.ac.in, drjitendrapanwar@yahoo.co.in (J. Panwar).

https://doi.org/10.1016/j.envexpbot.2020.104364
Received 27 October 2020; Received in revised form 15 December 2020; Accepted 20 December 2020
Available online 24 December 2020

Journal of Environmental Management 325 (2023) 116579

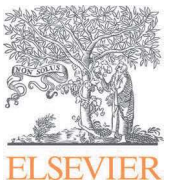

Contents lists available at ScienceDirect

Journal of Environmental Management

journal homepage: www.elsevier.com/locate/jenvman

Research article

Unveiling the potential of *Lichtheimia ramosa* AJP11 for myco-transformation of polystyrene sulfonate and its driving molecular mechanism

Vishalakshi Bhanot, Shobham, Mamta, Jitendra Panwar *

Department of Biological Sciences, Birla Institute of Technology and Sciences, Pilani, 333031, Rajasthan, India

ARTICLE INFO

Keywords:
Synthetic plastics
Polystyrene sulfonate
Myco-transformation
Fungal proteins
Hydrophobic surface binding protein
Molecular docking

ABSTRACT

Plastic pollution is a major environmental concern due to its deleterious effects on various ecosystems. The limitations and shortcomings of waste management strategies has led to the over-accumulation of plastic waste, mainly comprised of single-use plastics, such as polystyrene (PS). Considering the advantages of biotransformation over the other plastic disposal methods, it has become a major focus of the modern research. Biotransformation of plastics involves its microbial hydrolysis into short chain oligomers and monomers that are eventually assimilated as carbon source by the microbes leading to the release of CO_2. As fungi are known to possess multifarious and highly regulated enzyme system capable of utilizing diverse nutrient sources, the present study explored the potential of *Lichtheimia ramosa* AJP11 towards myco-transformation of polystyrene sulfonate (PSS), a structural analogue of polystyrene (PS). During the 30-day incubation period of *L. ramosa* AJP11 in minimal salt medium (MSM)+1% PSS, the fungus showed 41.6% increment in its fresh weight biomass, indicating the utilization of PSS as sole carbon source. Further analysis revealed the generation of various reaction intermediates such as alkanes and fatty acids, crucial for the continuum of fungal metabolic pathways. Moreover, detection of PS oligomers such as cyclohexane and 2,4-DTBP confirmed the myco-transformation of PSS. The extracellular fungal protein profile showed considerable overexpression of a 14.4 kDa protein, characterized to be a hydrophobic surface binding (Hsb) protein, which is hypothesized to adsorb onto the PSS to facilitate its transformation. Further, *in silico* analysis of Hsb protein indicated it to be an amphiphilic α-helical protein with ability to bind styrene sulfonate unit via both hydrogen and hydrophobic interactions, with a binding energy of −5.02 kcal mol^{-1}. These findings open new avenues for over expression of Hsb under controlled reactor conditions to accelerate the PS waste disposal.

1. Introduction

Plastics are an integral part of most of the daily requirements. The indiscriminate usage and disposal of plastics have led to the accumulation of massive quantities of waste over land and aquatic ecosystems [Kalia et al., 2021]. Since commercial-use plastics are synthetic and non-biodegradable in nature, they are difficult to manage and dispose due to their partial natural degradation [Patel et al., 2021]. Out of 6500 million metric tons (Mt) of plastic waste generated, only minor portions have been recycled (9%) and incinerated (12%), whereas the rest is left as litter in the environment [Geyer et al., 2017]. About 80% of plastic waste in environment releases microplastics that behave as support for microbial biofilm formation, for example, *Bacillus amyloliquefaciens* has been reported to bind and form biofilm over PVC-based support [Zettler et al., 2013; Prakash et al., 2018].

Polystyrene (PS) $(C_8H_8)_n$ is high molecular weight, synthetic and non-biodegradable polymer composed of aromatic styrene monomers, used in throw away products [Ho et al., 2018]. PS possesses desirable manufacturing attributes such as low specific weight, high transparency, low shrinkage, chemical inertness and brilliant mechanical properties such as resistance to compression, system strengthening, and porosity, which make it suitable for applications in engineering [Toksoy and Güden et al. 2005; Patel et al., 2019; Tang et al., 2019]. Also, its economic feasibility makes it widely applicable in packaging, construction material, food containers, disposable cutlery, fisheries, water sports, etc. The extensive applicability is accompanied with negligible recycling

* Corresponding author.
E-mail addresses: jpanwar@pilani.bits-pilani.ac.in, drjitendrapanwar@yahoo.co.in (J. Panwar).

https://doi.org/10.1016/j.jenvman.2022.116579
Received 12 July 2022; Received in revised form 16 October 2022; Accepted 17 October 2022
Available online 24 October 2022
0301-4797/

Received: 28 June 2022 | Revised: 31 October 2022 | Accepted: 15 November 2022

DOI: 10.1002/prot.26447

RESEARCH ARTICLE

PROTEINS WILEY

Understanding the in silico aspects of bacterial catabolic cascade for styrene degradation

Vishalakshi Bhanot | Snigdha Pali | Jitendra Panwar

Department of Biological Sciences, Birla Institute of Technology and Science, Pilani, Rajasthan, India

Correspondence
Jitendra Panwar, Department of Biological Sciences, Birla Institute of Technology and Science, Pilani, 333031 Rajasthan, India.
Email: drjitendrapanwar@yahoo.co.in; jpanwar@pilani.bits-pilani.ac.in

Abstract

Styrene is a nonpolar organic compound used in very high volume for the industrial scale production of commercially important polymers such as polystyrene resins as well as copolymers like acrylonitrile butadiene styrene, latex, and rubber. These resins are widely used in the manufacturing of various products including single-use plastics such as disposable cups and containers, protective packaging, heat insulation, and so forth. The large-scale utilization leads to the over-accumulation of styrene waste in the environment causing deleterious health risks including cancer, neurological impairment, dysbiosis of central nervous system, and respiratory problems. To eliminate the accumulating waste. Microbial enzyme-based system represents the most environmental friendly and sustainable approach for elimination of styrene waste. However, comprehensive understanding of the enzyme–substrate interaction and associated pathways would be crucial for developing large-scale disposal systems. This study aims to understand the molecular interaction between the protein-ligand complexes of the styrene catabolic reactions by bacterial enzymes of *sty* operon. Molecular docking analysis for catalytic enzymes namely, styrene monooxygenase (SMO), styrene oxide isomerase (SOI), and phenylacetaldehyde dehydrogenase (PAD) of the bacterial *sty* operon was carried out with their individual substrates, that is, styrene, styrene oxide, and phenylacetic acid, respectively. The binding energy, amino acids forming binding cavity, and binding interactions between the protein-ligand binding sites were calculated for each case. The obtained binding energies showed a stable association of these complexes indicating the future scope of their utilization for large-scale bioremediation of styrene, and its commercially used polymers and copolymers.

KEYWORDS
phenylacetaldehyde dehydrogenase, protein docking, *sty* operon, styrene, styrene catabolism, styrene isomerase, styrene monooxygenase

1 | INTRODUCTION

Styrene is an aromatic compound that naturally occurs in the environment as a petroleum component and used to produce wide range of functional polymers.[1,2] The main applications of styrene include its polymerization into polystyrene (PS) and copolymerization with butadiene rubber and acrylonitrile to form synthetic rubbers of diverse properties.[3] Styrene is of high relevance in various industries and produced in million tonne scale, causing substantial anthropogenic release.[4] Polymer mixtures of styrene are used for the production of beverage cups, and packaging containers for meat, egg, yogurt, cheese, and ready-to-eat foods causing migration of residual

